ELECTROCATALYSIS OF FUEL CELL MOLECULES ON CARBON NANOTUBE PLATINUM-RUTHENIUM BASED ELECTRODES

ELECTROCATALYSIS OF FUEL CELL MOLECULES ON CARBON NANOTUBE PLATINUM-RUTHENIUM BASED ELECTRODES

by

Nobanathi Wendy Maxakato

A dissertation submitted in fulfilment of the requirement for the degree of

Doctor of Philosophy

in the Faculty of Natural and Agricultural Science

University of Pretoria

Supervisor: Prof. K. I. Ozoemena

October 2012

DECLARATION

I declare that the dissertation which is hereby submitted to the Department of Chemistry, Faculty of Natural and Agricultural Sciences, University of Pretoria, is my work and has not been submitted by me for a degree at any other University, and that all material contained therein has been duly acknowledged.

DEDICATION

This dissertation is dedicated to God Almighty for helping me work through difficulties and challenges I have experienced throughout my studies, my Supervisor Prof. K.I. Ozoemena, my husband Sipho, my little boy Sonwabo and my late parents Ntombomntu and Ngqukuva Maxakato.

ACKNOWLEDGEMENTS

I am extremely grateful to my supervisor, Prof. K. I. Ozoemena for allowing me to be part of his research group and believing in me, his patience; his motivation and his guidance throughout in making this dream a reality. My appreciation also goes to my husband, my late parents, Dr O. Arotiba and my family at large for their love, prayers and unending support. University of Pretoria, the National Research Foundation and the CSIR for financial assistance are greatly acknowledged. Finally, I thank my colleagues in the same group for their love, encouragement and constant support, and every other person that made this work a success. Thank you all!

ABSTRACT

The investigation of the kinetics of fuel cell (FC) molecules such as methanol (MeOH), ethylene glycol (EG) and formic acid (FA) on platinum (Pt), platinum/ruthenium (PtRu) and platinum based metal complexes (ruthenium tetrakis(diaquaplatinum)octacarboxy-phthalocyanine (RuOcPcPt) modified basal plane pyrolytic graphite electrode (BPPGE) was carried out. One of the major limitations of FC molecules is that Pt undergoes surface poisoning by strongly adsorbed reaction intermediates, carbon monoxide (CO) that eventually decreases the fuel cell efficiency. Thus, the integration of Pt and or Pt/Ru with functionalized multi-walled carbon nanotubes (fMWCNTs) and some N4-macrocycles such as ruthenium phthalocyanine complexes on the BPPGE towards these FC molecules have been studied in this work. However, this study focused mainly on Pt, Pt/Ru, ruthenium octacarboxy-phthalocyanine (RuOcPc) and RuOcPcPt nanoparticles. The MWCNTs, metal and N4-macrocycles provided the needed platform for the efficient electrooxidation of FC molecules with minimum or no poisoning. The first part of the thesis deals with electrocatalytic oxidation of the FC molecules using electrodes prepared by electrodeposition techniques. The section describes the comparative electrocatalytic behaviour of MeOH, EG and FA at MWCNT-Pt/Ru immobilized on BPPGE. The Pt/Ru nanoparticles were deposited on the substrate using the electrodeposition technique. The

second part of this work deals with electrocatalysis of the FC molecules using BPPG electrode modified with chemically synthesized Pt nanoparticles integrated with RuOcPc. In both cases, successful modification of the electrodes with the metal nanoparticle/carbon nanotube or metal nanocomplex nanocomposite was established using the field emission /high resolution scanning electron microscopy (FESEM/HRSEM), high resolution transmission electron microscopy (HRTEM), x-ray diffraction (XRD) spectroscopy and electron dispersive x-ray spectroscopy (EDS). The average particle size for the synthesised Pt nanoparticles is 1.4 nm. The electrocatalytic behaviour of the modified electrodes was investigated using cyclic voltammetry (CV) and electrochemical impedance spectroscopy (EIS). The results of the electrodeposition study showed that the presence of Pt nanoparticles, together with Ru nanoparticles, gave better performance with the FA showing the least tolerance to electrode poisoning. The impedance spectra of the MWCNT-Pt/Ru hybrids in all the FC materials studied showed some dependence on the oxidation potential. These spectra were somewhat complicated but generally followed electrical equivalent circuit models characteristic of adsorption-controlled charge transfer kinetics. EG and MeOH showed conventional positive Faradaic impedance spectra, irrespective of the applied oxidation potential. FA impedance spectra exhibited an inductive loop only at the extreme forward anodic peak potential, characteristic of Faradaic current being governed by the occupation of an intermediate state.

On the other hand, the presence of phthalocyanine with the synthesized Pt-Ru nanocatalysts showed an improvement on the tolerance to CO poisoning during MeOH oxidation and therefore its application in the direct fuel cell oxidation is encouraged. The synthesized Pt-based nanoparticles gave better performance compared to the electrodeposited Pt-based nanoparticles. The comparative electrocatalytic behaviour of the chemically synthesized nanocatalysts indicated that the BPPGE-fMWCNT/RuOcPcPt electrode gives the best performance towards MeOH oxidation compared to other electrodes studied, while FA oxidation was favoured on the BPPGE-RuOcPcPt electrode without CNTs support. However, EG oxidation was not successful at the electrodes at all. The oxidation of these FC molecules are characterized by both diffusion (forward) and adsorption-controlled (reverse) processes. The two electrodes (BPPGE-fMWCNT/RuOcPcPt and BPPGE-RuOcPcPt) gave better tolerance to oxidation poison with the ratio of the current density of the forward anodic peak to the reverse anodic peak (J_{fa}/J_{ra}) and (J_{fa1}/J_{fa2}) of 4.0 and 1.0 respectively. The electrodeposited and chemical synthesized nanocatalysts results shown in this work have for the first time provided some useful insights into the electrocatalytic response of FC molecules (MeOH, FA, EG) for potential application in fuel cell technology.

The third part of the thesis describes the electrocatalytic reduction of molecular oxygen in alkaline solution using a novel ruthenium tetrakis

(diaquaplatinum)octacarboxyphthalocyanine (RuOcPcPt) electrocatalyst supported on MWCNTs. The results revealed that the MWCNT-RuOcPcPt electrode is electro-catalytically active than MWCNT, MWCNT-RuOcPc, RuOcPc and RuOcPcPt electrodes towards oxygen reduction reaction. The study shows that the oxygen reduction activity follows a direct 4-electron transfer process with high kinetic rate constant, 3.57 x 10^{-2} cm s^{-1}. The results obtained imply that more energy has been achieved and therefore the electrode is a promising candidate as a catalyst in the cathodic reaction of fuel cell.

TABLE OF CONTENTS

SECTION A

CHAPTER ONE

INTRODUCTION

CHAPTER TWO

EXPERIMENTAL

2.1 Materials and Reagents

2.2 Equipments and methods

2.3 Electrode Modification and Pretreatments

2.3.2 Electrode modification

2.4 Electrocatalytic and Electroanalysis

SECTION B

RESULT AND DISCUSSION

CHAPTER THREE

Insights into the electro-oxidation of ethylene glycol at Pt/Ru nanocatalysts supported on MWCNTs: Adsorption-controlled electrode kinetics

CHAPTER FOUR

Dynamics of electrocatalytic oxidation of ethylene glycol, methanol and formic acid at MWCNT platform electrochemically modified with Pt/Ru nanoparticles

CHAPTER FIVE

Efficient oxygen reduction reaction using ruthenium tetrakis (diaquaplatinum) octacarboxyphthalocyanine catalyst supported on MWCNT platform

CHAPTER SIX

Electrocatalytic Oxidation of Methanol and Formic Acid at MWCNT Platform Modified with synthesized Pt/Ru and Pt/RuOcPc Nanoparticles

LIST OF ABBREVIATIONS

A	Electrode surface area (cm^{-2})
AFM	Atomic force microscopy
Ag/AgCl	Silver/silver chloride reference electrode
BPPGE	Basal plane pyrolytic graphite electrode
BPPGE-MWCNT	Basal plane pyrolytic graphite electrode decorated multi-walled carbon nanotubes
CME	Chemically modified electrode
CMEs	Chemically modified electrodes
CV	Cyclic voltammetry
CV	Cyclic voltammogram
D	Diffusion coefficient ($cm^2\ s^{-1}$)
DMF	Dimethylformamide
EDX	Energy dispersive x-ray spectroscopy
EIS	Electrochemical impedance spectroscopy
E_i	Starting potential
E_f	Final potential
E_p	Peak potential
E_{pa}	Anodic peak potential
E_{pc}	Cathodic peak potential
E^o	Standard potential

$E^{o'}$ or $E_{1/2}$	Formal redox potential
F	Faraday's constant
FTIR	Fourier transform infra-red
$Fe(CN)_6^{4-}$	Hexacyanoferrate(II)
$Fe(CN)_6^{3-}$	Hexacyanoferrate(III)
Pt/Ru	Platinum-Ruthenium
Pt	Platinum
Ru	Ruthenium
RuOcPc	Ruthenium octa-carboxyphthalocyanine
RuOcPcPt	Ruthenium octa-carboxyphthalocyanine platinum (II) catalyst
RuTetPcPt	Ruthenium tetra-carboxyphthalocyanine platinum (II) catalyst
I_{pa}	Anodic peak current
I_{pc}	Cathodic peak current
L.B.	Langmuir-Blodgett
R	Gas constant
R.E.	Reference electrode
R_s	Solution resistance
SCE	Standard calomel electrode
SEM	Scanning electron microscopy
TEM	Transmission electron Microscope
W.E.	Working electrode
XRD	X-ray diffraction

LIST OF SYMBOLS

A	Rate of electron transfer
Γ	Surface coverage or concentration
π	Pi bonding
λ	Wavelength
A	Absorbance
C	Molar concentration of analyte
C	Capacitance
C_{dl}	Double-layer capacitance
CPE	Constant phase electrode
C_{Ox}	Concentration of the oxidised form of an analyte
C_{Red}	Concentration of the reduced form of an analyte
C_s	Specific interfacial capacitance
d	Diameter
D	Diffusion coefficient
E_{pa}	Anodic peak potential
E_{pc}	Cathodic peak potential
E	Potential

E^o	Standard potential
$E_{1/2}$	Half-wave potential
ΔE_p	Anodic-to-cathodic peak potential separation
f	Frequency
F	Faraday's constant
h	Plank's constant
Hz	Hertz
I_{abs}	Absorbed light
i_{pa}	Anodic peak current
i_{pc}	Cathodic peak current
k	Heterogeneous electron transfer coefficient
K	Equilibrium constant
K_a	Dissociation constant
K	Kelvin
N	Number of electron
N_A	Avogadro's constant
q	Electrical charge
Q	Electrical charge (C)
R	Universal gas constant
R_{ct}	Charge transfer resistance
R_s	Resistance of electrolyte
ν	Scan rate

V	Volts
Z_{im}	Imaginary impedance
Z_{re}	Real impedance
Z_w	Warburg impedance

LIST OF FIGURES

LIST OF SCHEMES

LIST OF TABLES

SECTION A

CHAPTER ONE

INTRODUCTION

1.1. BACKGROUND

Fuel Cell (FC) research and investigation of the electrochemical kinetics of FC molecules such as methanol (MeOH), ethylene glycol (EG) and formic acid (FA) have attracted great interest worldwide. This is due to their promising potential replacement for batteries in low power electronic applications such as laptops, computers and cellphones. However, during the electrooxidation of these FC molecules on platinum (Pt) electrocatalyst, the catalytic surface is poisoned by strongly adsorbed reaction intermediates, mainly carbon monoxide (CO) that eventually blocks the active sites [1]. Nanoparticulate alloys of Pt and other metals notably ruthenium (Ru) have shown to improve the electrocatatalytic activity and tolerance to CO poisoning compared to pure Pt [2]. Other existing problems in fuel cells include the high cost and the lack of the catalyst support and electrode materials.

In an attempt to solve these problems, efforts are being intensified on materials structured on the nanoscale since they are becoming a critical tool in the development of cleaner and higher performance energy devices. These nanostructured materials display a range of remarkable and unique properties, namely high surface area, mechanical strength, electronic conductivity and thermal stability which enhance the chemical reactivity of materials such as electrocatalyst [3, 4]. Among the energy devices that

could benefit from the unique properties of nanomaterials are fuel cells, photovoltaics, hydrogen storage systems, supercapacitors and rechargeable lithium ion batteries. Nanomaterials promise to improve the performance and reduce the cost of the electrocatalyst and electrode used in FCs [5-9].

Therefore in this study platinum-ruthenium carbon-nanotubes (PtRu-CNT) or ruthenium tetrakis (diaquaplatinum) octacarboxyphthalocyanine carbon nanotube (RuOcPcPt-CNTs) nanocomposite materials have been developed to improve the efficiency of the fuel cell electrocatalytic oxidation. The drawbacks associated with carbon black based electrodes are overcomed by choosing a CNT based graphite electrode. Carbon nanotubes are regarded as high quality pure supports and are essential for high catalytic activity due to their high surface area. Graphite electrode has the ability to interact with carbon nanotubes via π interactions. CNTs possess admirable conductive properties and also exhibit faster electrode kinetics compared to other electrodes such as the glassy carbon, boron-doped or carbon black electrode.

Finally, this work systematically explores the electron transport and electrocatalytic properties of fMWCNTs integrated with PtRu or RuOcPcPt nanoparticles supported on basal plane pyrolytic graphite electrode (BPPGE) platform towards electrooxidation of MeOH, EG, FA and in oxygen-reduction reaction (ORR).

This introductory chapter provides information on the general overview of the thesis, overview of electrochemistry, voltammetric techniques, electrochemical impedance spectroscopy, chemically modified electrodes, electrode modification techniques, metallophthalocyanine, fuel cells, microscopy and spectroscopy techniques and the analytes (MeOH, EG, FA and oxygen) used in this work as analytical probes. Chapter two describes the experimental procedure adopted while; chapter three to six discuss the results obtained.

1.2 Overview of Electrochemistry

1.2.1 Basic concepts

Electrochemistry is a broad field of physical science, encompassing those processes that involve the passage of charge across the interface between two phases. These involve electron transfer from a metal electrode to a redox active species in an electrolyte solution, and the transfer of an ion from an aqueous phase to an immiscible organic phase. It also deals with the study of chemical changes caused by the passage of an electric current and the production of electrical energy by chemical reactions and vice versa. The fundamental process in electrochemical reactions is the transfer of electrons between the electrode surface and molecules in the interfacial region, either in solution or immobilized at the electrode surface. Therefore, electrochemistry is one effective technique to study electron transfer properties [10-19]. When electron transfer is between a solid substrate and a solution species, it is termed heterogeneous process. Inversely, if electron transfer reaction occurs between two species, both of which are in solution, the reaction is homogeneous. Electrochemistry involves the measurement of potential (potentiometry) or current response (voltammetry) [12, 14-16]. Therefore, the work described in this thesis involves a number of voltammetric techniques, such as cyclic voltammetry (CV),

chronoamperometry (CA), and Rotating Disk Electrode (RDE) for studying the mechanism of electron transport and the electrocatalytic behaviour of the studied fuel cell (FC) molecules and oxygen at the electrode.

1.2.2 The electrode-solution interface

Charged particles exist at every material interface called the *electrical double layer*. In electrochemistry, this layer reflects the ionic zones formed in solution to compensate for the excess of charge on the electrode. The electrical double layer is made up of several layers when the electrode is immersed in solution as illustrated in Figure 1.1. Whether the charge on the metal is negative or positive with respect to the solution depends on the potential across the interface and the composition of the solution. A positively charged electrode thus attracts a layer of negative ions and vice versa. The inner layer closest to the electrode contains solvent molecules that are specifically adsorbed on the electrode. This layer is called the *Inner Helmholtz Plane* (IHP) or *compact layer* [17]. The outer layer called the *Outer Helmholtz Plane* (OHP) is the imaginary plane passing through the solvated cations. These planes cannot be measured nor do they exist so it can be assumed that the distance from the electrode to the IHP will be the radius of the ion. The IHP and OHP represent the layer of charges which is

strongly held by the electrode and can survive even when the electrode is pulled out of the solution [17, 18].

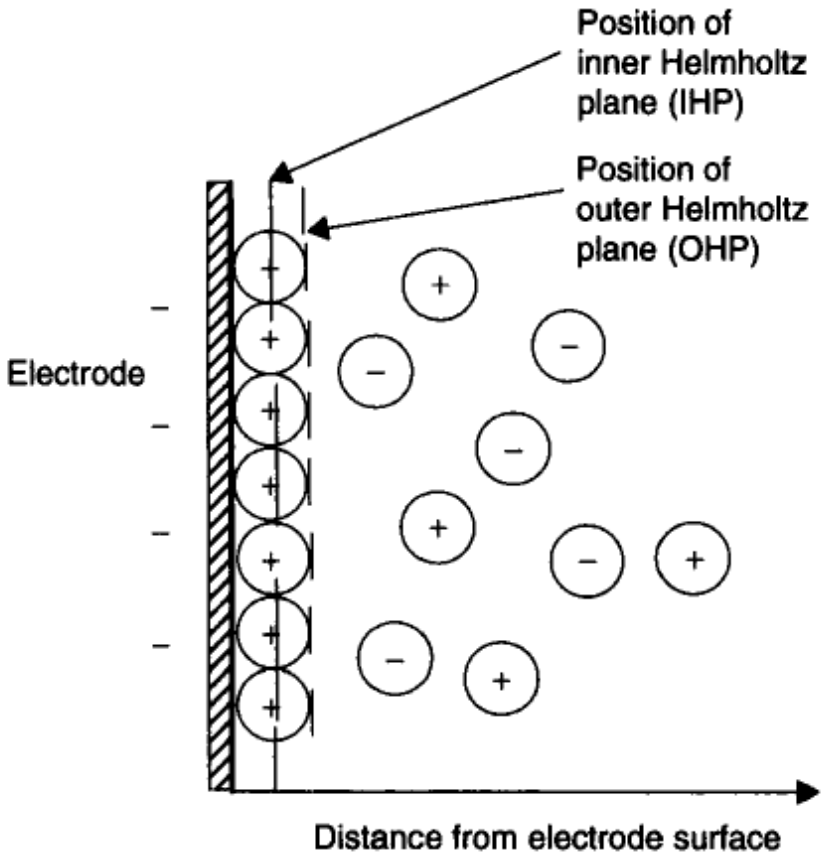

Figure 1.1: Schematic representation of the double-layer around an electrode, showing the positions of the inner and outer Helmholtz planes, and the way that ionic charges are separated. The circles represent solvated ions.

1.2.3 Faradaic and Non-Faradaic process

Oxidation and reduction processes are governed by Faraday's law which states that the amount of chemical reaction caused by the flow of current is proportional to the amount of electricity passed. These reactions are called Faradaic processes as electrons are transferred across the metal-solution

interface. Non-Faradaic process arise when an electrode-solution interface shows a range of potentials where no charge-transfer reactions occur. However, processes such as adsorption and desorption can occur, and the structure of the electrode-solution interface can change with changing potential or solution composition. Although charge does not cross the interface, external currents can flow (at least transiently) when the potential, electrode area, or solution composition changes [20].

1.2.4 Mass transport processes

Reaction at electrode surface can be complicated, and takes place in a sequence that involves several steps. In simple reactions, only mass transport of the electroactive species to the electrode surface, the electron transfer across the interface, and transport of the product back to the bulk solution occurs. However in complex reactions, additional chemical and surface processes that follow the actual electron transfer take place. Therefore, the overall measured current, may be limited by either mass transport of the reactant or by the rate of electron transfer. Hence, when the overall reaction is controlled solely by the rate at which the electroactive species get to the electrode, the measured current is said to be limited by mass transport [10, 17, 21]. Mass transport is a process which governs the movement of charged or neutral species and contributes to the flow of electricity through an electrolyte solution in an electrochemical cell. Mass

transfer in solution occurs by diffusion, migration, and convection. Diffusion and migration result from a gradient in electrochemical potential. Convection results from an imbalance of forces on the solution. Each of these processes is futher discussed below.

(a) Diffusion

This is a mass transport process which is aimed at minimising concentration differences at the electrode electrolyte interface. Diffusion is simply the movement of material from a high concentration region of the solution to a low concentration region, or the transport of particles as a result of difference in their chemical potential [10, 17, 21]. If the potential at an electrode oxidizes or reduces the analyte, its concentration at the electrode surface will be lowered, and therefore, mor analyte moves to the electrode from the bulk of the solution, which makes it the main current-limiting factor in voltammetric process. This process is represented in Figure 1.2a.

(b) Migration

Migration is a mass transport process involving movement of charge particles along an electrical field. The charge particles are carried through the solutions by ions according to their transference number. Migration of electroactive species can either enhance or diminish the current flowing at the electrode during reduction or oxidation of cations. It helps reduce the

electrical field by increasing the solution conductivity, and serves to decrease or eliminate sample matrix effects. Addition of high concentration of inert salt (i.e. hundred times higher than the electroactive ions concentration) as supporting electrolyte helps in eliminating current due to electromigration such that the current measured at the electrode is purely due to the diffusion of the electroactive species to the electrode surface. The supporting electrolyte also ensures that the double layer remains thin with respect to the diffusion layer, and it establishes a uniform ionic strength throughout the solution [14, 21]. Migration process is represented in Figure 1.2b.

(c) Convection

Convection is mass transport movement to the electrode by either physical movement such as fluid flow by stirring, or flow of solution and simultaneous vibration or rotation of the electrode (i.e forced convection) as found during the rotating disk electrode experiment [14, 22]. Convection can also occur naturally due to density gradient. In voltammetry, convection is eliminated by maintaining the cell under quiet and stable condition. Mass transport due to convection is represented in Figure 1.2c below.

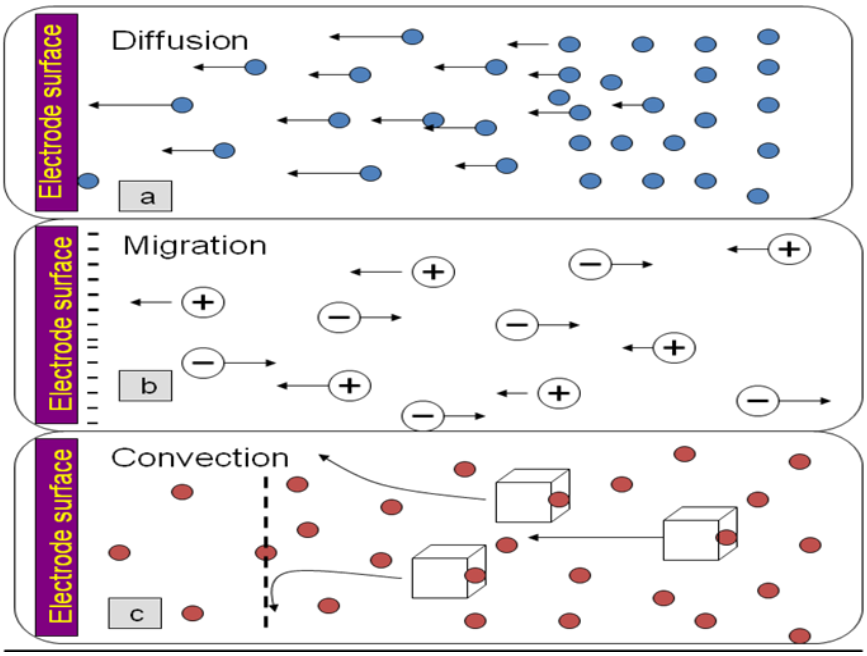

Figure 1.2: The three modes of mass transport process: (a) Diffusion, (b) Migration (c) Convection [14].

1.3 Voltammetric techniques

Voltammetric techniques measure current response in respect of variation in potential. The voltammetry techniques employed in this study are cyclic voltammetry (CV) and Rotating disc electrode voltammetry (RDE). This section gives the basic theoretical background underlying these techniques. Other electroanalytical techniques employed are Chronoamperometry (CA) and Electrochemical impedance spectroscopy (EIS) and are discussed below.

1.3.1 Cyclic voltammetry

Cyclic voltammetry (CV) has become a very popular technique for initial electrochemical studies of new systems and has proven very useful in obtaining information about fairly complicated electrode reactions. It is often the first experiment performed in an electroanalytical study, particularly due to its ability to rapidly provide considerable information on the thermodynamics of redox processes and the kinetics of heterogeneous electron transfer reactions. It offers a rapid location of redox potentials of the electroactive species and convenient evaluation of the effect of electrolyte on the redox process. In voltammetry the potential of the working electrode is ramped at a selected scan rate, ν. The resultant trace of current against potential is termed a voltammogram.

During cyclic voltammetry, the potential is similarly ramped from an initial potential E_i but, at the end of its linear sweep, the direction of the potential scan is reversed, usually stopping at the initial potential E_i (or it may commence an additional cycle). The potential at which the reverse occurs is known as the switch potential (E_λ). Almost universally, the scan rate between E_i and E_λ is the same as that between E_λ and E_i. Values of the scan rates $\nu_{forward}$ and $\nu_{backward}$ are always written as *positive* numbers.

There are three cyclic voltammetric processes that could take place, namely, reversible, irreversible and quasi-reversible [20].

1.3.1.1 Reversible process

The shape of the CV shown in Figure 1.3 is typical for a couple that is wholly reversible.

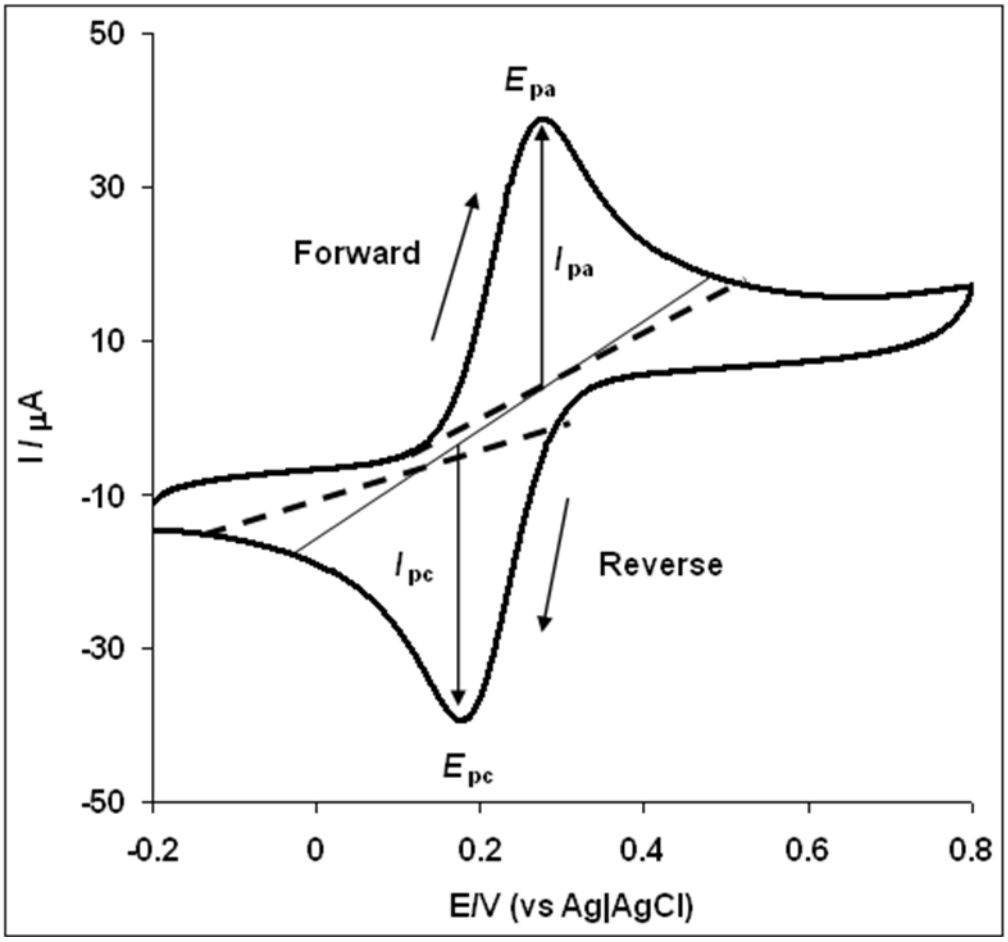

Figure 1.3: Typical cyclic voltammogram for a reversible redox process.

Simple diagnostic tests for electrochemical reversibility are listed in Table 1.1 [10]. A redox couple fulfilling all of the criteria given in Table 1.1 will probably be reversible. The couple is almost certainly not reversible if one or more of these criteria are not fulfilled. The amount of the oxidized species at

the electrode surface become reduced by the reduction process and replaced by the reduced species, which diffuses away into the solution. If the potential sweep process is reversed from the positive side, the reverse effect is observed. As the potential sweeps reverses back towards the redox potential, then the reduced species will start to be re-oxidized.

Table 1.1: Diagnostic tests for the electrochemical reversibility of a redox couple, carried out by using cyclic voltammetry.

1. $I_{pc} = I_{pa}$
2. The peak potentials, E_{pa} and E_{pc}, are independent of the scan rate.
3. E^0 is positioned midway between E_{pc} and E_{pa}, so $E^0 = (E_{pa} + E_{pc})/2$
4. I_p is proportional to $\nu^{1/2}$
5. The separation between E_{pc} and E_{pa} is 59 mV/n for an *n*-electron couple

Note: P_a is the anodic peak, P_c is the cathodic peak.

In Figure 1.3, it is assumed that only the oxidized form (analyte or electrolyte) is initially present, therefore a potential scan in the negative direction is chosen for the first half-cycle, starting from a point where no reduction occurs. As the applied potential approaches E^o, the standard potential, for a redox process, a cathodic current begins to increase until a peak reaches maximum. The potential at which the peak current occurs is known as the peak potential, E_p. At this potential, the redox species has

been depleted at the electrode surface and the current is diffusion limited. After potential region in which the reduction process takes place, the direction of the potential scan is reversed. During this scan, the molecules generated in the forward half-cycle and accumulated near the surface, are re-oxidized back, resulting in the anodic peak. The magnitude of the Faradaic current, called the anodic peak current, I_{pa}, or cathodic peak current, I_{pc}, is indicative of rate of electron transfer between the electrode and the redox species. The electrical signal is proportional to the concentration of the analyte [19].

For a reversible process, the Nernst equation is obeyed in which the electron transfer is fast, allowing the assumption that the concentration of both the oxidized, O and reduced, R species are in a state of equilibrium, Equation 1.1.

$$O + ne^- \leftrightarrows R \qquad \text{.....(1.1)}$$

In the case where electroactive species are stable, the magnitude of the reverse-to-forward peak current ratio is unity for a simple reversible couple. The peak-to-peak separation (ΔE_p) should be independent of the scan rate, ν but in practice it slightly increases with ν, this is due to the solution resistance, R_s, between the reference and working electrode [10, 17, 19]. Randles-Sevčik Equation 1.2 [13-18, 21,23] gives the peak current, I_p of a reversible process as:

$$I_p = (2.69\ x\ 10^5)\, n^{3/2} A D^{1/2} C \nu^{1/2} \qquad \text{.....(1.2)}$$

where n is the number of electrons, A the area of the electrode in cm^2, C the concentration in $mol.cm^{-3}$, D the diffusion coefficient in cm^2s^{-1} and ν the potential scan rate in Vs^{-1}. The current I_p, is directly proportional to concentration of the analyte [10, 15, 21] and increases with the square root of the scan rate. Using Equation 1.2, a linear plot of I_p vs. $\nu^{1/2}$ is obtained. The dependence of current on the scan rate is indicative of electrode reaction controlled by diffusion [10, 21, 17, 24-27].

The half-wave potential for a reversible process $E_{1/2}$ is given in Equation 1.3:

$$E_{1/2} = E^{o'} = E^o + \frac{RT}{2nF} \ln \frac{[O]}{[R]} \qquad \text{.....(1.3)}$$

where R is the gas constant, T the temperature in Kelvin, F the Faraday's constant and [**O**] is the concentration of oxidised species, [**R**] is the concentration of reduced species in mol l^{-1}. The formal redox potential, $E^{o'}$ can be calculated from Equation 1.4:

$$E_{1/2}\ or\ E^{o'} = \frac{E_{pa} + E_{pc}}{2} \qquad \text{.....(1.4)}$$

where E_{pa} is the anodic peak potential and E_{pc} is the cathodic peak potential.

1.3.1.2 Irreversible process

The characteristic of the cyclic voltammograms of an irreversible process is the absence of the reverse peak due to slow electron exchange or slow chemical reaction at the electrode surface [28]. This does not imply an irreversible electron transfer but could be due to a fast accompanying chemical reaction. In most cases, only forward peak for oxidation or reverse reduction peak is observed (Figure 1.4). There is usually lack of equilibrium between the oxidized and reduced species due to the insufficient electron transfer rate, thus the Nernst equation is not applicable. Because of the dynamic nature of the volatage-sweep voltammetry, current generated for an irreversible process is completely different from the reversible one and it is given as:

$$I_p = 2.99 \ x \ 10^5 n(\alpha n_a)^{1/2} A D^{1/2} C^b \nu^{1/2} \quad \text{at } 25^0\text{C} \qquad \text{.....(1.5)}$$

Where α is the rate of electron transfer and n_a is the number of electrons involved in the charge transfer step, and other terms already defined above. The electron transfer coefficient α has a value between 0.3 and 0.7. Irreversible process is also characterized by a shift of the peak potential with the scan rate, therefore, ΔE can be calculated from Equation 1.6:

$$\Delta E = E^o - \frac{RT}{\alpha n_a F}\left[0.78 - \ln\frac{k^o}{D^{1/2}} + \ln\left(\frac{\alpha n_a F \nu}{RT}\right)^{1/2}\right] \qquad \text{.....(1.6)}$$

where α, n_a, R, T, F and ν are already defined, k^o is the heterogeneous electron transfer coefficient in cm s^{-1}.

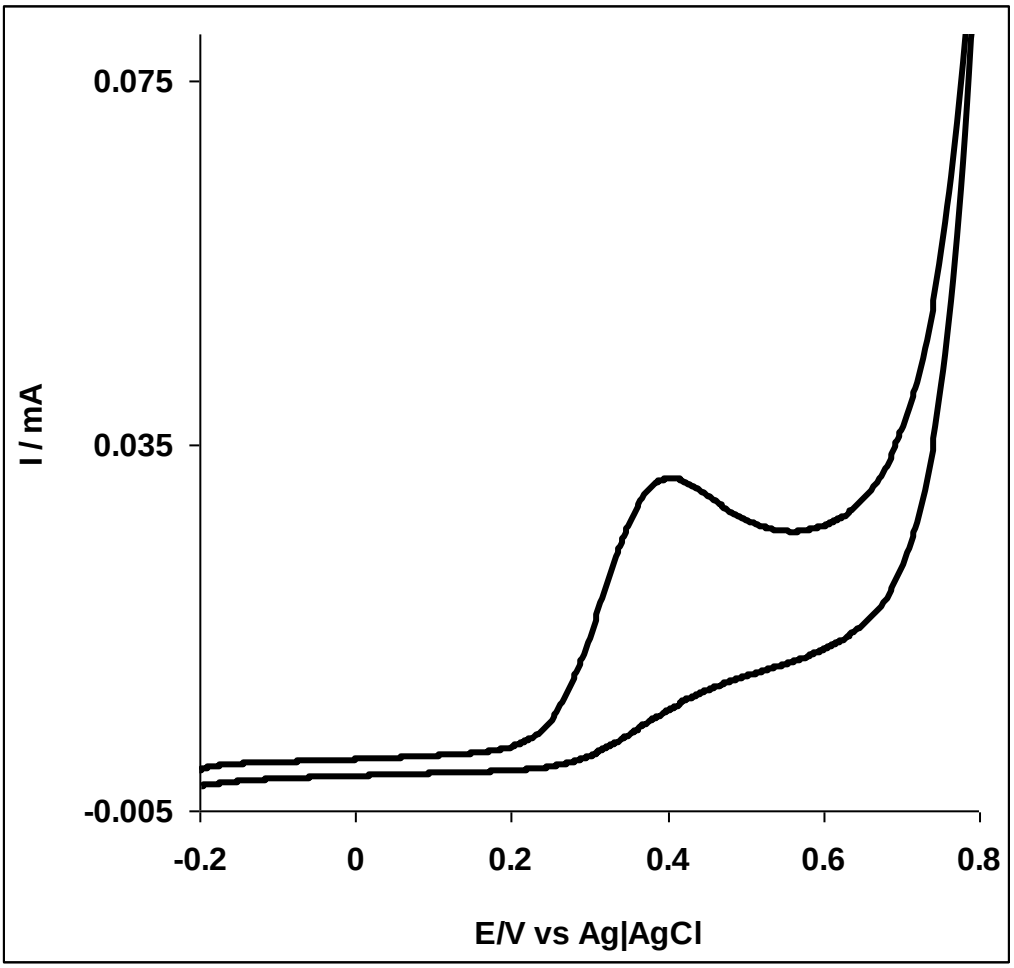

Figure 1.4: Typical cyclic voltammogram for an irreversible process.

1.3.1.3 Quasi-reversible process

The term quasi-reversible is commonly employed to denote a voltammetric wave which is controlled simultaneously by diffusion and by an electrochemical step whose backward rate is not negligible with respect to the forward one. The kinetics of the oxidation and reduction reactions has to

be considered simultaneously. The mathematical solution is therefore, more complex but there are numerical theoretical solutions.

In quasi-reversible process, the extent of irreversibility increases with increase in sweep rate, while at the same time there is a decrease in the peak current relative to the reversible case and an increasing separation between anodic and cathodic peaks (Figure 1.3). Thus, the voltammograms of a quasi-reversible process exhibit a large peak-to-peak separation compared to reversible processes. The peak current increase with $\nu^{1/2}$ but is not linear and ΔE is greater than 0.0059/n V. Current is controlled by both the mass transport and charge transfer kinetics unlike in reversible process where current control is purely by mass transport [28, 29].

In practice, quasi-reversibility is a relative term which depends on the time scale of the electrochemical technique employed [30]. More generally, the term quasi-reversibility can be extended so as to include those cases in which slight deviations from the reversible behaviour are due to a chemical step in non-equilibrium or to diffusion-controlled adsorption of reactants and/or products. A kinetic study of the overall electrode process is favoured by a decrease in the electrolysis time, which may sometimes cause a transition from quasi-reversible to totally irreversible behaviour. On the other hand, an increase in the electrolysis time causing a gradual transition from quasi-reversible to reversible behaviour may be useful in the

determination of the equilibrium constant of any homogeneous chemical reaction, such as complexation, coupled with the electron transfer process.

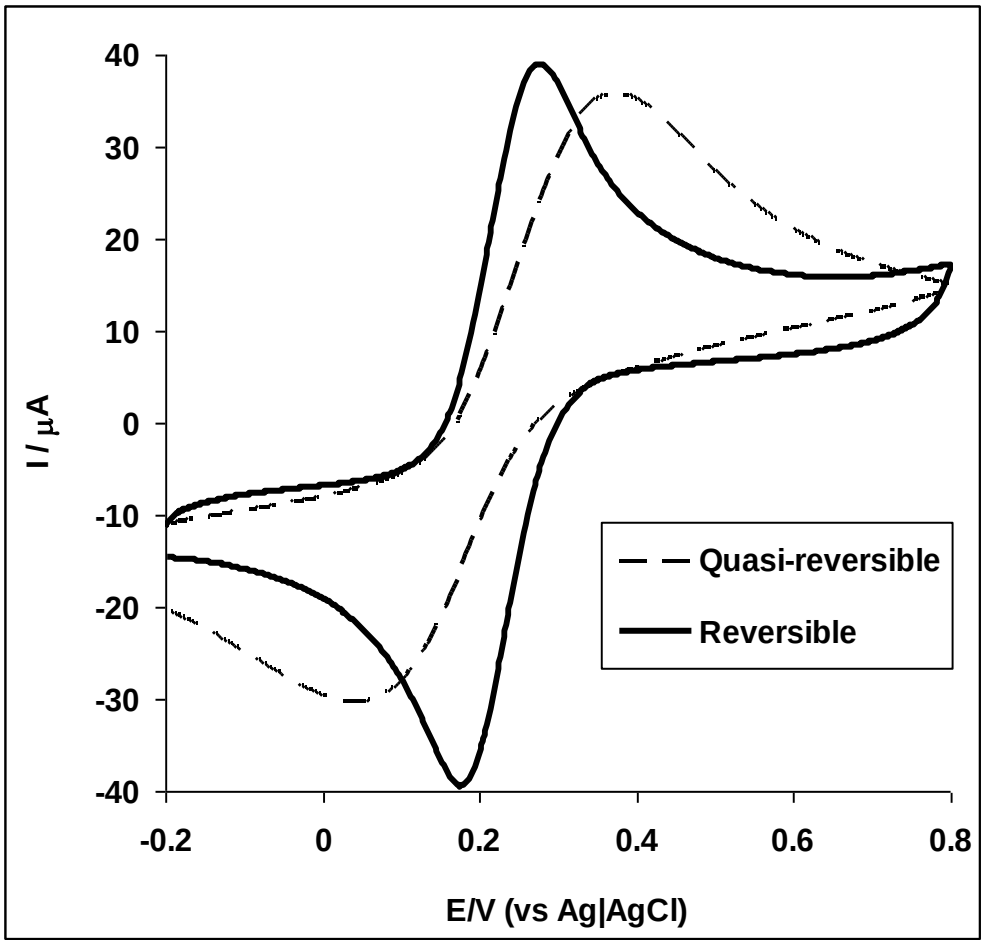

Figure 1.5: The effect of increasing irreversibility on the shape of cyclic voltammograms.

1.3.2 Chronoamperometry

In chronoamperometric technique, current is measured as a function of time. During the chronoamperometry experiment, the potential is stepped from an initial potential E_1 (at which no electromodification occurs, or no current

flows or oxidation/reduction of the electroactive specie occurs) to a second potential E_2 at which the electrode reaction is complete, i.e. the current is limiting (Figure 1.6a). The current flows at any time after the application of the potential step. A high charging current was generated which decay exponentially with time. Figure 1.6b shows a trace of current against time in response to the potential step. The trace shows a rapid rise in current, with this rise requiring perhaps as long as a few thousands of a second (i.e. milliseconds). The time between the potential step and the maximum is known as the rise time. The current trails off smoothly after the rise time until, eventually, it reaches zero. Such plots are often termed transients to emphasize their pronounced time dependence. The current that results from the semi infinite linear diffusion at the electrode is given by the Cottrell equation, (Equation 1.7) [10-15, 17-22].

$$I = \frac{nFAD^{1/2}C}{\pi^{1/2}t^{1/2}} \qquad \text{.....(1.7)}$$

where n, F, A, D, C, and t are number of electrons, Faraday constant, the surface area of the electrode, the diffusion coefficient, the concentration of analyte and time, respectively. This relationship holds not only for reversible cyclic voltammetry process, but for any electrochemical process that involves infinite linear diffusion and it is the basis for a variety of electrochemical method such as polarography, voltammetry, and controlled-

potential electrolysis. From Equations 1.6 and 1.7, the number of electrons transferred during the reversible process can be obtained.

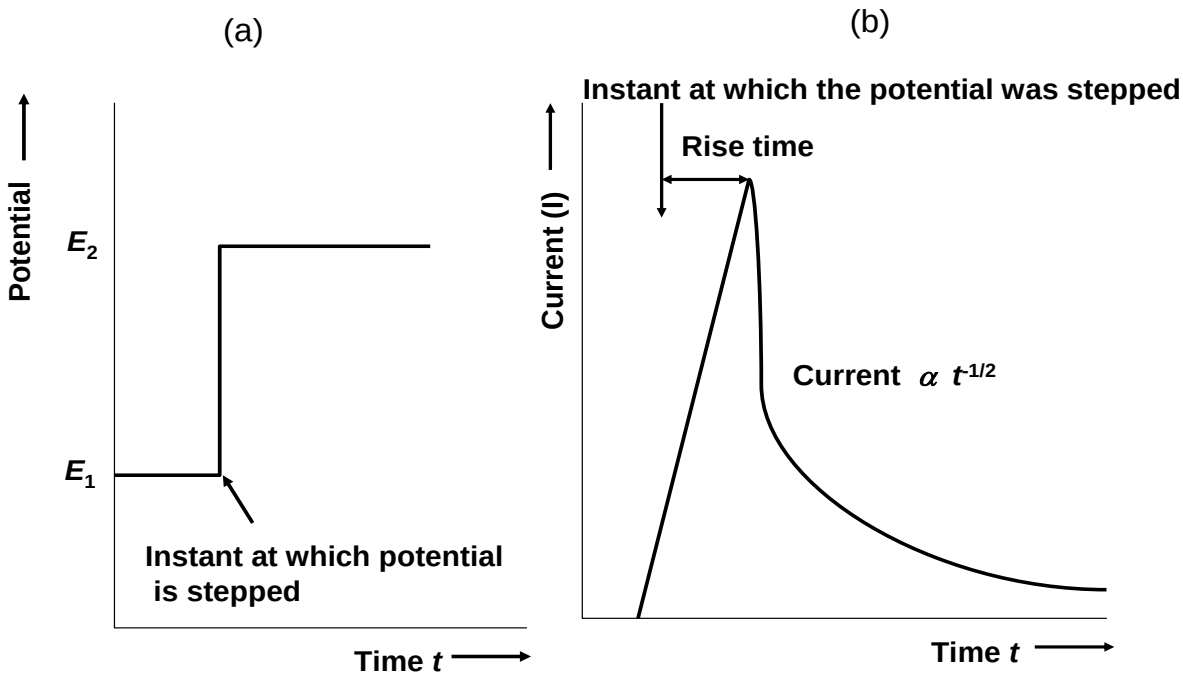

Figure 1.6: (a) Plot of potential against time (b) Plot of current against time [15].

1.3.3 Linear Sweep voltammetry (LSV)

LSV is the simplest voltammetric technique that uses a waveform. It can be used to measure the current at a working electrode while the potential between the working electrode and a reference electrode is swept linearly in time. LSV also measures the current signal that is registered as a peak or trough formed at the potential at which the species begins to be oxidized or reduced. The potential range is scanned starting at the initial potential and ending at the final potential. CV is an extension of LSV in that the direction

of the potential scan is reversed at the end of the first scan, and the potential range is scanned again in the reverse direction. This method includes rotating disk voltammetry [31].

1.3.4 Rotating disc electrode

This is an electrochemical technique in which the electrode moves with respect to the solution. A rotating disk electrode (RDE) is usually performed using LSV. It is a hydrodynamic working electrode that has advantage in a steady state being attained very quickly, and measurements can be made with high precision [15, 21]. The convective nature of the electrode results in very short response times. It also provides an efficient and reproducible mass transport, and hence the analytical measurement can be made with high sensitivity and precision. This technique is usually employed in electrochemical studies when investigating redox related mechanistic reactions. The electrode itself is a flat, circular disc of metal, graphite or another conductor, and has a radius of r; its area A, therefore, is estimated from πr^2. The disc is embedded centrally into one flat end of a cylinder of an insulatory material such as Teflon or epoxy resin (Figure 1.7). Behind the face of the electrode is an electrical connection which is made to the electrode through a brush contact leading ultimately to the potentiostat which controls the potential of the electrode. The rod is attached to a motor directly by a chuck or by a flexible rotating shaft or pulley arrangement and

is rotated at a certain frequency/(revolutions per second), and in so doing provides an influx of the analyte species at the electrode surface.

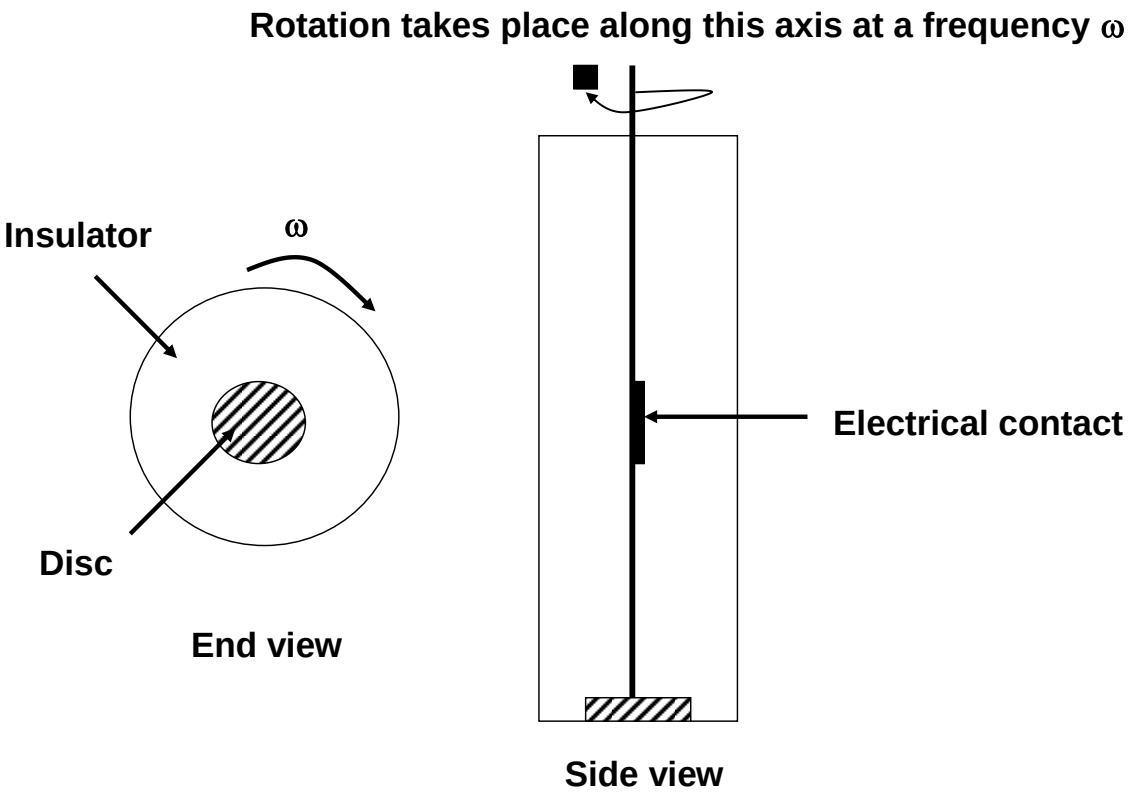

Figure 1.7: Schematic representation of a rotated disc electrode (RDE) of radius *r* [15].

The disk's rotation is often described in terms of angular velocity, ω (s^{-1}), where $\omega = 2\pi rf$. The limiting current (for a reversible system) is thus proportional to the square root of the angular velocity by the *Levich equation* (Equation 1.8) and Koutecky-Levich equation (Equation 1.9): [21, 32]

$$i_{l,c} = 0.62nFAD_0^{2/3}\omega^{1/2}\nu^{-1/6}C_0 \quad ..(1.8)$$

$$\frac{1}{I} = \frac{1}{I_k} + \frac{1}{I_{\lim}} = \frac{1}{I_k} + \frac{1}{0.62nFAD^{\frac{2}{3}}\omega^{\frac{1}{2}}\gamma^{\frac{1}{6}}} \quad ..(1.9)$$

where $i_{l,c}$ is the diffusion-limited currents, n is the number of electrons transferred, I is the measured current, I_k and $I_{\lim}$ are the kinetic and diffusion-limited currents, respectively, F is the Faraday constant, A is the geometric electrode area, D is the diffusion coefficient ω is the rotation rate in rad.s^{-1}, and γ is the kinematic viscosity of the solution.

1.4 Electrochemical Impedance Spectroscopy (EIS)

Electrochemical impedance spectroscopy is a powerful tool for examining processes occurring at electrode surfaces. A small amplitude ac (sinusoidal) excitation signal (potential or current), covering a wide range of frequencies, is applied to the system under investigation and the response (current or voltage or another signal of interest) is measured. This technique measures the impedance of a system over a range of frequencies, and therefore the frequency response of the system is revealed. Often, data obtained by EIS is expressed graphically in a Bode plot or a Nyquist plot [33].

EIS is a relatively new method for characterizing many of the electrical properties of materials and their interfaces with electronically conducting electrodes. It is widely used in different research areas. The technique has become a technique of significant importance and has been moved out of

academic laboratory to address the operation of difficult measuring techniques in the areas of industrial quality control of paints, emulsions, electroplating, thin-film technology, materials fabrication, mechanical performance of engines, corrosion, and so on. The technique is used in probing the dynamics of bound or mobile charge in ionic, semiconducting, mixed electronic–ionic and even insulators (dielectrics) [33, 34]; the properties of porous electrodes and passive surfaces [34], redox and structural features of a surface-confined species [35]; and in rapid acquisition of data such as ohmic resistance, capacitance, inductance, film conductivity, as well as charge or electron transfer at the electrode-film interface, or characterize interfacial properties in the absence of redox reactions.

1.4.1 Principle of impedance spectroscopy

There are three different types of electrical stimuli which are used in Impedance Spectroscopy (IS) [33-36]. First, in transient measurements a step function of voltage [$V(t) = V_0$ for $t > 0$, $V(t) = 0$ for $t < 0$] may be applied at $t = 0$ to the system and the resulting time-varying current $i(t)$ measured. The ratio $V_0 / i(t)$, often called the impedance or the time varying resistance, measures the impedance resulting from the step function voltage perturbation at the electrochemical interface. This quantity, although easily defined, is not the usual impedance referred to in IS. Rather, such time-varying results are generally Fourier or Laplace-transformed into the

frequency domain, yielding frequency-dependent impedance. The advantages of this approach are that it is experimentally easily accomplished and that the independent variable, voltage, controls the rate of the electrochemical reaction at the interface. Disadvantages include the need to perform integral transformation of the results and the fact that the signal-to-noise ratio differs between different frequencies, so the impedance may not be well determined over the desired frequency range. A second technique in IS is to apply a signal V(t) composed of random (white) noise to the interface and measure the resulting current. Again, one generally Fourier-transforms the results to pass into the frequency domain and obtain an impedance. This approach offers the advantage of fast data collection because only one signal is applied to the interface for a short time. The technique has the disadvantages of requiring the noise and then the need to carry out a Fourier analysis. Often a microcomputer is used for both the generation of noise and the subsequent analysis. Using a sum of well-defined sine waves as excitation instead of white noise offers the advantage of a better signal-to-noise ratio for each desired frequency and the ability to analyze the linearity of system response. The third approach, which is the most common and standard one, is to measure impedance by applying a single-frequency voltage or current to the interface and measuring the phase shift and amplitude, or real and imaginary parts, of the resulting current at that frequency using either analog circuit or fast Fourier transform (FFT)

analysis of the response [33-36]. Commercial instruments (like the one used in this study) are available which measure the impedance as a function of frequency automatically in the frequency ranges of about 1 mHz to 1 MHz and are easily interfaced to laboratory microcomputers. The advantages of this approach are the availability of these instruments and the ease of their use, as well as the fact that the experimentalist can achieve a better signal-to-noise ratio in the frequency range of most interest. In general, for a sinusoidal applied potential V generating a sinusoidal current I at a given time t, the impedance of the system is given in the relationship $Z = V_{(t)}/I_{(t)}$. From the relationship, $V(t)$ is the sinusoidal applied voltage at time t. $V(t) = V_o \sin \omega t$ where V_0 is the maximum potential amplitude, ω is the radial frequency (in rad.s^{-1}) which is related to frequency f (Hz) as $\omega = 2\pi f$. The current response $I(t)$ is also sinusoidal at the same frequency but with a shift in phase and therefore represented as $I(t) = I_o \sin(\omega t + \theta)$ where I_o is the maximum current applied and θ is the phase shift by which the voltage lags the current (Figure 1.8a) [33, 36] and it is zero for pure resistive behaviour. These properties of magnitude and direction makes impedance a vector quantity where $Z = V/I$ represents the magnitude and θ represents the direction (Figure 1.8b).

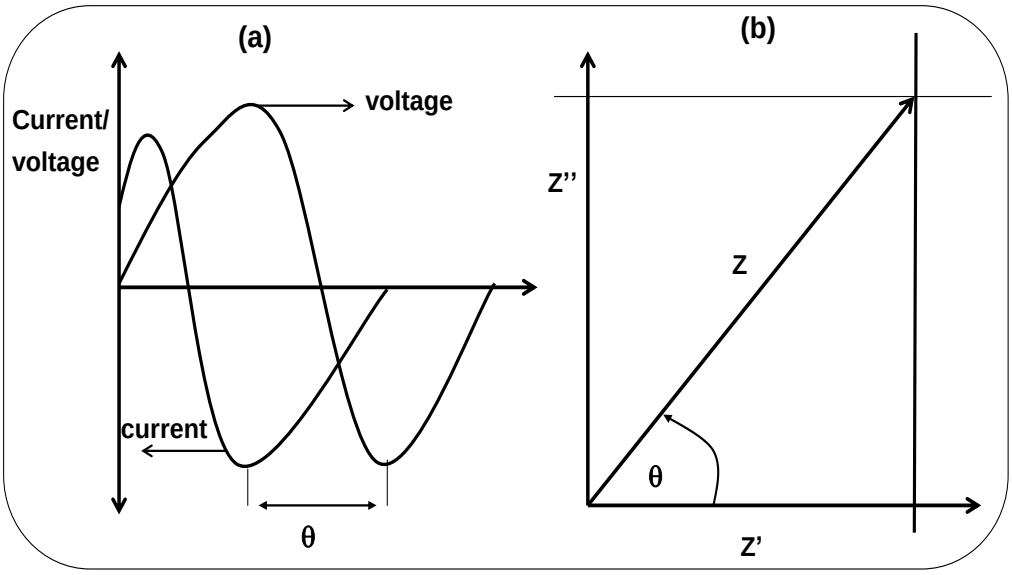

Figure 1.8: (a) Applied sinusoidal voltage and resulting sinusoidal current response. (b) Vector representation of real Z′ and imaginary Z′′ of impedance Z $= Z' + jZ'' = Z_{real} + jZ_{imaginary}$ [33, 36].

1.4.2 Application and data presentation

The Nyquist plot is the curve obtained from the impedance fitting and it is the plots of the imaginary Z′′ versus the real Z′ components of the impedance ($-Z_{imaginary}$ versus Z_{real}) (Figure 1.9). The plot consists of two separate processes namely semicircle and a straight line. The semicircle at higher frequencies corresponds to the charge-transfer-controlled process and its diameter is equal to the electron transfer resistance (R_{ct}), which controls the electron transfer kinetics of the redox probe at the electrode interface. The straight line at lower frequencies corresponds to the diffusion

process. The R_{ct} value is influenced by the film thickness and the nature of the films on the electrodes. The R_{ct} is the domain of kinetic control and it is proportionally related to the diameter of the semi-circle of the Nyquist plot.

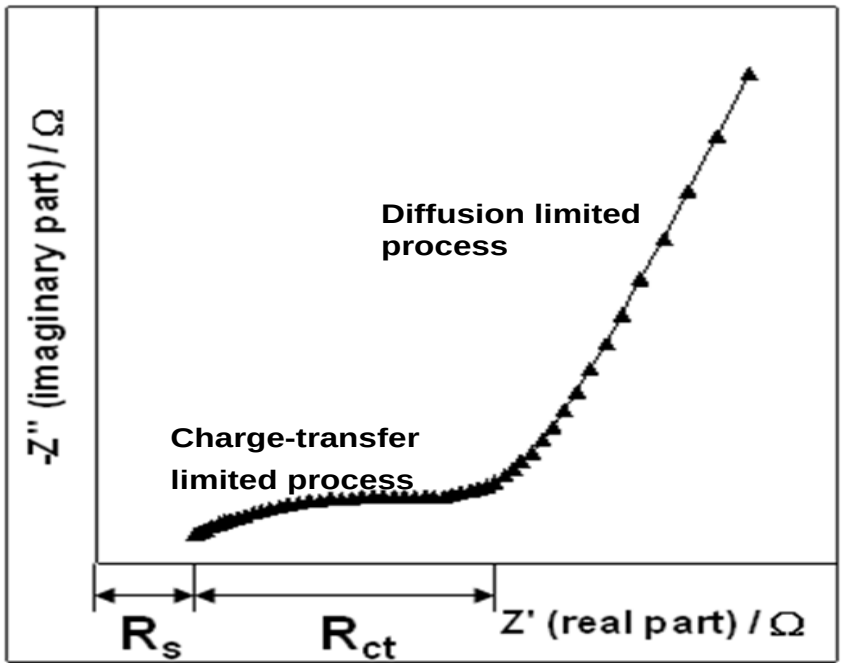

Figure 1.9: Typical Nyquist plot showing the charge transfer process at the electrode/electrolyte interface of a modified electrode.

The impedance data were fitted to an equivalent circuit using the FRA software package for complex non-linear least squares calculations based on the EQUIVCRT programme. Electrical elements such as resistors, capacitors and inductors in the circuit measure resistance, capacitance and inductance respectively during the electrochemical process [33]. Ideal Randles equivalent circuit (Figure 1.10a) incorporates various contributions to the interfacial barrier behaviour, which include the resistance of electrolyte (R_s),

the charge transfer resistance (R_{ct}), double-layer capacitance (C_{dl}) and Warburg impedance (Z_w). Modified Randles circuit uses CPE (Figure 1.10b) in place of C_{dl} especially in real life and practical application of EIS since the electrochemical process at the electrode/electrolyte interface are characterised by many factors such as roughness or polycrystallinity of the electrode, distribution of the relaxation times due to heterogeneities existing at the electrode/electrolyte interface, porosity and dynamic disorder associated with diffusion [33]. Therefore, the impedance of CPE has been defined as $Z_{CPE} = \frac{1}{[Q(j\omega)^n]}$

where Q is the frequency-independent constant relating to the surface electroactive properties, ω is the radial frequency, n arises from the slope of log Z vs log f (and has values $-1 \leq n \leq 1$). 0, 1 and -1 values of n indicate *CPE* behaving as a resistor, pure capacitor and an inductor respectively; while n = 0.5 corresponds to Warburg impedance (Z_w) which is associated with the domain of mass transport control arising from the diffusion of ions to and from the electrode|solution interface.

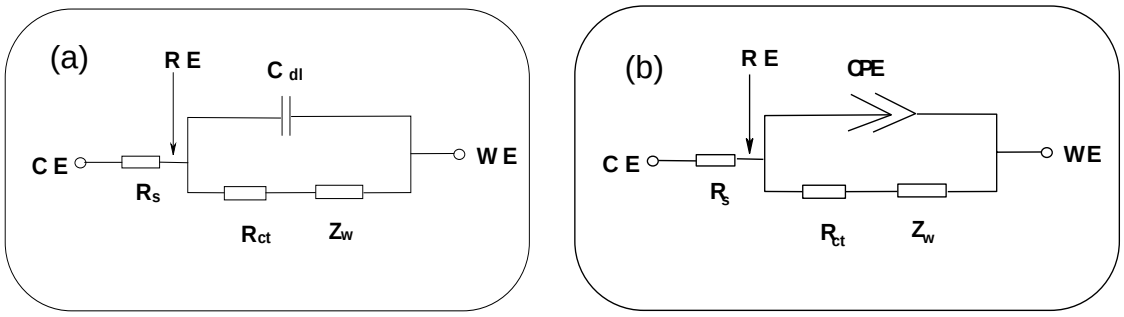

Figure 1.10: (a) Typical Randles equivalent circuit (for an ideal electrochemical system). (b) Modified Randles equivalent circuit (for real a practical situation).

In this study a half cell electrode setup was used. The resistance was recorded over the frequency range 10 kHz to 0.1 Hz. The obtained results were plotted. Two methods for measuring the resistance were used, namely Nyquist plot and Bode plot.

The Nyquist plots were explained in terms of equivalent circuits while Bode plot showed the absolute value of impedance log Z (o) and its phase angle (Θ) as a function of frequency. The results obtained from both Nyquist and Bode plots are interpreted as follows: From the Nyquist plot, the smaller the charge transfer resistance (Rct) value the faster the electron transfer and hence the higher the catalytic activity. From the Bode plot, the lower the phase angle, the lower the capacitive nature of the electrode and hence the faster the electron transfer.

Therefore in fuel cells, EIS was used to establish the kinetics of adsorption controlled reactions and electron transfer between the electrode surface and analyte/electrolyte. It was also used to reveal differences in FC molecule electrooxidation mechanisms on Pt-based nanoparticulate catalytic surfaces.

In this study, EIS has been used to monitor changes in the electron transport behaviour during different electrode modification procedure, and to probe the complex electrode reaction mechanism such as adsorption and carbon monoxide (CO) poisoning effect during the electrocatalytic oxidation of the fuel cell molecules, and during the reduction of molecular oxygen respectively.

Many researchers using EIS techniques have also found it informative when the impedance data are presented in Bode Plot (Figure 1.11). The plot provides information about the capacitive behaviour of an electrode at the frequency where the impedance was measured. Bode plot includes the plot of phase angle (θ) versus the logarithm of the frequency (log f), or the logarithm of impedance magnitude (log Z) versus the logarithm of the frequency (log f). From the formal plot, the peak height represents the capacitive nature of the electrode and a phase angle of 90^0 represents a pure and true capacitive behaviour of an electrode, while a phase angle less than 90^0 indicates pseudocapacitive properties of an electrode. On the other

hand, plot of log Z versus log f gives an idea of the relaxation process of the electrode|solution interface.

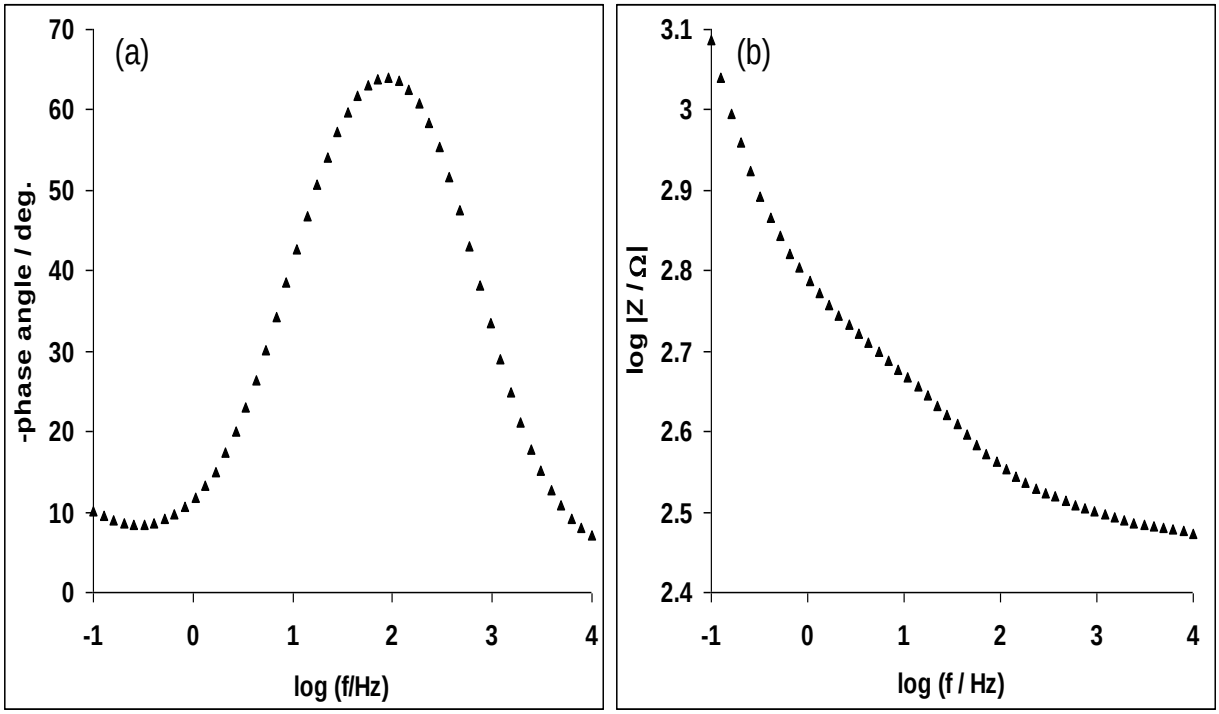

Figure 1.11: Typical Bode plots (a) the phase angle versus logarithm of frequency and (b) logarithm of impedance versus logarithm of frequency.

1.5 Introduction to Phthalocyanines (Pcs)

Phthalocyanines are an important class of organic materials with a very stable electronic configuration which makes them an important class of functional materials [37, 38]. Metal-free phthalocyanines and their metal complexes have been intensively investigated since the early-1930s. Phthalocyanine chemistry is undergoing a renaissance because phthalocyanines and many of their derivatives exhibit singular and unconventional physical properties which are interesting for applications in

materials science [39]. Pcs, especially due to the readily soluble peripherally substituted derivatives, posses a wide range of chemical and physical properties that make them interesting as building blocks for a number of applications as well as for obtaining new materials [40]. One of the important applications emerging in recent years includes the use of Pcs as chemically sensitive films for the detection of halogens such as chlorine (Cl_2) and nitrogen dioxide (NO_2) as well as organic vapors [41, 42]. Pcs have good sensitivity to toxic gases like NO_2. The properties of Pcs such as good chemical and thermal stability make them good candidates in gas sensing system [43]. Pcs exhibit excellent photochemical properties [44]. They can be used in jet printing inks [45], catalysts [46], gas sensors [47] and photonic devices [48, 49].

Recently, they are used as photosensitizers in the treatment of cancer [50, 51] and intimal hyperplasia [52] for photodynamic therapy (PDT). In photodynamic therapy (PDT), singlet oxygen is generated with appropriate kinds of photosensitizer and oxygen via several energy transfer steps [53]. It has been found that phthalocyanines are better photosensitizers for PDT than others, such as porphyrins, naphthalocyanines, etc. Some phthalocyanines and related macrocyclic complexes catalyze the electrooxidation of formic acid [54] CO [55]. Pcs are also promising as

electrode materials not only as catalysts but also as reactive species in lithium cells [56, 57].

1.6 Introduction to Metallophthalocyanines (MPcs)

MPcs are highly conjugated macrocyclic compounds, which have been extensively studied as catalysts for a variety of applications in organic synthesis, green chemistry and environmental treatment of pollutants [58-62]. A few examples of the hybrid materials between CNTs and MPcs have been described [63, 64] and those were used as photoelectric materials for solar energy conversation [65] or as electrode materials for electrocatalysis and electroanalysis [66-70]. The studies showed that cobalt tetraaminophthalocyanine immobilized on MWCNTs (CoTAPc-MWCNTs) exhibit an enhanced catalytic performance. In such systems, MWCNTs not only act as catalyst support [71-78], but also directly participate in catalytic process of electron transfer [79].

MPc was first reported more than four decades ago for ORR in a pioneering study by Jasinski [80, 81] while searching for non-noble catalysts for the oxygen cathode in fuel cells. He showed that Co phthalocyanine is active for the reduction of O_2. The feasibility of using phthalocyanines in practical fuel cells has been shown recently [82]. MPcs constitute an interesting type of catalysts since they present several advantages over noble metals. In particular, they provide very interesting models for theoretical and

experimental studies since their catalytic action can be described in terms of definite parameters such as chemical structure, chemical and physical properties.

MPcs complexes have attracted a great deal of research interest for many years because of their intense coloration and diverse redox chemistry associated with both 18π-electron system of the phthalocyanine (Pc) ring and central atom and also due to their chemical and physical properties [83-89]. They belong to a class of transition metal complexes known as N4-macrocyclic complexes and they possess a N4 inner structure that is common in naturally occurring molecules such as chlorophyll, heme groups in hemoglobin, cytochrome C, vitamin B12, etc. Due to the rich and varied chemistry in the transition metal ruthenium [90, 91] numerous ruthenium phthalocyanine complexes (Figure 1.12) have been reported.

Due to their macrocyclic nature including extended π systems, Pcs are capable of undergoing fast redox processes, with minimal reorganizational energies and can act as mediators in electron transfer processes involving a great variety of molecules [92-94]. In particular, MPc complexes have traditionally been used as dyes and pigments, and more recently as photoconducting agents in photocopiers because of their easy in synthesis, high stability, and the presence of intense π transitions in the visible region [95]. In recent decades, there has been renewed interest in the use of

these compounds in technological applications fields including semiconductor devices, photovoltaic, solar cells and non-linear optics [96]. Exploiting their interesting properties, MPc thin films have been scrutinized for possible applications as sensitive, selective and stable active layers of transducers in solid state opto-chemical gas sensors [97, 98].

MPcs can be immobilized on various supports such as zeolites [99] and zeolites embedded in polydimethylsiloxane membranes [100, 101] activated carbon black [102, 103]. MPcs are known to exhibit good electrocatalytic activities towards the oxidation and reduction of a wide range of chemical substances [104-106]; among which are oxygen, sulfur-containing compounds, some neurotransmitters and nitrite, to mention a few. Almost all of the catalytic reactions with MPcs occur through electron exchange, following the coordination between central metal ions and reactants.

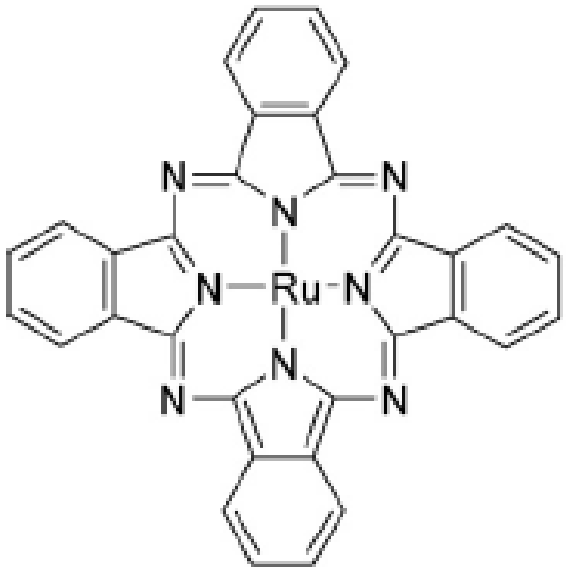

Figure 1.12: The structure of ruthenium phthalocyanine (RuPc).

The MPc complexes have also attracted immense attention in electrocatalysis and for fuel cells applications [107-111]. Since methanol and formic acid oxidation on platinum or platinum alloy electrodes have been characterized by poisoning effect due to adsorbed intermediates, an approach has been defined to include macrocycles such as phthalocyanine (containing non-noble transition elements) with standard platinum as anodic catalysts for enhancing electro-catalytic activity. Many reports on the use of platinum in combination with macrocycles for methanol oxidation have been reported [112-115]. In fact, metal complexes including metal porphyrins and phthalocyanine have been studied as electrocatalysts for oxygen reduction reaction (ORR) in fuel cells for more than 30 years [116]. The platinum catalyst metal complexes [117, 118] were also tested as anodic

electrocatalysts, which demonstrate a promising electrocatalytic activity towards methanol oxidation.

MPc complexes integrated or supported on carbon nanotubes (CNTs) improve electrocatalytic performance of electrodes [66]. Also, electrodes modified with acid treated MWCNTs (fMWCNT) electro-decorated with platinum-ruthenium (Pt/Ru) or ruthenium octa-carboxy Pt (II) phthalocyanine (RuOcPcPt) nanoparticles exhibited an ability to enhance the electrooxidation response of fuel cell molecules [119, 120], thus making them more promising anodic materials for use in fuel cells. However, it is noteworthy that one of the well known properties of CNTs is their increased surface areas which make them susceptible to adsorption of solution molecules and reaction intermediates. Thus, despite the use of Ru to enhance the tolerance of CO, adsorption of reaction intermediates onto the Pt/Ru catalyst (that poison and adversely affect the reaction kinetics and reduce the life time of the catalyst) still prevails to certain extent, depending on the employed liquid fuel. From literature survey, it is easily seen that despite the huge interests on the use of fuel cell molecules for the development of fuel cells, the extent to which the reaction intermediates affect the heterogeneous electro-oxidation kinetics of these fuel cell molecules is still unclear or poorly understood. For example, the two available reports [121, 122] claim diffusion-controlled reaction, whereas

other works on Pt based electrodes for the oxidation of EG [123, 124] and other alcohols [125] claim adsorption-controlled. Indeed, many reports claim that such reaction is diffusion-controlled or adsorption-controlled based mainly on voltammetric evolutions notably the response of peak currents with varying scan rates. It is without doubt therefore that for a successful application of this type of platform for making direct ethylene glycol fuel cell (DEGFC) stack requires an understanding of factors that impact on the reaction kinetics. The current study interrogated the impact of such factors as scan rate, reaction potential and concentration on the kinetics of FC molecules electrooxidation.

In this study the electrocatalytic oxidation of methanol and formic acid using a novel ruthenium tetrakis (diaquaplatinum) octacarboxy-phthalocyanine (RuOcPcPt) as a catalyst supported on multi-walled carbon nanotubes (MWCNTs) is reported. The results obtained indicate that the RuOcPcPt/MWCNTs electrode platform can enhance the electrocatalytic performance of methanol whereas formic acid oxidation was favoured on the complex even in the absence of the MWCNTs. For some clearer insights into the adsorptive behaviour, the electrochemical impedimetric behaviour was studied. This is the first time this type of electrocatalytic investigation has been undertaken for these model fuel cell molecules at the BPPGE modified electrodes with a consistent methodology in the same laboratory.

1.7 Novelty of Ruthenium (II) tetrakis (diaquaplatinum) octacarboxyphthalocyanines (RuOcPcPt)

The use of ruthenium phthalocyanine (RuPc) complexes in ORR and in electrooxidation of alcohols has rarely been studied. RuOcPcPt/MWCNTs electrode platform enhances the electrocatalytic performance of the ORR in alkaline medium (in terms of the onset potential and the catalytic current density of the oxygen reduction). From the slope of the Koutecky-Levich plot, the number of electrons (*n*) transferred per oxygen molecule was calculated as 3.78±0.30, indicating that ORR at the MWCNT-RuOcPcPt platform proceeds mainly via a single-step 4-electron transfer process which is the desired one for fuel cells. The kinetic rate constant (*k*) was calculated as 3.57 x 10-2 cm s^{-1}. This value is in the same magnitude (1.96 x 10-2 – 5.87 x 10-2 cms^{-1} range) obtained using gold nanoclusters catalyst of different core sizes [11] and tungsten carbide nanocrystals [29], but slightly better than the one observed for anthraquinone [28]. The high value of the Tafel slope –221 mV obtained is characteristic of porous electrode with high internal surface area leading to high electrocatalytic activities. The preliminary results suggest that ORR at the MWCNT-RuOcPcPt involves 4-electrons with high kinetic rate constant compared to recent reports, thereby making this catalyst a promising candidate for cathodic reactions of fuel cells.

In electrooxidation reactions, formic acid oxidation was favored on the BPPG-RuOcPcPt electrode without CNTs support. The oxidation of fuel cell molecules is characterized by both diffusion (forward) and adsorption controlled (reverse) processes. When comparing these results with the previous study using electrodeposited Pt/Ru, MeOH gives better tolerance to CO poisoning while FA gives about the same J_{fa}/J_{ra}. The presence of phthalocyanine in the modified electrode used for MeOH has improved their tolerance to CO poisoning and therefore its application in the direct fuel cell oxidation is encouraged.

1.8 Modification of electrodes

The slow electron transfer behaviour at the bare electrode can be improved by surface modification with electron transfer mediators such as carbon nanotubes and redox active metal catalyst. Therefore, a chemically modified electrode is an electrode decorated with a mediator to facilitate the charge transfer between the redox active specie/molecule and the electrode. In most cases, the mediator or surface modifier reduces the over potential and enhances catalysis. The efficiency of the electrocatalytic process may also depend upon the actual distance between the bound redox site and the surface.

1.8.1 Carbon electrodes

Recent studies on carbon based electrode materials such as glassy carbon (GC) and the highly ordered pyrolytic graphite (HOPG) electrodes namely basal and edge-plane pyrolytic graphite electrodes (BPPGE and EPPGE) have attracted immense interest in the field of electrochemistry due to their several advantages such as low cost, chemical inertness and wide potential window in most electrolyte solutions over metal electrodes (e.g. nickel, gold, platinum, aluminium, silver, copper), and their potential to be used as supporting platforms for electroanalysis [126]. Among these carbon based electrodes, basal plane pyrolytic graphite electrode (BPPGE) and the edge plane pyrolytic graphite electrode (EPPGE) have been reported to have a better catalysis and reactivity due to edge plane sites/defects (Figure 1.13) which are responsible for the fast heterogeneous charge transfer [127]. BPPGE is said to possess properties intermediate between those of the glassy carbon electrode (GCE) and edge plane pyrolytic graphite electrode (EPPGE) [128]. BPPGE has rarely been used as platform for the immobilisation of Pt/Ru catalysts for electrooxidation of fuel cell molecules. However, the choice of BPPGE over EPPGE in this study is its ability to withstand rough treatment during electrode cleaning, and chemical stability in acidic medium during electrooxidation of the fuel cell molecules.

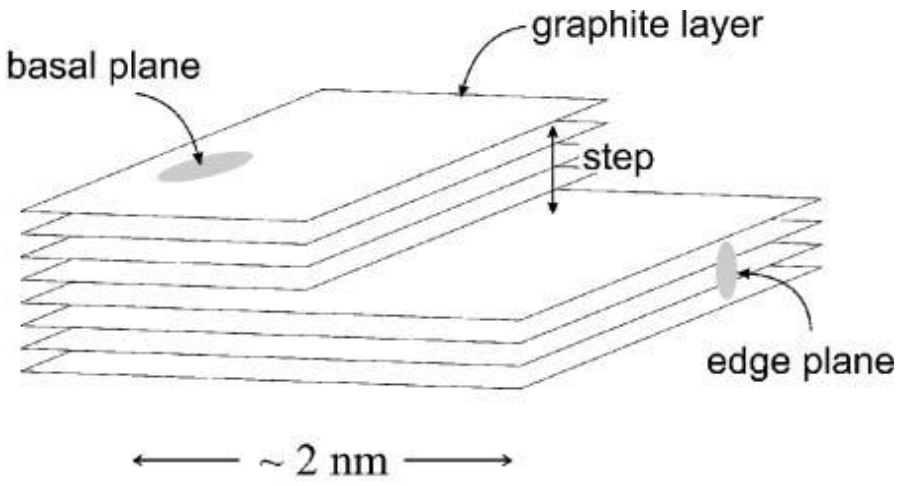

Figure 1.13: Pyrolytic graphite plate showing the basal and the edge plane sites [127, 129].

It is now widely recognized that materials structured on the nanoscale display remarkable properties that are not seen in the same material when in bulk form. Interest is focused on exploiting nanostructured materials for portable fuel cells and improved battery technologies, which are needed to power a new generation of mobile electronics devices. Nanomaterials promised to improve the performance and reduce the cost of the catalyst, membranes and electrodes used in polymer-electrolyte membrane fuel cells (PEMFC) and direct methanol fuel cells (DMFC). At the same time, nanoparticles made from alloys of Pt and other metals, notably ruthenium have been shown to improve tolerance to CO poisoning

1.8.2 Carbon nanotubes as electrode modifiers

Carbon nanotubes (CNTs), a new class of nanoscale carbon, have gained special interest in recent years due to their unique physical, electrical and mechanical properties. Because CNTs have excellent electrical conductivity and mechanical strength, they have been successfully used as catalyst support for fuel cell applications [130, 131].

The carbon nanotube material is considered to have several advantages over conventional support materials, which includes (i) having more defined crystalline structure with higher conductivity, (ii) containing little impurities, such as metals and sulfides, and thus eliminating potential poisoning effects to electrocatalysts, and (iii) possessing three dimensional structure thus favoring the flow of reactant and providing a large reaction zone when fabricated into electrodes. The carbon nanotubes are also chemically stable and resistant to thermal decomposition. Due to these distinctive characteristics, the carbon nanotube material is very suitable for use as a novel electrocatalyst support. With this in view, the objective of this study was to investigate the electrocatalytic oxidation of industrially important fuel cell molecules such as methanol, formic acid and ethylene glycol using metal nanoparticles modified multi-walled carbon nanotubes.

Carbon Nanotubes (CNTs) were discovered in the late 1950's [132] and the work on multi-walled carbon nanotubes (MWCNTs) was improved by the

report made by Iijima in 1991 [133]. The formation of single-walled carbon nanotubes (SWCNTs) was first reported by Iijima S et al. [134] and Bethune D.S. et al. [135]. CNTs are sp^2 hybridised carbons arranged in graphene sheets, which have been rolled up to form a hollow tube. They are one of the nanomaterials being investigated to improve the performance of supercapacitors and fuel cell electrodes and they exist in two main classes, namely SWCNTs which consist of a hollow tube with diameters between 1-5 nm and MWCNTs which are composed of multiple nanotubes 0.34 nm apart, where the final MWCNT has diameters of 2-100 nm. The synthesis of CNTs can be accomplished by a wide variety of methods including arc discharge, laser ablation and chemical vapour deposition [136]. CNTs offer potential applications in electronic devices, catalysts, sensors, field-emission devices and hydrogen-storage media [137-143]. MWCNTs contain concentric SWCNTs in their structure, and therefore, they possibly have analogous physicochemical properties to those corresponding to SWCNTs such as mechanical strength, electronic conductivity, thermal stability and high surface area [133, 144]. These nanomaterials are robust and they have been reported as the strongest of all the synthetic fibres [133]. The structures of SWCNT and MWCNT are represented in figure 1.14 below.

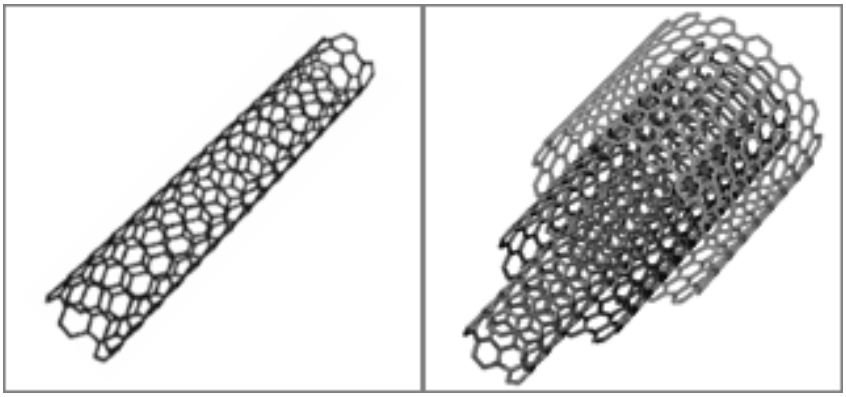

Figure 1.14: Structures of (a) SWCNT and (b) MWCNT [145]

The size and morphology of CNTs enable them to be used as suitable catalyst support, in which active metal particles are either dispersed on the external walls or be encapsulated in the interior of the nanotubes. The metal particles on the external walls make contact with the reactant molecules more easily than those encapsulated inside the internal channels of the CNTs [136, 146-149]. The presence of CNTs on the surface of bare electrodes such as glassy carbon, [150] graphite, [151] carbon fiber, [152], gold (Au) [153] and platinum (Pt) electrodes [154] has enhanced their electrical properties tremendously. Electrodes modified with CNTs have increased surface areas and adsorption efficiency compared to other common electrodes, and exhibit intriguing ability to enhance the electrochemical responses of several fuel cell molecules. Several workers have reported the use of CNTs in fuel cells as catalyst supports for electrode materials [155-157]. CNTs have also shown to be promising candidates for new chemical nanoarchitectures in electrocatalysis and nanoelectronic circuitry [158, 159].

Other applications of CNTs modified electrodes are found in electrocatalytic response of hydrazine [160], glucose [161], dihydronicotinamide adenine dinucleotide (NADH) [162], dopamine [163], nitric oxide [164], ascorbic acid [165] and hydrogen peroxide [166].

1.8.3 Metal-catalyst modified electrodes for fuel cell application

Today, the search of new catalysts for fuel cell applications is a very active field. The oxidation of fuel cell molecules for example MeOH on platinum (Pt) and on platinum based electrocatalysts has been extensively studied during the last decade. Platinum catalyst has been found to have high activity for methanol oxidation. However, previous studies revealed that Pt undergoes surface poisoning by strongly adsorbed reaction intermediates, carbon monoxide (CO) that blocks the active sites [167]. A solution to this problem has been to replace platinum catalyst with nanoparticles made from an alloy of platinum and ruthenium (Ru) rather than pure Pt. This combination offers an improved tolerance to CO poisoning [168].

1.9 Role of CNTs in electrochemistry and its role in electrocatalysis

Recently, as new forms of carbon, carbon nanotubes (CNTs) appeared to be promising supporting materials for new chemical nanoarchitectures in electrocatalysis [169, 170] and nanoelectronic circuitry [171] due to their unique structure and excellent mechanical, electronic and surface properties [172]. Several papers have reported the application of carbon nanotubes in fuel cells as potential supports in heterogeneous catalysts and electrode materials [173-176].

CNTs as a support have been extensively studied to improve the catalyst utilization and electrochemical activity in fuel cells [177-179]. Some results show that the CNT support induced the higher catalytic activity than conventional Vulcan XC-72 carbon black [180, 181].

One of the main powerful properties of carbon nanotubes is that it can enhance the electron transfer between the electroactive species and the electrodes. The carbon nanotubes as an electrode material can be used in electrochemical sensing. The CNT electrodes display superior performance than other electrodes in terms of promoting electron-transfer and improving reversibility of electrochemical reaction [182, 183].

The application of a multiwalled carbon nanotube modified basal plane pyrolytic graphite electrodes (MWCNT-BPPGE) for ultra sensitive detection of paracetamol in pharmaceutical products with cyclic voltammetric and adsorptive stripping voltammetric techniques has been reported in the literature. It has been reported that oxidation of paracetamol at MWCNT-BPPGE shows a remarkable improvement in analytical response in comparison with bare basal plane pyrolytic graphite electrode (BPPGE). A MWCNT-BPPGE has been successfully utilised for the adsorptive stripping voltammetric determination of paracetamol in standard laboratory and real pharmaceutical samples [184].

1.9.1 The importance of Pt/Carbon Nanotubes over Pt/Carbon Black

Carbon-related nanomaterials are considered to be one of the most ideal catalyst supports for fuel cells and have been widely used. In the past decades, carbon black has been most frequently used as a catalyst support [185-188], especially for Pt or Pt alloy electrodes for the oxygen cathode, or low-loading Pt electrodes for a hydrogen anode in an acid fuel cell. However, the efficiency of methanol oxidation is low partly due to low platinum utilization on this conventional carbon support, which is, in turn, related to the low electrochemically accessible surface area for the deposition of Pt particles [189-191]. Compared with the carbon black, carbon nanotubes (CNTs) are attractive materials used as the catalyst support for fuel cell

applications due to their particular morphologies and properties, such as high specific surface area and corrosion resistance, good electronic conductivity and high stability [192, 193].

It has been found that MWNTs exhibit better performance in DMFCs as compared to carbon black (XC-72) [194, 195] under identical conditions for catalysts preparation and cell performance test. The reasons for the high performance of CNTs supported Pt or Pt alloy nanoparticles (Pt/CNT) as compared with carbon black supported Pt (Pt/C) nanoparticles are due to the following [196]:

- The unique structure and electrical properties of CNTs.
- CNTs have few impurities while carbon black contains significant quantities of organosulfur impurities which poison Pt metal [197].
- Pt/C has Pt nanoparticle that are trapped in deep cracks of carbon black which cannot work as catalysts of electrodes.
- CNTs do not have such cracks hence Pt nanoparticles on CNTs can be used as effective catalysts [198].
- Pt/C is sensitive to CO poisoning.

PtRu alloys are nowadays the catalysts of choice for oxidation of fuel cell molecules and oxygen reduction reactions because of their high tolerance for CO poisoning, which is generally explained by a bifunctional mechanism, in

which CO is oxidized by the oxygenated species formed on the Ru surface atoms. In the bifunctional mechanism, Ru plays the role of dissociating water to form adsorbed OH species, which then reacts with the adsorbed CO to generate CO_2. In the electronic ligand effect mechanism, the electronic properties of Pt are said to be modified by the overlap of the Pt-Ru orbital so that the binding strength of the adsorbed CO on the Pt is weakened resulting to enhanced electrocatalysis [199,200].

The problem of the poor performance of the fuel cell molecules is a problem of poor catalyst performance. It is well known that when pure platinum is used as the catalyst, it will be rapidly poisoned by the adsorption of CO produced during the oxidation of methanol. However, many investigations have shown that some Pt-based alloy or Pt-metal oxide catalysts exhibit enhanced tolerance of CO and, consequently, improved electrocatalytic activities compared to those with platinum alone [201]. For instance, two mechanisms have been proposed to account for the promotional effect of Pt–Ru alloy catalysts. One is the so-called bifunctional mechanism [202, 203] in which the role of ruthenium is to dissociate water to form adsorbed OH species, which then reacts with adsorbed CO to generate CO_2. Another explanation is the electronic ligand effect mechanism, i.e. the electronic properties of platinum are modified by Pt–Ru orbital overlaps so that the binding strength of CO adsorbed on Pt is weakened, leading to the

enhancement of electrocatalytic activities for methanol electrooxidation [204].

Prior to presenting the results obtained the initial objectives of this thesis have to be clearly exposed. It can be seen from the tables above that the literature on FC oxidation at Pt-based electrode surfaces is very large, and that interest on this topic is not recent. The aim of this thesis was not that of exhaustively reviewing the literature on this subject, but to rather giving a good overview of the major achievements in the field. More particularly, there has been a strong interest in the development of a new Pt-based catalyst for both methanol and ethanol electrooxidation, and it was shown that alloying Pt with other transition metals greatly enhance the catalytic activity of the surface. Among all Pt-M combinations tested, Pt/Ru and Pt/Sn can be designated as the most efficient for the electrocatalysis of methanol and ethanol oxidation, respectively. We propose within this thesis to synthesize and electrocatalytically characterize Pt-based nanocatalysts. Our aim was to find a new type of catalyst by to preparing alloyed nanoparticles with controlled composition and high dispersion of the two metals, and determine the differences between the oxidation mechanisms on each fuel cell molecule. For practical reasons, the particles were deposited on basal plane pyrolytic graphite electrodes. The choice of such a substrate was motivated by its admirable conductive properties, ability to interact with

CNTs via π-π interactions and exhibition of faster electrode kinetics. The use of BPPGE as substrate for the study of supported nanoparticles should be a good approach to the problems usually encountered with common substrates such as those metioned above. It is well known, for instance, that Au substrates will undergo surface oxide formation. Moreover, electron transfer will occur from Au to Pt, modifying the electronic and catalytic properties of the Pt deposit. Glassy carbon substrate will also undergo surface oxides formation and corrosion. The work function of BPPGE is not well known, but it was expected that with this electrode, it should be possible to study the oxidation of FC molecules without any major interference.

Table 1.2 below summarises different types of metals that have been used in combination with Pt for methanol electrooxidation. Since most work has been carried out on methanol FC molecule for a direct methanol fuel cell (DMFC) due to its potential application in fuel cells, (Table 1.2) in this study alternative FC molecules were investigated

Table 1.2: Metal-carbon nanotube electrode for electrooxidation of methanol.

Nature of electrode	Electrode additives & treatment	Electrolyte	E_{foward}	$E_{reverse}$	Comments	Ref
Graphite-CNTs/Pt electrode	CNTs were grown directly on graphite disk	0.5M H_2SO_4	0.65 V	-	SCE reference electrode was used. Electrode modified with CNTs and Pt is better than the electrode modified with Pt only	205
GC-Pt/SWCNT	SWCNTs were functionalised with 0.5M Na_2SO_4 by electrochemical treatment	1M H_2SO_4	0.89 V	0.45 V	SCE reference electrode was used. Methanol oxidation peaks were observed	206
Pt/Ru (50:50)-graphitized/pristine/ template	Pt-Ru particles were deposited on three types of nanotubes (NTs), namely pristine, graphitized and template High temperature (800ºC) used	1M H_2SO_4	0.10 V	0.30 V	Hg/Hg_2SO_4 reference electrode was used. The highest peak current was observed on graphitized NTs	207
Graphite-CNT-Pt/Ru electrode	CNT/graphite electrode pretreated in 30 wt% HNO_3	0.5M H_2SO_4	0.40 V	0.70 V	SCE reference electrode was used. No current peaks of methanol oxidation observed when CNTs and Pt-Ru nanoparticles are not used	208
CNT-Pt (-.25V) CNT-Pt/Ru (-.25V) CNT-Pt(-.30V) CNT-Pt/Ru(-.30V)	CNTs grown directly on PTFE treated carbon cloths via a thermal CVD process	0.5M H_2SO_4	0.37 V 0.19 V 0.37 V 0.15 V	0.63 V 0.63 V 0.71 V 0.60 V	SCE reference electrode was used. Pt-Ru deposits exhibited relatively higher peak current densities	209

Pt/SWCNT PtRu/SWCNT Pt/Vulcan Carbon PtRu/Vulcan carbon	SWCNTs prepared by a microwave-assisted polyol process	1M H_2SO_4	0.31 V 0.19 V 0.35 V 0.20 V	~0.7 V 0.60 V 0.70 V 0.60 V	Ag/AgCl reference electrode was used. PtRu catalyst dispersed on SWCNT exhibits the best performance	210
Pt/GN Pt/MWCN Pt/SWCN	Prepared via self-regulated reduction by surfactant	1M H_2SO_4	*ca*. 0.45 V	*ca*. 0.95 V	NHE reference electrode was used. Higher catalytic activity in Pt/GN	211
Polycrystalline gold dics electrode-Pt/Ru 80:20	Nanoparticles synthesized by reduction with sodium borohydride of H_2PtCl_6 and $RuCl_3$	0.5M H_2SO_4	0.73 V	-	RHE reference electrode was used. Different ratios of Pt to Ru were studied and 80:20 gave the best performance	212
GCE-Pt/Ru/Ni (60:30:10)	Ni used as a promoting agent High temperature used	0.5M H_2SO_4	*ca.* 0.5 V	-	SCE reference electrode was used. Different metal ratios used and 60:30:10 was found to be the best. Results better than commercial Pt/Ru Catalyst available from Johnson- Matthey	213
Carbon paper electrode-Pt/Ru/Ni	No support used	1M H_2SO_4	*ca.* 0.7 V	0.39 V	Ag/AgCl reference electrode was used. Pt/Ru/Ni nanoparticles have high tolerance towards electrocatalytic poison	214
GCE- CNTs-Pt/Ru/Ni	MWCNTs were functionalized with sulfuric and nitric acids	0.5M H_2SO_4	-	0.40 V	SCE reference electrode was used. Improved catalytic activity and stability of Pt/Ru/Ni-CNTs catalyst electrode	215

					than Pt/Ru CNTs catalyst	
GCE/Pt/CNTs-POM GCE/Pt/C GCE/Pt/C-POM (same Pt loading)	The CNTs were purified with solutions of HNO_3 and HCl. Polyoxometalate (POM) modification on the prepared Pt/CNT catalysts was done by suspension of Pt/CNTs in solutions of $H_3PMo_{12}O_{40}$ and 2-propanol	0.5M H_2SO_4	0.72 V	0.43 V	Ag|AgCl reference electrode was used. Pt/CNT-POM catalysts show a superior performance over the other systems due to presence of CNTs and POM.	216
Pt–Co/Ppy-MWCNT before over-oxidation Pt–Co/PPy-MWCNT after over oxidation	Bimetallic Pt–Co nanoparticles were co-deposited on PPY-MWCNT composite by formaldehyde reduction route.PPy-MWCNT support was prepared by in situ polymerization of pyrrole on MWCNT.	0.5M H_2SO_4	0.71 V 0.66 V	0.52 V 0.48 V	Ag|AgCl reference electrode was used. The over-oxidation treatment improves electrochemical activity of Pt–Co/PPy-MWCNTs catalyst	217
GC/Pde-Ag(1:1)/C GC/Pde-Ag(1:1)/aCNT	MWNTs were activated by alkali treatment. High temperature was used (750-800 °C)	1M KOH	-0.18 V -0.14 V	-0.29 V -0.30 V	Hg/HgO reference electrode was used. PdeAg(1:1)/aCNT catalyst exhibits better catalytic activity than PdeAg/C) catalyst	218
Pd-1%MWCNTs-1%Ni/GC	MWCNTs were activated by refluxing in concentrated HNO_3	1M KOH	0.08 V	-0.26 V	Hg/HgO reference electrode was used. Pd–1%MWCNT–1% Ni/GC composite electrode has greatest active and more poisoning tolerant	219

					electrocatalyst compared to other electrodes studied.	
Pt/CCE	preparation of a carbon ceramic as an electrode matrix by sol–gel technique	0.2M H_2SO_4	0.89 V	0.43 V	SCE reference electrode was used. The prepared electrodes exhibit satisfactory stability and reproducibility	220
Pt-MoOx/CNTs/ graphite	purification was done by agitating the CNTs in concentrated nitric acid	0.5M H_2SO_4	0.76 V	0.48 V	SCE reference electrode was used. Pt-MoOx/CNTs/graphite electrode delivers excellent electrocatalytic properties while in CNTs/graphite has no electrocatalytic activity. T he existence of MoOxc plays an important role towardselectrocatalysis.	221
Gold/Pt-FTO/MWCNTs Gold/Pt-SnO2/MWCNTs	Fluorine tin oxide (FTO) and MWCNT composites were synthesized by a sol–gel process followed by a hydrothermal treatment process	0.1M $HClO_4$	0.79 V	0.58 V	SCE reference electrode was used. Pt–FTO/MWCNT catalyst exhibits a higher catalytic activity with high stability during potential cycling than Pt-SnO_2/MWCNTs	222
Pt-f-MWCNTs/ITO Electrode polycrystalline Pt electrode.	MWCNTs were prepared by the catalytic CVD method. Ptf-MWCNTs were prepared by radiolysis of K_2PtCl_6 in the presence of HOOC-fMWCNT	1M H_2SO_4	0.90 V 0.69 V	0.66 V 0.73 V 0.51 V	Ag|AgCl reference electrode was used. Unlike the polycrystalline Pt electrode, no CO desorption peak was observed on Pt-f-	223

					MWCNTs due to the presence of oxy groups on the f-MWCNTs.	
GCE/Pt/MWCNT GCE/Pt-Fe/MWCNT	MWNTs was subjected to strong acids (H_2SO_4–HNO_3)	0.5M H_2SO_4	069 V 0.68 V	0.50 V 0.47 V	Ag|AgCl reference electrode was used. Higher electrocatalytic activity and stability on Pt–Fe/MWNTs catalyst than a comparative Pt/MWNTs catalyst.	224
GCE/PtNi/MWCNT GCE/PtNi/Si-MWCNT	CNT functionalized with HNO_3 and H_2SO_4. PtNi/Si-MWCNT composite synthesized by nocovalent MWCNTsurface within polysiloxane. Siloxane (Si) was polymerized on the nanotube surfaces.	1M H_2SO_4	0.69 V 0.67 V	0.47 V 0.48 V	SCE reference electrode was used. PtNi/Si-MWCNT composite shows excellent electrocatalytic activity and enhanced CO tolerance.	225
GC/Pt-Ru/C GC/Pt-Ru/CNTs	CNTs were surface oxidized by H_2SO_4-HNO_3 mixture	0.5M H_2SO_4	0.53 V 0.53 V	-	Ag|AgCl reference electrode was used. Pt-Ru /CNTs catalysts exhibit better methanol oxidation activities than commercial Pt-Ru/C (E-TEK) catalyst	226
Pt/sulfonated-CNTs/GC Pt/HNO_3-CNTs/GC Pt/pristine-CNTs/GC	MWCNTs prepared by the catalytic decomposition of CH_4 using $LaNiO_3$ catalysts	0.5M H_2SO_4	0.62 V	0.50 V	Ag|AgCl reference electrode was used. The Pt/sulfonated-CNTs/GC electrode has extraordinarily high electrocatalytic stability and storage properties.	227
Ni@Pd/MWCNTs /GC (Ni@Pd = core-	MWCNTs were dispersed in a concentrated H_2SO_4–HNO_3 mixture	0.5M NaOH	-0.50 V	-0.38 V	SCE reference electrode was used. Ni@Pd/ MWCNTs increases the	228

shell nanoparticle) PdNi/MWCNTs/GC Pd/MWCNTs/GC					electrocatalytic activity and stability of the electrode considerably than that of PdNi/MWCNTs and Pd/MWCNTs catalysts	
Pd/MWCNTs Pd-MnO_2/MWCNTs	MWCNTs was refluxed in a concentrated H_2SO_4 - HNO_3 mixture	0.5M NaOH	-0.16 V	-0.48 V	SCE reference electrode was used. The presence of MnO_2 improves the electrocatalytic activity of Pd/MWCNTs	229
Graphite/Pt–Ru/PPy–CNT electrode Graphite/Pt/PPy –CNT electrode	Commercial MWCNTs were rinsed with double distilled water and dried.	0.5M H_2SO_4	*ca.* 0.60 V	*ca.* 0.40 V	SCE reference electrode was used. Methanol oxidation current of Pt–Ru/PPy–CNT/graphite electrodes is higher than that of Pt/PPy/graphite electrodes.	230
GC/Pt–Ru–STA/CNF GC/ Pt–Ru–STA/C GC/ Pt–Ru/C	CNF was treated with mixed acid solution of HNO_3 and H_2SO_4	0.5M H_2SO_4	0.80 V	0.60 V	Ag|AgCl reference electrode was used. Pt–Ru/STA–CNF electrode showed better electro-catalytic activity than the commercially Pt–Ru/C and Pt–Ru/STA–C catalyst.	231
GC/Pt/CNT-S GC/Pt/C	Carbon nanotubes used	0.5M H_2SO_4	0.70 V	0.50 V	Ag|AgCl reference electrode was used. High catalytic activities on Pt/CNTs synthesized on sulfur-coated CNTs than that of Pt/C.	232

CNTs = carbon nanotubes, **Pt** = platinum, **Ru**=ruthenium, **SWCNT**= single walled carbon nanotubes, **GC**= glassy carbon electrode, **MWCNT**=multi-walled carbon nanotubes, **Pt/Ru** = platinum-ruthenium, **GN**=graphite nanofiber, **Ni=**nickel, **POM=** Polyoxometalate, **Pt-Co/PPy** =platinum cobalt polypyrrole, **CCE**=carbon ceramic electrode, **Pd**=palladium, **Pt-MoOx**= platinum and molybdenum oxide particle, **Pt-FTO**=, Pt-Fluorine tin oxide, **ITO=**indium tin oxide, **Si**-MWCNT= Siloxane MWCNT, **C**=carbon black, **@** = core shell nanoparticle, **STA=** Silicotungstic acid, **CNF**=carbon nanofiber, **Ag|AgCl**= silve/silver chloride electrode, **SCE**=standard calomel electrode, **Hg/HgO**=mercury/mercury oxide electrode, **Hg/Hg_2SO_4**=mercury/mercurouis sulphate, **NHE**=standard hydrogen reference electrode, **RHE**=reversible hydrogen electrode **CVD**= chemical vapour deposition,**CNT-S**=sulphurcoatedCNT.

In my study I used highly ordered pyrolytic graphite (HOPG) which exhibit faster electrode kinetics in comparison with the glassy carbon that has been reported in the literature. HOPG has the ability to interact with carbon nanotubes via π-π interactions. Also, it helps in improving the electro-oxidation of FC molecules to take place at lower potentials and high current as this is seen when comparing the work done previously [223-225] with my work. Lower potential is favourable in FC technology as it indicates that electro-oxidation can be achieved by using less energy.

Most works report on the use of very long methods which required a lot of expensive reagents/solvents for the synthesis whereas in my study I used a very simple cheap method. Also, most reseachers did not conduct EIS studies hence cannot claim whether the oxidation of these FC molecules is controlled by diffusion or adsorption processes.

In other works reported for example Zhibin et al, no current peaks of MeOH oxidation were observed which indicated that the substrate used has no obvious electrocatalytic activity for MeOH oxidation. In other reports for example Selvaraj et al [121] on EG oxidation the first peaks for all prepared electrodes are slightly higher than the second peaks.

Electrooxidation of FC molecules such as ethylene glycol and formic acid on carbon nanotubes (CNTs) has been studied with the intention of overcoming the drawbacks of methanol such as adsorption and electro-oxidation behavior of CO-containing species. Electro-oxidation of methanol,

ethylene glycol and formic acid at platinum-based electrocatalysts supported on CNTs [233-235] has continued to receive attention because of its importance in the design and development of high-performance fuel cells for use in various applications such as in hybrid electric vehicles.

Weber et al. [236] have reported formic acid (FA) to show slightly more efficiency than methanol on Pt/Ru catalysts. It is expected that electrooxidations of EG and FA would offer a better solution to the problems associated with MeOH oxidation. Zhu et al. [237] reported formic acid oxidation on Pt–MWNT/PANI and concluded that composite films show excellent electrocatalytic activity for formic acid oxidation and offer good stability. Habibi et al. [238] has recently studied the Pt/Ni catalyst supported on carbon ceramic electrode (CCE) where it was discovered that it shows satisfactory stability and reproducibility than a comparative Pt/CCE catalyst and hence shows great potential as less expensive electrocatalyst for FA electrooxidation. Other work done on formic acid oxidation and reported in literature is summarised in Table 1.3.

Table 1.3: Metal-carbon nanotube electrode for electrooxidation of formic acid.

Nature of electrode	**Electrode additives & treatment**	**Electrolyte**	**E_{foward}**	**$E_{reverse}$**	**Comments**	**Ref**
Pt/GC/TMWNT Pt/GC/TAMWNT Pt/GC-Vulcan carbon XC-72	MWCNTs were functionalized first by using mixed acid treatment and then an amine treatment.	0.5M H_2SO_4	0.60-0.70 V	0.45-0.60 V	Ag/AgCl reference electrode was used. FA oxidation is improved when MWNT is used as a suport for Pt catalyst instead of Vulcan XC 72. Pt on acid and amine treated MWNTs demonstrate better electrochemical oxidation of FA compared to Vulcan carbon.	239
Carbon disk/Pt/C electrode Carbon disk/PtRu/C electrode	Catalysts on carbon XC-72 were prepared by a microwave-assisted polyolprocess	1M H_2SO_4 1M H_2SO_4	-0.75 V -0.61 V	0.50 V 0.41 V	Ag/AgCl reference electrode was used. For the PtRu/C catalyst, the FA oxidation shift to lower potentials indicating better electrocatalytic activity compared to the Pt/C catalyst.	240
Fe_xPt_{100-x}/Au: Fe10Pt90; Fe15Pt85; Fe42Pt58; Fe58;Pt42; Fe54Pt46;	FePt nanoparticles prepared by refluxing a mixture of oleylamine, oleic acid and $Fe(CO)_5$ High temperature was used (297°C)	0.1M $HClO_4$	 0.083 V 0.378 V Only one anodic peak at	 0.14 V 0.088 V	Ag/AgCl reference electrode was used. Results show that the catalytic activity depends on the composition of the alloy nanoparticles. The catalytic activity decreases in the sequence with Ja/Jc in brackets:	241

Fe63Pt37			0.045 V Only one anodic peak at 0.40V	0.017 V	Fe42Pt58(0.51)>Fe54Pt46 (0.47)>Fe58Pt42(0.42)> Fe15Pt85 (0.52)>Fe10Pt90 (0.29)> Fe63Pt37 (0.17)	
Pt/C GC rotating disk	Catalyst ink produced by dispersing Pt or PtPd supported on Vulcan XC-72 in ethanol	0.5M $HClO_4$	*ca.* 0.3 V 0.68 V	0.38 V	Ag/AgCl reference electrode was used. CO_{ads} is oxidized in the same potential range for the PtPd/C and Pt/C	242
Graphite/PtPd/CNTs Graphite E-TEK/Pt/CNTs Graphite/E-TEK PtPd/C	CNT purified by refluxing in concentrated nitric acid	0.5M H_2SO_4	0.35 V 0.65 V SAME	0.4 V SAME	SCE reference electrode was used. Has the highest electrocatalytic activity compared to Graphite E-TEK/Pt/CNTs and Graphite/E-TEK PtPd/C	243
nanoPtSn/Ti	Platinum and tin were co-deposited using a simple hydrothermal process to form stable nano-size bimetallic particles.Medium temerature was used (180°C)	0.5M H_2SO_4	0.31 V 0.72 V	0.49 V	SCE: Hg/Hg_2Cl_2 reference electrode was used. The high electrocatalytic activity may be directed to its large surface electro-active area.	244
GC/Pt-Ru 1:1 GC/Pt-Ru 10:1	Prepared by immersing clean GC electrode in the solution containing H_2PtCl_6 and $RuCl_3$	0.1M H_2SO_4	0.44 V 0.46 V - 0.62 V	0.31 V	SCE reference electrode was used. Oxidation current is higher than that of GC/Pt-Ru 10:1. Peak potential on forward scan shifts	245

				0.44 V	negatively to more than 60mV.	
Pt-modified MWCNT/PANI composite film Pt-modified pure PANI composite film	MWCNTs were functionalised via chemical deposition method. MWCNT/PANI was prepared by refluxing FWCNT with aniline.	0.5M $HClO_4$	0.34 V 0.69 V	0.46 V	SCE reference electrode was used. Lower peak potentials observed. Onset potential is over 100 times more negative than the film without MWCNTs.	246
HOPG/Pt/Co HOPG/Pt	Pt/Co nanoparticles prepared by aqueous solutions of H_2PtCl_6 and various concentrations of $CoCl_2$.	0.28M $HClO_4$	0.2 V	-	Ag/AgCl reference electrode was used. Only one oxidation peak observed in the forward scan which is about one order of magnitude higher than that of pure Pt particles. The enhanced activity of bimetallic particles is the bi-function effect of Pt and Co.	247
GC/Pd/FMWCNT GC/Pd/PMWCNT GC/Pd/RWCNT	MWCNT was functionalized with H_2SO_4 and $(NH_4)_2S_2O_8$	0.5M H_2SO_4	0.06 V 0.11 V 0.11 V	0.43 V 0.44 V 0.44 V	SCE reference electrode was used. Peak potential is more negative and is 1.4 and 2.4 times higher in current density compared to the other two electrodes.	248
Pt thin film	Electrode prepared by electroless deposition of thin Pt films	0.5M H_2SO_4	0.4-0.7 V 0.68 V	0.87 V	RHE reference electrode was used.	249
$Fe_{20}Pt_{80}$ paticles coated gold film	FePt nanoparticles prepared by refluxing a mixture of oleylamine, oleic acid and $Fe(CO)_5$	0.1M $HClO_4$	0.07 V 0.36 V	0.07 V	Ag/AgCl reference electrode was used. Film thickness/coverage was used and it was found	250

					that with thicker films the catalyst surface is partially poisoned leading to appearance of two oxidation peaks in anodic scans	
GC/Pt1Pd3/CNT GC/Pt1Pd1/CNT Pd/CNT Pt/CNT	CNTs were produced by a CVD approach. Small Pt, Pd and PtxPdy alloy nanoparticles supported on CNT were prepared through a modified ethylene glycol method.	0.5M H_2SO_4	0.26 V;0.64 V;0.92V 0.6 V;0.9 V 0.44 V (1); 0.77 V(shoulder) 0.5 V(2) 0.9 V(3)	-	RHE reference electrode was used. Three distinct peaks with comparatively similar height are observed for PtxPdy/CNT catalyst.The results indicates a 'direct oxidation pathway' of FAOR occurred on the Pd surface,while on the Pt surface, the FAOR goes through COads intermediate pathway.	251
Graphite/ Pt–Pd/CNT	CNTs first oxidized in hot conc. HNO_3 solution.	0.5M H_2SO_4	0.38 V 0.70 V	0.22 V	SCE reference electrode was used. The electrode exhibits ehanced rate of oxidation than the corresponding Pt nanoparticles modified SWCNT electrodes due to uniform dispersion of nanoparticles on SWCNTs and the efficacy of Pd species in Pt–Pd system.	252
GCE/nPd/MWCNT	MWCNTs were purified according to the conventional procedures.	0.1M H_2SO_4 0.1M	0.64 V	-	SHE reference electrode was used. One peak was observed. CNT-	253

		$HClO_4$			supported catalysts facilitate the electron transfer kinetics for the electrode reactions. The current obtained in H_2SO_4 is significantly 1.8 times less than that in $HClO_4$ solution.	

Au=gold, **PANI**=polyaniline, **HOPG**=highly ordered pyrolytic graphite, **RMWCNT**=raw multi-walled crbon nanotubes, **PMWCNT**=purified multi-walled carbon nanoubes, **SHE**= saturated hydrogen electrode, **SCE: Hg/Hg_2Cl_2** = SCE: Mercury/mercury chloride, **TMWNT**= MWNT functionalized with mixed acid treatrment, **TAMWNT**= MWNT functionalized with amine treatment.

Ethylene glycol (EG) has not only been studied as a fuel cell molecule for possible use in fuel cells but also due to its high solubility in aqueous solutions and relatively high reactivity [254]. Sieben et al. reported the synergistic effect between the facilitation of FA oxidation via oxygen-containing species adsorbed on Sn atoms in Pt/Sn catalyst, the alteration of the electronic structure of Pt atoms that weakens CO and intermediates adsorption, and the adequate Pt ensembles size [255]. Jin et al. observed a further positive shift in peak potential in acidic solution compared to other studies [256]. More literature on EG is summarised in Table 1.4 below.

Table 1.4: Metal-carbon nanotube electrode for electrooxidation of ethylene glycol.

Nature of electrode	**Electrode additives & treatment**	**Electrolyte**	**E_{foward}**	**$E_{reverse}$**	**Comments**	**Ref**
Carbon rod/ Pt/CMS	Carbon microspheres were prepared from sucrose by a hydrothermal method.	1.0M KOH	-0.07 V	-0.12 V	Hg/HgO reference electrode was used. The electrocatalytic activity for alcohol oxidation on catalysts supported on carbon microspheres is higher than that supported on carbon black. The activity and stability order of alcohol oxidation on Pt/C and Pt/CMS is EG > methanol > ethanol.	257
Pt/C electrode (treated) Pt/C electrode (untreated)	THF and acetone solutions were used to treat Pt/C electrode surface	0.5M H_2SO_4	0.55 V 0.82 V 0.80 V		Ag|AgCl reference electrode was used. Surface treatment can promote the eletrooxidation of Coad	258
Graphite/Pt-Ru/CNT Graphite/Pt/CNT Graphite/Pt/C	CNTs were oxidized in a hot concentration of HNO_3 solution.	0.5M H_2SO_4	0.55 V 0.60 V 0.64 V	0.35V 0.38V 0.44V	SCE reference electrode was used. Pt and Pt-Ru nanoparticles decorated CNT electrodes shows better catalytic performance. Pt-Ru/CNT displays a higher performance than Pt/CNT.	123
GC/S-MWNTS/Pd	MWNTs were purified by CVD method. novel sulfonated-MWNTS (S-MWNT) was derived from concentrated H_2SO_4 and acetic anhydride through a facile synthesis	0.2M KOH	-0.09 V	-0.38V	SCE reference electrode was used. S-MWNTS/Pd catalysts shows best electrocatalytic activities and stabilty in contrast to the unsulfonated and traditional sulfonated counterparts.	259
Pt/MCNT/Graphite PtRu/MCNT/Graphite electrode	MWCNT used	0.5M H_2SO_4	0.58 V 0.54 V	0.36V 0.32V	SCE reference electrode was used. Addition of Ru increased catalytic activity	260

PTh= Polythiopene, **s-**MWCNT=sulfonated- MWCNT, **THF**=tetrahydrofuran, **CMS**= carbon microspheres.

The complete electro-oxidation of ethanol at low temperature (below 100°C) would enhance the commercialization prospect of direct ethanol fuel cell (DEFC) compared to direct methanol fuel cell. The use of ethanol as fuel has distinctive advantage over methanol. Ethanol is relatively non toxic. The complete electro-oxidation of ethanol involves 12 electrons and breaking of C-C bond in contrast to methanol electro-oxidation, which involves only 6 electrons. However, for small scale applications, such as powering electronic devices or as a sensor in breathalyzers, the DEFC durability and reliability are the main requirements.

Ethanol oxidation in acid media occurs with the adsorption of acetyl species and the formation of stable intermediate products such as acetaldehyde and acetic acid. Generally, the overall electrooxidation of ethanol follow Equation 1.10:

$$Pt + R\text{-}CH_2OH + H_2O \rightarrow Pt\text{-}Rads + CO_2 + 5H^+ + 5e^- \quad \text{.....(1.10)}$$

Table 1.5: Metal-carbon nanotube electrode for electrooxidation of ethanol.

Nature of electrode	**Electrode additives & treatment**	**Electrolyte**	**$E_{forward}$**	**$E_{reverse}$**	**Comments**	**Ref**
PdNPs–CFCNTs–Nafion modified GCE	CFCNTs prepared by immersing MWCNTs in a mixture of concentrated H_2SO_4 and HNO_3	1.0M H_2SO_4 1.0 M NaOH	-0.29 V 0.09 V	-0.39 V	SCE reference electrode was used. PdNPs do not present activity in an acidic medium. However, in an alkaline solution, an oxidation peak was observed.	261
Pd/p-CNFs/GC (platelet) Pd/f-CNFs/GC (fish-bone) Pd/t-CNFs/GC (tubular)	Surface functionalized CNF (CNFs) was sonochemically treated in a solution containing HNO_3 and conc. H_2SO_4. Pd nanoparticles were deposited onto the CNFs modified GC electrode by pulse electrodeposition (PED) technique.	1M KOH	-0.261 V -0.256 V -0.231 V	-0.39 V -0.38 V -0.38 V	SCE reference electrode was used. p-CNFs supported Pd electrocatalyst improved the catalytic activity due to PdeCNFs interaction	262
Pd-1%MWCNTs-1%Ni/GC	MWCNTs were activated by refluxing in conc. HNO_3	1M KOH	0.07 V	-0.26 V	Hg/HgO reference electrode was used. Addition of 1%Ni to the active Pd–1%MWCNT composite improved the electrocatalytic activity further, but its higher additions (2–5%) showed an adverse effect on the apparent catalytic activity.	263
Pt/CCE	Preparation of a carbon ceramic as an electrode matrix by sol–gel technique	0.2M H_2SO_4	0.63 V 1.05 V	0.35 V	SCE reference electrode was used. Electrodes exhibit satisfactory stability and reproducibilitywhen stored in ambient conditions	264
Gold/Pt–ATO/MWCNT	Preparation of MWCNT supported platinum–antimony tin oxide(Pt–	1.0M H_2SO_4	0.70 V 1.02 V	0.41 V 0.91 V (small	SCE reference electrode was used. The electrocatalytic activity and utilizaton of Pt–ATO/MWCNT	265

Gold/ Pt–SnO2/MWCNT Gold/ Pt/C	ATO/MWCNT) nanoparticles was based on the polyol method			reduction peak)	was better than that of Pt–SnO_2/MWCNT and commercial Pt/C catalysts. Its CO tolerance performance is comparable to that of Pt–SnO_2/MWCNT but largely improved compared with commercial Pt/C.	
Pt/C/GC PtSn/MWNTs/GC	Functionalization of MWNTs has been achieved by refluxing in concentrated HNO_3	1M H_2SO_4	0.72 V 0.745 V	0.44 V 0.48 V	Ag|AgCl reference electrode was used. PtSn/MWNTs show good catalytic activity.	266
Gold/Pt–S–TiO_2/MWCNTs Gold/Pt–TiO_2/MWCNTs Gold/Pt/C		1M $HClO_4$	0.71 V 1.10 V 0.72 V 1.12 V 0.71 V 1.10 V	*ca.* 0.40 V *ca.* 0.40 V *ca.* 0.40 V	SCE reference electrode was used. Pt–S–TiO_2/MWCNT catalysts show higher catalytic activit due to incorporation of sulfated TiO_2.	267
Pt/CNT-X (based composite) X=Mg^{2+}/Ni^{2+} Pt/CNTs(comm.)	CNTs were used	0.5 M H_2SO_4	0.4-1.1 V	0.2-0.6 V	SCE reference electrode was used. Electrodes of platinum particles supported on the CNT based composites exhibited excellent electrocatalytic activity	268

NP=nanoparticles, **CF**=carbon fiber, **ATO**= antimony tin oxide.

Platinum based alloys with numerous transition metals have been prepared using a wide range of experimental techniques, and it is now well accepted that amongst the combinations tested Pt/Ru [269] appear as one of amongst the most appropriate ones for the electrocatalysis of ethylene glycol, methanol and formic acid electrooxidations. The use of these Pt-based alloys rather than pure Pt nanoparticles allows improvement of the catalytic activity. These new catalytic surfaces have exhibited enhanced electrocatalytic properties and higher CO tolerance than pure Pt. There are two main mechanisms that have been proposed to account for the promotional effect of Pt-Ru; (i) the *"bifunctional mechanism"* [270-272] and (ii) "*electronic ligand-effect mechanism*" [273, 274]. In the former, Ru plays the role of dissociating water to form adsorbed OH species, which then reacts with the adsorbed CO to generate CO_2. In the latter, the electronic properties of Pt are said to be modified by the overlap of the Pt-Ru orbital so that the binding strength of the adsorbed CO on the Pt is weakened resulting to enhanced electrocatalysis. A number of studies have indicated that electrodes modified with carbon nanotubes (CNTs) decorated with the nanoparticles of Pt/Ru or Pt/Fe exhibit an ability to enhance the electrooxidation response of fuel cell molecules [119, 121, 122, 275-279], thus making them more promising anodic materials for use in fuel cells.

1.10 Electrode modification techniques

Several methods have been developed to fabricate chemically modified electrodes. Some of these methods are described below.

1.10.1 Electrodeposition

Electrodeposition is one of the most efficient methods for the growth of metal nanoparticles. This is a powerful technique for the deposition of many metals which allows easy control of nucleation and growth of metal nanoparticles with various sizes, shapes and distributions [280, 281]. This process is used in electroplating in which the current is used to reduce cations of a desired material from a solution and coat a conductive metal with a thin layer of the material. To acquire this, the electrode is immersed in an electrolyte solution containing one or more dissolved salts as well as other ions that permit the flow of electricity, followed by repetitive voltammetric scanning within a specified potential window [282]. Hassan [282] used this method for the co-electrodeposition of Pt and Sn on Ti or Pt electrodes from K_2PtCl_6 and $SnCl_2$ salts in 0.5 mol/L H_2SO_4 solution by using different molar ratio of Pt:Sn (8:1 and 1:1) with the potentiostatic deposition at –850 mV vs Hg/Hg_2SO_4 /1.0 mol/L H_2SO_4 for 15 min. After the preparation of the modified Ti and Pt electrodes, no further pretreatment of the electrode was necessary to avoid any changes in the substrate surface.

1.10.2 Drop-dry method

This method involves drop-coating the electrode with small droplets of the desired (metal or compound etc) solution of volatile solvent such as DMF and then allowing it to dry out. The films prepared in this way are usually non-uniform and this is the greatest drawback for the method. However, the morphology of the film depends on the concentration of the casting solution, rate of solvent evaporation, nature of the solvent and the roughness of the electrode surface [283].

1.10.3 Dip-dry coating

Dip-dry coating involves immersion of the electrode in a solution for a period sufficient for spontaneous film formation to occur by adsorption. Then the electrode is withdrawn from the solution and the solvent is allowed to dry out [284].

1.10.4 Spin coating

The spin coating technique is a straightforward and fast growing technique in which the excess amount of a solution is placed on the substrate and rotated at high speed in order to spread the fluid by centrifugal force and obtained a desired thickness of the film after drying. The spin-coating film has a large surface/volume ratio and porous structure, which make such thin films especially useful for sensor applications. Many previous investigations reveal that spin-coating films containing pyrrole (Py) and Pc complexes have

excellent gas sensitivity [285,286]. Spin-coating films of tetra-(tert-butyl)-5,10,15,20-tetraazaporphyrin copper (CuTAP(t-Bu)$_4$) and tetra- (tert-butyl) phthalocyanine copper (CuPc(t-Bu)$_4$) have been studied by Bin Wanga et al. [287]. However, the thickness of the film depends on the concentration of the solution and the solvent. Spin coating is widely used in microfabrication and photolithography and the film may show lower percentage coverage of crystallites than a simple evaporated film.

1.10.5 Vapour deposition

Minimizing the cost of fuel-cell catalysts is highly desirable and the synthesis of nano-sized Pt particles is one of the ways to reduce the Pt loading without losing the catalytic activity. Chemical vapor deposition (CVD), which involves reactions between the surface sites of catalyst carriers and vapors of metal compounds, is a useful method for preparing nano-sized metal particles [288]. However, CVD rarely has been used to prepare Pt nanoparticles, although it is frequently used to obtain Pt thin films for electronic and optical devices [289-291]. Fuel-cell electrode catalysts with improved electrochemical properties have been prepared by dispersing Pt nanoparticles onto carbon nanotubes (CNT) using a CVD method. The method is used to produce high-purity and high performance thin films. In a typical CVD process the substrate is exposed to one or more volatile precursors which react and decompose on the substrate surface to produce the desired deposit [292].

1.10.6 Langmuir-Blodgett

In 1930, Langmuir and Blodgett invented the technique that involves forming an ordered monolayer or multilayer films at the air-water interface and then transfering the film onto the electrode surface by immersing the solid substrate into or from the liquid. A monolayer is added with each immersion step thus films with accurate thickness can be formed and can be repeated with several layers, if desired, of different properties [293]. It is also used extensively to build up monolayers or multilayers of organic amphiphilic molecules in which the order and 2D structure are controlled at the molecular level [294-296]. By this way, it is possible to obtain ultrathin films characterized by long range order, which can provide new insights on electron transfer processes at molecularly ordered interfaces [297-299].

1.10.7 Electropolymerisation

Electropolymerisation is a simple method for deposition of polymers such as polyaniline thin films on electrode surface. In this method the electrode is immersed in solution of the modifier followed by repetitive voltammetric scanning within a specified potential window. The resulting voltammogram of the first scan is different from the subsequent scans indicative of the formation of the new species on the electrode surface [300].

1.11 Overview of Fuel Cell (FC) technology and its shortcomings

Over the past few years, the development and application of Fuel Cells (FCs) has been a topic of intense investigation. FCs is an important technology for a wide variety of applications including stationary power, portable power and transportation power. This technology seeks to provide a solution to the problems of limited availability and atmospheric pollution in the use of fossil fuels. One of the most important components for the development of FC is the electrocatalyst. Finding new and better electrocatalysts is undoubtedly one of the keys to the development of FCs. The electrocatalysts will help with the internal combustion engines in cars, with batteries to fit for portable systems such as cellphones, and laptops, and with FC-based electricity and heat generation systems.

In 1839 Sir Willian Grove began the history of fuel cells when he reported the invention of fuel cells as electrical energy conversion system [301]. Grove demonstrated that electricity could be generated from the electrochemical reactions of hydrogen oxidation and oxygen reduction taking place at separate electrodes. This "primary" FC has since been improved continuously, and new types of FC were established. There are six major types of fuel cells under development worldwide namely (i) Proton Exchange Membrane Fuel Cell (PEMFC), (ii) Direct Methanol Fuel Cell (DMFC), (iii) Alkaline Fuel Cell (AFC), (iv) Phosphoric Acid Fuel Cell (PAFC), (v) Molten

Carbonate Fuel Cell (MCFC), (vi) Solid Oxide Fuel Cell (SOFC). These FC types are divided into three groups, namely low temperature FCs (PEMFC and DMFC), medium temperature FCs (AFC and PAFC) and high temperature FCs (MCFC and SOFC) [302]. They differ amongst themselves by the type of the electrolyte employed in the cell and the temperature of operation. The operating mode of all of these FC types is basically the same. The physical structure of a fuel cell consists of a membrane that is in contact with the anode and cathode electrodes [303, 304]. Oxidation of the fuels (hydrogen, methanol, ethanol etc.) takes place at the anode generating electrons and protons. Reduction of oxygen occurs at the cathode. The overall process yields water and electrical current, as well as CO_2 when a methanol is used as the fuel. The subject of this thesis is the synthesis and characterization of different Pt-based nanoparticulate electrocatalysts that can be used in methanol, formic acid and ethylene glycol-fed FC. Fuel cell molecules such as methanol or ethanol are attractive as fuels because they are inexpensive, widely available and can be handled and distributed easily. These fuels could alleviate problems associated with H_2 storage and transportation because of higher energy density in methanol compared to H_2. Important aspects for a possible industrial application of the DAFC based on PEMFC are the development of better catalysts, both for the cathodic and anodic processes in order to reduce the required overpotentials and also the surface poisoning that occurs at the anode as well as improvements of the separating

membranes, so as to avoid the crossover of methanol from the anode compartment to the cathode resulting in significant fuel inefficiency and reduced cell voltage at higher current, which causes a significant loss in overall cell efficiency.

The main requirements for any fuel for FC development are non-toxicity, safe to handle (high boiling point (for application at T > 100^{o}C at near-ambient pressure), high energy density, and ability to be completely oxidized to CO_2 with little or no accumulation of oxidation by-products [305].

1.12 JUSTIFICATION OF THIS WORK

To date, most works on fuel cell molecules for FC development have been devoted to methanol. However, DMFCs still have a number of significant drawbacks. One drawback is dealing with the high price of the final devices. The main contributor to the high cost is the use of platinum and platinum alloys at both sides of the MEAs. This problem can be solved by using a modified catalyst since Pt is sensitive to CO poisoning which reduces the cell efficiency and the lifetime of the device. The second problem is the high toxicity of methanol, which can be solved only by strict safety regulations for methanol container design. The third drawback is the methanol crossover from the anode side to cathode.

There are limited studies on the use of other fuels such as ethylene glycol and formic acid. These two fuel cell molecules have been reported to exhibit properties that could make them as possible alternatives to methanol as already mentioned in section 1.5.3. FA and EG meet these requirements, which explains why they are being considered as the most viable alternative to MeOH for FC in this study. The oxidation of methanol (MeOH) on platinum (Pt) and on platinum based electrocatalysts has been extensively studied during the last decade. The researcher studied the electro oxidation of ethylene glycol and formic acid with the intention of overcoming the drawbacks of methanol such as adsorption and electro oxidation behavior of CO-containing species.

Ethylene glycol (EG) has a number of advantages that make it superior to methanol for fuel cell applications. The boiling point of EG (bp 198 °C) is higher than that of methanol (bp 64.7 °C), which makes it safer to work with and is much less volatile. It has higher theoretical energy density than that of methanol and can be electrochemically oxidized [306]. Because ethylene glycol is widely used in the automobile industry, the supply chain is already established, which is not true for methanol. All these benefits make fuel cells based on EG a promising source of alternative energy. However, it should be mentioned, that in direct liquid fed fuel cells the fuel should be oxidized completely (or close to 100%), what is still challenging task for DEGFCs.

This issue is making the development of new catalysts for complete ethylene glycol oxidation extremely important.

The application of EG electrooxidation on direct alcohol fuel cells (DAFCs) has attracted increased interests [307, 308]. The fuel cells based on EG fuel show certain advantages such as low fuel cross-over and high power density [309, 310].

The electrochemical activity of formic acid is much higher than that of methanol. Unlike methanol, formic acid is non-toxic and non-flammable, and is also a strong electrolyte that is able to facilitate the proton transport within the anode catalyst layer [311]. Additionally, its crossover flux through a Nafion® membrane is two orders of magnitude lower than that of methanol [312] which makes it possible for DFAFC to work at concentrations as high as 15M formic acid [313, 314]. Thus, the practical power density of DFAFC could be higher than that of direct methanol fuel cells (DMFC) despite the specific energy density of formic acid being lower than methanol. Although the commercial price of formic acid is a little higher than that of methanol, it is still acceptable in portable applications due to its unique merits. Explained below are the different types of fuel cells.

1.13 Fuel Cell Types

There are six major types of fuel cells under development worldwide. These fuel cell types are Polymer Electrolyte Membrane Fuel Cell (PEMFC), Direct Methanol Fuel Cell (DMFC), Alkaline Fuel Cell (AFC), Phosphoric Acid Fuel Cell (PAFC), Molten Carbonate Fuel Cell (MCFC) and Solid Oxide Fuel Cell (SOFC).

1.13.1 Polymer Electrolyte Membrane Fuel Cell (PEMFC)

PEMFC deliver high power density and efficiency, smaller and lighter than other fuel cells providing the same power output. PEMFC is typically fueled with hydrogen. This FC type uses a fluorinated sulphonic acid polymer as an electrolyte and operates at relatively low temperature (80-100°C) and is currently the most popular choice for portable power and small-scale stationary applications. The electrode in PEMFC consists of a porous carbon material containing a platinum (Pt) catalyst. PEMFC uses platinum catalyst to separate hydrogen's electrons and protons. However, the platinum is extremely sensitive to CO poisoning. Therefore, PEMFCs are fuelled with pure hydrogen since the Pt catalyst is sensitive to CO poisoning. Existing PEMFCs deliver high power density and efficiency but the cost reduction and improving durability remain key priorities. Nanomaterials are believed to improve the performance and reduce the cost of the catalyst, the associated electrode material and the polymer membrane [315].

1.13.1.1 Principle of PEMFC

PEMFC consist of two electrochemical reactions, namely Hydrogen and Direct Methanol Fuel Cell reactions. These reactions are taking place at the anode and cathode electrodes to produce electric current and are described below: A schematic view of a hydrogen fuel cell is shown in scheme 1.1.

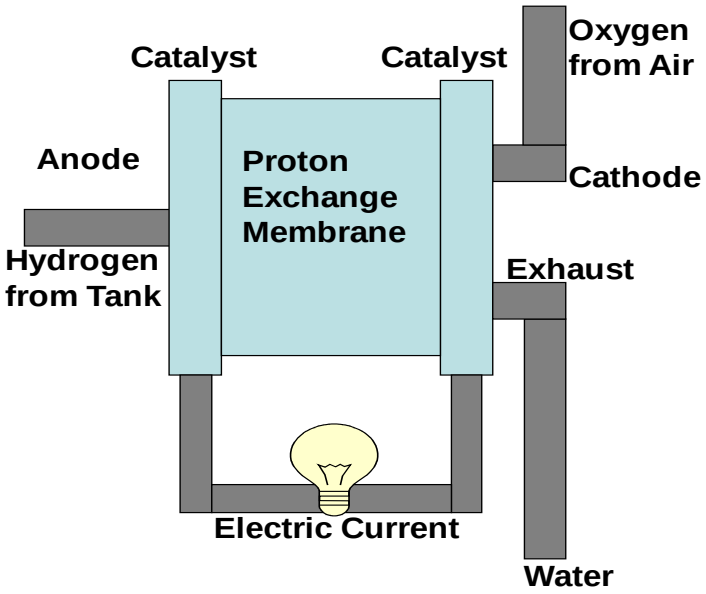

Scheme 1.1: Hydrogen Fuel Cell [316].

The oxidation of hydrogen takes place at the anode and the overall oxidation reaction involves the release of two electrons, and can be described by the following Equation:

Reactions of Hydrogen (H_2) Fuel Cell

$$Anode: \quad H_2 \rightarrow 2H^+ + 2e^- \tag{1.11}$$

$$Cathode: \quad O_2 + 4e^- \rightarrow 2O^{2-} \tag{1.12}$$

$$O^{2-} + 2H^+ \rightarrow H_2O \tag{1.13}$$

Pure H_2 fuel cell gives the best performance; however, due to storage and transportation problems alternative fuels have been investigated. One alternative is the Direct Methanol Fuel Cell (DMFC) which utilizes a liquid fuel (methanol). Since the subject of this thesis is the preparation of carbon based electrodes for electrocatalysis of fuel cell molecules therefore, only the Direct Methanol Fuel Cell (DMFC) will be presented in greater detail below. The use of organic molecule (methanol) is one of the most interesting solutions to avoid problems in the storage and handling of the fuel that are decisive for practical applications in vehicles and portable instrumentation.

1.13.2 Direct Methanol Fuel Cells (DMFCs)

DMFCs are based on the same principle as PEMFC but are specifically designed to be powered by pure methanol which is mixed with steam or water and fed to the fuel-cell anode rather than pure hydrogen. Methanol is one of the most intensively investigated fuel cell molecule for the development of DMFCs. The DMFC has been an extremely promising power source for portable applications due to its simple handling and processing of fuel [317-319]. However, it has some disadvantages as being poisonous, the quality of getting evaporated easily, having a high crossover through the polymer membrane and a complicated reaction process whereas formic acid has a higher theoretical electromotive force (EMF) in a fuel cell, as calculated

from the Gibbs free energy, than either hydrogen or direct methanol fuel cells (DMFCs) [320].

1.13.2.1 Principle of DMFC

A schematic view of a direct methanol fuel cell (DMFC) is shown in scheme 1.2. The DMFC consists of two electrodes (anode and cathode) that are separated by a membrane and are connected to the external circuit. At the anode the methanol is oxidized electrochemically to carbon dioxide (CO_2) and protons (H^+) (equation 1.14). The protons produced at the anode enter the membrane and are transported to the cathode. At the cathode the supplied oxygen reacts with the protons (H^+) to form water (equations 1.15)

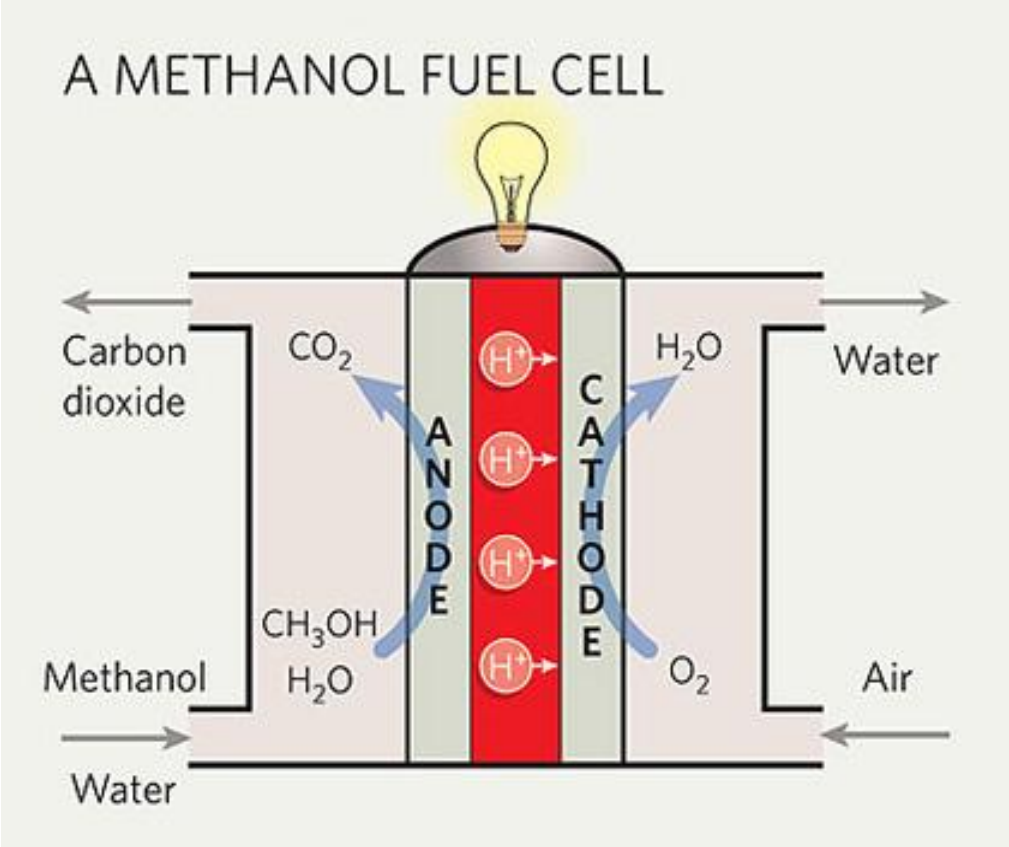

Scheme 1.2: Direct Methanol Fuel Cell (DMFC) [321].

The oxidation of the methanol takes place at the anode and the overall oxidation reaction involves the release of six electrons as shown in the following Equation:

$$Anode: CH_3OH + H_2O \rightarrow CO_2 + 6H^+ + 6e^- \quad (1.14)$$

$$Cathode: O_2 + 6e^- + 6H^+ \rightarrow 3H_2O \quad (1.15)$$

$$CH_3OH + \frac{3}{2}O_2 \rightarrow CO_2 + 2H_2O \quad (1.16)$$

1.13.3 Alkaline Fuel Cell (AFC)

The electrolyte in this FC type is potassium hydroxide, KOH (85 wt. %) and is operated at medium temperature (150- 200°C). AFC requires platinum (Pt) as the catalyst for both the anode and cathode electrodes. AFC is easily poisoned by carbon monoxide (CO) [301, 303].

1.13.4 Phosphoric Acid Fuel Cell (PAFC)

This fuel cell type utilizes phosphoric acid electrolyte and is operated at medium temperatures (180 - 220°C). The catalyst used in PAFC at both the anode and cathode electrodes is usually Platinum (Pt). PAFC can tolerate up to 2 % carbon monoxide poisoning [303, 322, 323].

1.13.5 Molten Carbonate Fuel Cell (MCFC)

MCFC uses alkali carbonates namely, sodium carbonate (Na_2CO_3) as an electrolyte and operates at high temperatures (600-650°C). MCFC uses nickel catalyst at the anode electrode and nickel oxide at the cathode electrode. MCFC is insensitive to CO poisoning. The alkali carbonates provide ionic conduction by forming highly conductive molten salts with carbonate ions [324].

1.13.6 Solid Oxide Fuel Cell (SOFC)

The electrolyte in this cell is zirconium oxide (ZrO_2). These fuel cells operate at very high temperatures (900-1000°C). SOFCs do not suffer from CO poisoning. These cells use Co-ZrO_2 or Ni-ZrO_2 catalysts at the anode electrode and Sr-doped $LaMnO_3$ catalyst at the cathode electrode [301, 303].

Table 1.6: Different types of fuel cells classified according to the electrolyte.

Type	**Electrolyte**	**Optimal working temperature (°C)**
PEMFC	Fluorinated sulphonic acid polymer	85-105 (low)
DMFC	Fluorinated sulphonic acid polymer	80 (low)
AFC	KOH	150-200 (medium)
PAFC	H_3PO_4	180-220 (medium)
MCFC	Na_2CO_3	600-650 (high)
SOFC	ZrO_2	900-1000 (high)

1.14 Applications of fuel cells

Fuel cells are an important technology for a wide variety of applications including stationary power, portable power and transportation power.

Both low-temperature (PEMFC and DEMFC) and high-temperature fuel cells (MCFC and SOFC) could be utilized for stationary applications. PEMFC could also be used for transportation applications. MCFC play an important role in power conversion for stationary power. SOFC type can be used in big, high power applications including industrial and large-scale central electricity generating stations. AFCs were initially developed for Space applications. Unlike stationary power, low temperature fuel cells are favoured for Space applications and therefore PEMFCs are the best candidates. Portable devices require less power output, and thus DMFC systems could well be suited for this kind of application [325].

1.15 Advantages and disadvantages of fuel cell system

Kordesch et al [303] compared fuel cell systems to other energy conversion systems and a summary of the advantages and disadvantages are as follows:

Advantages of fuel cell systems:

- Fuel cells produce little pollution, i.e. no noxious exhaust gases are formed.

- They will reduce the use of fossil fuels due to their high efficiency of energy conversion.
- Fuel cell systems produce good quality drinking water in hydrogen-oxygen and methanol systems.
- They use only a small number of moving parts (pumps, fans and blowers).
- Fuel cell systems are low maintenance and employ exchangeable parts (i.e. mass-produced components).
- High temperature fuel cell systems have the ability to use low cost fuels.

Disadvantages:

- A major disadvantage is the high cost of the system (i.e. catalysts, membranes and accessories).
- The hydrogen gas fuel storage is also a problem in PEMFC.

1.16 Mechanism of adsorption of methanol oxidation intermediates at Pt-modified electrodes

Methanol adsorption on Pt is a sequence of fast, consecutive dehydrogenation steps as shown in Equation 1.17, rather than a simple adsorption phenomenon. All the steps listed in Equation 1.17 are accompanied by the release of one proton and one electron, and this sequence leads to the formation of adsorbed carbon monoxide (CO):

$$CH_3OH \longrightarrow CH_2OH_{ads} \longrightarrow CHOH_{ads} \longrightarrow COHads \longrightarrow CO_{ads} \quad (1.17)$$

Adsorbed CH_3OH cannot be detected on Pt; methanol chemisorption on platinum is dissociative, and mainly leads to adsorbed CO which acts as a poison for the direct electrocatalytic oxidation of methanol, since it blocks the reactive sites on the Pt surface. The results suggested that the tolerance to surface poisoning is worst at methanol [326]. Adsorbed CO is then oxidized to CO_2. It can be reasonably concluded that the irreversible adsorption of methanol on Pt is accompanied by the simultaneous and spontaneous dehydrogenation of the molecule (combined with charge transfer) that is catalytically activated by Pt.

Polycrystalline bulk Pt and Pt nanoparticles do not behave in exactly the same manner with respect to methanol adsorption. Christensen et al [327] compared the behaviour of Pt particles (15 nm) with that of bulk

surfaces and showed that methanol adsorption takes place at a lower potential on particles (< 50 mV, as compared to 150 mV for bulk Pt). These authors postulated that migration of singly bonded CO from terraces to edge sites occurred on particles, and that the appearance of triply bonded CO was much more pronounced on particles. Overall methanol oxidation including dehydrogenation followed by oxidation of the poisoning surface residue can thus be described in terms of Equations 1.18 to 1.21:

$$Pt + CH_3OH_{(bulk)} \longrightarrow Pt\text{-}(CH_3OH)_{ads} \quad (1.18)$$

$$Pt\text{-}(H_2O)_{ads} \longrightarrow Pt\text{-}(OH)_{ads} + H^+ + e^- \quad (1.19)$$

$$Pt\text{-}(CH_3OH)_{ads} \longrightarrow Pt\text{-}CO_{ads} + 4H^+ + 4e^- \quad (1.20)$$

$$Pt\text{-}CO_{ads} + Pt(^{\cdot}OH) \longrightarrow CO_2 + 2Pt + H^+ + e^- \quad (1.21)$$

With respect to the potential required for this reaction, the removal of the poison may occur as the result of a direct surface reaction with water molecules or reversible Pt surface oxides (Equations 1.22 and 1.23).

$$Pt(CO) + H_2O \rightarrow Pt + CO_2 + 2H^+ + 2e^- \quad (1.22)$$

$$Pt(CO) + PtO_x \rightarrow Pt + PtO_{x-1} + CO_2 \quad (1.23)$$

This complex overall mechanism is summarized in the catalytic cycle of methanol electrooxidation at Pt in Figure 1.15 [274].

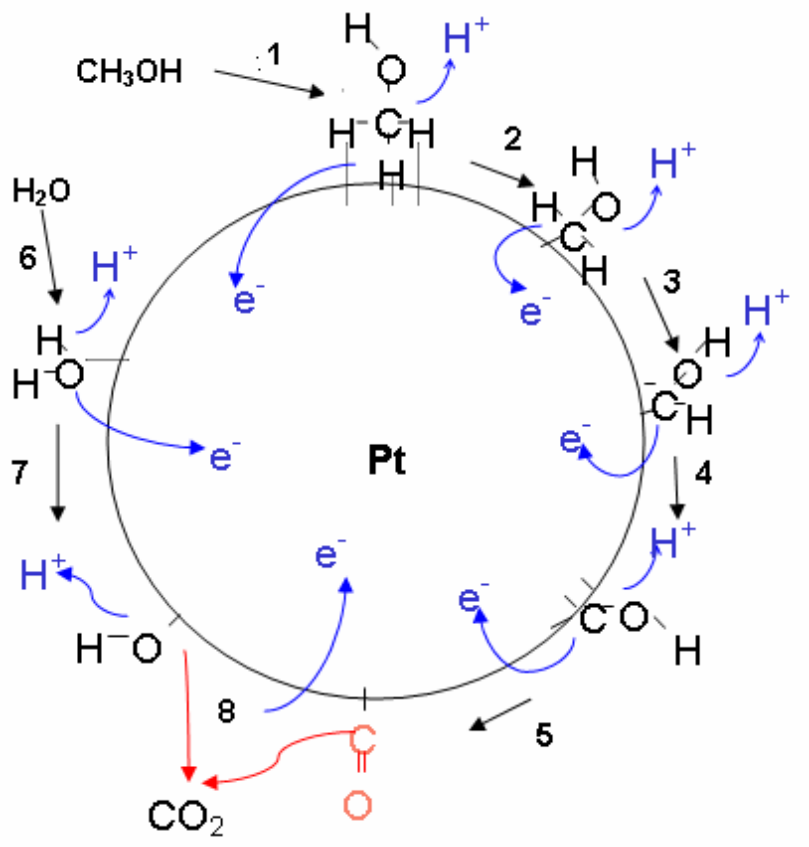

Figure 1.15: Catalytic cycle of methanol electrooxidation at a Pt electrode.

This cycle involves the following steps: adsorption (1) of one methanol molecule on three adjacent Pt sites, followed by the four successive, fast dehydrogenation steps (2-5) of adsorbed methanol leading to CO. In parallel water activation and adsorption (6) of hydroxyl radicals at Pt sites (7) take place in parallel. Finally, the surface reaction between adsorbed CO and $^{\bullet}OH$ yields free sites and CO_2 (8).

1.17 Microscopy and spectroscopic techniques

Microscopy is the technical field of using microscopes to view samples and objects that cannot be seen with the unaided eye (objects that are not within the resolution range of the normal eye). There are three well-known branches of microscopy namely optical, electron, and scanning probe microscopy.

Optical and electron microscopy involve the diffraction, reflection, or refraction of electromagnetic radiation/electron beams interacting with the specimen, and the subsequent collection of this scattered radiation or another signal in order to create an image. This process may be carried out by wide-field irradiation of the sample (for example standard light microscopy and transmission electron microscopy) or by scanning of a fine beam over the sample (for example confocal laser scanning microscopy and scanning electron microscopy). Scanning probe microscopy involves the interaction of a scanning probe with the surface of the object of interest. The development of microscopy revolutionized biology and remains an essential technique in the life and physical sciences [328]. Spectroscopy is the study of the interaction between matter and radiated energy. Historically, spectroscopy originated through the study of visible light dispersed according to its wavelength, e.g., by a prism. Later the concept was expanded greatly to comprise any interaction with radiative energy as a

function of its wavelength or frequency. Spectroscopic data is often represented by a spectrum, a plot of the response of interest as a function of wavelength or frequency [329].

1.17.1 Raman Spectroscopy

Raman spectroscopy is a spectroscopic technique used to study vibrational, rotational, and other low-frequency modes in a system. It relies on inelastic scattering, or Raman scattering, of monochromatic light, usually from a laser in the visible, near infrared, or near ultraviolet range. The laser light interacts with molecular vibrations, phonons or other excitations in the system, resulting in the energy of the laser photons being shifted up or down. The shift in energy gives information about the vibrational modes in the system [330].

1.17.2 Scanning Electron Microscope (SEM)

A scanning electron microscope (SEM) is an electron microscope type that images a sample by scanning it with a high-energy beam of electrons in a raster scan pattern. The electrons interact with the atoms that make up the sample producing signals that contain information about the sample's surface topography (Fig. 1.16), composition, and other properties such as electrical conductivity.

The SEM can produce very high-resolution images of a sample surface, revealing details less than 1 nm in size. Due to the very narrow electron beam, SEM micrographs have a large depth of field yielding a characteristic three-dimensional appearance useful for understanding the surface structure of a sample [328, 331]. This is exemplified by the micrograph of Pt/Ru nanoparticles on modified electrode.

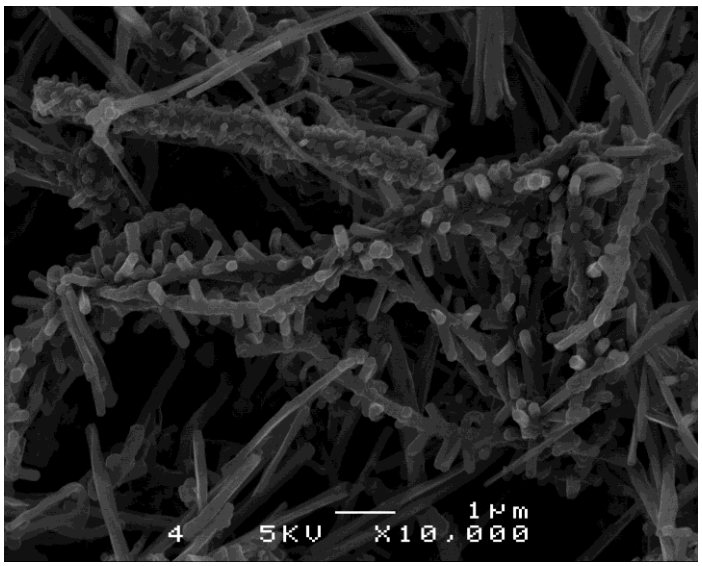

Figure 1.16: A Typical SEM Image showing formation of Pt/Ru nanoparticles on modified electrode.

1.17.3 Fourier Transform Infra-Red Spectroscopy (FTIR)

Infrared spectroscopy is a well known analytical technique which deals with the infrared region of the electromagnetic spectrum. It can be used to identify compounds or investigate sample composition. Infrared

spectroscopy is widely used in both research and industry as a simple and reliable technique for measurement, quality control and dynamic measurement. It is of special use in forensic analysis in both criminal and civil cases, enabling identification of polymer degradation for example. It is perhaps the most widely used method of applied spectroscopy [332].

1.17.4 Transmission Electron Microscope (TEM)

Transmission electron microscopy (TEM) is a powerful microscopy technique whereby a beam of electrons is transmitted through an ultra thin specimen, interacting with the specimen as it passes through. An image is formed from the interaction of the electrons transmitted through the specimen (Fig. 1.17); the image is magnified and focused onto an imaging device, such as a fluorescent screen, on a layer of photographic film, or to be detected by a sensor such as a CCD camera.

TEMs are capable of imaging at a significantly higher resolution than light microscopes. This enables for examination of fine detail—even as small as a single column of atoms, which is tens of thousands times smaller than the smallest resolvable object in a light microscope. TEM forms a major analysis method in a range of scientific fields, in both physical and biological sciences. TEMs find application in cancer research, virology, materials science as well as pollution, nanotechnology and semiconductor research

[333]. The image (Fig. 1.17) of CNT decorated with metal nanoparticles is shown below.

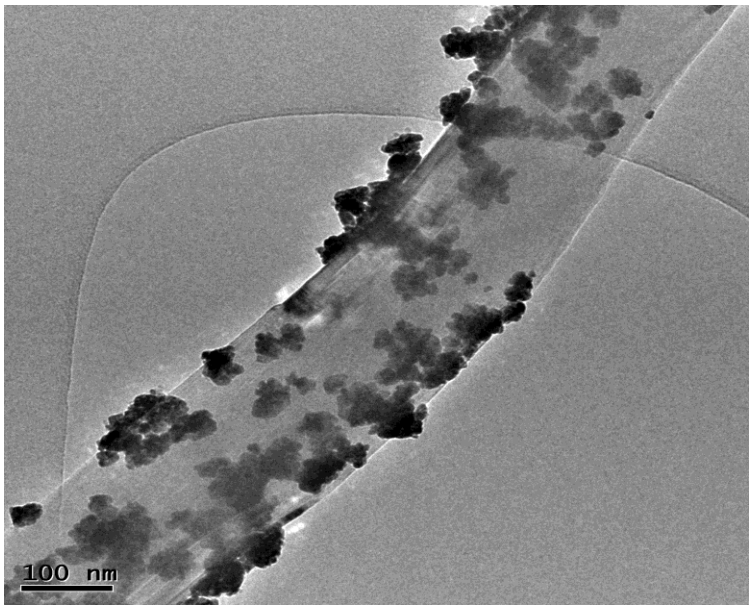

Figure 1.17: A Typical TEM Image of CNT decorated with metal nanoparticles.

1.17.5 Atomic force microscope

Atomic force microscope (AFM) or scanning force microscope (SFM) is a very high-resolution type of scanning probe microscope, with demonstrated resolution of fractions of a nanometer, more than 1000 times better than the optical diffraction limit. AFM is one of the foremost tools for imaging, measuring and manipulating matter at the nanoscale. The information is gathered by "feeling" the surface with a mechanical probe. Piezoelectric

elements that facilitate tiny but accurate and precise movements on (electronic) command enable the very precise scanning.

The AFM consists of a microscale cantilever with a sharp tip (probe) at its end that is used to scan the specimen surface (Fig. 1.18). The cantilever is typically silicon or silicon nitride with a tip radius of curvature on the order of nanometers. When the tip is brought into proximity of a sample surface, forces between the tip and the sample lead to a deflection of the cantilever according to Hooke's law. Typically, the deflection is measured using a laser spot reflected from the top surface of the cantilever into an array of photodiodes. A feedback mechanism is employed to adjust the tip-to-sample distance to maintain a constant force between the tip and the sample. The AFM can be operated in a number of modes, depending on the application. In general, possible imaging modes are divided into static (also called Contact) modes and a variety of dynamic (or non-contact) modes where the cantilever is vibrated [334].

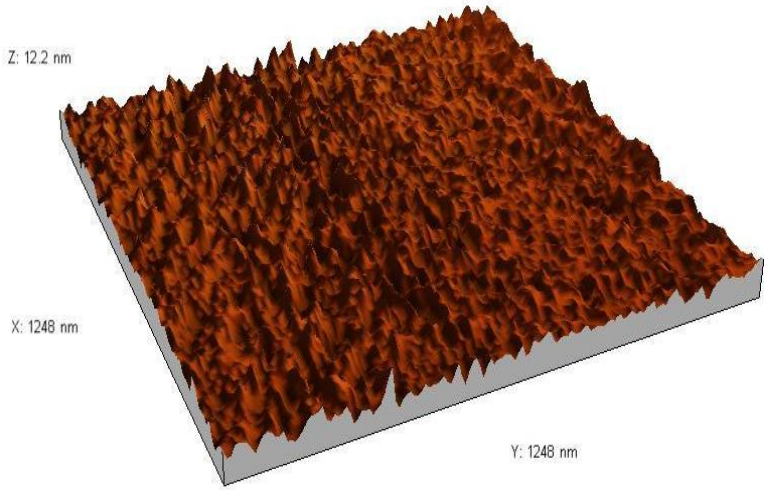

Figure 1.18: AFM three dimentional (3D) image of a nanomaterial growth on a modified electrode [334].

1.17.6 Energy Dispersive X-ray Spectroscopy (EDX)

Energy dispersive X-ray spectroscopy (EDS or EDX) is an analytical technique used for the elemental analysis or chemical characterization of a sample. It relies on the investigation of a sample through interactions between electromagnetic radiation and matter, analyzing X-rays emitted by the matter in response to being hit with charged particles. Its characterization capabilities is that, each element has a unique atomic structure allowing X-rays that are characteristic of an element's atomic structure to be identified uniquely from one another. The EDX spectrum of a particular sample is shown below [335].

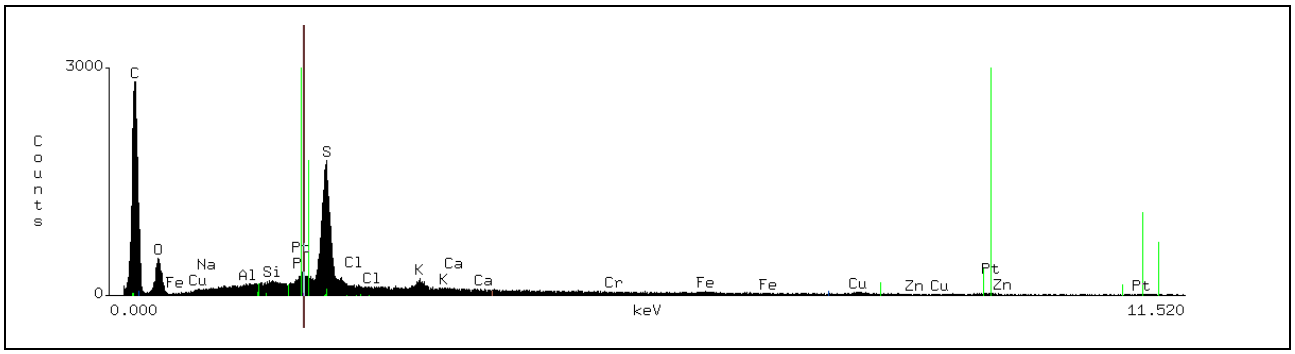

Figure 1.19: EDX profile of a material showing the possible elemental composition.

1.17.7 X-ray diffraction spectroscopy

X-ray diffraction (XRD) yields the atomic structure of materials and is based on the elastic scattering of X-rays from the electron clouds of the individual atoms in the system. The most comprehensive description of scattering from crystals is given by the dynamical theory of diffraction: Single-crystal X-ray diffraction is a technique used to solve the complete structure of crystalline materials, ranging from simple inorganic solids to complex macromolecules, such as proteins. Powder diffraction (XRD) is a technique used to characterise the crystallographic structure, crystallite size (grain size), and preferred orientation in polycrystalline or powdered solid samples. Powder diffraction is commonly used to identify unknown substances, by comparing diffraction data against a database maintained by the International Centre for Diffraction Data. It may also be used to characterize heterogeneous solid

mixtures to determine relative abundance of crystalline compounds and for determining strains in crystalline materials [336].

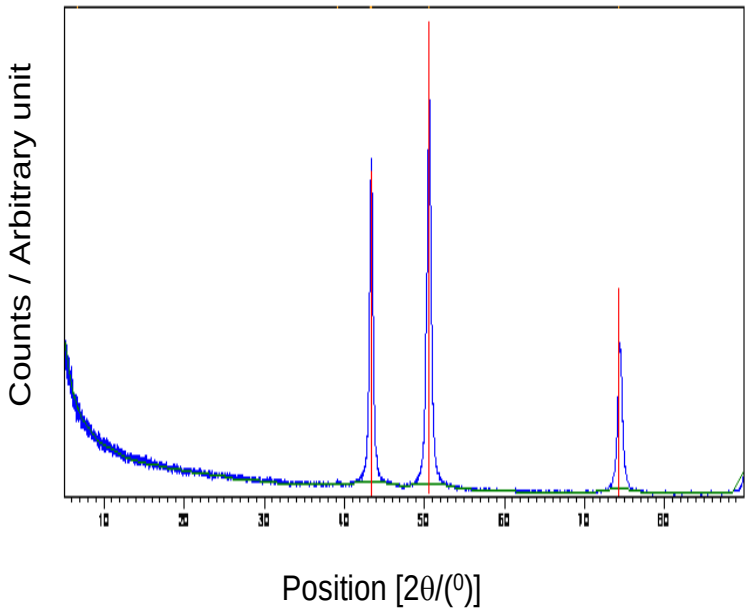

Figure 1.20: XRD spectrum of synthesised metal nanoparticles showing identified peaks of the metal at different 2θ position [336].

1.18 Background of the studied Analytes

The electrochemical oxidation of fuel cell molecules such as CH_3OH, HCOOH, and HCHO has been the field of intensive research for the development of direct fuel cell [337-341].

1.18.1 Methanol electrooxidation

Due to the problems associated with methanol which have already been mentioned in sections 1.10 and 1.11.2, intense efforts have been devoted towards investigating other fuel cell molecules such as formic acid and ethylene glycol.

1.18.2 Formic acid electrooxidation

Formic acid (FA) has been considered an alternative fuel cell molecule to methanol due to its advantages. The oxidation of formic acid commences at less positive potentials than that of methanol. The direct formic acid fuel cells (DFAFCs) are quite interesting for portable power applications. Unlike methanol, formic acid has a low crossover through the Nafion membrane and possesses a high kinetic activity. These unique characteristics of formic acid allow operating DFAFCs at higher voltages than DMFCs. Further, formic acid fuel cells run more efficiently at higher voltages and in practice, DFAFCs have about a factor of three to six higher power densities than DMFCs and can operate well at room temperatures [311, 342-345]. Formic acid aqueous solution is non-combustible and nonexplosive; its chemical properties are relatively benign at room temperature. It is recognized as safe and facile in handling and distribution compared with methanol. Consequently, formic acid is an emerging and a promising substitute for methanol [346, 347].

Proton exchange membrane (PEM) based direct formic acid fuel cells (DFAFCs) have recently attracted enormous attention, due to their unique advantages, such as (1) DFAFCs have a high theoretical open circuit potential, e.g. emf of 1.450V (compared to 1.229V for H_2-proton exchange membrane fuel cells and 1.190V for direct methanol fuel cells at room temperature; (2) formic acid is a non-toxic liquid fuel; (3) formic acid has a lower cross-over flux than methanol and ethanol; (4) although the neat energy density of formic acid (2086 Wh/L) is lower than that of methanol (4690 Wh/L), high concentrated formic acid can be used as fuel, e.g. 20M (70 wt%), compared to low concentrated methanol, e.g. 1–2 M, therefore, formic acid carries more energy per volume than methanol; (5) formic acid itself is an electrolyte, thus, it can facilitate proton transport within anode compartment [348-357].

Recent studies also demonstrate that DFAFC can be successfully used as an energy source for portable devices and microelectromechanical systems [343]. The electrocatalytic oxidation of formic acid is known to proceed via dehydrogenation and dehydration pathways [311]. The dehydrogenation reaction pathway is preferred to achieve high efficiency, as it does not involve the generation of poisoning intermediate species CO. It has been shown that formic acid oxidation on Pd surface follows the direct oxidation

pathway and CO-like intermediate does not form during the reaction [358-361].

1.18.3 Ethylene glycol electrooxidation

Among the different fuel cell molecules studied (methanol and formic acid) as model fuels; ethylene glycol (EG) was also fascinating to investigate due to its high solubility in aqueous solutions and relatively high reactivity [362]. The electrochemical oxidation of EG on platinum metal electrodes and catalysts has been receiving significant attention during the last decades, both as a model compound for studies of the adsorption and electrooxidation behavior of CO-containing organic species and due to its potential application as an attractive anodic fuel in direct oxidation fuel cells in acidic medium [363-370] and in alkaline solution [367, 371].

Recently, Peled et al. [372, 373] reported that methanol/oxygen and ethylene glycol/oxygen fuel cells equipped with a new nanoporous proton-conducting membrane and using PtRu/C (atomic ratio of 1:1) as anode catalyst provided a maximum power density of 400 and 300 mW cm^{-2}, respectively, which puts ethylene glycol in direct competition with methanol as a promising candidate for practical electric vehicles and stationary applications Kelaidopoulou et al. [374, 375] observed that the addition of

ruthenium and tin onto platinum dispersed in polyaniline increases the electro-oxidation of ethylene glycol in acid medium.

1.18.4 Oxygen reduction reaction (ORR)

Electrochemical reduction of oxygen (O_2) has been a pivotal subject for extensive studies in view of its importance in achieving the current density needed for practical applications of electrochemical energy conversion systems such as fuel cells and metal-air batteries and in the detection of oxygen levels in research fields of fish culture, biochemistry, neuroscience, physiology, electrochemical caustic concentrators, air depolarized cathodes, and oxidant production [376-383]. Platinum is regarded as the best ORR catalyst for low temperature fuel cells because it provides the lowest overpotential and the highest selectivity towards direct oxygen reduction to water [384]. However, in spite of the extensive research in this field, full commercialization of fuel cells has been hampered by the sluggish reaction dynamics as well as the high cost and limited supply of platinum. But even on pure Pt, potential in excess of 0.3 V are lost from the thermodynamic potential for ORR because of competing water activation reaction and sluggish kinetics [384].

Researchers have found that gold nanoparticles electrodeposited on bulk Au and Pt electrodes demonstrate electrocatalytic effects to oxygen

reduction as indicated by a significant positive shift of the oxygen reduction peak potential and a concurrent increase of the peak current [385-387]. Rather than the use of bulk metals (such as platinum and ruthenium) for ORR, research direction is now geared towards the use of their molecular complexes or nanoparticles [388]. Metal-phthalocyanine (MPc) complexes represent a unique class of N4-macrocyclic metal compounds that have applications in various fields already mentioned in section 1.7, and in ORR [389-391].

MPc is an interesting kind of compound with a conjugated ligand and a transition central metal ion. A delocalized conjugated π bond in the molecule makes MPc liable to oxidation and reduction [392-394], which is an advantage for the compound to be used as electrocatalysts [395]. MPc compounds used as catalysts for ORR have been paid much attention [396-406]. N4-macrocyclic complexes of transition metals, especially of Fe or Co, exhibit remarkable catalytic activity towards oxygen reduction reaction. It has been established that most of the monomeric cobalt porphyrins (capable of adsorbing irreversibly on glassy carbon, graphite or gold electrodes) can catalyze the reduction of oxygen only through two-electrons pathway to produce H_2O_2 [407, 408].

CNT-supported MPc compounds used as catalysts for ORR have attracted much interest [409-411]. It has been reported that nitrogen atoms in the backbone strongly affect the properties of MPc derivatives [412-416]. Few work related to the properties of CNTs decorated with diverse nitrogen atoms in the backbone of MPc derivatives for ORR has been shown. In an attempt to show the effects of nitrogen atoms in the backbone of CoPc derivatives on the electrochemical performance of MWCNT-supported CoPc derivatives, Z. Xu et al prepared MWCNT-supported CoPc, cobalt tetrapyridinoporphyrazine (CoTAP) and cobalt tetrapyrazinoporphyrazine (CoPTpz) assemblies, and used them as catalysts for ORR [417]. Despite the popularity of ruthenium-based electrocatalysts for ORR, as elegantly reviewed recently by Lee and Popov [382], the use of ruthenium phthalocyanine (RuPc) complexes in ORR is virtually unknown.

The importance of the reduction of oxygen to water in fuel cells and metal/air batteries is well-known. The oxygen reduction reaction proceeds either as a direct four electron process or a two-electron process [418, 419]. It is well known that molecular oxygen can be reduced on the chemically modified electrodes by a two-electron process to H_2O_2 or via a direct four-electron reduction mechanism to H_2O. Usually oxygen is reduced in a two electron process to hydrogen peroxide and this is often followed at more negative potentials by a further two electron reduction of hydrogen peroxide

to water. From the viewpoint of fuel cell application the four electron reduction of water is more desirable.

1.19 Problem statement

Fuel cell research based on use of fuel cell molecules and alcohols has attracted great interest worldwide. This is due to their promising potential replacement for batteries in low power electronic devices such as laptops and cellphones. Most works for fuel cell development have been devoted to methanol and ethanol. The electrooxidation of methanol (MeOH) on platinum (Pt) and on platinum based electrocatalysts has been extensively studied during the last decade. Platinum catalyst has been found to have high activity for methanol oxidation. However, previous studies revealed that Pt undergoes surface poisoning by strongly adsorbed reaction intermediates, carbon monoxide (CO) that blocks the active sites [1]. Due to the high cost and limited supply of platinum, the development of non-Pt based, cheap and abundantly available electrocatalyst for oxygen reduction reaction (ORR) is essential for the commercialization of the fuel cells.

1.20 Hypothesis

In an attempt to overcome the drawbacks of Pt, nanoparticulate alloys of Pt and Ruthenium (Ru) have been investigated. This combination offered an improved tolerance to CO [2].

Since most work has been carried out on methanol fuel for a direct methanol fuel cell (DMFC) due to its potential application in fuel cells, in this study alternative fuels have been investigated. The electro oxidation of ethylene glycol (EG) and formic acid (FA) have been investigated with the intention of overcoming the drawbacks of methanol such as adsorption and electro oxidation behavior of CO-containing species. These chosen fuel cell (FC) molecules have been reported to exhibit properties that could make them possible alternatives to methanol and ethanol; for example EG is highly soluble in aqueous solutions and relatively reactive [254]. Weber et al have reported FA to be slightly more efficient than methanol on Pt/Ru catalysts [236]. It is expected that electrooxidations of EG and FA would offer a better solution to the problems associated with MeOH oxidation.

1.21 Aims and Objectives

The main aim of the study was the preparation of novel and effective platinum group metal (PGM) based nanocatalysts supported on carbon nanotube based electrode for potential applications in alcohol and formic acid fuel cells and oxygen reduction reaction (ORR). To achieve this aim, the study has the following objectives:

- To explore the unique physical, chemical and electronic properties of CNTs to tackle the CO poisoning problems associated with carbon black supported Pt-based nanocatalysts (Pt/C) used in FCs.
- To compare the electrocatalytic behaviour of Pt-based nanocatalysts made by both electrodeposition and chemical synthesis, and integrated with fMWCNT for applications in FCs.
- To establish the heterogenous electron transfer kinetics and adsorption reactions of these FC molecules (MeOH, EG and FA) during electrocatalysis.
- To investigate the electrocatalytic properties of CNT-based electrode towards oxygen reduction reactions (ORRs).

1.22 Structure of the thesis:

Chapter 1 (Introdution) provides information on the general overview of the thesis, overview of electrochemistry, voltammetric techniques, electrochemical impedance spectroscopy, chemically modified electrodes, electrode modification techniques, metallophthalocyanine, fuel cells, microscopy and spectroscopy techniques and the analytes (MeOH, EG, FA and oxygen) used in this work as analytical probes.

Chapter 2 (Experimental work) summarizes the methods employed in functionalizing carbon nanotubes, synthesizing metallophthalocyanine, methods used in preparing carbon nanotube based electrodes and the techniques used for characterization.

Chapter 3-6 (Results and discussions) presents the experimental results and gives an interpretation of the data obtained.

Chapter 7 (Conclusion) summarizes the main finding of the study and future work.

1. C.Y. Chen, P. Yang, J. Power Sources 2002, 123, 37.
2. M. Gotz and H. Wendt, Electrochim. Acta 43 (1998) 363.
3. K.H. An, W.S. Kim, Y.S. Park, J.M. Moon, D.J. Bae, S.C. Lim, Y.S. Lee and Y.H. Lee Adv. Funct. Mater. 11 (2001) 387.
4. P. Serp, M. Corrias, P. Kalck, Appl. Cat. A: General 253 (2003) 337.
5. G. Wu, Y.S. Chen, and B. Q. Xu, Electrochem. Commun. 7 (2005) 1237.
6. K. Jurkschat, S.J. Wilkins, C.J. Salter, H.C. Leventis, G.G. Wildgoose, L. Jiang, T.G. J. Jones, A. Crossley and R.G. Compton, Small 2 (2006) 95.
7. Z.L. Liu, X.H. Lin, J.Y. Lee, W. Zhang, M. Han, L.M. Gan, Langmuir 18 10 (2001) 4054.
8. W.Z. Li, C.H. Liang, J.S. Qiu, W.J. Zhou, H.M. Han, Z.B. Wei, G.Q. Sun, Q.Xin, Carbon 40 (2002) 787.
9. B. Rajesh, V. Karthik, S. Karthikey, K.R. Thampi, J.M. Bonard, B. Viswanathan, Fuel 80 (17) (2002) 2177.
10. P.A. Christensen and A. Hamnett, Techniques and Mechanisms in Electrochemistry, Blackie Academic & Professional, An Imprint Of Chapman & Hall, Glasgow (1994).
11. D.T. Sawyer, A. Sobkowiak, J. L. Roberts Jr, Electrochemistry for Chemists, 2nd editions, John Wiley and Sons Inc. New York (1995).
12. V.F. Bagotsky, Fundamentals of Electrochemistry, 2nd Edition, John Wiley and Sons Inc. New Jersey (2006).
13. K. Rajeshwar, J. G. Ibanez, Environmental Electrochemistry, Elsevier Science and Technology Book ISBN: 0125762607 (1997).
14. J. Wang, Analytical Electrochemistry, 2nd Edition, VCH Publishers Inc. New York (2000).

15. P.M.S. Monk, Fundamentals of Electroanalytical Chemistry, John Wiley and Sons Ltd, Chichester, New York (2001).
16. P.T. Kissinger, C.R. Preddy, R.E. Shoup, W.R. Heineman in Laboratory Techniques in Electroanalytical Chemistry 2nd ed.,P.T. Kissinger and W.R. Heineman, Eds.; Marcel Dekker Inc., New York (1996).
17. J. Wang, Analytical Electrochemistry, VCH Publishers Inc. New York (1994).
18. D.B. Hibbert, Introduction to Electrochemistry, Macmillan, London (1993).
19. A.E. Kaifer, M. Gómez-Kaifer, Supramolecular Electrochemistry, Wiley-VCH, New York (1999).
20. J. Wang, Analytical Electrochemistry, 2nd Edition, Wiley-VCH, (2000).
21. A.J. Bard, L.R. Faulkner, Electrochemical methods:Fundamental and applications, 2nd ed., John Wiley and Sons, Hoboken, NJ, (2001).
22. M.A.B. Christopher, M.O.B. Ana, Electrochemistry, Principles, methods and Applications, Oxford University Press Inc., New York (1994).
23. G. Inzelt, Kinetics of electrochemical reactions. In: Scholz F (ed), Electroanalytical methods Springer, Berlin (2002) 38.
24. P.A. Christensen, A. Hamnet, Techniques and Mechanisms in Electrochemistry, 1st ed, Blackie Academic and Professional, London (1994).
25. B.S. Flaven, J. Yu, A.V. Ellis, J.G. Shapter, Electrochim. Acta 54 (2009) 3191.
26. J.E.B. Randles, Trans. Faraday Soc. 44 (1948) 327.
27. R.S. Nicholson, I. Shain, Anal. Chem. 36 (1964) 1351. A.

28. A. Sevcik, Coll. Czech. Chem. Comm. 13 (1958) 349.
29. J.Wang, Analytical Electrochemistry, 3rd ed, Wiley-VCH John Wiley & Sons Publishers Inc., Hoboken, New Jersey (2006).
30. L.F. Maria, G. Roland, N. Leif, J. Electroanal. Chem. 269 (1989) 27.
31. R.G. Compton, C.E. Banks, Understanding Voltammetry, World Scientific Publishing Co. Pte. Ltd (2007).
32. R.D. Rocklin, R.W. Murray, J. Phys. Chem. 85 (1981) 2104.
33. E. Barsoukov, J.R. Macdonald, Impedance Spectroscopy, 2nd Edition, Wiley and Sons Inc., New Jersey (2005).
34. J.R. Macdonald, Ed., Impedance Spectroscopy Emphasizing Solid Materials and Systems, Wiley/Interscience, New York, 1987.
35. E. Katz, I. Wilner, in: Ultrathin Electrochemical Chemo- and Biosensors. Technology and Performance, V.M. Mirsky Ed. Springer- Verlag, New York, 2004, pp. 68–116, Chapter 4.
36. J.R. Macdonald, W.B. Johnson in : E. Barsoukov, J.R. Macdonald (Eds.), Impedance Spectroscopy, 2nd ed., John Wiley and Sons Inc., 2005.
37. T. Rawling, A. McDonagh Coordin. Chem. Rev. 251 (2007) 1128.
38. N.B. Mckeown. Phthalocyanine materials: synthesis, structure and function. Cambridge University Press (1998).
39. C.J. Claessens, W.J. Blau, M.Cook, M. Hanack, R.J.M. Nolte, T. Torres, et al. Monatshefte für Chemie (2001) 132 3.
40. J.S. Simon, J.J. Andre, Molecular Semiconductors, Springer, Berlin, Chapter III, 1985. M.I. Newton, T.K.H. Starke, M.R. Willis, G. McHale, Sens. Actuators B 67 (2000) 307.
41. S. Chakane, A. Gokarna, S.V. Bhoraskar, Sens. Actuators B 92 (2003) 1.
42. C.C. Leznoff and A.B.P. Lever eds.1, Phthalocyanines,Properties and Applications, VCH Publisher, New York (1993).

43. J.D. Spikes, Photochem. Photobiol. 43 (1986) 691, I. Rosenthal, Photochem. Photobiol. 53 (1991) 859.
44. K.K. Canon, Japanese Patent 59191775 (1984).
45. M. Walter, US Patent 4088569 (1978).
46. D. Xie, W. Pan, Y.D. Jiang, Y.R. Li, Mater. Lett. 57 (2003) 2395.
47. K. Petrisch, J.J. Dittmer, E.A. Marseglia, R.H. Friend, A. Lux, G.G. Rozenberg, S.C. Moratti, Holmes, Solar Energy Mater. Solar Cells 61 (2000) 63.
48. T.H. Wei, T.H. Huang, Opt. Quantum Electron. 28 (1996) 1495.
49. I. Rosenthal, Photochem. Photobiol. 53 (1991) 859.
50. J. Griffiths, J. Schofield, M. Wainwright, S.B. Brown, Dyes and Pigments 33 (1997) 65.
51. A.Visona, A. Angelini, S. Gobbo, A. Bonanome, G. Thiene, A. Pagnan, D. Tonello, E. Bonandini, G. Jori, J. Photochem. Photobiol. B: Biol. 57 (2000) 94.
52. J.H. Weber, D.H. Busch, Inorg. Chem. 4 (1965) 469.
53. V. Duarte, D. Gasparutto, L.F. Yamaguchi, J.L. Ravanat, G.R. Martinez, M.H.G. Medeiros, P.D. Mascio, J. Cadet, J. Am. Chem. Soc. 122 (2000) 12622.
54. R.D. Patent, 2,128,842 (1972) Chem. Abs. 78 (1973) 79028.
55. J. Ma, Y. Liu, P. Zhang, J. Wang, Electrochem. Commun. 10 (2008) 100.
56. D. Worhle, M. Kirschmann, N.I. Jaeger, J. Electrochem. Soc. 132 (1985) 1150.
57. J. H. Zagal, S. Griveau, J.F. Silva, T. Nyokong, F. Bediouib, Coord. Chem. Rev. 254 (2010) 2755.
58. K. Hanabusa, H. Shirai. Catalytic functions and application of metallophthalocyanine polymers. In: Leznoff CC, Lever ABP,

editors. Phthalocyanines: properties and applications, Vol.2. New York: VCH; (1993) 197.

59. M. Kimura, H. Shirai. Enzyme-like catalytic reactions of metallophthalocyanines and polymeric metallophthalocyanines. In: Kadish KM, Smith KM, Guilard R, editors. The porphyrin handbook, applications of phthalocyanines. Amsterdam: Academic Press; (2003). 151.
60. N.B McKeown. Phthalocyanine materials: synthesis structure and function. Cambridge: Cambridge University Press; (1998).140.
61. A.Sorokin, J.L. Se´ ris, B. Meunier. Science (1995) 268 1163.
62. X. Tao, W. Ma, T. Zhang, J. Zhao Angew Chem Int Ed (2001) 40 3014.
63. G. de la Torre, W. Blau, T. Torres. Nanotechnol. (2003) 14 765.
64. Z.L. Yang, H.Z. Chen, L. Cao, H.Y. Li, M. Wang. Mater. Sci. Eng. B (2004) 106.73.
65. B. Ballesteros, G. de la Torre, C. Ehli, GMA Rahman, F. Agullo´ - Rueda, D.M. Guldi, et al. J. Am. Chem. Soc. (2007) 129 5061.
66. J.H. Zagal, S. Griveau, K.I. Ozoemena, T. Nyokong, F. Bedioui J. Nanosci. Nanotechnol. (2009) 9 2201.
67. M. Siswana, K.I. Ozoemena, T. Nyokong Sensors (2008) 8 5096.
68. M. Siswana, K.I. Ozoemena, T. Nyokong. Electrochim Acta (2006) 52 114.
69. J. Pillay, K.I. Ozoemena Electrochim Acta (2007)52 3630.
70. B.O. Agboola, K.I. Ozoemena, T. Nyokong T, T. Fukuda, N. Kobayash, Carbon (2010) 48 763.
71. L. Gan, R. Lv, H. Du, B. Li, F. Kang Carbon (2009) 47 1833.
72. B. Yoon, C.M. Wai, J. Am. Chem. Soc. 127 (2005) 17174.
73. X. Pan, Z. Fan, W. Chen, Y. Ding, H. Luo, X. Bao, Nat. Mater. 6 (2007) 507.

74. H. Vu, F. Gonc¸alves, R. Philippe, E. Lamouroux, M. Corrias, Y. Kihn, J. Catal. 240 (2006) 18.
75. A.Kongkanand, K. Vinodgopal, S. Kuwabata, P.V. Kamat J. Phys. Chem B 110 (2006) 16185.
76. A.Solhy, B.F. Machado, J. Beausoleil, Y. Kihn, F. Gonc¸alves, MFR Pereira, Carbon 46 (2008) 1194.
77. D. Guo, X. Qiu, L. Chen, W. Zhu, Carbon (2009) 47 1680.
78. H.B. Zhang, X. Dong, G.D. Lin, X.L.Liang, H.Y.Li, Chem Commun (2005) 5094.
79. L. Wangyang, Li Nan, S. Bao, W. Chen, Y. Yao, CARBON 49 (2011) 1699.
80. R. Jasinski, Nature 201 (1964) 1212.
81. R. Jasinski, J. Electrochem. Soc. 112 (1965) 526.
82. J. Ma, Y. Liu, P. Zhang, J. Wang, Electrochem. Commun. 10 (2008) 100.
83. J. Sorokin, S. De Suzzonl-Dezard, D.Poull-ain, J.P. Noel, B. Meunier, J. Am. Chem. Soc.118 (1996) 7418.
84. A.Sorokin, B. Meunier,J. Chem.Soc. Chem. Commun. (1991) 1799.
85. A.Sorokin, J.L. Seris, B. Meubier, Science 268 (1995) 1163.
86. N.Grootboom, T.Nyokong, J.Mol. Catal.179 (2002) 113.
87. A.L.Thomas, Phthalocyanine Research and Applications, CRC Press, Boca Raton, Fla, (1990).
88. K.M. Kadish, K.M.Smith,R. Guilard (Eds.), The Porphyrin Handbook, vol. 16-20,Academic Press,New York, (2003).
89. C.C.Leznoff, A.B.P. Lever (Eds.), Phthalocyanines: Properties and Aplications, VCH, New York, (1989).
90. K.Kasuga, M. Tsutsui, Coord. Chem. Rev.32 (1980) 67.
91. G.Wilkinson, R.D.Gillard,J.A. McCleverty (Eds.), Comprehensive Coordination Chemistry:The synthesis, Reactions,Properties &

Applications of Coordination Compounds, Pergamon Press, Oxford, (1987).

92. J.A. McCleverty, T.J.Meyer (Eds.), Comprehensive Coordination Chemistry. II: From biology to nanotechnology, vol. 5, Elsevier Ltd., Oxford, (2004).
93. F.H. Moser, A.L. Thomas, The Phthalocyanines, vols. 1 and 2, CRC Press, Boca Raton, FL, 1983, Katalyse und Phthalocyaninen, M. Kropf, F. Steinbach (Eds.), Georg Thieme, Verlag Stuttgart, (1973).
94. J. Manassen, Catal. Rev. Sci. Eng. 9 (1974) 223, L.J. Bocler, in: G.A. Melson (Ed.), Coordination Chemistry of Macrocyclic Compounds, Plenum Press, New York, (1979).
95. J. Simon, J.-J. Andre, Molecular Semiconductors, Springer, Berlin, 1985 (Chapter 3).
96. D. Worhrle, D. Meissner, Organic solar cells, Adv. Mater. 3 (1991) 129; C.W. Tang, Appl. Phys. Lett. 60 (1986) 1047.
97. R. Zhou, F. Josse, W. Gopel, Z. Ozturk, O. Bekaroglu, Appl. Organomet. Chem. 10 (1996) 557.
98. J. Spadavecchiab, G. Ciccarellaa, R. Rellab, Sens. Actuators B 106 (2005) 212.
99. K.J. Balkus Jr., M. Eissa, R. Levado, J. Amer. Chem. Soc. 117 (1995) 10753.
100. R.F. Parton, I.F.J. Vankelecom, M.J.A. Casselman, C.P.Bezoukhanova, J.B. Uytterhoeven, P.A. Jacobs, Nature 370 (1994) 541.
101. R.F. Parton, I.F.J. Venkelecom, D. Tas, K.B.M. Janssen, P.-P. Knops-Gerrits, P.A. Jacobs, J. Mol. Catal. A: Chem. 113 (1996) 283.
102. R.F. Parton, P.E. Neys, P.A. Jacobs, R.C. Sosa, P.G. Rouxhet, J. Catal. 164 (1996) 341.

103. A.B. Sorokin, A. Tuel, Catal. Today 57 (2000) 45.
104. S. Zecevic, B. Simic-Glavaski, E. Yeager, A.B.P. Lever, P.C. Minor, Spectroscopic and electrochemical studies of transition metal phthalocyanines. Part V. J. Electroanal. Chem. 196 (1985) 339.
105. J.H. Zagal, Coord. Chem. Rev. 119 (1992) 89, M.K. Halbert, R.P. Baldwin, Anal. Chem. 57 (1985) 591.
106. W.J. Todd, F. Bailly, J. Pavez, P.W. Faguy, R.P. Baldwin, R.M. Buchanan, J. Am. Chem. Soc. 120 (1998) 4887.
107. Y. Tse, P. Janda, H. Lam, J. Zhang, W.J. Pietro, A.B.P. Lever, J. Porphyr. Phthalocya. 1 (1997) 3.
108. J.H. Zagal, M. Gulppi, M. Isaacs, G. Cardenas-Jiron, M.J. Aguirre, Electrochim. Acta 44 (1998) 1349.
109. S. Griveau, J. Pavez, J.H. Zagal, F. Bedioui, J. Electroanal. Chem. 497 (2001) 75. S. Griveau, F. Bedioui, Electroanal. 13 (2001) 253.
110. W. Jingjie, T. Haolin, P. Mu, W. Zhaohui Electrochim. Acta 54 (2009) 1473.
111. Y. Lu, R.G. Reddy, Int. J. Hydrogen Energy 33 (2008) 3930.
112. S. Sarangapani, B. Morriseau, Electrochem. Soc. Mtg., Abstract No. 476. Reno, Nevada, (1995).
113. J.S. Bett, H.R. Kunz, A.J. Aldykiewicz Jr., J.M. Fenton,W.F. Baileyb, D.V. McGrath, Electrochim. Acta 43 (1998) 3645.
114. N. Martz, C. Roth, H. Fuess, J. Appl. Electrochem. 35 (2005) 85.
115. J.A.R. van Veen, J.F. van Baar, C.J. Kroese, J.G.F. Coolegem, N. de Wit, H.A. Colijn, B. Bunsenges, Phys. Chem. 85 (1981) 693.
116. F. van den Brink, E. Barendrecht, W. Visscher, Rec. J. Roy. Neth. Chem. Soc. 99 (1980) 253.
117. J.S. Bett, H.R. Kunz, A.J. Aldykiewicz Jr., J.M. Fenton,W.F. Baileyb, D.V. McGrath, Electrochim. Acta 43 (1998) 3645.

118. T. Okada, Y. Suzuki, T. Hirose, T. Ozawa, Electrochim. Acta 49 (2004) 385.
119. Z. He, J. Chen, D. Liu, H. Zhou, Y. Kuang, Diam. & Relat. Mater. 13 (2004) 1764.
120. V. Baglio, A. Di Blasi, C. D'Urso, V. Antonucci, A. S. Arico, R. Ornelas, D. Morales-Acosta, J. Ledesma-Garcia, L. A. Godinez, L. G. Arriaga and L. Alvarez-Contreras, J. Electrochem. Soc. 155 (2008) B829.
121. V. Selvaraj, M. Vinoba, M. Alagar, J. Colloids Interf. Sci. 322 (2008) 537.
122. V. Selvaraj, M. Alagar, Nanotechnol. 19 (2008) 045504.
123. H. Wang, Z. Jusys, R.J. Behm, J. Electroanal. Chem. 595 (2006) 23.
124. W. Hauffe, J. Heitbaum, Electrochim. Acta 23 (1978) 299.
125. M.S. Ureta-Zañartu, A. Alarcón, G. Muñoz, C. Gutiérrez, Electrochim. Acta 52 (2007) 7857.
126. A.S. Adekunle, K.I. Ozoemena, J. Solid State Electrochem. 12 (2008) 1325.
127. Craig E. banks, R.G. Compton, Analyst 131 (2006) 15.
128. X. Ji, C.E. Banks, A. Crossley, R.G. Compton, ChemPhyChem 7 (2006) 1337.
129. R.R. Moore, C.E. Banks, R.G. Compton, Analyst 129 (2004) 755.
130. R.H. Baughman, A.A. Zakjidov, W.A.d. Heer, Science 297 (2002) 787.
131. Y. Mu, H. Liang, J. Hu, L. Jiang, L. Wan, J. Phys. Chem. B 109 (2005) 22212.
132. L.V. Radushkevich, VM Lukyanovich, Zurn Fisic Chim 26 (1952) 88.
133. S. Iijima, Nature 354 (1991) 56.
134. S Iijima, T. Ichihashi Nature 363 (1993) 603.

135. D.S. Bethune, C.H. Kiang, M.S. De Vries, G. Gorman, R. Savoy, J. Vazquez, Nature 363 (1993) 605.
136. P.M. Ajayan, S. Iijima, Nature 361 (1993) 333.
137. T. Hertel, R. Martel, P. Avouris, J. Phys. Chem. B 102 (1998) 910.
138. S.S. Wong, J.D. Harper, P.L. Lansbery, C.M. Lieber, J. Am. Chem.Soc. 120 (1998) 603.
139. A.C. Dillon, K.M. Jones, T.A. Bekkedahl, C.H. Kiang, D.S. Bethune,M.J. Heben, Nature 386 (1997) 377.
140. N. Rajalakshmi, K.S. Dhathathreyan, B.C. Sathish Kumar, A.Govinda Raj, Electrochim. Acta 45 (2000) 4511.
141. G. Gundiah, A. Govindaraj, N. Rajalakshmi, K.S. Dhathathreyan, C.N.R. Rao, J. Mater. Chem. 13 (2003) 209.
142. H. Dai, J.H. Hafner, A.G. Rinzler, D.T. Colbert, R.E. Smalley, Nature 384 (1996) 147.
143. S. Hynek, W. Fuller, J. Bentley, Int. J. Hydrogen Energy 22 (1997) 601.
144. K.H. An, W.S. Kim, Y.S. Park, J.M. Moon, D.J. Bae, S.C. Lim, Y.S. Lee, Y.H. Lee, Adv. Funct. Mater. 11 (2001) 387.
145. P.M. Ajayan, O.Z. Zhou, 80 (2001) 391.
146. G. Che, B.B. Lakshmi, C.R. Martin, E.R. Fisher, Langmuir 15 (1999) 750.
147. B. Rajesh, K.R. Thampi, J.M. Bonard, B. Viswanathan, J. Mater.Chem. 10 (2000) 1757.
148. R. M. Lago, S.C. Tsang, K.L. Lu, Y.K. Chen, M.L.H. Green, J. Chem. Soc., Chem. Commun. (1955) 1355.
149. L.M. Ang, T.S.A. Hor, G.Q. Xu, C.H. Tung, S.P. Zhao, J.L.S. Wang, Carbon 45 (2000) 134.
150. Rubianes, G.A. Rivas, Electrochem. Commun. 9 (2007) 480.

151. F. Valentini, A. Amine, S. Orlanducci, M.L. Terranova, G. Palleschi, Anal. Chem. 75 (2003) 5413.
152. N. Maleki, A. Safavi, F. Tajabadi, Anal. Chem. 78 (2006) 3820.
153. R.S. Chen, W. Huang, H.Tong, Z. Wang, J. Cheng, Anal. Chem. 75 (2003) 6341.
154. A.Abbaspour, A. Izadyar, Talanta 71 (2007) 887.
155. Y. Xing, J. Phys. Chem. B108 (2004) 19255.
156. K.I. Han, J.S. Lee, S.O. Park, S.W. Lee, Y.W. Park, H. Kim, Electrochim. Acta 50 (2004) 791.
157. D.J. Guo, H.L. Li, J. Electroanal. Chem. 573 (2004) 197.
158. G. Wu, Y.S. Chen, and B. Q. Xu, Electrochem. Commun. 7 (2005) 1237.
159. K. Jurkschat, S.J. Wilkins, C.J. Salter, H.C. Leventis, G.G. Wildgoose, L. Jiang, T.G. J. Jones, A. Crossley, R.G. Compton, Small 2 (2006) 95.
160. H. R. Zare, N. Nasirizadeh, F. Chatraei, S. Makarem, Electrochim. Acta 54 (2009) 2828.
161. J. Wang, M. Musameh, Analyst 11 (2003) 1382.
162. M. Musameh, J. Wang, A. Merkoci, Y. Lin, Electrochem. Commun. 4 (2002) 743.
163. Z. Wang, Q. Liang, Y. Wang, G. Luo, J. Electroanal. Chem. 540 (2003) 129.
164. F.H. Wu, G.C. Zhou, X.W. Wei, Electrochem. Commun. 4 (2002) 690.
165. H. Luo, Z. Shi, N. Li, Z. Gu, Q. Zhuang, Anal. Chem. 73 (2001) 915.
166. J. Wang, M. Mosameh, Y. Lin, J. Am. Chem. Soc. 125 (2003) 2408.
167. C.Y. Chen, P. Yang, J. Power Sources 123 (2002) 37.
168. M. Gotz, H. Wendt, Electrochim. Acta 43 (1998) 3637.

169. G. Wu, Y.S. Chen, B.Q. Xu, Electrochem. Commun. 7 (2005) 1237.
170. Z.B. He, J.H. Chen, D.Y. Liu, H.H. Zhou, Y.F. Kuang, Diam. Relat. Mater. 13 (2004) 1764.
171. K. Jurkschat, S.J. Wilkins, C.J. Salter, H.C. Leventis, G.G. Wildgoose, L. Jiang, T.G.J. Jones, A. Crossley, R.G. Compton, Small 2 (2006) 95.
172. K.H. An, W.S. Kim, Y.S. Park, J.M. Moon, D.J. Bae, S.C. Lim, Y.S. Lee, Y.H. Lee, Adv. Func. Mater. 11 (2001) 387.
173. Y.C. Xing, J. Phys. Chem. B 108 (2004) 19255.
174. T. Matsumoto, T. Komatsu, K. Arai, T. Yamazaki, M. Kijima, H. Shimizu, Y. Takasawa, J. Nakamura, Chem. Commun. 7 (2004) 840.
175. Y.L. Yao, Y. Ding, L.S. Ye, X.H. Xia, Carbon 44 (2006) 61.
176. C.H. Liang, Z.L. Li, J.S. Qiu, C. Li, J. Catal. 211 (2002) 278.
177. J. Prabhuram, T.S. Zhao, C.W. Wong, J.W. Guo, J. Power Sources 134 (2004) 1.
178. C. Zhou, S. Kumar, C.D. Doyle, J.M. Tour, Chem. Mater. 17 (2005) 1997.
179. J.J. Niu, J.N. Wang, Electrochim. Acta 53 (2008) 8058.
180. H. Shi, Electrochim. Acta 41 (1996) 1633.
181. S.C. Roy, P.A. Christensen, A. Hamnett, K.M. Thomas, V.Trapp, J. Electrochem. Soc. 143 (1996) 3073.
182. J. Wang, M. Li, Z. Shi, N. Li, Z. Gu, Electrochim Acta 47 (2001) 651.
183. H.X. Luo, Z.J. Shi, N.Q. Li, Z.N. Gu, Q.K. Zhuang, Anal. Chem. 73 (2001) 915.
184. R.T. Kachoosangi, G.G. Wildgoose, R.G. Compton, analytica chimica acta 618 (2008) 54.

185. U.A. Paulus, U. Endruschat, G.J. Feldmeyer, T.J. Schmidt, H. Bonnemann, R.J. Behm, J. Catal. 195 (2000) 383.
186. T. Frelink, W. Visscher, J.A.R. Van Veen, Electrochim. Acta 39 (1994) 1871.
187. K. Amine, K. Yasuda, H. Takenaka, Ann. Chim. Sci. Mater. 23 (1998) 331.
188. O. Antoinea, Y. Bultel, R. Durand, J. Electroanal. Chem. 499 (2001) 85.
189. V. Rao, P.A. Simonov , E.R. Savinova , G.V. Plaksin, S.V. Cherepanova, G.N. Kryukova, J. Power Sources 145 (2005) 178.
190. Z.B. Wang, G.P. Yin, P.F. Shi, Carbon 44 (2005) 133.
191. Z. Zhou, S. Wang, W. Zhou, G. Wang, L. Jiang, W. Li, Chem. Commun. (2003) 394.
192. Y. Liang, H. Zhang, B. Yi, Z. Zhang, Z. Tan, Carbon 43 (2005) 3144.
193. J. Su, G. Wang, H. Deng, X. Fan, J. Funct. Polym. 2 (2002) 122
194. W.Z. Li, C.H. Liang, W.J. Zhou, J.S. Qiu, Z.H. Zhou, G.Q. Sun, Q.Xin, J. Phys. Chem. B 107 (2003) 6292.
195. G. Wu, Y.S. Chen, B.Q. Xu, Electrochem. Commun. 7 (2005) 1237.
196. X.S. Zhao, W.Z.Li, L.H. Jiang, W.J. Zhou, Q. Xin, B.L. Yi, G.Q. Sun, Carbon 42 (2004) 3263.
197. S. Litster, G. McLean, J. Power Sources 130 (2004) 61.
198. T. Matsumoto, T. Komatsu, H. Nakano, K. Arai, Y. Nagashima, E. Yoo, Catal. Today 90 (2004) 191.
199. O.A. Petrii, J. Solid State Electrochem. 12 (2008) 609.
200. K. Ruth, M. Vogt, R. Zuber, In: W. Vielstich, H.A. Gasteiger, A. Lamm, editors. Handbook of fuel cells e fundamentals, technology and applications, vol. 3. Chichester (UK): John Wiley & Sons, Ltd; (2003).

201. J.W. Long, R.M. Stroud, K.E. Swider-Lyons, D.R. Rolison, J. Phys. Chem. B 104 (2000) 9772.
202. H.N. Dinh, X.M. Ren, F.H. Garzon, P. Zelenay, S. Gottesfeld, J. Electroanal. Chem. 491 (2000) 222.
203. N.W. Maxakato, K.I. Ozoemena, C.J. Arendse, Electroanalysis 22 (2010) 519.
204. H.F. Oetjen, V.M. Schmidt, U. Stimming, F. Trila, J. Electrochem. Soc. 143 (1996) 3838.
205. Z. He, J. Chen, D. Liu, H. Tang, W. Deng, Y.Kuang, Materials Chemistry and Physics, 85 (2004) 396.
206. D.-J. Guo, H.-L. Li J. Electroanal. Chem. 573 (2004) 197.
207. E. Frackowiak, G. Lota, T. Cacciaguerra, F. Beguin, Electrochem. Commun. 8 (2006) 129.
208. Z. He, J. Chen, D. Liu, H. Zhou, Y. Kuang, Diam. & Relat. Mater. 13 (2004) 1764.
209. M.-C. Tsai, T.-K. Yeh, Z.-Y. Juang, C.-H. Tsai Carbon 45 (2007) 383.
210. Z. Liu, X.-Y. Ling, B. Guo, L. Hong, J. Yang Lee, J. Power Sources 167 (2007) 272.
211. C.-L.Lee, Y.-C. Ju, P.-T.Chou, H. Y.-C. Huang, K. L.-C. Kuo, J.-C. Oung, Electrochem. Commun. 7 (2005) 453.
212. J. Solla-Gullo`n, F.J. Vidal-Iglesias, V. Montiel, A. Aldaz, Electrochim. Acta 49 (2004) 5079.
213. J. Liu, J. Cao, Q. Huang, X.Li, Z. Zou, H. Yang, J. Power Sources 175 (2008) 159.
214. X. Zhang, F. Zhang, R.-F. Guan, K.-Y. Chan, Mater. Research Bulletin 42 (2007) 327.
215. F.Ye, S. Chen, X.Dong, W. Lin, J. Natural Gas Chemistry 16 (2007) 162.

216. M.-H. Seo, S- M. Choi, H.-J Kim, J.-H. Kim, B-K Chou, W. B. Kim, J. Power Sources 179 (2008) 81.
217. H. Zhao, J. Yang, L. Li, H. Li, J. Wang, Y. Zhang, Int. J. Hydrogen Energy 34 (2009) 3908.
218. Y.Wanga, Z. M. Sheng, H. Yang, S. P. Jiang, C. M. Li, Int. J. Hydrogen Energy 35 (2010) 10087.
219. R.N. Singh, A. Singh, Anindita, Int. J. Hydrogen Energy 34 (2009) 2052.
220. H. Razmi, Es. Habibi, H. Heidari, Electrochim. Acta 53 (2008) 8178.
221. G. Yong-ping, H. Hui, Z. Wen-kui, Trans. Nonferrous Met. SOC. China 17 (2007) 214.
222. D-J. Guo, Z-H. Jing, J. Colloid and Interf. Sci. 359 (2011) 257.
223. K.M. Samanta, V.S. Joshi, G. Sharmaa, S. Kapoorb, S.K. Harama, Electrochim. Acta 56 (2011) 2081.
224. J. Xu, K. Hua, G. Sun, C.Wang, X. Lv, Y. Wang, Electrochem. Commun. 8 (2006) 982.
225. Z-C. Wanga, Z-M. Mab, H-L. Li, Applied Surf. Sci. 254 (2008) 6521.
226. Z. Cui, C. Liu, J. Liao, W. Xing, Electrochim. Acta 53 (2008) 7807.
227. H.J. Wang, H. Yu, F. Peng, P. Lv, Electrochem. Commun. 8 (2006) 499.
228. Y. Zhao, X. Yang, J. Tian, F. Wang, L. Zhan, Int. J. Hydrogen Energy 35 (2010) 3249.
229. Y. Zhao, L. Zhan, J. Tian, S. Nie, Z. Ning, Int. J. Hydrogen Energy 35 (2010) 10522.
230. V. Selvaraj, M. Alagar, Electrochem. Commun. 9 (2007) 1145.
231. T. Maiyalagan, Int. J. Hydrogen Energy 34 (2009) 2874.
232. R. Ahmadi, M. K. Amini, Int. J. Hydrogen Energy 36 (2011) 7275.
233. B. Wieland, J. P. Lancaster, C. S. Hoaglund, P. Holota, W. J. Tornquist, Langmuir 12 (1996) 259.

234. V. Livshits, M. Philosoph, E. Peled, J. Power Sources 178 (2008) 687.
235. H. Wang, Z. Jusys, R. J. Behm, J. Electroanal. Chem. 595 (2006) 23.
236. M. Weber, J.T. Wang, S. Wasmus, R. F. Savinell, J. Electrochem. Soc. 143 (1996) L158.
237. Z-Z. Zhu, Z. Wang, H-L. Li., Applied Surf. Sci. 254 (2008) 2934.
238. B. Habibi, N. Delnavaz, Int. J. Hydrogen Energy 36 (2011) 9581.
239. S. Murugesan, K. Myers, V. (Ravi) Subramanian, Appl. Cat. B Environ. 103 (2011) 266.
240. Z. Liu, L. Hong, J. Appl. Electrochem. 37 (2007) 505.
241. W. Chen, J. Kim, S. Sun, S. Chen, 23 (2007) 11303.
242. X. Wang, J-M Hu, I-M Hsing, J. Electroanal. Chem. 562 (2004) 73.
243. B. Liu, H.Y. Li,L. Die, X.H. Zhang, Z. Fan, J.H. Chen, J. Power Sources 186 (2009) 62.
244. Q. Yi, J. Zhang, A. Chen, X. Liu, G. Xu, Z. Zhou, J. Appl. Electrochem. 38 (2008) 695.
245. Q. Zhong, P. Huang, B. Zhang, X. Yang, Y. Ding, H. Zhou, B. Ren, Z. Tian, Acta Physico-Chimica Sinica 22 (2006) 291.
246. Z.-Z. Zhu, Z. Wang, H.-L. Li, Applied Surf. Sci. 254 (2008) 2934.
247. N. Chi, K.-Y. Chan, D. Lee Phillips, Catal. Lett. 71 (2001) 21.
248. S. Yang, X. Zhang, H. Mi, X. Ye, J. Power Sources 175 (2008) 26.
249. Y.-X. Chen, M. Heinen, Z. Jusys, R.J. Behm, Langmuir 22 (2006) 10399.
250. W. Chen, J. Kim, L.-P. Xu, S. Sun, S. Chen, J. Phys. Chem. 111 (2007) 13452.
251. O. Winjobia, Z. Zhanga, C. Liangb, W. Li, Electrochim. Acta 55 (2010) 4217.

252. V. Selvaraj, A. Nirmala Graceb, M. Alagarc, J. Colloids Interf. Sci. 333 (2009) 254.
253. S. Chakraborty, C. R. Raj, Carbon 48 (2010) 3242.
254. N. Dalbay, F. Kadirgan, J. Electroanal. Chem. 296 (1990) 559.
255. J.M. Sieben, M.M.E. Duarte, Int. J. Hydrogen Energy 36 (2011) 3313.
256. C. Jin, Y. Song, Z. Che, Electrochim. Acta 54 (2009) 4136.
257. C. Xu, Y. Liu, D. Yuan, Int. J. Electrochem. Sci. 2 (2007) 674.
258. B. Wu, Y. Gao, G. Li, W. Qu, Z. Jiang, Catalysis Letters, 106, (2006) 167.
259. Z.-P. Suna, X.-G. Zhanga, Y.-Y. Lianga, H.-L. Li, J. Power Sources 191 (2009) 366.
260. A. Serov, C. Kwak, Appl. Catal. B. Environ. 97 (2010) 1.
261. X.-M. Chena, Z.-J. Lina, T.-T Jia, Z.-M. Caia, X.-L. Huanga, Y-Q Jianga, X. Chena, G. Chen, Anal. Chim. Acta 650 (2009) 54.
262. Y.-H. Qin a, H.-H. Yang, X.-S. Zhang a, P. Li, C.-A. Mab, Int. J. Hydrogen Energy 35 (2010) 7667.
263. R.N. Singh, A. Singh, Anindita, Carbon 47 (2009) 271.
264. Razmi, Es. Habibi, H. Heidari Electrochim. Acta 53 (2008) 8178.
265. D.-J. Guo J. Power Sources 196 (2011) 679.
266. R. I. Jafri, S. Ramaprabhu, Int. J. Hydrogen Energy 35 (2010) 1339.
267. D.-J. Guoa, X.-P. Qiua, L.-Q. Chena, W.-T. Zhu, Carbon 47 (2009) 1680.
268. L. Zhang, F. Li, Appl. Clay Sc. 50 (2010) 64.
269. B.V. Derjaguin, B.V. Spitsyn, A. E. Gorodetsky, A. P. Zakharov, L. L. Bouilov, A. E. Aleksenko, J. Cryst. Growth 31 (1975) 44.
270. H.A. Gasteiger, N. Markovic, P. N. Ross, E. J. Cairns, J. Electrochem. Soc. 141 (1994) 1795.

271. H. N. Dinh, X. M. Ren, F. H. Garzon, P. Zelenay, S. Gottesfeld, J. Electroanal. Chem. 491 (2000) 222.
272. H. F. Oetjen, V. M. Schmidt, U. Stimming, F. Trila, J. Electrochem. Soc., 143 (1996) 3838.
273. T. Frelink, W. Visscher, J. A. R. vanVeen, Langmuir 12 (1996) 3702.
274. J. B. Goodenough, A. Hamnett, B. J. Kennedy, R. Manoharan, S. A. Weeks, J. Electroanal. Chem. 240 (1988) 133.
275. A.L. Ocampo, M. Miranda-Hernandez, J. Morgado, J.A. Montonya, P.J. Sebastian, J. Power Sources 160 (2006) 915.
276. M.-C. Tsai, T-K Yeh and C-H Tsai, Mater. Chem. Phys. 109 (2008) 0422.
277. J.Li, Y. Liang, Q. Liao, X. Zhu and X. Tian, Electrochim. Acta 54 (2009) 1277.
278. V. Baglio, A. Di Blasi, C. D'Urso, V. Antonucci, A. S. Arico, R. Ornelas, D. Morales-Acosta, J. Ledesma-Garcia, L. A. Godinez, L. G. Arriaga and L. Alvarez-Contreras, J. Electrochem. Soc. 155 (2008) B829.
279. Y.-C Tsai, Y.-H Hong and P.-C Hsu, Advanced Mat. Research (2008) 99.
280. J. Rasko, T. Kecskes, J. Kiss. J. Catal. 224 (2004) 261.
281. H.A. Gasteiger, M.N. Markovic, P.N. Ross, Catal. Lett. 36 (1996) 1.
282. H.B. Hassan, J. Fuel Chem. Technol. 37 (2009) 346.
283. V. Bambagionia, C. Bianchinia, A. Marchionnia, J. Filippi, F. Vizzaa, J. Teddy, P. Serpb, M. Zhiania, J. Power Sources 190 (2009) 241.
284. S.-M. Hwang, O. J. Kwon, J. J. Kim Appl. Catal. A: General 316 (2007) 83.

285. J. Spadavecchia, R. Rella, P. Siciliano, M.G. Manera, A. Alimelic, R. Paolesse, C.Di. Natale, A.D. Amico, Sens. Actuators B 115 (2006) 12.
286. X.Y. Li, S.Y. Shen, Q.F. Zhou, Thin Solid Films 324 (1998) 274.
287. B. Wanga, X. Zuoc, Y. Wua, Z. Chena, C. Hea, W. Duana, Sensors and Actuators B 152 (2011) 191.
288. K. Inumaru, T. Okuhara, M. Misono. J. Phys. Chem. 95 (1991) 4826.
289. T. Aaltonen, M. Ritala, T. Sajawaara, J. Keinonen, M. Leskela Chem. Mater. 15 (2003) 1924.
290. M. Hiratani, T. Nabatame, Y. Matsui, S. Kimura, Thin Solid films 410 (2002) 200.
291. C. Thurier, P. Doppelt, Coordin. Chem. Rev. 252 (2008) 155.
292. H. Kim, S. Heup Moon, Carbon 49 (2011) 1491.
293. H.Li, T.F.Guarr, J. Chem.Soc.Chem.Commun. (1989) 832.
294. I. Langmuir, V.J. Schaefer, J. Am. Chem. Soc. 57 (1938) 1007.
295. M. Petty, Langmuir–Blodgett Films, Cambridge University Press, Cambridge, (1996).
296. A. Ulman, Ultrathin Organic Films, Academic press, New York, (1991).
297. R. Bilewicz, M. Majda, J. Am. Chem. Soc. 113 (1991) 5464.
298. B. Lindholm-Sethson, Langmuir 12 (1996) 3305.
299. P. Ugo, P. Bertoncello, F. Vezzà Electrochim. Acta 49 (2004) 3785.
300. S. A. Jamadade, S. V. Jadhav, V.Puri, Appl. Surf. Sc. 255 (2009) 4201.
301. L. Carrette, K.A. Friedrich, U. Stimming, 1 (2001) 5.
302. N.W. Maxakato, MSc Thesis 2003.
303. K.V. Kordesch, G.R. Simade, Chem. Rev.95 (1995) 191.

304. Z. Poltarzewski, W. Wieczorek, J. Przyluski, V. Antonucci, Solid State Ionics 119 (1999).
305. N.P. Lebedeva, G.N. Kryukova, S.V. Tsybulya, A.N. Salanov, Electrochim. Acta 44 (1998) 1431.
306. E.M. Belgsir, E. Bouhier, H.E. Yei, H.K. Kokoh, B. Beden, Electrochim. Acta 36 (1991) 1157.
307. K. Matsuoka, M. Inaba, Y. Iriyama, T. Abe, Z. Ogumi, M. Matsuoka, Fuel Cells 2 (2002) 35.
308. H. Wang, Y. Zhao, Z. Jusys, R.J. Behm, J. Power Sources 155 (2006) 33.
309. E. Peled, V. Livshits, T. Duvdevani, J. Power Sources, 106 (2002) 245.
310. V. Livshits, E. Peled, J. Power Sources 161 (2006) 1187.
311. C. Rice, S. Ha, R.I. Masel, P. Waszczuk, A. Wieckowki, T. Barnard, J. Power Sources 111 (2002) 83.
312. R. Larsen, S. Ha, J. Zakzeski, R.I. Masel, J. Power Sources 157 (2006) 78.
313. Y.W. Rhee, S. Ha, C. Rice, R.I. Masel, J. Power Sources 117 (2003) 35.
314. C. Rice, S. Ha, R.I. Masel, A. Wieckowki, J. Power Sources 115 (2003) 229.
315. F. Barbir PEM Fuel Cells-Theory and Practice. Elsevier Academic Press (2005).
316. D. Mark, The Story of Hydrogen, Uehling (1995), Grolier publishing. The Elements Hydrogen, John Farndom (2000), Benchmark Books.
317. X. Ren, P. Zelenay, S. Thomas, J. Davey, S. Gottesfeld, J. Power Sources 86 (2000) 111.

318. C.K. Witham, W. Chun, T.I. Valdez, S.R. Narayanan, Electrochem. Solid-State Lett. 3 (2003) 497.
319. C.Y. Chen, P. Yang, J. Power Sources 123 (2002) 37.
320. Z. Wang, K. Qiu, Electrochem. Commun. 8 (2006) 1075.
321. S. Prakash, G. A. Olah, University of Southern California's Loker Hydrocarbon Institute (1990).
322. T. Lehtinen, G. Sundholm, S. Holmberg, F. Sundholm, P. Bjornborn, M. Bursell, Electrochimica Acta 43 (1998) 1881.
323. A.D. Little, The new role of Fuel Cell Technology in Utility Planning. Prepared for The World Fuel Cell Council, Frankfurt, Germany (1992).
324. T.D. Kaun, A. Shoeler, C.J. Centeno, M. Krumpelt, The Electrochem. Soc., Pennington, NJ Proceedings 99-20 (1999) 219.
325. C. Lamy, E. M. Belgsir, in: W. Vielstich, H. A. Gasteiger, A. Lamm (Eds.), Handbook of Fuel Cells - Fundamentals, Technology and Applications, John Wiley & Sons, Ltd., New York (2003) 323.
326. T. Iwasita, F. C. Nart, J. Electroanal. Chem. 317 (1991) 291.
327. P. A. Christensen, A. Hamnett, J. Munk, G. L. Troughton, J. Electroanal. Chem. 370 (1994) 251.
328. C.A. Gervasi, P.E. Alvarez, M.V. Fiori Bimbi, M.E. Foilquer, J. Electroanal. Chem. 601 (2007) 194.
329. T.G. Rochow, E.G. Rochow, An Introduction to Microscopy by Means of Light, Electrons, X-Rays, or Ultrasound, Plenum Press, New York (1978).
330. P. Hermann, A. Hermeling, V. Lausch, G. Holland, L. Möller, N. Bannert, D. Naumann, Analyst 136 (2) (2011) 1148.
331. E. Suzuki, J. Microscopy 208 (3) (2002) 153.
332. C.L. Copper, G.E. Collins, Electrophoresis 25 (2004) 897.
333. E. Le Bourhis, G. Patriarche, Micron 38 (2007) 377.

334. Y. Roiter, S. Minko, J. Am. Chem. Soc. 127 (2005) 15688.
335. P.J. Orr, S.L. Kearns, (2011). "X-Ray Microanalysis of Burgess Shale and Similarly Preserved Fossils".
336. B.E. Warren, X-Ray Diffraction, Addison-Wesley Publishing Company, Reading (1969).
337. C. Lamy, A. Lima, V. Lerhun, F. Delime, C. Coutanceau, J.M. Leger, J. Power Sources 105 (2002) 283.
338. J. Nordlund, G. Lindberbh, J. Electrochem. Soc. 149 (2002) A1107.
339. T. Iwasita, Electrochim. Acta 48 (2002) 289.
340. R. Parson, Y. Vatsumura, J. Electroanal. Chem. 257 (1988) 9.
341. H. Nonaka, Y. Matsumura, J. Electroanal. Chem. 520 (2002) 101.
342. C. Rice, S. Ha, R.I. Masel, A. Wieckowski, J. Power Sources 115 (2003) 229.
343. S. Ha, B. Adams, R.I. Masel, J. Power Sources 128 (2004) 119.
344. Y. Zhu, S. Ha, R.I. Masel, J. Power Sources 130 (2004) 8.
345. S. Ha, R. Larsen, Y. Zhu, R.I. Masel, Fuel Cells 4 (2004) 337.
346. Y.W. Rhee, S.Y. Ha, Richard I. Masel, J. Power Sources 117 (2003) 35.
347. X. Wang, J.-M. Hu, I.-M. Hsing, J. Electroanal. Chem. 562 (2004) 73.
348. P. Waszczuk, T.M. Barnard, C. Rice, R.I. Masel, A. Wiechowski, Electrochem. Commun. 4 (2002) 599.
349. Y. Zhu, Z. Khan, R.I. Masel, J. Power Sources 139 (2005) 15.
350. R. Larsen, J. Zakzeski, R.I. Masel, Electrochem. Solid State Lett. 8 (2005) 291.
351. R.S. Jayashree, J.S. Spendelow, J. Yeom, C. Rastogi, N.A. Shannon, P.J.A. Kenis, Electrochim. Acta 50 (2005) 4674.
352. W.J. Zhou, J.Y. Lee, J. Phys. Chem. C 112 (2008) 3789.

353. W.P. Zhou, A. Lewera, R. Larsen, R.I. Masel, P.S. Bagus, A. Wieckowski, J. Phys. Chem. B 110 (2006) 13393.
354. Z.L. Liu, L. Hong, M.P. Tham, T.H. Lim, H.X. Jiang, J. Power Sources 161 (2006).831.
355. V. Mazumder, S.H. Sun, J. Am. Chem. Soc. 131 (2009) 4588.
356. W.P. Zhou, A. Lewera, R. Larsen, R.I. Masel, P.S. Bagus, A. Wieckowski, J. Phys. Chem B 110 (2006) 13393.
357. X. Yu, P.G. Pickup, J. Power Sources 182 (2008) 124.
358. J.M. Feliu, E. Herrero. In: W. Vielstich, A. Lamm, H. Gasteiger, editors, Handbook of fuel cells: fundamentals, technology applications, vol. 2. New York: Academic Press/Wiley (2003) 625.
359. R. Larson, S. Ha, J. Zakzeski, R.I. Masel, J. Power Sources 157 (2006) 78.
360. N. Hoshi, K. Kida, M. Nakamura, M. Nakada, K. Osada, J. Phys. Chem. B 110 (2006) 12480.
361. C. Jung, C.M. Sanchez-Sanchez, C.L. Lin, J. Rodriguez-Lopez, A.J. Bard, Anal. Chem. 81 (2009) 7003.
362. N. Dalbay, F. Kadirgan, J. Electroanal. Chem. 296 (1990) 559.
363. F. Kadirgan, B. Beden, C. Lamy, J. Electroanal. Chem. 136 (1982) 119.
364. G. Horanyi, V.E. Kazarinov, Y.B. Vassiliev, V.A. Andreev, J. Electroanal. Chem. 147 (1983) 263.
365. F. Hahn, B. Beden, F. Kadirgan, C. Lamy, J. Electroanal. Chem. 216 (1987) 169.
366. L.W.H. Leung, M.J. Weaver, J. Phys. Chem. 92 (1988) 4019.
367. P.A. Christensen, A. Hamnett, J. Electroanal. Chem. 260 (1989) 347.
368. J.M. Orts, A. Fernandez-Vega, J.M. Feliu, A. Aldaz, J. Clavilier, J. Electroanal.Chem. 290 (1990) 119.

369. E.M. Belgsir, E. Bouhier, H.E. Yei, K.B. Kokoh, B. Beden, H. Huser, J.M.Leger, C. Lamy, Electrochim. Acta 36 (1991) 1157.
370. S.G. Sun, A.-C. Chen, T.-S. Huang, J.-B. Li, Z.-W. Tian, J. Electroanal.Chem. 340 (1992) 213.
371. F. Hahn, B. Beden, F. Kadirgan, C. Lamy, J. Electroanal. Chem. 216 (1987) 169.
372. E. Peled, T. Duvdevani, A. Aharon, A. Melman, Electrochem. Solid-State, Lett. 4 (2001) A38.
373. E. Peled, V. Livshits, T. Duvdevani, J. Power Sources 106 (2002) 245.
374. A. Kelaidopoulou, E. Abelidou, A. Papoutsis, E.K. Polychroniadis, G.Kokkinidis, J. Appl. Electrochem. 28 (1998) 1021.
375. R.B. De Lima, V. Paganin, T. Iwasita, W. Vielstich, Electrochim. Acta 49 (2003) 85.
376. M.S. El-Deab, T. Ohsaka, Electrochem.Commun. 4 (2002) 288.
377. Y.J. Komai, Exp. Biol. 201 (1998) 2359.
378. A. Andreasen, G. Danscher, S. Juhl, M. Stoltenberg, N.P. Revsbech, H. Jensen, K.B.J. Jensen, Neurosci. Meth. 72 (1997) 15.
379. P.G. Osborne, X.F. Li, Y.Z. Li, H.W. Han, J. Neurosci. Res. 63 (2001) 224.
380. P.G. Osborne, Physiol. Behav. 61 (1997) 485.
381. J.C. Huang, R. K. Sen, E. Yeager, J. Electrochem. Soc. 126 (1979) 786.
382. J.M. Zen, R. Manoharan, J.B. Goodenough, J. Appl. Electrochem. 22 (1992) 140.
383. N.R.K. Vilambi, E. Taylor, Separ. Sci. Technol. 25 (1990) 627.
384. J-W Lee, B.N. Popov, J. Solid State Electrochem. 11 (2007) 1355.
385. Y.J. Komai, Exp. Biol. 201 (1998) 2359.
386. M.S. El-Deab, T.J. Ohsaka, Electroanal. Chem. 553 (2003) 107.

387. M.S. El-Deab, T. Ohsaka, Electrochim. Acta 47 (2002) 4255.
388. W. Chen, S. Chen, Angew. Chemie, Int. Ed. 48 (2009) 4386.
389. N. Sehlotho, T. Nyokong, J. Electroanal. Chem. 595 (2006) 161.
390. S.A. Mamuru, K.I. Ozoemena, Electroanalysis 22 (2010) 985.
391. S.A. Mamuru, K.I. Ozoemena, Electrochem. Commun. 12 (2010) 1539.
392. M. Kimura, T. Kuroda, K. Ohta, K. Hanabusa, H. Shirai, N. Kobayashi, Langmuir 19 (2003) 4825.
393. N. Nishiyama, A. Iriyama, W.D. Jang, K. Miyata, K. Itaka, Y. Inoue, H. Takahashi, Y. Yanagi, Y. Tamaki, H. Koyama, K. Kataoka, Nat. Mater. 4 (2005) 934.
394. A. Sorokin, J.L. Seris, B. Meunier, Science 268 (1995) 1163.
395. M. Stantney, W. Ham, Chem. Rev. 104 (2004) 4271.
396. J.H. Zagal, Coord. Chem. Rev. 119 (1992) 89.
397. A.B.P. Lever, J. Porph. Phthalocya. 3 (1999) 488.
398. R.R. Chen, H.X. Li, D. Chu, G.F. Wang, J. Phys. Chem. C 113 (2009) 20689.
399. M. Ozer, A. Altındal, A.R. Ozkaya, O. Bekaroˇglu, Dalton Trans. (2009) 3175.
400. I˙. Koc, M. Ozer, A.R. Ozkaya, O. Bekarogˇlu, Dalton Trans. (2009) 6368.
401. N. Sehlotho, T. Nyokong, J. Electroanal. Chem. 595 (2006) 161.
402. J. Obirai, T. Nyokong, Electrochim. Acta 50 (2005) 3296.
403. R. Baker, D.P. Wilkinson, J.J. Zhang, Electrochim. Acta 54 (2009) 3098.
404. F. Harnisch, S. Wirth, U. Schroer, Electrochem. Commun. 11 (2009) 2253.
405. G.I. Cardenas-Jiron, M.A. Gulppi, C.A. Caro, R. delRio, M. Paez, J.H. Zagal, Electrochim. Acta 46 (2001) 3227.

406. C.J. Song, L. Zhang, J.J. Zhang, J. Electroanal. Chem. 587 (2006) 293.
407. E. Song, C. Shi, F.C. Anson, Langmuir 14 (1998) 4315.
408. N. Kobayashi, D. Janda, A.P. Lever, Inorg. Chem. 31 (1982) 5172.
409. J.F. Silva, S. Griveau, C. Richard, J.H. Zagal, F. Bedioui, Electrochem. Commun. 9 (2007) 1629.
410. A. Baba, Y. Kanetsuna, S. Sriwichai, Y. Ohdaira, K. Shinbo, K. Kato, S. Phanichphant, F. Kaneko, Thin Solid Films 518 (2010) 2200.
411. D.A. Geraldo, C.A. Togo, J. Limson, T. Nyokong, Electrochim. Acta 53 (2008) 8051.
412. M. Pomerantz, A. Aviram, R.A. McCorkle, L. Li, A.G. Schrott, Science 255 (1992) 1115.
413. C.Y. Tsai, S.P. Chen, T.C. Wen, Chem. Phys. 240 (1999) 191.
414. B.H. Lee, J.Y. Jaung, S.C. Jang, S.C. Yi, Dyes Pigments 65 (2005) 159.
415. D. Dini, M. Hanack, H.J. Egelhaaf, J.C. Sancho-Garcia, J. Cornil, J. Phys. Chem. B109 (2005) 5425.
416. Z.W. Xu, G.X. Zhang, Z.Y. Cao, J.S. Zhao, H.J. Li, J. Mol. Catal. A318 (2010) 101.
417. Z. Xu, H. Li , G. Cao, Q. Zhang, K. Li, X. Zhao, J. Molecular Catalysis A: Chemical 335 (2011) 89.
418. E. Yeager, NBS Special Publication 455 (1976) 203.
419. M. Tarasevich, A. Sadkowaski, E. Yeager E (1983) vol 7. Plenum Press, New York.

CHAPTER TWO

EXPERIMENTAL

Approach

The following phases were the approaches used for this project:

Phase 1: Literature review

- Literature review of the past and recent publications in the area of this project were carried out in order to be informed on the progress and challenges involved in this research.

Phase 2: Methodology and Equipments

- Functionalization of Carbon Nanotubes (CNTs) with strong acids to improve its solubility and reactivity for effective modification.
- Chemical synthesis of metallophthalocyanine (MPc), Octa-carboxy ruthenium phthallocyanine, RuOcPc [1] with platinum salt.
- Surface characterisation with Raman Spectroscopy, Scanning Electron Microscopy (SEM), Fourier Transform Infra-Red Spectroscopy (FTIR), Atomic Force Microscopy (AFM), X-ray Diffraction (XRD) and High Resolution Transmission Electron Microscopy (TEM).
- Electrode modification with Platinum-Ruthenium (Pt/Ru) and Ruthenium Tetrakis(diaquaplatinum)- Octacarboxyphthalocyanine Catalysts (RuOcPcPt).
- Electrochemical characterisation of the modified electrodes with Cyclic Voltammetry (CV) and Electrochemical Impedance Spectroscopy (EIS).
- Electron transfer kinetics studies of the modified electrodes.

Electrodeposition of PtRu on BPPGE was performed for which Pt^{4+} ions are reduced to Pt^{0}, to a 0.2 mM K_2PtCl_6 in 0.5 M H_2SO_4 solution that was previously saturated with nitrogen gas. The reduction reaction occurred following Equation 2.1:

$$PtCl_6^{2-} + 4e^- \rightarrow Pt + 6Cl^- \quad (2.1)$$

The dropcasting of the chemically synthesized nanoparticles was also performed.

For this purpose the three-electrode cell was used, with modified BPPGE as working electrode (exposed surface: 5 mm), Ag|AgCl (sat'd KCl)) as reference and a platinum wire as counter electrode. The electrodeposition process was followed by means of chronoamperometry (CA), and all other types of electrochemical measurements presented in this Chapter were done using the same set-up. All solutions were made with ultra-pure (Millipore®) water using analytical grade reactants without further purification and were saturated with nitrogen gas prior to each experiment.

Introduction

This chapter presents a detailed preparation of the functionalized carbon nanotube (fCNTs) and catalysts that were used to prepare nanocomposite electrodes. The sources (starting materials) employed to prepare nanocomposite electrodes are basal plane pyrolytic graphite (BPPG), fCNTs, Platinum-Ruthenium (PtRu) and Ruthenium (II) tetrakis (diaquaplatinum) octacarboxyphthalocyanine (RuOcPcPt) nanoparticles. The preparation methods on the synthesis of nanoparticles and fabrication of BPPG electrodes are discussed. The methods of preparing the nanocomposite electrodes are of two main types, i.e. electrodeposition and drop-casting of the chemically synthesized nanoparticles. This chapter also outlines a brief summary on the techniques (physical and electrochemical) used to characterize catalysts and nanocomposite electrodes. The major electrochemical techniques used were cyclic voltammetry (CV) and electrochemical impedance spectroscopy (EIS) and the information extracted from such experiments will be described in Chapters 4-6.

2.0 Experimental details

2.1 Materials and Reagents

Pristine multi-walled carbon nanotubes (MWCNT, purity >90 %, 110-170 nm in diameter, 5-9 μm in length) obtained from Sigma Aldrich were acid-functionalised (converted mainly into carboxylated and abbreviated as fMWCNT) by undergoing acid treatment following the procedure described by J. Liu et al. [2]. Acid treatment serves the purposes of transforming the CNTs into shorter, uncapped nanotubes for easy incorporation of Pt based nanoparticles. Potassium hexa-chloroplatinate(IV) 99% (K_2PtCl_6), ruthenium(III) chloride anhydrous ($RuCl_3$), Potassium tetra-chloroplatinate (K_2PtCl_4) salts and sodium hydroxide (NaOH) were purchased from Merck and Fluka chemicals.

Ethylene glycol (EG or $C_3H_8O_3$), methanol (MeOH or CH_3OH), formic acid (FA or HCOOH), sulphuric acid (H_2SO_4), acetone (C_3H_3O), diethyl ether and hydrazine sulphate ($N_2H_4.H_2SO_4$) were of analytical grades (All from Sigma Aldrich chemicals) and used as received without further purification. N,N-Dimethyl formamide (DMF) was purchased from Sigma-Aldrich, and was distilled before use. Oxygen (technical grade) was supplied by Afrox. The ruthenium(II) tetrakis (diaquaplatinum) octacarboxyphthalocyanine (RuOcPcPt) was synthesised by adopting a similar strategy used for the cobalt derivative [3]. Ultra-pure water of resistivity 18.2MΩ.cm was obtained from a Milli-Q Water System (Millipore Corp., Bedford, MA, USA) and was

used throughout for the preparation of solutions. All solutions were purged with pure nitrogen before use to eliminate oxygen and any form of oxidation during experiment. All electrochemical experiments were performed with nitrogen-saturated analytes.

2.1.1 Synthesis of functionalised CNTs

Briefly, MWCNTs were purified and cut into short and uncapped nanotubes bearing acid functional groups (CNT-COOH) by refluxing a known weight of the MWCNTs in 2.6 M HNO_3 for 48 h. The product was washed with copious amounts of water, centrifuged to separate water which was decanted from the solids and dried at 30^0C in an oven for 36 h. The residue was ultrasonicated at 40^0C in a mixture of concentrated H_2SO_4 and HNO_3 (3:1, v/v) for 24 h. The material was filtered again, washed with copious amounts of water and dried in an oven for 48 h at 40^0C. Finally, the dried powder was suspended in a mixture of concentrated H_2SO_4 and 30% aqueous H_2O_2 (4:1, v/v) and stirred at 70^0C for 4 h. The product was filtered and washed with copious amounts of water until the pH of the filtrate was neutral. The black solid material obtained was dried in an oven at 40^0C over night and characterised using FTIR (to confirm the carbonyl functional group (C=O) of the –COOH), Raman for structural properties, SEM and TEM (for surface morphology). The acid treatment employed cut the nanotubes to smaller sizes to allow for COOH modification.

2.1.2 Synthesis of Potassium tetra-chloroplatinate(II), K_2PtCl_4

About 0.27 g of hydrazine sulphate ($N_2H_4.H_2SO_4$) was added to *ca.* 2.0 g of K_2PtCl_6 dissolved in 20 mL of distilled water. The solution was brought to boil by heating on a water bath for 40 min. The resulting solution was filtered and the product was precipitated by addition of acetone:diethyl ether mixture (1:1). The K_2PtCl_4 product formed was washed with acetone and ether. The obtained product was used for analysis [3].

2.1.3 Synthesis of ruthenium (II) tetrakis (diaquaplatinum) octacarboxyphthalocyanine

Ruthenium(II) tetrakis (diaquaplatinum) octacarboxyphthalocyanine (RuOcPcPt) [3] nanoparticles were synthesised by adopting the method described by Dolota et al. [3]. The procedure is summarized in scheme 2.1 below.

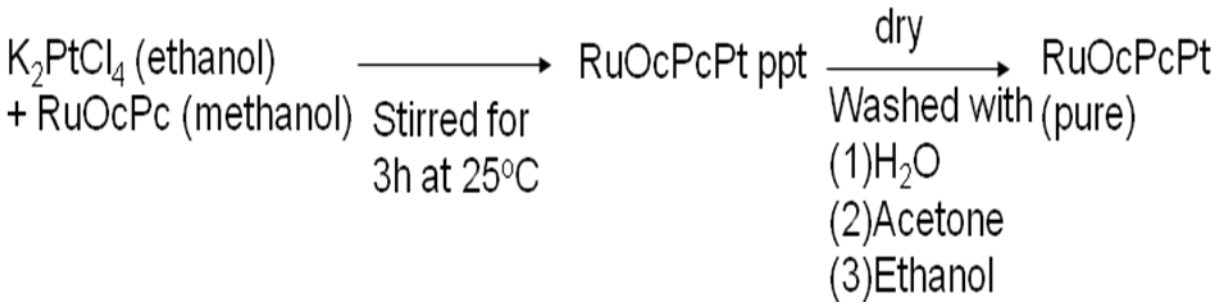

Scheme 2.1: Procedure for the chemical synthesis of RuOcPc nanoparticle.

A solution of K_2PtCl_4 (0.24g) in 50% ethanol (350 mL) was added to a suspension of octa-carboxyrutheniumphthalocyanine (0.27g) in water:methanol (50 mL:210 mL). The mixture was stirred for 3 h at room temperature. After 48 h the precipitate was filtered off and washed sequentially with distilled water, ethanol, acetone and diethyl ether to remove possible adsorbed ions such as Pt. The precipitate was finally dried in air.

2.1.4 Synthesis of fMWCNT Ruthenium (II) tetrakis (diaquaplatinum) tetracarboxyphthalocyanine (RuTetPcPt)

Pt nanoparticles were synthesized using the method described by Li et al. [4]. FMWCNT (50 mg) was suspended in EG solution (10 mL of 95 mL EG + 5 mL distilled water) and dispersed in an ultrasonic bath for 20 min. A solution of K_2PtCl_6 (5.4 mg/mL EG solution) and ruthenium phthalocyanine nanoparticles (5.4 mg/mL EG solution) was added drop-wise to fMWCNT dispersion under mechanically stirred conditions for 4 h. NaOH solution was added to adjust the pH of the solution to above 13. The solution was heated at 140^0C for 3 h. The solid was filtered using whatman grade 1 filter paper, washed with copious amounts of distilled water (1.5 L) and dried at 70^0C for 8 h.

2.1.5 Synthesis of Pt/fMWCNT catalyst

Pt catalyst was synthesized using the method described by Li et al. [4]. fMWCNT (20 mg) was suspended in EG solution (10 mL of 95 mL EG + 5 mL distilled water) and stirred in ultrasonic bath for 20 min. K_2PtCl_6 (3 mg) in EG solution (1 mL) was added to the above solution drop-wise and the solution was allowed to stir for 4 h. Upon stirring NaOH (2.5 M in EG solution) was added to adjust the pH of the solution to above 13. The solution was refluxed at 140^0C for 3 h to ensure that Pt was completely

reduced. The solution was filtered, washed with 2 L distilled water and dried at 70^0C for 12 h. The obtained Pt / fMWCNT catalyst was used for analysis.

2.2 Equipments and methods

The basal plane pyrolytic graphite electrode plate, BPPGE (5.0 mm diameter) was purchased from Le Carbone, Sussex, UK and was constructed in-house at the University of Pretoria technical workshop by placing it in a Teflon tube, extended outside with a copper wire (held in place with conducting silver varnish L 100 (Kemo Electronic, Germany) to make electrical contact with the electrochemical equipment.

Raman spectra of samples were recorded by a Jobin-Yvon T64000 and LabRam HR 800. For these measurements an excitation wavelength of 514.5 nm with power setting of 1.2 mW was used. Field emission scanning electron microscopy (FESEM) images were obtained from JEOL JSM 5800/6000 LV FESEM (Japan). High resolution scanning electron microscope (HRSEM) images were obtained using the Zeiss Ultra Plus 55 HRSEM (Germany), while the energy dispersive x-ray spectra were obtained from NORAN VANTAGE (USA), at the Microscopy and Microanalysis Laboratory of the University of Pretoria. Infrared spectroscopy data were obtained with PerkinElmer GX 2000 FT-IR Spectrometer attached to a Perkin Elmer Auto Image Microscope System equipped with liquid nitrogen cooled MCT detector. TEM images were

obtained with a JEOL JEM – 2100 F/HT high-resolution transmission electron microscope (HRTEM), Tokyo (Japan). AFM experiments were performed with AFM 5100 System (Agilent Technologies, USA) using a contact mode AFM scanner interfaced with a PicoView 1.4.3 controller (scan range 1.25 μm in x–y and 2.322 μm in z). Silicon type PPP-CONT-20 (Nanosensors®) of thickness 2.0±1.0 μm, length 450±10 μm, width 50±7.5 μm, spring constants 0.02-0.77 N m^{-1}, resonant frequencies of 6–21 kHz and tip height of 10-15 μm were used. All images (256 samples/line × 256 lines) were taken in air at room temperature and at scan rates 0.5–0.6 lines s^{-1}. The X-ray Diffraction (XRD) analysis was done using a back loading preparation method. The sample was analysed using a PANalytical X'Pert Pro powder diffractometer with X'Celerator detector and variable divergence- and receiving slits with Fe filtered Co-Kα radiation. The samples are scanned at 2θ angle ranges (5^o – 90^o). The phases were identified using X'Pert Highscore plus software. The voltage and current was 35 kV and 50 mA respectively.

Electrochemical experiments (cyclic voltammetry) were carried out using an Autolab Potentiostat PGSTAT 100/20 (Eco Chemie, Utrecht, The Netherlands) driven by the GPES software version 4.9. The RDE experiments were performed using AUTOLAB-RDE, (Eco Chemie, Utrecht, The Netherlands) with a locally fabricated RDE BPPGE electrode (5.0 mm in diameter) as the working electrode. Electrochemical impedance spectroscopy

(EIS) measurements were performed with an Autolab Frequency Response Analyser (FRA) software between 10 kHz and 1.0 Hz using a 5 mV rms sinusoidal modulation in a solution of 5 mM of $K_4Fe(CN)_6$ and a 5 mM $K_3Fe(CN)_6$ (1:1) mixture in phosphate buffer solution (PBS) of pH 7.0, or buffer solution containing different concentrations of the analytes MeOH, EG, FA, oxygen saturated NaOH, and at the $E_{1/2}$ of the $[Fe(CN)_6]^{4-}/[Fe(CN)_6]^{3-}$ or the analytes respectively vs. Ag|AgCl in sat'd KCl. The FRA software allowed the automatic fitting of the raw EIS data to equivalent circuit models using a *non-linear least squares* (CNLS) method based on the EQUIVCRT programme [5], with *Krammers-Kronig rule check*. Bare and modified BPPGE electrodes were used as working electrode. A Ag|AgCl in saturated KCl and platinum wire were used as reference and counter electrodes respectively. A bench top pH/ISE ORION meter, model 420A, was used for pH measurements. All solutions were de-aerated by bubbling nitrogen for 5 min prior to each electrochemical experiment. All experiments were performed at 25 ± 1 °C.

2.3 Electrode Modification and Pretreatments

2.3.1 Electrode cleaning

Prior to modification, electrodes were prepared using the following procedures. First, the BPPGE surface was cleaned by gentle polishing on a p1200C Norton carborundum paper (Saint-Goban Abrasives, Isando, South Africa) followed by cleaning with cellotape process of removing graphite layers and finally subjected to ultrasonic vibration in acetone or absolute ethanol to remove adhesives that might be trapped at the surface. Edge plane pyrolytic graphite electrode (EPPGE) was also tried in this work but did not give any reasonable results towards the electrocatalysis of the studied analytes.

2.3.2 Electrode modification

In this study, two methods of electrode modification were employed namely, electrodeposition and drop-casting of the chemically synthesized nanoparticles.

2.3.2.1 Drop-dry / electrodeposition techniques

BPPGE-fMWCNT was prepared by drop-coating 20 µL of the fMWCNT/DMF solution (1 mg (fMWCNTs)/1 mL DMF) onto the BPPGE and oven-dried at

50°C for 5 min. Pt nanoparticles (0.2 mM in 50 mL 0.5 M H_2SO_4), and different mass ratios of Pt-Ru nanoparticles (Pt/Ru; in 0.5 M H_2SO_4 aqueous solution containing hexachloro-platinate(IV) and ruthenium chloride) were electrodeposited on the BPPGE-fMWCNT using chronoamperometry technique at a deposition potential of -0.30 V (vs Ag|AgCl, sat'd KCl) for 5 min, following the procedure that has been reported by others for the deposition of metal nanoparticels on carbon electrodes [6-13] to obtain BPPGE-fMWCNT-Pt and the BPPGE-fMWCNT-Pt/Ru electrodes. The electrode modification process is summarised in scheme 2.2.

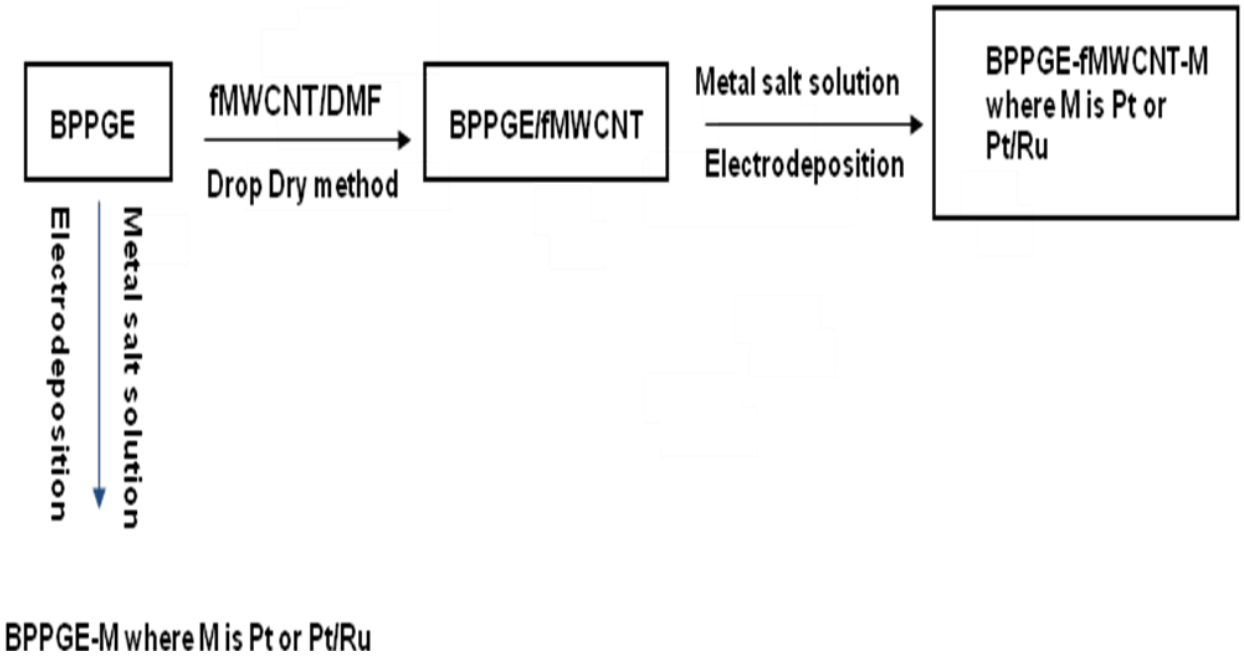

Scheme 2.2: Procedure for the fabrication of metal nanoparticle modified electrodes by electrodeposition.

The electrodes morphology were examined with HRSEM, TEM, EDX) and XRD using CoKα radiation. The electroactive surface coverage area of the

electrodes was determined in 5 mM ferri/ferro ($[Fe(CN)_6]^{3-/4-}$) redox probe and estimated by using the relationship; $Q = nFA\Gamma$ [14] where Q= the background-corrected charge under cathodic or anodic waves, n= the number of electrons involved in the redox process, F is the Faraday constant (96485°C mol^{-1}) , A is the experimentally determined area of the electrode and Γ is the surface coverage.

The electrocatalytic properties of the bare and the modified electrodes were investigated in 0.5M H_2SO_4 containing 0.5 M of $C_2H_6O_2$ (ethanol) or CH_3OH (methanol) or HCOOH (formic acid) by cyclic voltammetry and electrochemical impedance spectroscopy. A 4:1 molar ratio (RPt/Ru) of BPPGE-fMWCNT-Pt/Ru was found to give the best performance in terms of catalytic activity when compared with others and for this reason studies were carried out using this ratio.

2.3.2.2 Electrode modification with synthesised RuOcPcPt nanoparticles

The chemical synthesis was employed since it produces Pt and Pt/Ru nanoparticles in commercial quantity compared to electrodeposition method. For the chemical synthesis experiment, acidified MWCNT was combined with N4-macrocycles (MPc). Electrode modification follows simple drop-dried procedure. fMWCNT (1 mg) was dispersed in DMF (1 mL) with the aid of ultrasonic stirring. fMWCNT solution (15 µL) was cast on the BPPGE surface

and allowed to dry at room temperature to prepare the BPPGE-fMWCNT electrode. RuOcPc or RuOcPcPt complex (15 µL) prepared in the same manner as the fMWCNT was cast onto the surface of the BPPGE-fMWCNT to obtain the BPPGE-fMWCNT-RuOcPc or BPPGE-fMWCNT-RuOcPcPt electrodes. A similar procedure was adopted to obtain the electrodes without fMWCNTs (i.e., BPPGE-RuOcPcPt or BPPGE-RuOcPc). Scheme 2.3 summarises the electrode modification procedure.

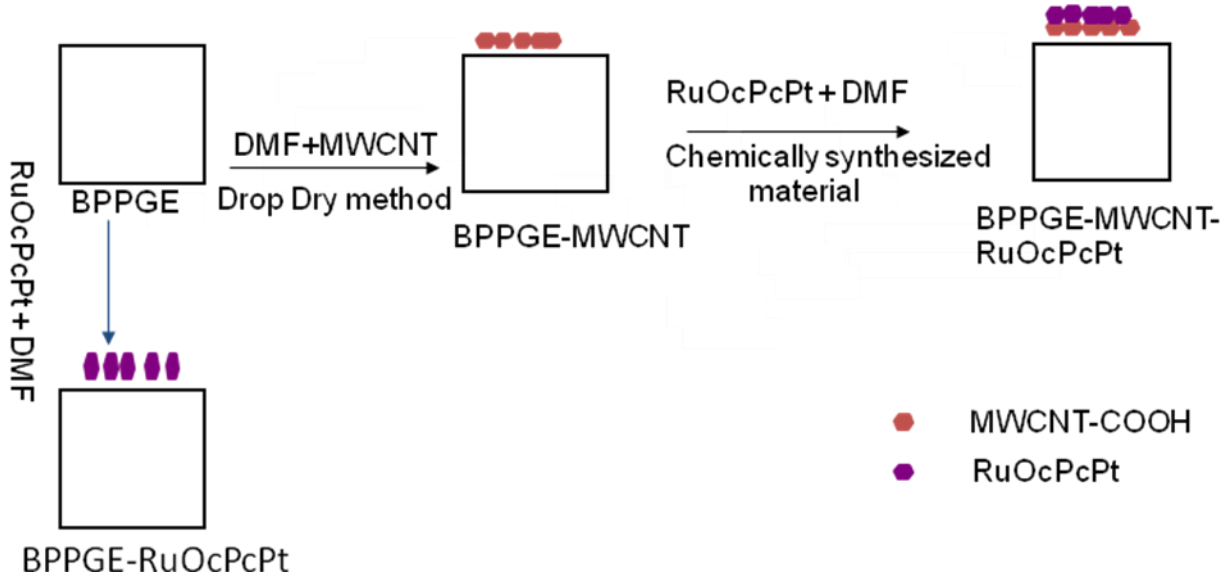

Scheme 2.3: Procedure for the electrode modification procedure using chemical synthesized material.

2.3.2.3 Electrode modification with synthesised RuTetPcPt nanoparticles

A solution of Pt the (II) tetracarboxyruthenium phthalocyanine, *RuTetPcPt* (1mg) and ethanol (1.0 mL) was sonicated for 30 min to obtain a homogeneous ink. A 0.5 µl of the ink was dropped onto the electrode surface

and dried at 80°C for 10 min and finally, 0.5 µl of 50 wt % Nafion solution was dropped onto the electrode, dried for 10 min [15].

2.4 Electrocatalysis and Electroanalysis

Experiments for electrocatalytic oxidation of the analytes were carried out using N_2 purged 0.5 M H_2SO_4 containing a 0.5 M of MeOH or EG or FA, while the O_2 reduction reaction was done in an O_2-saturated 0.1 M NaOH. The oxidation experiments were carried out at a scan rate of 50 mV s^{-1}, and oxidation potential window of -0.2 to 0.6 V, while the O_2 reduction reaction was carried out at scan rate of 25 mV s^{-1}, potential window of 0.4 to -0.8 V using cyclic voltammetry. The EIS experiment was also conducted at the $E_{1/2}$ at which the analytes perform best on the electrodes. The electrocatalytic experiments were divided into two parts. The first part involves catalysis using electrode modified by electrodeposition of metal nanoparticles. The second electrocatalytic experiment was the catalysis using electrode modified with chemically synthesised metal nanoparticles. In each case, a comparative study of the electrocatalytic behaviour of the modified electrodes towards the analyte was investigated and reported. The electrodes investigated were: bare BPPGE, BPPGE-fMWCNT, BPPGE-fMWCNT-Pt, BPPGE-Pt/Ru, BPPGE-fMWCNT-Pt/Ru, BPPGE-RuOcPc, BPPGE-fMWCNT-RuOcPc, BPPGE-RuOcPcPt, and BPPGE-fMWCNT-RuOcPcPt. More importantly, the effect of MPc complex such as octacarboxy ruthenium phthalocyanine

(RuOcPc) on the electrodes with and without CNTs towards MeOH, EG and FA electrooxidations was studied and compared with electrode modified with Pt/Ru nanoparticles.

From CV experiments, electrochemical parameters such as peak current (I_p), peak potential (E_p), ΔE and formal potential ($E_{1/2}$) were measured and discussed. In addition, rotating disc electrode (RDE) experiments were carried out for O_2 reduction experiments to monitor its kinetic at the modified electrode. In all the electrocatalytic experiment, the bare or modified electrode is the working electrode while Ag|AgCl, sat'd KCl and platinum electrodes are the reference and counter electrodes respectively.

The analysis of the analytes involves studying their kinetics using the best electrodes from the electrocatalytic experiment. The effect of scan rate (scan rate range 10 to 1200 mVs^{-1}) was studied. Several kinetic parameters such as E_p, I_p, the peak-to-peak separation (ΔE_p) were obtained. The plot of the anodic peak current (I_{pa}) against square root of scan rate ($\nu^{1/2}$) was obtained. The intercept of the plots gives an insight to the diffusion or adsorption process at the electrode. Zero intercept indicates diffusion-controlled electrode kinetics while a negative intercept suggest an adsorption-controlled electrode reactions [16].

Similarly, concentration study on the analytes was carried with the best electrode, at their respective peak potentials of catalysis using

chronoamperometric techniques. From the chronoamperogram, the catalytic current (I_{cat}) and the buffer current (I_{buff}) were estimated and recorded. The catalytic rate constant *K* [17,18] and the diffusion coefficient *D* [16] of the analyte on the electrode were calculated. From the plot of peak current response I_p versus different analyte concentration *[analyte]*, the electrode sensitivity and its limit of detection (LoD =3.3 s/m [19], where *s* is the relative standard deviation of the intercept and *m*, the slope of the linear current versus the concentration of analyte) were estimated.

To evaluate the extent of catalyst tolerance to CO poisoning at the working electrode, the electrolyte solution containing MeOH, EG and FA were saturated with CO gas [20,21]. The modified electrode was run in the CO saturated analyte solution and the poisoning effect due to CO adsorption on the electrode was evaluated using the the Langmuir adsorption isotherm theory (Equation 2.2) [22].

$$\frac{[\text{Analyte}]}{\text{I}_{\text{cat}}} = \frac{\text{I}}{\beta \text{I}_{\text{max}}} + \frac{[\text{Analyte}]}{\text{I}_{\text{max}}} \qquad \text{.....(2.2)}$$

where all the symbols are already defined in chapter 1. The adsorption equilibrium constant (β) and the standard free energy (ΔG^o) due to adsorption were calculated. These parameters give an idea of the level of CO tolerance or poisoning of the working electrode.

References

1. N. Kobayashi, Thohoku University, Japan.
2. J.A. Liu, , G. Rinzler, H. Dai, J.H. Hanfer, R.K Bradley, P.J. Boul, A. Lu, T Iverson, K. Shelimov, C.B. Huffman, F.R. Macias, Y.S. Shon, T.R. Lee, D.T. Colbert, *Science* 280 (1998) 1253.
3. O.V. Dolotova, O.L. Kaliya, Russ. *J. Coord. Chem*. 33 (2007) 111.
4. W-Z Li, C. Liang, W. Zhou, J. Qiu, Z. Zhou, G. Sun, Q. Xin, *J. Phys. Chem. B* 107 (2003) 6292.
5. B.A. Boukamp, *Solid State Ionics* 20 (1986) 31.
6. Z. He, J. Chen, D. Liu, H. Zhou, Y. Kuang, *Diamond Relat. Mater.* 13 (2004) 1764.
7. Z. He, J. Chen, D. Liu, H. Tang, W. Deng, Y. Kuang, *Mater. Chem. Phys.* 85 (2004) 396.
8. M-C Tsai, T-K Yeh, Z-Y Juang, C-H Tsai, *Carbon* 45 (2007) 383.
9. A. Salimi, R. Hallaj, S. Soltanian, *Biophys. Chem.* 130 (2007) 122.
10. A. Salimi, E. Sharifi, A. Noorbakhsh, S. Soltanian, *Electrochem. Commun.* 8 (2006) 1499.
11. A. Salimi, E. Sharifi, A. Noorbakhsh, S. Soltanian, *Biophys. Chem.* 125 (2007) 540.
12. A. Salimi, E. Sharifi, A. Noorbakhsh, S. Soltanian, *Biosens. Bioelectron.* 22 (2007) 3146.

13. D. Giovanelli, N.S. Lawrence, S.J. Wilkins, L. Jiang, T.G.J. Jones, R.G. Compton, *Talanta* 61 (2003) 211.

14. J. Wang, *Analytical Electrochemistry*, VCH, New York, 1994, ch. 6, p. 171.

15. Z.D. Wei, C. Yan, Y. Tan, L. Li, C.X. Sun, Z. G. Shao, P.K. Shen and H.W. Dong, *J. Phys. Chem. C* 112 (2008) 2671.

16. A.J. Bard, L.R. Faulkner *Electrochemical Methods: Fundamentals and Applications*, 2nd ed, John Wiley & Sons, Hoboken NJ (2001)]

17. M.H. Pournaghi-Azar, R. Sabzi, *J. Electroanal. Chem.* 543 (2003) 115

18. K.M. Manesh, P. Santosh, A.I. Gopalan, K.P. Lee, *Electroanalysis* 18 (2006) 894.

19. G. D. Christian, Analytical Chemistry, 6th ed. John Wiley and Sons New York, 2004, p 113.

20. F, Hu, C. Chen, Z. Wang, G. Wei, P. K. Shen, *Electrochim. Acta* 52 (2006) 1087.

21. A. N. Gavrilov, E. R. Savinova, P. A. Simonov, V. I. Zaikovskii, S. V. Cherepanova, G. A. Tsirlina, V. N. Parmon, Phys-Chem ChemPhys. 9 (2007) 5476.

22. H.X. Ju, L. Donal, *J. Electroanal. Chem.* 484 (2000) 150.

SECTION B

RESULTS AND DISCUSSION*

* Chapters 3 – 6 comprise the results and discussion. Four publications (in peer reviewed journals) presented in chapters 3-6 resulted from this study and are not referenced further in this thesis.

CHAPTER THREE

Insights into the electro-oxidation of ethylene glycol at Pt/Ru nanocatalysts supported on MWCNTs: Adsorption-controlled electrode kinetics*

*__N.W. Maxakato__, C.J. Arendse, K.I. Ozoemena, *Electrochemistry Communications* 11 (2009) 534.

Introduction

In this section the results of different characterization techniques and their interpretations are discussed. The first chapter (chapter 3) deals with the electrocatalytic oxidation of EG at Pt/Ru nanocatalysts supported on MWCNTs, the second chapter (chapter 4) is about the electrocatalytic oxidation of EG, MeOH and FA at MWCNT platform electrochemically modified with Pt/Ru nanoparticles, the third chapter (chapter 5) presents the ORR in alkaline solution using RuOcPcPt catalysts supported on MWCNT electrode, the fourth chapter (chapter 6) outlines the electrocatalytic oxidation of FA and MeOH at MWCNT platform modified with RuOcPcPt and the last chapter summarizes the main fundings of the study and future work.

The MWCNT/Pt-Ru or MWCNT/ RuOcPcPt catalysts discussed in Chapter 3 were used to prepare the nanocomposite electrodes (BPPGE-MWCNT/Pt-Ru or BPPGE-MWCNT/ RuOcPcPt). The previous chapter also dealt with the characterization techniques namely; Raman Spectroscopy, Scanning Electron Microscopy (SEM), Fourier Infra-Red Spectroscopy (FTIR), Atomic Force Microscopy (AFM), Transmission Electron Microscopy (TEM), X-Ray Diffraction (XRD), Cyclic Voltammetry (CV) and Electrochemical Impedance Spectroscopy (EIS) used for the analysis of nonfunctionalized and

functionalized multi-walled carbon nanotubes and nanocomposite membranes prepared from different catalysts.

3.1 Characterisation

Surface characterization was performed in this study to investigate the surface morphology and to obtain information on the distribution of Pt/Ru or RuOcPcPt nanoparticles on BPPGE substrate/platform.

3.1 1 Comparative Raman Spectra

Fig 3.1 below demonstrates overlay comparison of non-functionalized multi-walled carbon nanotubes (MWCNT) and functionalized multi-walled carbon nanotubes (MWCNT-COOH). The peak at ~1340 cm^{-1} can be attributed to D line (a diamond sp^3) while the strongest peak at ~ 1540 cm^{-1} is due to G line (a highly graphitized sp^2 carbon nanotubes). From the graph it can be seen that there is a change in structural form (i.e more defects have been increased). The calculated ID/IG ratio of MWCNT and functionalized MWCNTs indicate more functional groups on the walls of MWCNTs after modification. The ID/IG ratio was calculated by intergrating the height of D and G bands.

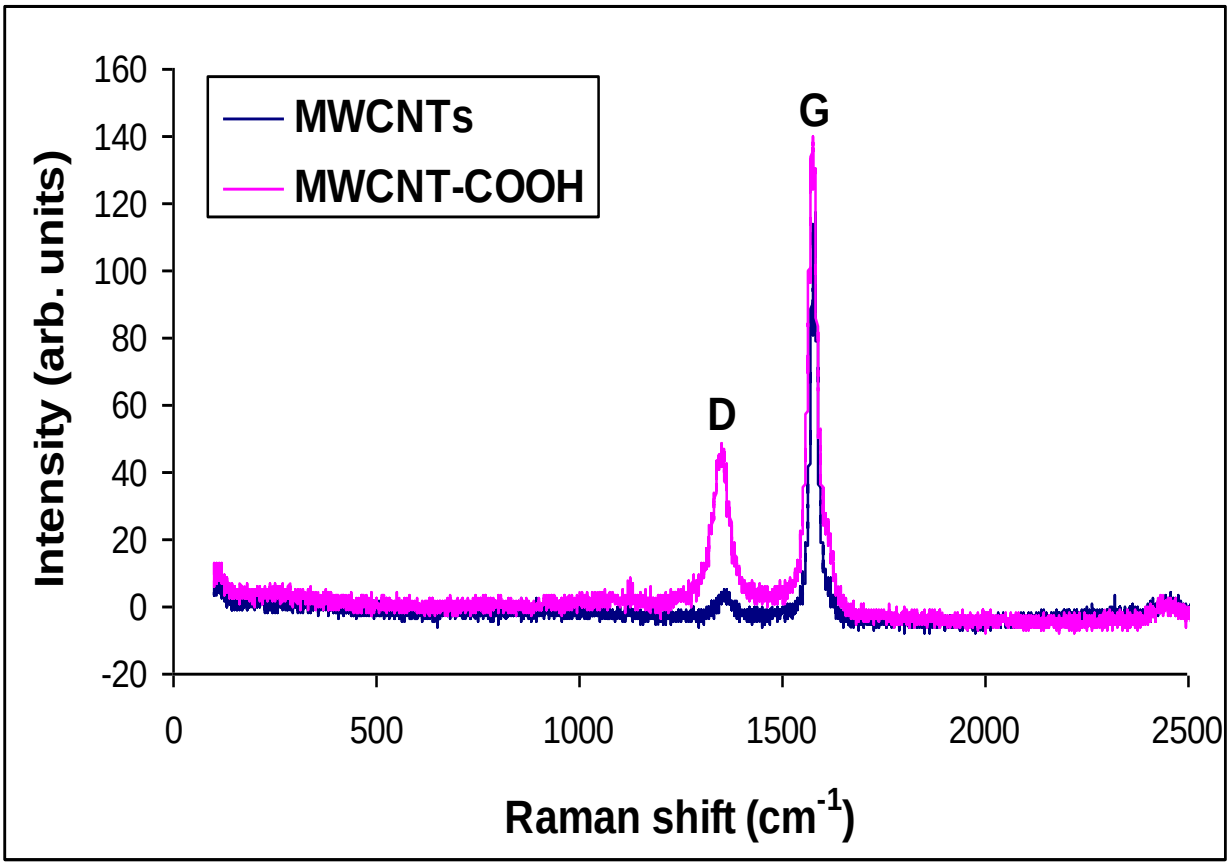

Fig 3.1: Raman spectra of MWCNT and MWCNT-COOH

3.1.2 Comparative FESEM images

The figure below gives the comparison of SEM micrographs of non-functionalized and functionalized carbon nanotubes. In image 1, it appears that the tubes were long before functionalization and short after (image 2) indicating the reduction in length of the nanotubes. The modification of MWCNTs by functionalization method changes the size of the tubes. This implies a change in the morphology of of the functionalized carbon nanotubes.

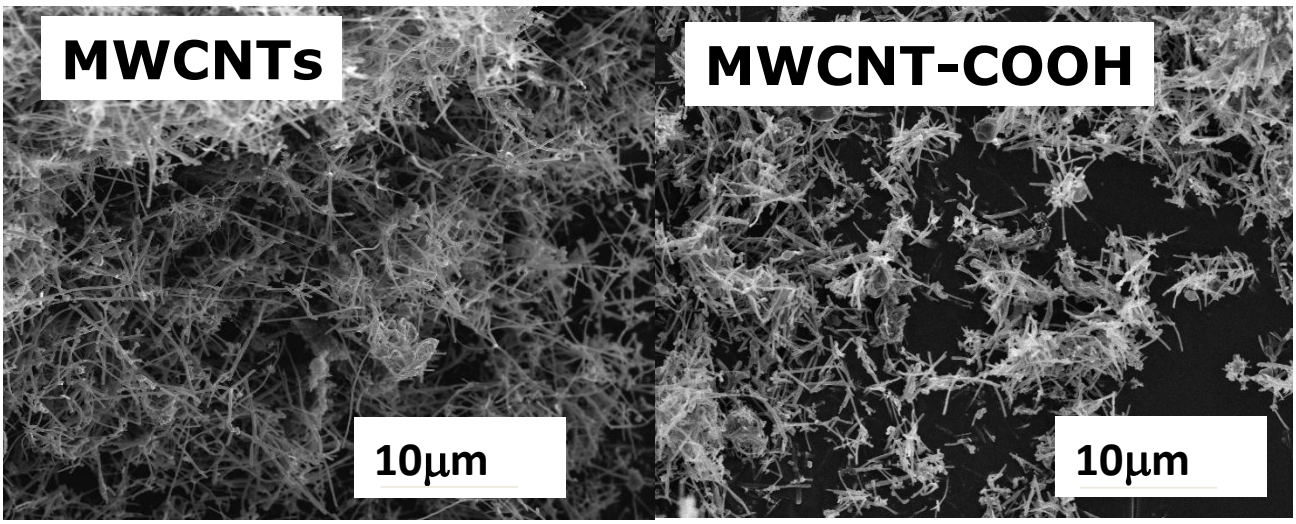

Fig 3.2: FESEM images of MWCNT and MWCNT-COOH

3.1.3 Comparative Infra-Red Spectra

The presence of the peak at ~2840 cm^{-1} in MWCNT-COOH spectrum which is not present in MWCNT spectrum could be assigned to the C=O stretching mode of the COOH group. The peak at ~2800 cm^{-1} is due to the OH stretching mode of COOH group. The presence of C=O and OH groups are evidence of the functionalization of MWCNTs after acid treatment. However, the C=O peak is observed at high values than that reported in the literature and the factor responsible for the shifting may be due to the interaction between carboxylic acid groups.

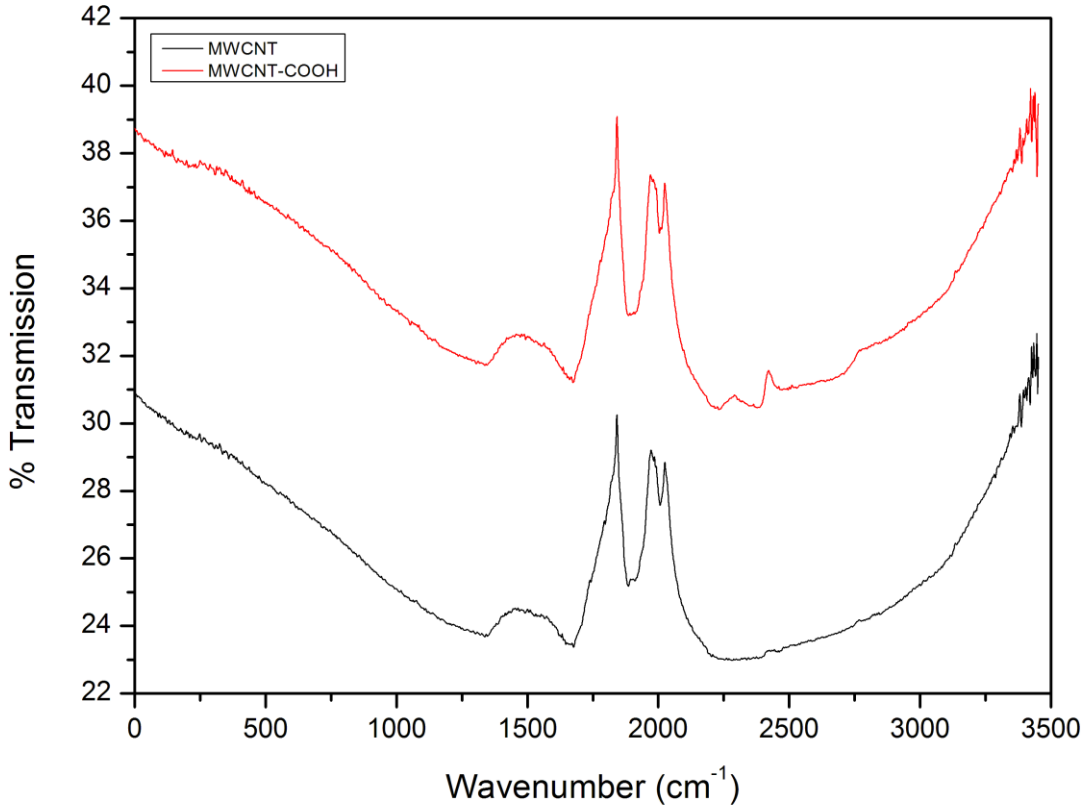

Fig 3.3: FESEM images of MWCNT and MWCNT-COOH

3.1.4 Comparative FESEM images and Energy Dispersive X-rays

Figure 3.4 compares the scanning electron micrographs of (a) bare BPPGE, (b) BPPGE-fMWCNT and (c) BPPGE-fMWCNT-Pt/Ru. Pt and Ru nanoparticles were electrodeposited onto BPPGE-fMWCNT from the solution containing the Pt and Ru salts (Pt/Ru molar ratio = 4:1). From the figure it is observed that Pt/Ru nanoparticles are uniformly distributed on the fMWCNTs. Qualitative EDX spectrum (d) confirms the successful electrodeposition of Pt and Ru

nanoparticles on the surface of MWCNTs, in agreement with the work of He *et al.* [1]. From the quantitative analysis it can be seen that the % elemental weight of Pt:Ru is 3.36:0.05. The % Pt weight agrees closely to the 4.0 expected from the experimental procedure employed while the 0.05 for Ru was lower than the expected 1.0. This behavior can be attributed to the very low concentration of Ru used thus making it impossible to be detected quantitatively by the equipment.

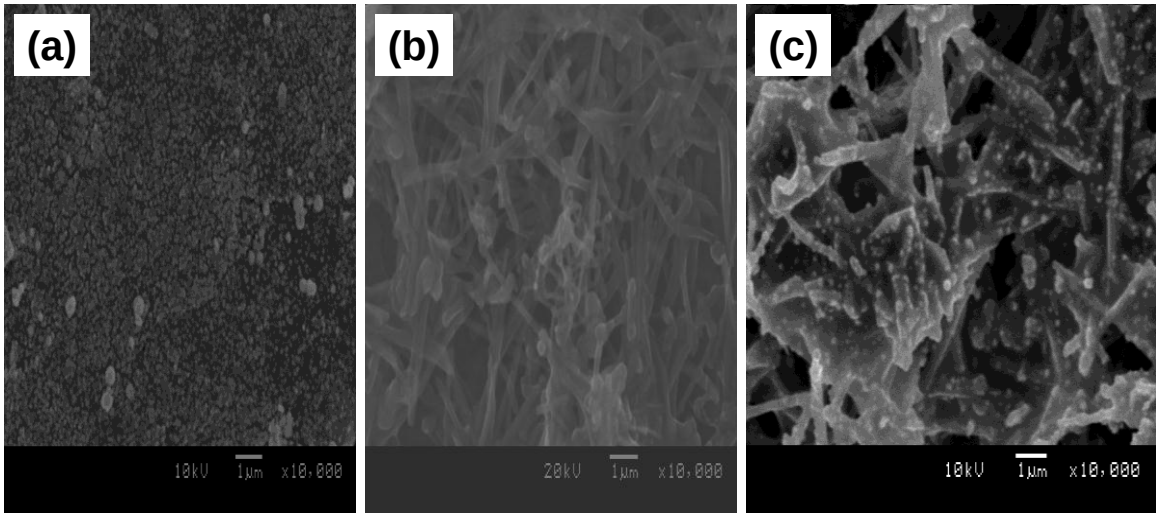

Figure 3.4: Comparative FESEM images of (a) bare BPPGE, (b) BPPGE-fMWCNT and (c) BPPGE-fMWCNT-Pt/Ru. Deposition vessel solution, 0.2 mM K_2PtCl_6 and 0.2 mM $RuCl_3$ (RPt/Ru = 4:1).

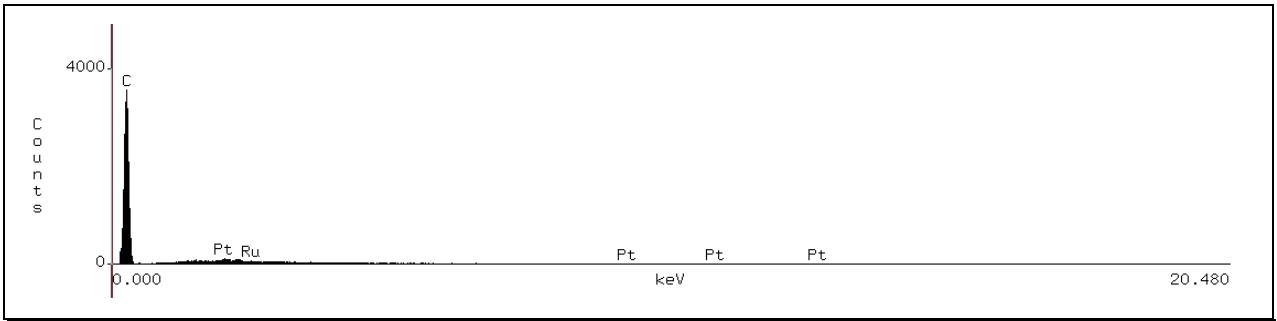

Quantitative Analysis

Chi-sqd = 10.06 Livetime = 100.0 Sec.

Element	k-ratio (calc.)	ZAF	Atom % Wt %	Element Wt (1-Sigma)	% Err.
C -K	0.7964	1.208	99.63	96.20	+/- 0.62
Pt-L	0.0218	1.546	0.21	3.36	+/- 0.68
Ru-L	0.0005	1.113	0.01	0.05	+/- 0.11
S -K	0.0034	1.112	0.15	0.38	+/- 0.05
Total			100.00	100.00	

Figure 3.5: EDX and quantitative analysis of Pt/Ru nanoparticles.

3.1.5 AFM studies

AFM was used to establish the successful fabrication of the electrodes. The AFM images show different morphology for all electrodes. For the bare electrode the surface is open and after modification with CNTs the surface is evenly covered with CNT particles in a paste form. Further modification with 4:1 ratio of Pt/Ru nanoparticles shows the presence of nanoparticles sticked on the CNT paste. When comparing the topographic scales the growth and successful deposition of CNTs and nanoparticles on electrode (c) can be seen.

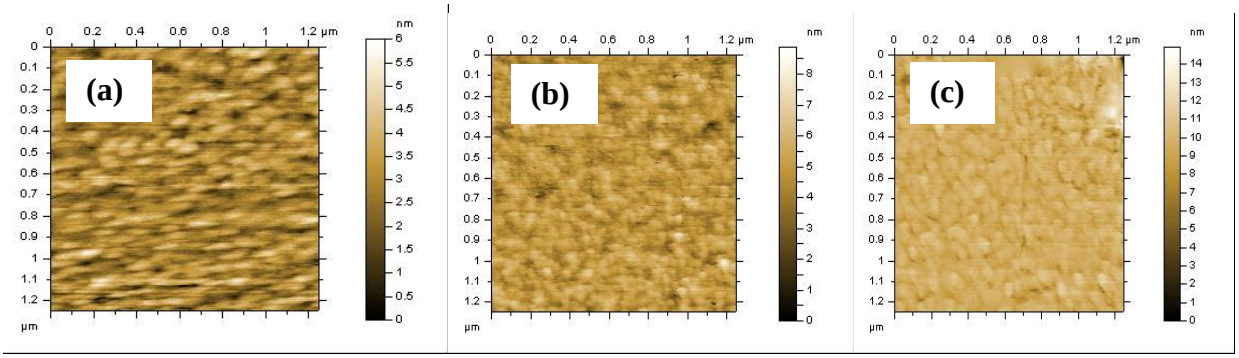

Figure 3.6: AFM images and height profiles of (a) bare GC plates, (b) GC-fMWCNT, and (c) GC-fMWCNT-Pt/Ru.

3.2 Impact of scan rates, concentrations and repetitive scannings

Scan rate study was done to investigate the electrochemical process taking place between the electrode and the analyte solution, concentration study was conducted to determine sensitivity of the electrode while repetitive scanning study was performed to study the reproducibility and stability of the electrode.

Figure 3.7a shows the cyclic voltammetric evolutions of the bare BPPGE, BPPGE-fMWCNT, BPPGE-fMWCNT-Pt, BPPGE-Pt/Ru and BPPGE-fMWCNT-Pt/Ru in 0.5M H_2SO_4 solution containing 0.5M EG. Comparative studies was done in order to compare current responses and to investigate which electrode gives the highest current response during electro-oxidation. The fMWCNT-Pt/Ru gave higher current density compared to other electrodes with well-defined forward and reverse anodic peaks. The reverse anodic peak may be attributed to the removal of incompletely oxidised

carbonaceous species formed in the forward anodic scan. Hence, the ratio of the current density of the forward anodic peak (J_{fa}) to the reverse anodic peak (J_{ra}) is a measure of the fraction of the catalyst surface that is free from the accumulation of the carbonaceous species [2, 3] (e.g., CO, glycolic and oxalic acids in our case) and can be used to describe the catalyst's tolerance to poisoning. For the Pt/Ru nanocatalyst system, the J_{fa}/J_{ra} ratio is close to unity implying that the voltammetric currents are due mainly to direct oxidation of the EG into CO_2.

As also suggested by others [4], the reaction mechanism may be ascribed to the bifunctional mechanism. In acidic medium, EG is known to be completely oxidized to CO_2 in a complex series of reaction steps by Pt based electrodes. De Lima *et al* [5] reported the use of Pt-Ru catalyst for the oxidation of EG and found that CO_2, glycolic acid and oxalic acid as reaction products, and that the complete oxidation to CO_2 is favoured by high Pt content. Ru is not only used to oxidize CO to CO_2, but also promotes the oxidation of other poisonous intermediates of EG oxidation, notably glycolic and oxalic acids. However, the exact mechanism explaining the involvement of the Ru and these poisonous intermediates is still unknown [6].

Figure 3.7 b shows the impact of the oxidation at varying scan rates (0.01 – 1.2 Vs^{-1} range). On increasing scan rates, the peak currents shift to more cathodic (for reverse) and more anodic (for the forward peak) except at high scan rates. At higher scan rates the reverse peak stabilises while the

forward peak continued to increase. It is seen that as the scan rate increases, the J_{fa}/J_{ra} becomes greater than unity, about 2.5 at 1.2 Vs^{-1} implying an apparent tolerance to the poisonous intermediate adsorption. This result can be interpreted as follows: At the higher scan rates, the CO poisoning (as well as other adsorbates) is drastically reduced due to the shorter time spent in the low potential region. The results are similar to the reports of Wang et al on EG oxidation on Pt catalyst supported on carbon [7].

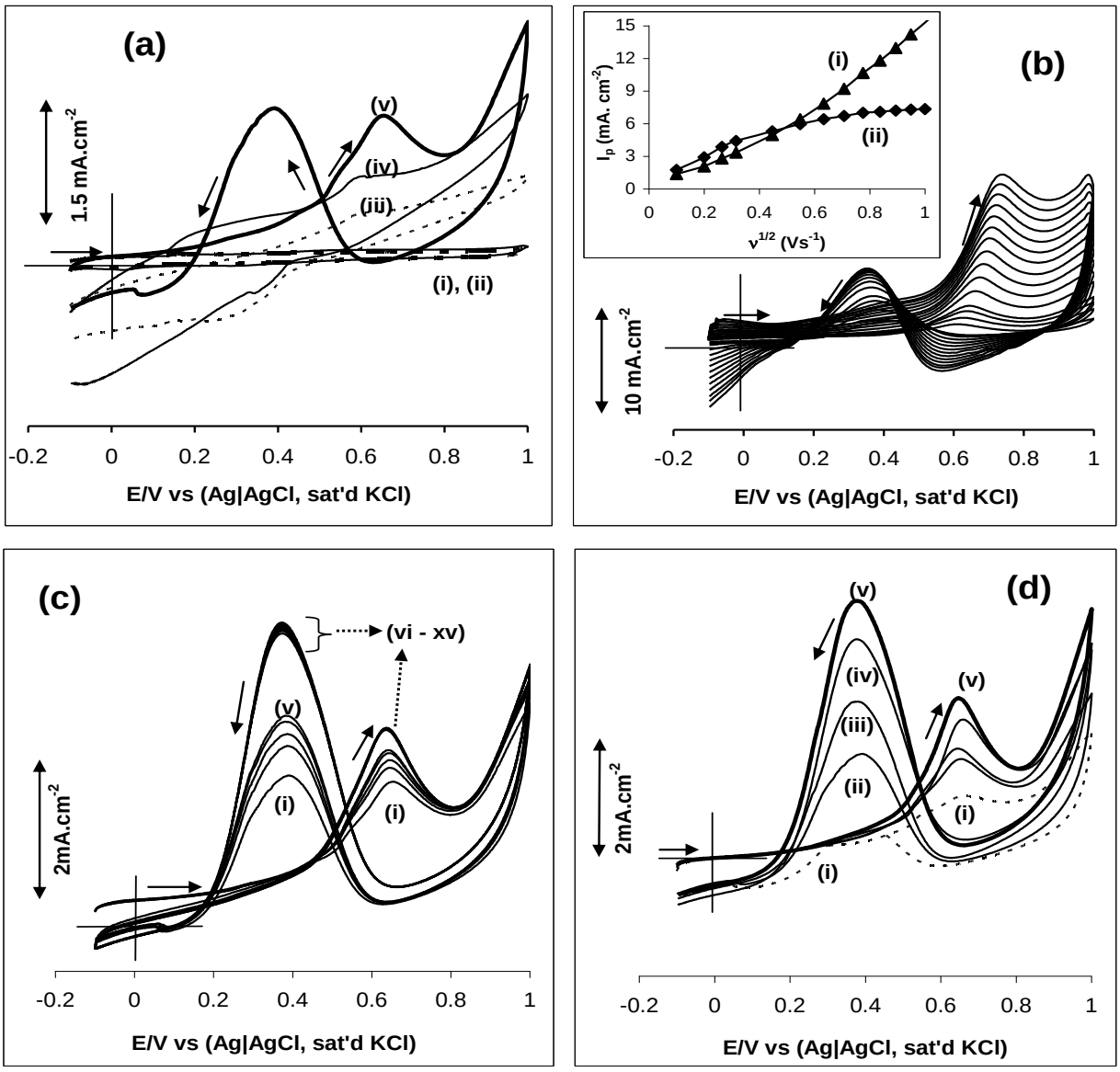

Figure 3.7: (**a**) Comparative cyclic voltammetric evolutions in 0.5 M H_2SO_4 solutions containing 0.5 M EG at different electrodes: (i) BPPGE, (ii) BPPGE-fMWCNT, (iii) BPPGE-fMWCNT-Pt, (iv) BPPGE-Pt/Ru and (v) BPPGE-fMWCNT-Pt/Ru (**b**) scan rate studies of BPPGE-fMWCNT-Pt/Ru in 0.5 M H_2SO_4 solutions containing 0.5 M EG (inset: plots of Ip vs $\nu^{1/2}$, where (i) is the forward peak and (ii) is the reverse peak)**, (c)** cyclic voltammetric evolutions during 15 repetitive scanning (i – xv) of BPPGE-fMWCNT-Pt/Ru in 0.5 M H_2SO_4 solutions containing 0.5 M EG, and (**d**) cyclic voltammetric evolutions following changes in concentrations of EG (0.3, 0.5, 0.7, 0.9 and 1.1 M, from (i) to (v)) at BPPGE-fMWCNT-Pt/Ru increasing at scan rate of 0.5 Vs^{-1}.

The plots of the peak current for both forward and reverse peaks versus the square root of scan rates (I_p vs $\upsilon^{1/2}$) are not truly linear (Figure 3.7b inset), suggesting that in the conditions used in this work, the overall reaction is not diffusion-controlled (i.e., mainly kinetic-controlled). Simply put, both the forward and reverse anodic peaks indicate that the initial oxidation of EG as well as the adsorbed EG and CO (and other poisonous intermediates) inhibit the reaction kinetics. Adsorption phenomena should be expected since one of the important attributes of CNTs is their increased surface areas which make them susceptible to adsorption of solution molecules and reaction intermediates [8]. The results are in agreement with the works of Wang *et al.* [7] that found that EG is not fully diffusion-controlled at Pt/C platform as well as the claim of Ureta-Zañartu *et al*. [9] that claimed diffusion-controlled CV reaction was not possible with EG. It should be mentioned that Selvaraj *et al*. [10] have claimed that the oxidation of 0.5 M EG in 0.5 M H_2SO_4 is diffusion-controlled reaction. However, a closer look at the reported I_p vs $\upsilon^{1/2}$ plots (also using 0.5 M EG in 0.5 M H_2SO_4 as our present report) showed their plots to be non-zero intercepts as would be expected of the Randles-Sevčik theory for reversible cyclic voltammetry. It should also be noted that even in alkaline solution where EG oxidation is expected to be more efficient, [11,12] Hauffe and Heitbaum [13] observed diffusion-controlled reaction only at EG concentration ≤ 5 mM.

Figure 3.7c shows the impact of repetitive scanning on the oxidation of the EG. The current densities of the two anodic peaks increased from the 1st – 5th scan stabilising at the 6th scan. Interesting, at the 6th scan the reverse peak increased sharply resulting in the J_{fa}/J_{ra} being about 0.5, indicating that approximately 50% of the active sites of the catalyst have been poisoned compared to the initial 1 – 5th scans.

Figure 3.7d showed the effect of EG concentration on its oxidation reaction, showing that at EG concentration ≤ 0.5 M, that the J_{fa}/J_{ra} is about 1.0, but at concentration > 0.5 M, the J_{fa}/J_{ra} is reduced to about 0.5 for every 0.1 M EG increase, indicative of catalyst surface poisoning by the adsorption of CO and other imtermediates. Also the peak currents are not proportional to the concentration of EG for the reverse peak, poorly linear (R^2 < 0.9) with the forward peak, confirming again that the overall reaction is not fully diffusion-controlled.

To establish the level of adsorption, we interrogated the Langmuir adsorption isotherm to obtain the electrochemical adsorption equilibrium constant *(β)*, using the equation [14]:

$$\frac{[EG]}{\Gamma} = \frac{[EG]}{\Gamma_{max}} + \frac{1}{\beta\Gamma_{max}} \quad \text{.....} \quad \text{... (3.1)}$$

where Γ is the surface coverage and Γ_{max} is the maximum surface coverage. Assuming that the CV catalytic peak current (I_{cat}) is proportional to the surface concentration of EG, equation 1 may be re-written as:

$$\frac{[EG]}{I_{cat}} = \frac{[EG]}{I_{cat,max}} + \frac{I}{\beta I_{cat,max}} \quad \text{.....} \quad (3.2)$$

By plotting the ratio of the EG concentration to the catalytic current response against the concentration of EG, β value was estimated from the slopes and intercepts of the linear relation as 1.47 M^{-1} for the forward anodic reaction. The electrochemical adsorption Gibbs energy change (ΔG^o) was calculated as -0.95 $kJ.mol^{-1}$ (n = 5, 95% confidence limit) using Equation 3.3:

$$\Delta G^o = - RT \ln\beta. \quad \text{.....} \quad (3.3)$$

where R and T have their usual meaning. The low negative ΔG^o value further suggest weak adsorption of EG at the fMWCNT-Pt/Ru. It was not possible to estimate the values for the reverse anodic peak as the Langmuir plot was non-linear.

3.3 Comparative EIS measurements

For further insights into the oxidation of EG at this modified electrode platform, we used electrochemical impedance spectroscopy (EIS). EIS provides vital information about processes at the electrode|electrolyte interface and is extensively used in probing electrooxidiation of fuel cell molecules for fuel cell application [15-18]. Fig. 3.8a shows the Nyquist plots obtained at two different potentials representing the forward and reverse peak potentials.

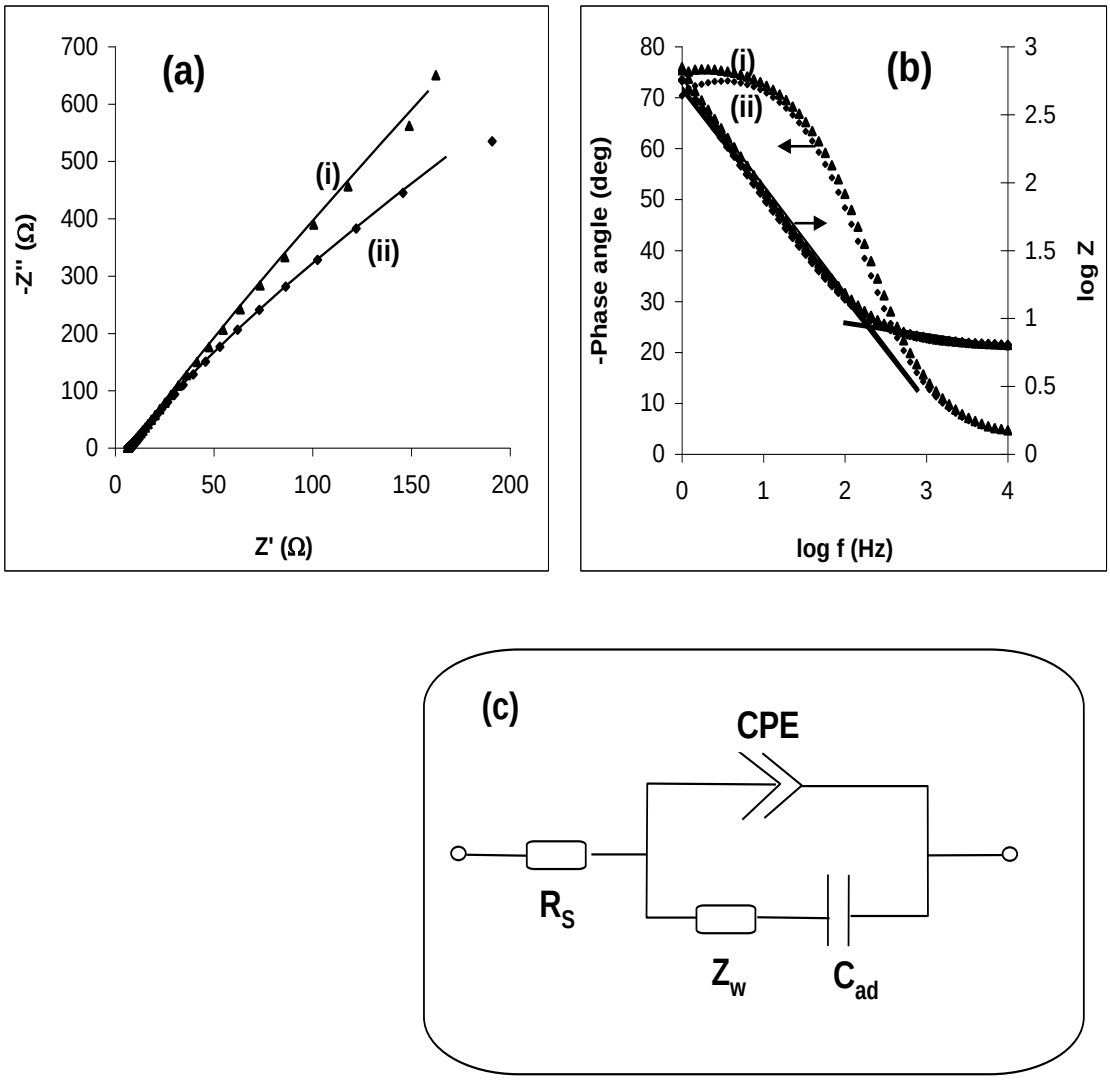

Figure 3.8: (**a**) Typical Nyquist plots (i for forward and ii for reverse peaks) and (**b**) Bode plots of BPPGE-fMWCNT-Pt/Ru obtained in 0.5 M H_2SO_4 containing 0.5 M EG between 10 kHz and 0.1 Hz at forward and reverse peak potentials. The data points are experimental while the solid lines represent fitted (theoretical) spectra obtained from the proposed equivalent circuit model shown in (**c**).

The experimental data were satisfactorily fitted with the modified Randles equivalent circuit (Fig. 3.8c) involving solution resistance (R_s), double layer (Helmholtz layer) capacitance (C_{dl}), electron-transfer resistance across the film (R_{ct}) representing the domain of kinetic control, and constant phase element (CPE) representing the capacity of the film. The chosen equivalent circuit shows satisfactory fittings (solid lines) with the experimental results (data points). The impedance of the CPE (Z_{CPE}) is given as [18]:

$$Z_{CPE} = \frac{1}{Q(j\omega)^n} \quad \text{.....(3.4)}$$

where Q is the frequency-independent constant relating to the surface electroactive properties, ω is the radial frequency, the exponent n arises from the slope of log Z vs log f ($0 \leq n \leq 1$). An n value of zero corresponds to a pure resistor; a unit value of n corresponds to a pure capacitor, while a 0.5 value corresponds to Warburg impedance (Z_w) which is associated with the domain of mass transport control arising from the diffusion of ions to and from the electrode|solution interface. The EIS data seen here have certain implications. First, the replacement of the Z_w with the CPE in the Randles equivalent circuit (Fig. 3.8c), coupled with the fact that the n>0.5 clearly suggests that the CPE is due to the adsorption of intermediates rather than semi-infinite diffusion of the EG to the electrode. This again confirms the CV results that predicted adsorption rather than diffusion-limited reaction. Second, this circuit is opposite to what has been reported

for the methanol or formic acid oxidation that involve both positive and negative Faradaic impedance indicative of pseudo-inductive behaviour as a result of serious poisoning of electrode surfaces [15-17]. From the other type of Bode plot (i.e., –phase angle vs log f, Fig. 3.8b), the phase angles for the forward and reverse potentials are –75^{o} and –70^{o}, respectively, confirming the presence of CPE and pseudocapacitive nature of the electrodes since the angles are less than the –90^{o} expected for an ideal capacitive behaviour. The slopes for the forward and reverse scans are approximately the same (ca. -0.78 and -0.10 at mid and high frequency regions, respectively) indicative of pseudocapacitive and resistive behaviour at these respective frequency regions.

Table 3.1: Impedance data obtained at the BPPGE-MWCNT-Pt/Ru platform in 0.5 M H_2SO_4 containing 0.5 M EG.

Biased potential (vs Ag|AgCl, sat'd KCl)	**Electrochemical Impedance spectral data**				
	R_s / Ω	**CPE / F**	**N**	**Z_w / Ω**	**C_{ad} / μF**
0.66 V (Forward process)	6.11 (0.78)	2.3 x 10^{-4} (3.40)	0.75 (3.16)	6. 6 x 10^{-3} (9.50)	111.20 (10.55)
0.39 V (Reverse process)	6.04 (0.56)	3.1 x 10^{-4} (1.94)	0.62 (3.60)	8.9 x 10^{-3} (2.50)	166.00 (4.39)

The forward and reverse oxidative reactions of EG at MWCNT-Pt/Ru platform exhibit distinct electrochemical behaviour following changes in EG concentrations, scan rates and during repetitive cyclic voltammetric

scanning. The results suggest that the overall electro-oxidation reaction of EG is governed by adsorption-controlled kinetics.

Conclusion

MWCNTs were successfully converted to MWCNT-COOH by employing functionalization method. This was confirmed by Raman, SEM and FTIR. Electrocatalytic investigations by cyclic voltammetry showed that BPPGE-MWCNT-COOH-Pt/Ru is the best electrode in comparison with others. The presence of bright particles observed in HR-SEM image of BPPGE-MWCNT-COOH-Pt/Ru confirm the successful electrodeposition of Pt and Ru nanoparticles on MWCNTs. Several ratios of Pt to Ru were studied and it was found that 4:1 ratio is the best in terms of catalytic activity towards ethylene glycol oxidation. BPPGE-MWCNT-COOH-Pt/Ru 4:1 exhibited excellent electrocatalytic activity for ethylene glycol oxidation due to high dispersion of Pt-Ru nanoparticles with small size. The electrocatalytic properties of Pt/Ru nanoparticle-electrodecorated MWCNT platform towards the oxidation of ethylene glycol have been interrogated. The forward and reverse oxidative reactions of EG at MWCNT-Pt/Ru platform exhibit distinct electrochemical behaviour following changes in EG concentrations, scan rates and during repetitive cyclic voltammetric scanning. The results suggest that the overall electrooxidation reaction of EG is governed by adsorption-controlled kinetics.

References

1. Z. He, J. Chen, D. Liu, H. Tang, W. Deng and Y. Kuang, *Mat. Chem. Phys.* 85 (2004) 396.
2. R. Manohara, J.B. Goodenough, *J. Mater. Chem.* 2 (1992) 875. L. Zhang, D. Xia, *Appl. Surf. Sci.* 252 (2006) 2191.
3. G-Y Zhao, H-L Li, *Appl. Surf. Sci.* 254 (2008) 3232.
4. R. Manohara, J.B. Goodenough, *J. Mater. Chem.* 2 (1992) 875. L. Zhang, D. Xia, *Appl. Surf. Sci.* 252 (2006) 2191.
5. R. B. de Lima, V. Paganin, T. Iwasita, W. Vielstich, *Electrochim. Acta* 49 (2003) 85.
6. V. Selvaraj, M. Alagar, *Nanotechnol.* 19 (2008) 045504. R. B. de Lima, V. Paganin, T. Iwasita, W. Vielstich, *Electrochim. Acta* 49 (2003) 85.
7. H. Wang, Z. Jusys, R.J. Behm, *J. Electroanal. Chem.* 595 (2006) 23.
8. R.T. Kachoosangi, G.G. Wildgoose, R.G. Compton, *Electroanalysis* 20 (2008) 1714.
9. M.S. Ureta-Zañartu, A. Alarcón, G. Muñoz, C. Gutiérrez, *Electrochim. Acta* 52 (2007) 7857.
10. V. Selvaraj, M. Vinoba, M. Alagar, *J. Colloids Interf. Sci.* 322 (2008) 537. V. Selvaraj, M. Alagar, *Nanotechnol.* 19 (2008) 045504.
11. R. Parsons and T. van der Noot, *J. Electroanal. Chem.* 257 (1988) 9.
12. K. Nishimura, M. K-i Machida and M. Enyo, *J. Electroanal. Chem.* 251 (1988) 117.

13. W. Hauffe, J. Heitbaum, *Electrochim. Acta* 23 (1978) 299.

14. H.X. Lu, L. Donal, *J. Electroanal. Chem*. 484 (2000)150.

15. W. Chen, J. Kim, S. Sun, S. Chen, *Phys.Chem.Chem.Phys.* 8 (2006) 2779.

16. J. Zhou, J. He, G. Zhao, C. Zhang, T.W.X. Chen *Electrochem. Commun.* 10 (2008) 76.

17. Z. Zhang, X. Zhou, C. Liu, W. Xing, *Electrochem. Commun.* 10 (2008) 131.

18. E. Barsoukov and J.R. Macdonald, Editors, *Impedance Spectroscopy: Theory Experiment, and Applications* (2nd ed.), Wiley, Hoboken, New Jersey (2005).

CHAPTER FOUR

Dynamics of electrocatalytic oxidation of ethylene glycol, methanol and formic acid at MWCNT platform electrochemically modified with Pt/Ru nanoparticles*

* **N.W. Maxakato**, K.I. Ozoemena, C.J. Arendse, Electroanalysis 22 (2010) 519.

4.1 SEM characterization

SEM technique was employed for the direct observation of BPPGE surfaces modified by chemically synthesized carbon nanotubes and electrodeposited Pt/Ru nanoparticles. Pt/Ru nanoparticles were successfully electrodeposited on MWCNTs. BPPGE-MWCNT-COOH-Pt/Ru 4:1 exhibited excellent electrocatalytic activity for oxidation of fuel cell molecules (as already described in chapter 3).

4.2 Comparative cyclic voltammetric evolutions

Comparative CV studies was done in order to compare current responses and to investigate which electrode gives the highest current response during electrooxidation reactions. Voltammogram obtained at the fMWCNT/Pt-Ru showed a higher current density compared to that of the bare BPPGE or BPPGE containing fMWCNT or fMWCNT with Pt catalyst in acidic medium. The fMWCNT-Pt/Ru (Ratio Pt/Ru = 4:1) gave a higher current density compared to other electrodes with well-defined forward and reverse anodic peaks. Figure 4.1 exemplifies the voltammetric evolutions in 0.5 M H_2SO_4 solutions containing 0.5 M EG (Fig. 4.1a), 0.5 M MeOH (Fig 4.1b) and 0.5 M FA (Fig. 4.1c). The shapes of the voltammograms for EG, MeOH and FA are in good agreement with most published work [1-6] However; there are some deviations from some literature. For example, the activity of our MWCNT/Pt towards MeOH (figure 4.1b (iii)) is poor compared to the recent work by Shi

et al. [7] where Pt nanoparticles/MWCNT multilayers were immobilised onto a gold electrode using the layer-by-layer self-assembly strategy. This clearly indicates that the CNT/Pt based electrode platform and its modification strategy play a major role in the electrocatalytic activity.

Given the enhanced electrocatalytic activity at the BPPGE-fMWCNT-Pt/Ru, all subsequent studies were performed at this electrode platform. There are two main observations here for these three FC molecules.First In terms of the on-set potentials for oxidation, the catalysis of FC molecules follow the trend FA (0.25V) < EG (0.40V) ≤ MeOH (0.42V). The results indicate that the electrooxidation of FA was more favoured than the other FC molecules. However, the current density followed the trend: FA (1.31 μA cm^{-2}) <EG (1.67 μA cm^{-2}) < MeOH (5.96 μA cm^{-2}) which indicates less CO poisoning tolerance on FA compared with others. Second, the reverse anodic peak may be attributed to the removal of incompletely oxidised carbonaceous species formed in the forward anodic scan. Hence, the ratio of the current density of the forward anodic peak (J_{fa}) to the reverse anodic peak (J_{ra}) is a measure of the fraction of the catalyst surface that has not been poisoned by the accumulation of the carbonaceous species (notably CO) and can be used to describe the catalyst's tolerance to poisoning; the higher the value the less poisoned is the electrode. The ratio of the current densities of the forward to the reverse oxidation peaks (J_{fa}/J_{ra}) at this electrode are approximately 2.0, 2.0 and 1.0 for the MeOH, EG and FA

respectively, indicating that FA showed the least electrode poisoning tolerance. The first anodic peak of the FA around 0.2 V is weak, more visibly observed during the concentration studies (discussed latter). The catalyst's tolerance to the direct oxidative pathway for FA, which is the ratio of the first forward anodic to the second forward anodic peaks is also ~ 0.5. In summary, these two observations are indicative of the extent to which the Pt/Ru nanoparticles tolerate poisoning generated by these fuel cell molecules.

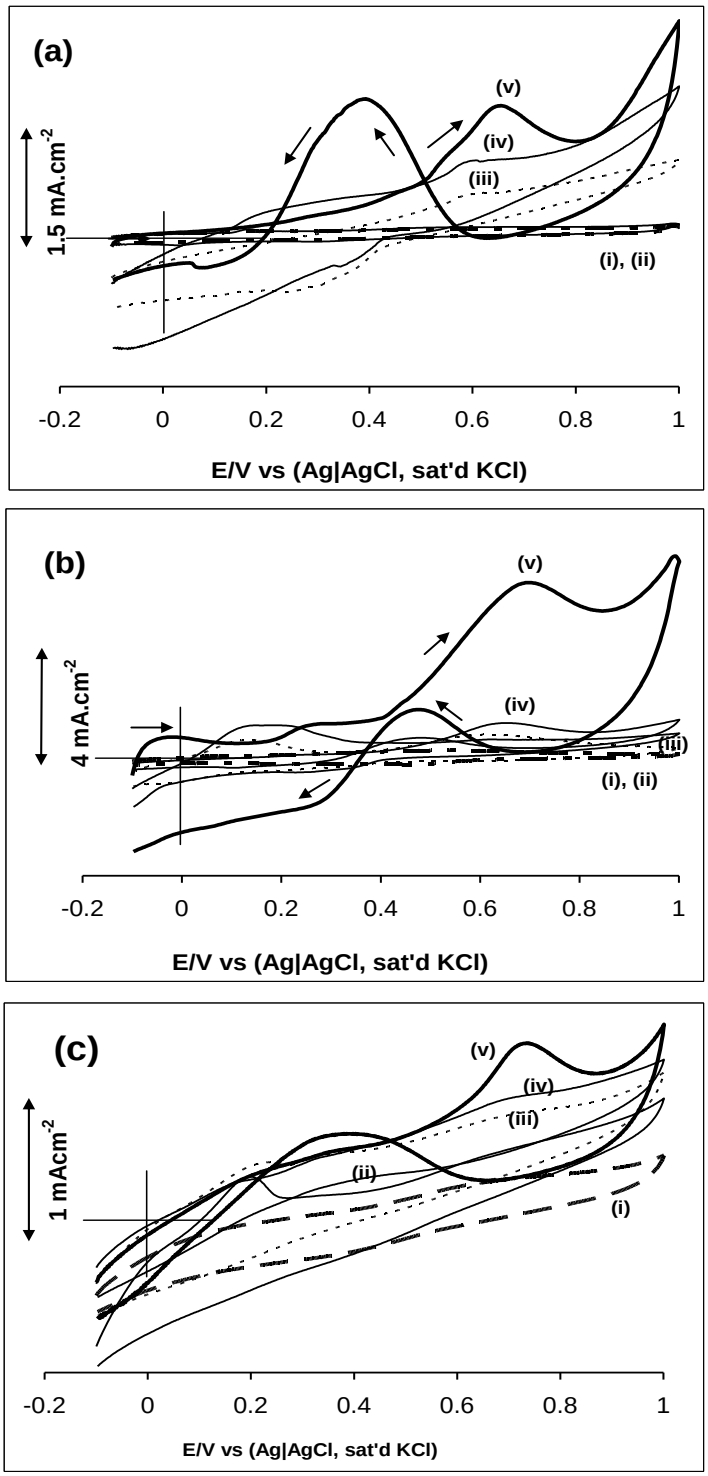

Figure 4.1: Comparative cyclic voltammetric evolutions in 0.5 M H_2SO_4 solutions containing 0.5 M EG (a), 0.5 M MeOH (b) and 0.5 M FA (c) at different electrodes: (i) BPPGE, (ii) BPPGE-fMWCNT, (iii) BPPGE-fMWCNT-Pt, (iv) BPPGE-Pt/Ru and (v) BPPGE-fMWCNT-Pt/Ru. Scan Rate = 0.5 Vs^{-1}.

The electrocatalysed oxidation mechanism for these three molecules at the BPPGE-fMWCNT-Pt/Ru are proposed to follow the well known *"bifunctional mechanism"* [4,7], wherein Ru plays the role of dissociating water to form adsorbed OH species, which then reacts with the adsorbed CO to generate CO_2. Equations 4.1–4.4 summarise those accompanying the MeOH oxidation:

$$Pt + CH_3OH_{(bulk)} \longrightarrow Pt\text{-}(CH_3OH)_{ads} \quad (4.1)$$

$$Pt\text{-}(CH_3OH)_{ads} \longrightarrow Pt\text{-}CO_{ads} + 4H^+ + 4e^- \quad (4.2)$$

$$Ru\text{-}(H_2O)_{ads} \longrightarrow Ru\text{-}(OH)_{ads} + H^+ + e^- \quad (4.3)$$

$$Pt\text{-}CO_{ads} + Ru\text{-}(OH)_{ads} \longrightarrow CO_2 + Pt + Ru + H^+ + e^- \quad (4.4)$$

The first step involves the dehydrogenation process of the MeOH at the Pt surface leading to the formation of the poisonous CO deposited on the active sites of the Pt. To continue with the catalytic oxidation reaction process, the adsorbed CO must be oxidatively removed from the surface to regenerate the active Pt sites. The adsorbed CO molecules are further oxidised into CO_2 (step 4.4) by reacting with the hydroxyl species generated by water electrolysis on the catalyst surface. It is to be noted that steps 4.3 and 4.4 can still occur without Ru but usually at high onset potentials. Ru enhances the activity as the reaction occurs at lower onset potential due to the ability of Ru to activate water molecules at lower potential than on Pt hence oxidising CO at lower potential. This is confirmed by Figure 4.1 where

the onset potential of BPPGE-MWCNT-Pt/Ru was observed at about 0.30 V while at BPPGE-MWCNT-Pt alone it was at 0.40 V.

For the EG, the equations are shown below:

$$(CH_2OH)_2 \longrightarrow (:COH)_2 \quad (4.5)$$

$$Pt + (:COH)_2 + 2H_2O \longrightarrow Pt\text{-}(HCOOH)_{ads} + 2H^+ + 2e^- \quad (4.6)$$

$$Pt\text{-}(CHOOH)_{ads} \longrightarrow Pt\text{-}CO_{ads} + H_2O \quad (4.7)$$

$$Ru + H_2O \longrightarrow Ru\text{-}(OH)_{ads} + H^+ + e^- \quad (4.8)$$

$$Pt\text{-}CO_{ads} + Ru\text{-}(OH)_{ads} \longrightarrow CO_2 + Pt + Ru + H^+ + e^- \quad (4.9)$$

The oxidation of the EG first occurs at the Pt surface yielding formic acid (FA), which in turn leads to the formation of the poisonous CO deposited on the active sites of the Pt. As for the MeOH, the adsorbed CO molecules are then oxidised into CO_2 (step 4.9) by reacting with the hydroxyl species generated by water electrolysis on the catalyst surface. Note again that the the presence of Ru lowers the onset potential where it was observed that with fMWCNT-Pt/Ru the onset potential was about 0.40 V while at fMWCNT-Pt alone it was at 0.50 V. Unlike other reports for FA, [4.9-4.10] the oxidation of FA at the BPPGE-fMWCNT-Pt/Ru platform is associated with a broad reverse peak, which may be ascribed to overlap of two or more peaks mainly due to CO and FA. Also, unlike the MeOH and EG, the forward

scan of FA showed two peaks at 0.40V (with onset potential at 0.0 V) and at 0.70 V for the FA. Similar behaviour has been observed by Chen *et al.* [8-9] at FePt where the first peak was attributed to direct oxidation initiated by the surface-adsorbed hydroxyl species. The same explanation is likely to hold for this system (steps 4.10 and 4.11):

$$Pt/Ru + H_2O \longrightarrow Pt/Ru\text{-}(OH)_{ads} + H^+ + e^- \quad (4.10)$$

$$Pt/Ru\text{-}(OH)_{ads} + HCOOH \longrightarrow CO_2 + H_2O + H^+ + e^- \quad (4.11)$$

The second forward anodic peak and the corresponding reverse broad anodic peak occur via the bifunctional mechanisms (steps 4.12-4.15), which commence with the adsorption of the FA followed by its rapid dissociation into water and CO (step 4.13), and subsequent oxidation of the adsorbed CO molecules into CO_2 enhanced by the Ru-$(OH)_{ads}$ species.

$$Pt + CHOOH_{(bulk)} \longrightarrow Pt\text{-}(CHOOH)_{ads} \quad (4.12)$$

$$Pt\text{-}(CHOOH)_{ads} \longrightarrow Pt\text{-}CO_{ads} + H_2O \quad (4.13)$$

$$Ru\text{-}(H_2O)_{ads} \longrightarrow Ru\text{-}(OH)_{ads} + H^+ + e^- \quad (4.14)$$

$$Pt\text{-}CO_{ads} + Ru\text{-}(OH)_{ads} \longrightarrow CO_2 + Pt + Ru + H^+ + e^- \quad (4.15)$$

Also, the impact of scan rates on the current responses of these three fuel cell molecules was studied. The plots of peak current density against the square root of scan rates (I_p vs $\upsilon^{1/2}$) at scan rates ranging from 10 – 1200

mVs^{-1}. In general, both the forward and reverse oxidation processes are associated with adsorption of intermediates that seriously impact on the global reaction kinetics. Adsorption phenomena should perhaps not be surprising since one of the major attributes of CNTs is their high surface area that makes them most susceptible to adsorption of solution molecules and reaction intermediates [10].

Next, the effect of varying concentrations on the electrooxidation dynamics of the fuel cell molecules was explored. Figure 4.2 illustrates the impact of changes in the concentrations (0.3 – 1.1 M) of EG (Fig. 4.2a), MeOH (Fig. 4.2b) and FA (Fig. 4.2c) on their oxidation reactions. From the plots of peak current density ($mAcm^{-2}$) vs concentration the following observations were made; (i) for EG, a linear plot for the forward (r^2 = 0.9889) and poor linearity for the reverse (r^2 = 0.9128) oxidations were observed. (ii) for MeOH, the forward plot confirms linearity (R^2 = 0.9946) while for the reverse plot showed poor linearity (R^2 = 0.9836) while (iii) the FA showed much better linearity for both the forward (R^2 = 0.9941) and reverse (R^2 = 0.9974) peaks. This result is indicative of catalyst surface poisoning due to the adsorption of CO and other intermediates for EG and MeOH oxidations [11]. In a nutshell, the results seem to suggest that the ability of the electrode platform studied in this work to tolerate poisoning at increasing concentrations of the molecules is best at FA, compared with other fuel cell molecules.

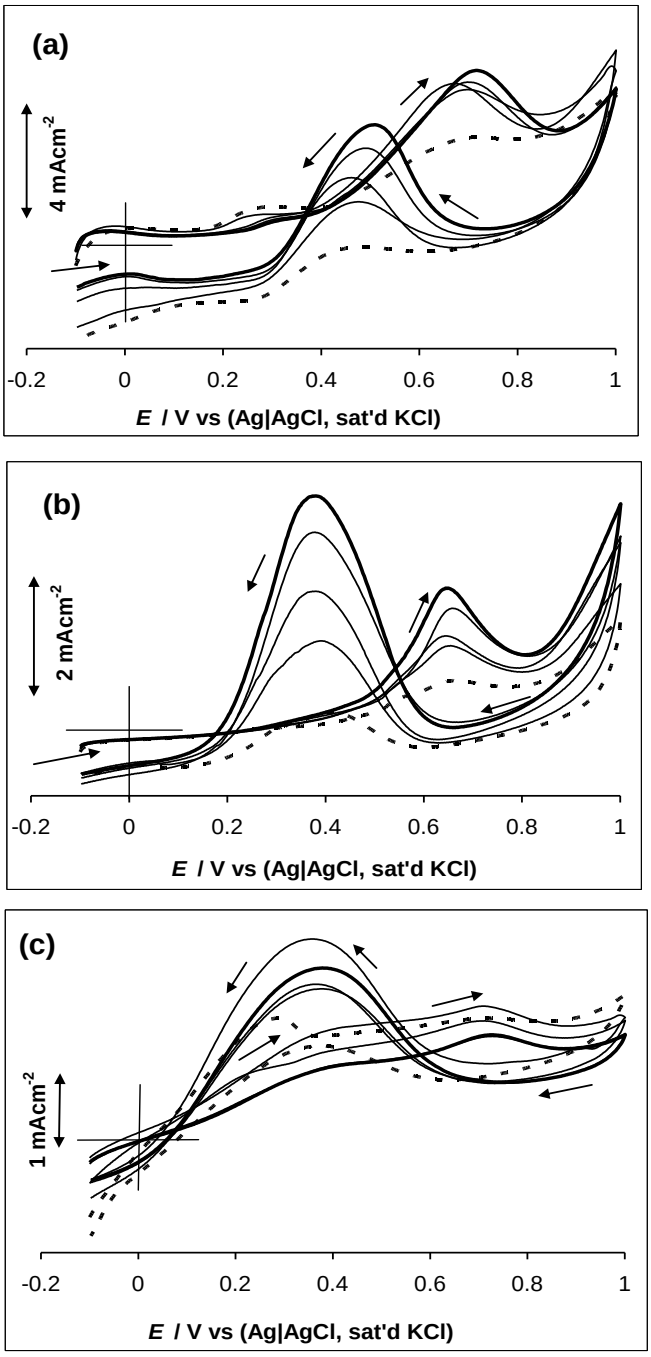

Figure 4.2: Cyclic voltammetric evolutions following changes in concentrations of (a) EG, (b) MeOH and (c) FA (0.3, 0.5, 0.7, 0.9 and 1.1 M) at BPPGE-fMWCNT-Pt/Ru. Scan rate = 0.5 Vs^{-1}.

4.3 Studies on the Catalysts Tolerance to CO Poisoning

To obtain an unequivocal insight into a catalysts ability to tolerate CO poisoning, it is crucial to perform CV experiments with the fuel cell molecules in the presence of CO [12-13]. Figure 4.3 shows the CV responses of the three molecules obtained at fMWCNT-Pt/Ru electrode for the (a) EG, (b) MeOH and (c) FA saturated with CO gas (i), electrolyte saturated with CO gas alone (ii), and electrolyte in the absence of fuel solvent and CO gas (iii). As evident from the Figure 4.3, in the presence of CO, the forward and reverse waves of the EG and MeOH, observed in the previous Figures 4.1 and 4.2, are almost completely suppressed. With the FA, however, the electrocatalytic waves are still clearly observed. The only negative impact seen for the FA is the absence of the first forward peak as well as the increase in the onset potential of the second forward potential from ~0.5 V to about 0.7 V, occuring at the same potential as the CO oxidation. Simply stated, the CO experiment proves that the electrode (BPPGE-fMWCNT-Pt/Ru) tolerates CO when used for the electrocatalytic oxidation of FA much better than when used for the EG and MeOH. Also, note that the reverse oxidation peak that occurred at 0.78 V is possibly due to the oxidation of the adsorbed CO or FA species. These findings are noteworthy as the author is not aware of any such comparative investigations as performed in this work. In this study, the high suppression of the EG and MeOH activity in the presence of CO may not rule out the operation of the proposed bifunctional mechanism,

but may simply suggest that generation of high concentration of CO during electrooxidation negatively impact the catalysis of EG and MeOH.

4.4 Impedance spectroscopy measurements

Electrochemical impedance spectroscopy (EIS) provides vital information about processes at the electrode|electrolyte interface and extensively used in probing electrooxidiation of fuel cell molecules at carbon substrates for fuel cell application [8, 14-15]. First, the researcher explored the impedimetric evolutions at the potentials where the forward and reverse anodic peaks were obtained for the EG, MeOH and FA (Figure 4.4).

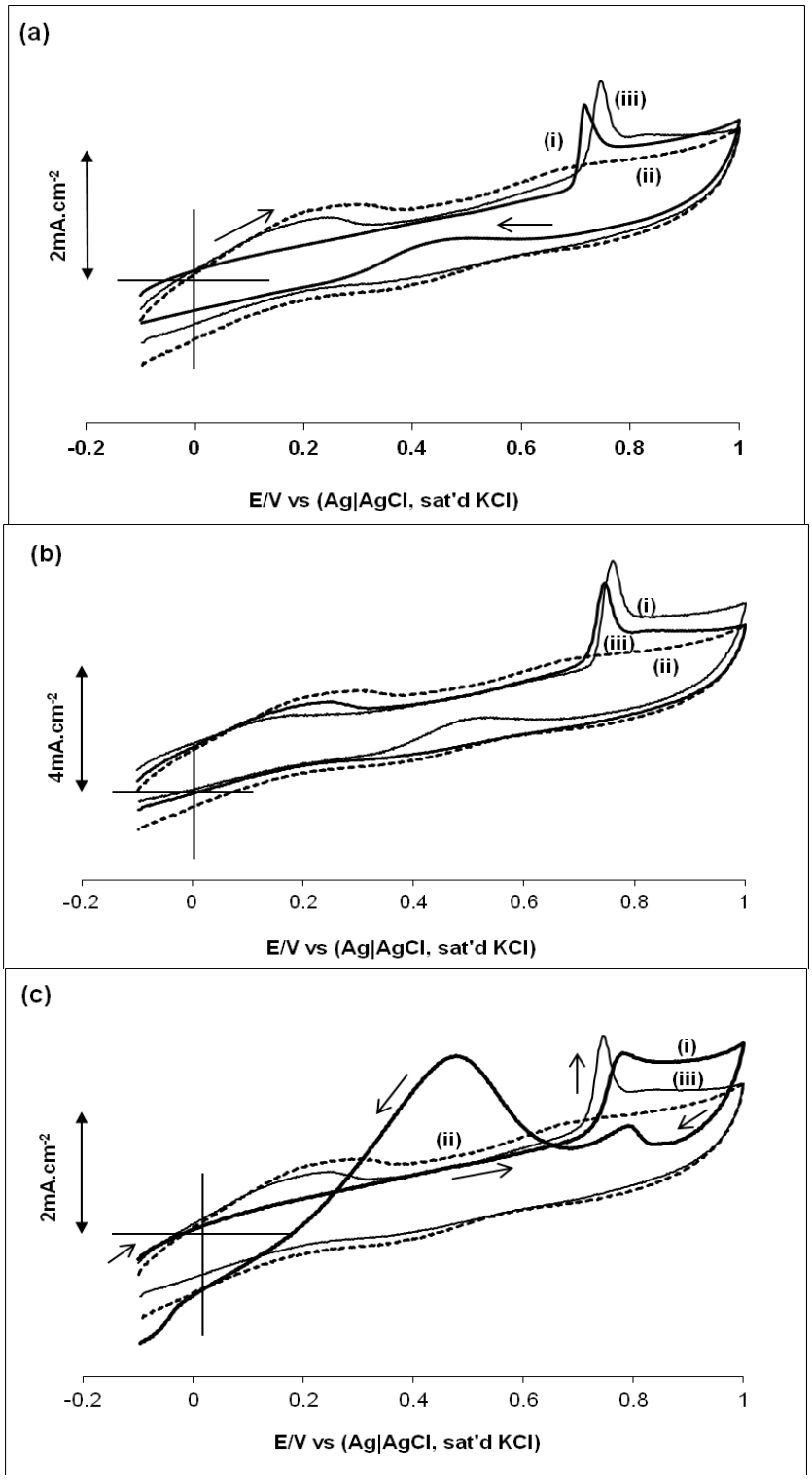

Figure 4.3: Comparative cyclic voltammetric evolutions in 0.5 M H2SO4 containing 0.5M EG (a) 0.5M MeOH (b) and 0.5M FA (c) in the presence of CO gas (i). Curve (ii) represents the electrolyte alone, while curve (iii) represents electrolyte saturated with CO gas. Working electrode is the BPPGE-fMWCNT-Pt/Ru. Scan Rate = 0.05 V.s-1.

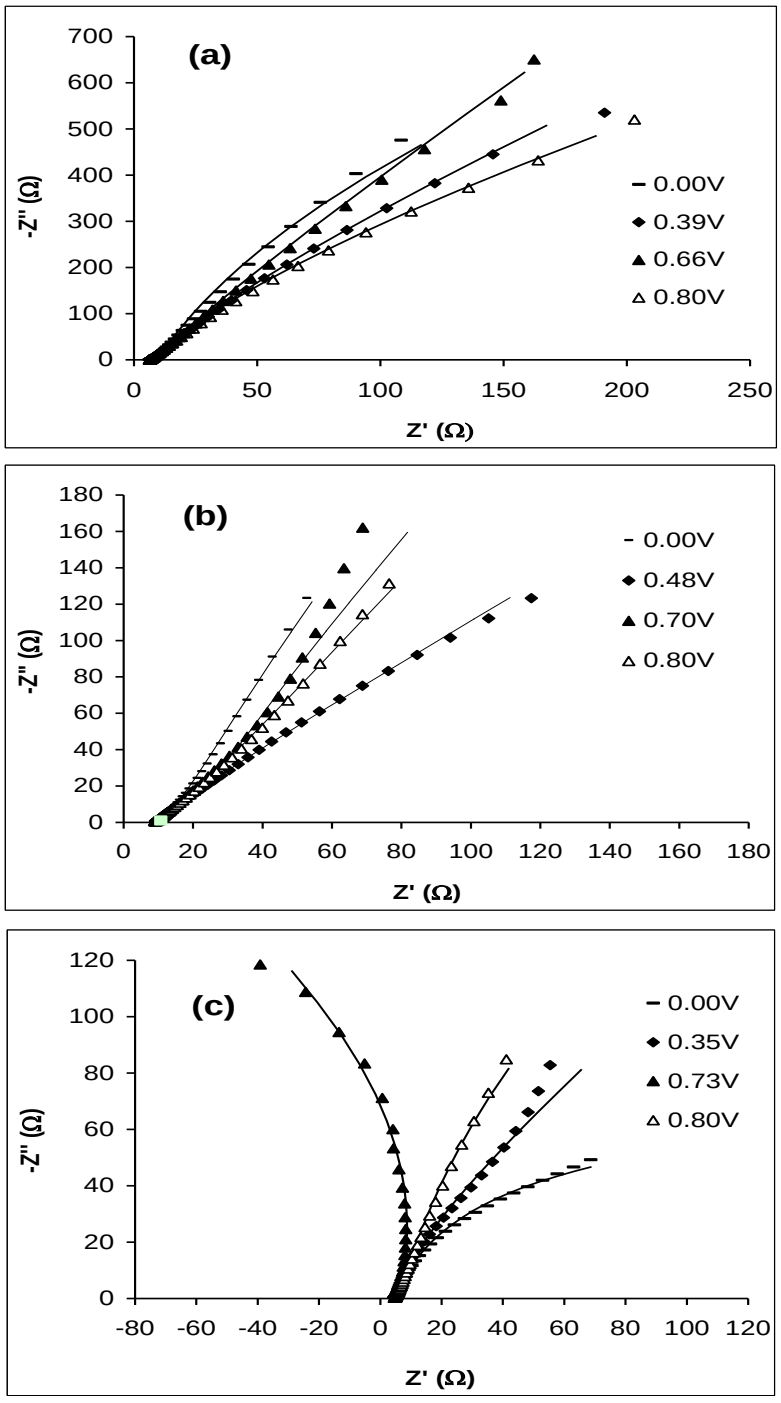

Figure 4.4: Typical Nyquist plots at different potentials and Bode plots of BPPGE-fMWCNT-Pt/Ru obtained in 0.5M H_2SO_4 solutions containing 0.5M EG (a), 0.5M MeOH (b) and 0.5M FA (c) between 10kHz and 0.1 Hz at forward and reverse peak potentials.

The experimental spectra obtained for the three molecules at the forward and reverse potential peaks were fitted with theoretical electrical equivalent models (Figure 4.5). Aside from visual inspection of goodness of the fitting lines, two accurate ways to establish how well the modeling functions reproduce the experimental data sets are the relative error estimates (in %) and pseudo chi-square functions (χ^2) resulting from the Kramers-Kronig (K-K) test. The χ^2 values in this work are in the 10^{-5} and 10^{-4} range. For the EG, impedance spectra obtained at both the forward (0.70 V) and reverse (0.4 V) potentials, were satisfactorily fitted with the modified Dolin-Ershler equivalent circuit (Fig. 4.5a), where R_s and CPE represent the solution resistance and constant phase element (CPE) instead of the true double layer capacitance, R_{ads} and C_{ads} represent the adsorption (or partial charge-transfer resistance) and adsorption capacitance arising from the oxidation of adsorbed carbonaceous species on the electrode's surface. The fitted data were summarized in Table 4.1a.

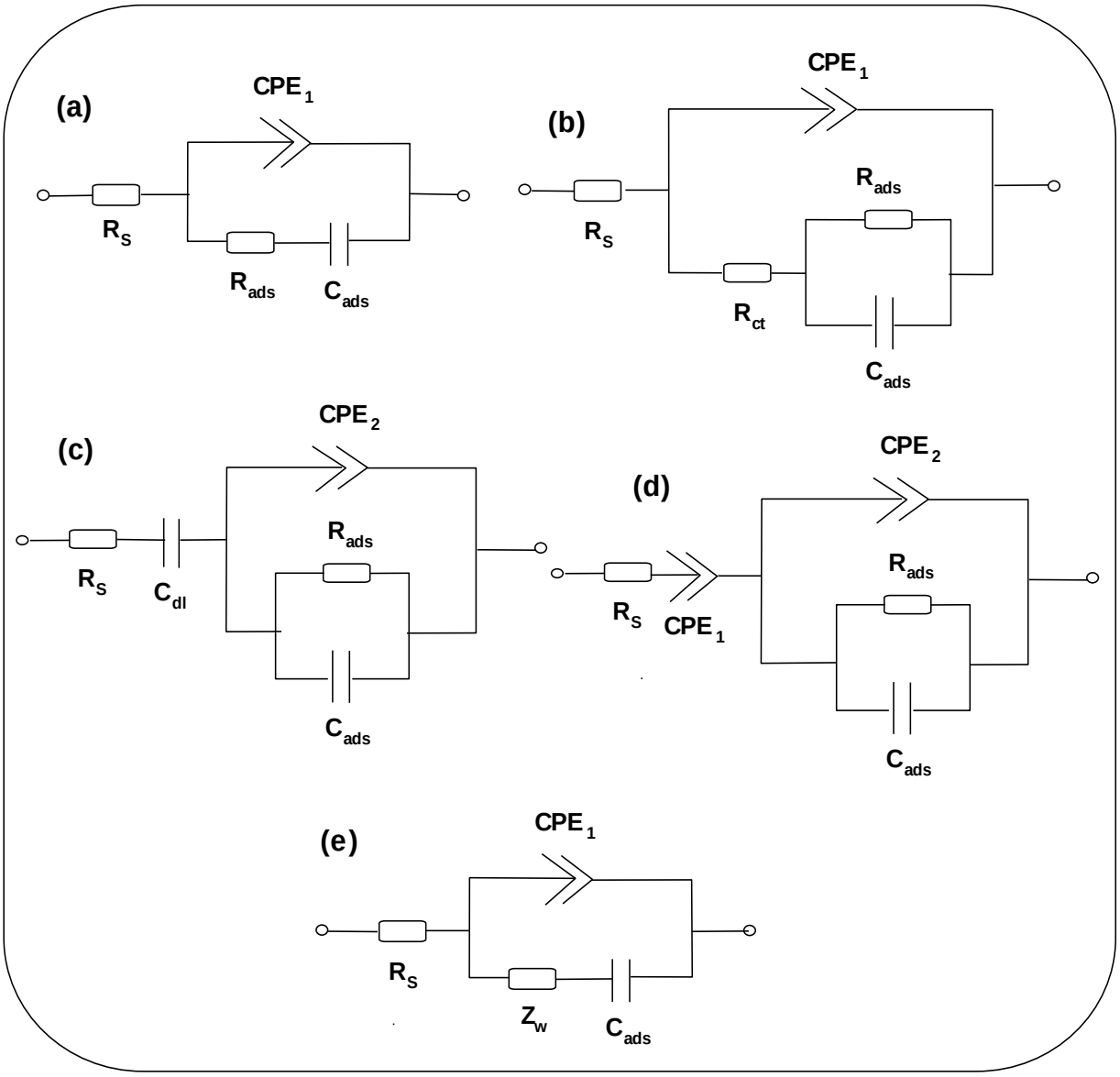

Figure 4.5: Equivalent circuits used to fit the EIS data of BPPGE-fMWCNT-Pt/Ru in 0.5 M H_2SO_4 solutions containing 0.5 M EG, 0.5 M MeOH and 0.5 M FA.

Table 4.1: Impedance data obtained at the BPPGE-fMWCNT-Pt/Ru platform in 0.5 M H_2SO_4 containing 0.5 M of the fuel cell solvents (ethylene glycol, methanol or formic acid) at the foward and reverse peak potentials. Value in parenthesis is fitting error in percent.

***Ethylene Glycol*: Circuit Figure 4.5a was used to fit the spectra for both 0.4 and 0.70 V**

Bias potential / V (vsAg|AgClsat'd KCl)	R_s / Ω	CPE / mF	N	R_{ads} / Ω	C_{ads} / μF
0.40 (Reverse process)	8.83 (0.34)	1.71 (2.49)	0.62 (0.60)	8.98 (23.82)	32.91 (15.83)
0.70 (Forward process)	9.02 (2.22)	3.10 (5.74)	0.60 (2.57)	20.90 (25.11)	21.59 (14.38)

***Methanol*: Circuit Figure 4.5b was used to fit spectrum for the 0.48V while Figure 4.5c was used for the 0.70 V.**

Bias potential / V (vs Ag|AgCl sat'd KCl)	R_s / Ω	C / mF	CPE / mF	N	R_{ct} / Kω	R_{ads} / kΩ	C_{ads} / μF
0.48 (Reverse process)	8.83 (0.34)	-	1.71 (2.49)	0.62 (0.60)	0.537 (19.16)	0.467 (10.32)	99.1 (21.53)
0.70 (Forward process)	9.02 (2.22)	1.26 (2.62)	3.10 (5.74)	0.60 (2.57)	-	0.140 (13.15)	78.1.00 (43.4)

***Formic acid*: Circuit Figure 4.5a was used to fit the spectrum for the 0.35V while Figure 4.5d was used for the 0.73 V.**

Bias potential / V (vsAg|AgClsat'd KCl)	R_s / Ω	CPE_1 / mF	n_1	R_{ads}/ Ω	C_{ads} / μF	CPE_2 / mF	n_2
0.35(Reverse process)	4.00 (1.67)	3.20 (2.23)	0.53 (1.78)	1.45 (10.10)	3.75 (3.75)	-	-
0.73(Forward process)	2.44 (0.00)	1.00 (6.06)	0.56 (5.59)	-25.77 (0.00)	150.60 (50.73)	1.70 (3.80)	0.73 (8.73)

For the MeOH, the spectrum at the low potential (0.48 V) was fitted with the modified Randles circuit (Figure 4.5b), comprising the charge transfer resistance (R_{ct}), CPE used instead of C_{dl}, and the Warburg impedance (Z_w) replaced by one Voigt RC element. The spectrum at the higher potential (0.70 V) was fitted with circuit shown as Figure 4.5c with R_s and C_{dl} in series. The fitted data are summarized in Table 4.1b. Note that systems comprising resistor and capacitor in series are considered to exhibit blocking or ideally polarisable behavior [16]. Also, R_{ads} in parallel with C_{ads} is characteristic of an electrochemical response with a strongly adsorbed intermediate. Thus, R_{ads} and C_{ads} are associated with contributions of the surface concentrations (coverage) of the adsorbed intermediates and the rate of adsorption or desorption arising from the oxidation of MeOH and/or adsorbed carbonaceous species on the electrode.

For the FA, the forward anodic peak potential (0.73 V) gave negative Faradaic impedance, while the spectrum obtained at the lower potential (0.38 V) exhibited conventional positive Faradaic impedance. The negative Faradaic impedance is indicative of the presence of an inductive component characteristic of adsorbed intermediates. Similar spectrum was also observed by Chen *et al.* [8,9] and was attributed to the formation of chemisorbed hydroxyl species (steps 10 and 14) that competes for surface adsorption sites against the CO and, at the same time, enhances their oxidative removal from the electrode surface. The spectrum at the low

potential (0.35 V) was fitted with the modified Dolin-Ershler equivalent circuit (Figure 4.5a), while the spectrum at higher potential (0.73 V) was fitted with circuit Figure 4.5d with R_s and CPE_1 in series. The fitted data values are summarized in Table 4.1c.

The three circuits so far used to fit the impedance spectra of these FC molecules describe the absence of mass transport, suggesting that the oxidation of any of these molecules is controlled mainly by adsorption process, in good agreement with the CV results. To obtain further insights into the adsorption of the oxidation intermediates, more EIS experiments were performed at different potentials ranging from 0.0 – 0.8 V Figure 3.4. Interestingly, we found that only the modified Frumkin-Melik-Gaikazyan (FMG) equivalent circuit (Figure 4.5e), incorporating the diffusive resistance (Warburg impedance), could be satisfactorily used to fit all the spectra, except for the spectrum at the 0.73 V for FA that could only be fitted with circuit (d). EIS data for the proposed GMG equivalent circuit model are summarized in Table 4.2.

Table 4.2: Impedance data obtained at the BPPGE-fMWCNT-Pt/Ru platform in 0.5 M H_2SO_4 containing 0.5 M of the fuel cell solvent (ethylene glycol, methanol or formic acid) at different potentials. Circuit Figure 5e was used to fit the data. Value in parenthesis is fitting error in percent.

Bias potential /V(vs Ag|AgCl sat'd KCl)	R_s / Ω	CPE / mF	N	$10^3 Z_w$ / Ω	C_{ads} / μF
		Ethylene Glycol			
0.00	6.04 (0.51)	0.25 (8.88)	0.29 (18.80)	9.70 (1.99)	310.40 (1.60)
0.39	6.04 (0.56)	0.31 (1.94)	0.62 (3.60)	8.90 (2.50)	166.00 (4.39)
0.66	6.11 (0.78)	0.23 (3.40)	0.75 (3.16)	6.60 (9.50)	111.20 (10.55)
0.80	6.01 (0.64)	0.36 (3.04)	0.52 (4.80)	9.60 (2.98)	187.10 (3.24)
		Methanol			
0.00	8.98 (0.64)	0.93 (8.88)	0.50 (26.26)	8.80 (9.99)	1.14 (14.76)
0.48	8.63 (0.61)	2.20 (0.10)	0.53 (1.42)	2.20 (7.73)	0.07 (16.52)
0.70	9.13 (0.77)	0.40 (33.84)	0.75 (4.92)	3.20 (7.83)	1.19 (13.38)
0.80	8.69 (0.59)	1.40 (5.26)	0.62 (1.66)	2.30 (7.81)	0.57 (11.23)
		Formic acid			
0.00	4.39 (0.48)	6.80 (1.56)	0.25 (3.00)	18.0 (2.87)	0.53 (2.26)
0.35	4.58 (1.11)	3.30 (2.83)	0.48 (3.46)	40.0 (22.04)	0.37 (7.09)
0.80	4.46 (0.35)	2.40 (5.08)	0.24 (18.18)	19.0 (1.35)	1.63 (3.08)

It is interesting to note that the FMG model is most popular for analyzing the adsorption of organic molecules [17]. Thus, the satisfactory fitting with the modified FMG model is a further confirmation of the dominance of adsorption process on the global electro-oxidation processes.

The notable impedance spectral features observed in this work should be emphasised. First, the spectral features for MeOH and EG are dependent on potential with no inductive behaviour. This is a contrast to many other reports for MeOH [17-19]. Unfortunately, I cannot make any comparison for EG as I am not aware of any impedimetric investigation of EG as done in this work. Second, the electrical equivalent circuits used in this work to model our experimental impedimetric data are unique as they differ remarkably from every known literature reports. I attribute these discrepancies to various factors ranging from the nature of the electrodes to differing experimental conditions employed. The impedance of the CPE (Z_{CPE}) is already described in chapter 3 (equation 3.4).

Generally speaking, CPE may occur as a result of several factors [20,21] including (i) the nature of the electrode (e.g., roughness and polycrystallinity), (ii) distribution of the relaxation times due to heterogeneities existing at the electrode/electrolyte interface, (iii) porosity and (iv) dynamic disorder associated with diffusion. From the Tables, n_1 and n_2 are ≥ 0.53 for CPE_1 and CPE_2, respectively meaning pseudocapacitive behaviour. CPE_2 is associated with the CO_{ads} oxidation [7].

From the Bode plots (i.e., –phase angle (θ/°) vs log f (Hz), Fig. 4.6, the phase angles of EG, MeOH and FA for the forward and reverse potentials are ~ 75°, < 70° and ≥ -85° respectively, confirming the presence of CPE and pseudocapacitive nature of the electrodes since the angles are less than the –90° expected for an ideal capacitive behaviour.

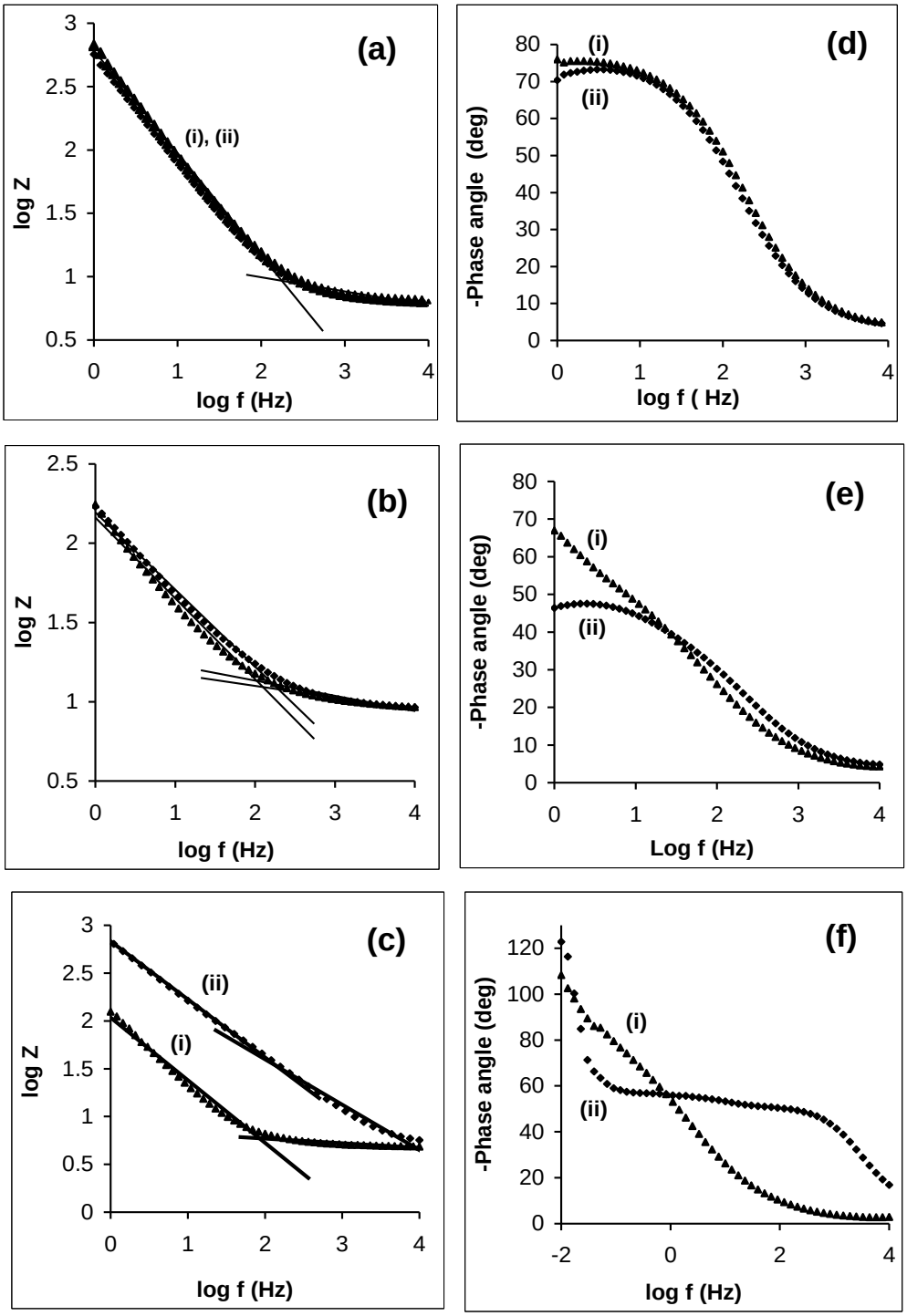

Figure 4.6: Bode plots (log |Z| vs log f) for EG (a), MeOH (b) and FA (c). Plots (d), (e) and (f) are the corresponding Bode plots (phase angle vs log f), respectively.

The slopes of EG, MeOH and FA recorded for the forward and reverse scans are (ca. -0.78 and -0.10, -0.50 and -0.07, and -0.66 and -0.05 at mid and high frequency regions, respectively) indicative of pseudocapacitive and resistive behaviour at these respective frequency regions. Notice that at 0.73 V for FA, phase angle greater than the ideal -90^{o} for pure capacitive behaviour appeared at low frequencies, suggesting that the reaction kinetics change to pseudo-inductive behaviour. In electrocatalytic reactions, inductive behaviour occurs when the Faradaic current is governed by the occupation of an intermediate state [22-24], thus, the observation here is interpreted as the consequence of the domination of adsorption of the intermediate(s) on the electrodes.

Conclusion

Several ratios of Pt to Ru were studied and it was found that 4:1 ratio is the best in terms of catalytic activity towards electrooxidations of ethylene glycol (EG), methanol (MeOH) and formic acid (FA) fuel cell molecules. Electro-oxidation of EG, MeOH and FA at bare BPPGE and BPPGE modified with MWCNTs and decorated with metal nanoparticles has been investigated. From cyclic voltammograms (CV) it was found that BPPGE-fMWCNT-Pt/Ru exhibited excellent electrocatalytic activity than other electrodes. Comparative studies on the electrocatalytic behaviour of EG, MeOH and FA fuel cell molecules at MWCNT-Pt/Ru supported on basal plane pyrolytic

graphite electrode have been investigated. From the cyclic voltammetric results, the ratio of the forward anodic to the reverse anodic peak current densities follow this order: MeOH > EG > FA. Oxidation was favored in FA since it oxidizes at lower potentials than MeOH and EG. From CV and Impedance, it has been proven that FA gives better electrocatalytic response (faster kinetics, higher current density). FA impedance spectrum exhibited inductive loop, characteristic of Faradaic current being governed by the occupation of an intermediate state. Our results proved that the electro-oxidation reactions of EG, MeOH and FA are governed by adsorption-controlled kinetics. Based on the above observations, it can be concluded that electro-oxidation of FA performs better than that of MeOH and EG. We believe that the novel results in this work have provided some useful insights into the potential application of these FC molecules in fuel cell technology.

References

1. V. Selvaraj, M. Vinoba, M. Alagar, *J. Colloid and Interf. Sc.* (2008) 322 537.
2. G.L. Che, B.B. Lakshmi, E.R. Fisher, C.R. Martin, *Nature* (1998) 393 346.
3. Z. Liu, X-Y Ling, B. Guo, L. Hong and J-Y Lee, *J. Power Sources* (2007) 167 272.
4. Q. Zhong, P. Huang, B. Zhang, X. Yang, Y. Ding, H. Zhou, B. Ren and Z. Tian, *Acta Phys.-Chim. Sin. (*2006) 22 291.
5. V. Selvaraj, M. Alagar, *Nanotechnol.* (2008)19 045504.
6. J. Shi, Y-Q. Hu, Y-X. Hua, *Electroanalysis (*2008) 20 1483.
7. A.L. Ocampo, M. Miranda-Hernandez, J. Morgado, J.A. Montoya and P.J. Sebastian, *J. Power Sources (*2006) 160 915.
8. W. Chen, J. Kim, S. Sun, S. Chen, *Phys. Chem. Chem. Phys.* (2006) 8 2779.
9. W. Chen, J. Kim, S. Sun, S. Chen, *Langmuir* (2007) 23 11303.
10. A.S. Adekunle, J. Pillay, K.I. Ozoemena, *Electroanalysis (*2008) 20 2587.
11. H.X. Lu, L. Donal, *J. Electroanal. Chem*. (2000) 484 150.
12. F, Hu, C. Chen, Z. Wang, G. Wei, P. K. Shen, Electrochim.Acta (2006) 52 1087.

13. A. N. Gavrilov, E. R. Savinova, P. A. Simonov, V. I. Zaikovskii, S. V. Cherepanova, G. A. Tsirlina, V. N. Parmon, Phys-ChemChemPhys. (2007) 9 5476.

14. J. Zhou, J. He, G. Zhao, C. Zhang, T.W.X. Chen, *Electrochem. Commun. (*2008) 10 76.

15. M.E. Orazem, B. Tribollet, Electrochemical Impedance Spectroscopy, John Wiley & Sons Inc, Hoboken, NJ., 2008, Chapter 16.

16. G. Nurk, H. Kasuk, K. Lust, A. Janes, E. Lust, J. Electroanal.Chem (2003) 553.

17. F. Ye, S. Chen, X. Dong, W. Lin, *J. Nat. Gas. Chem*. (2007) 16, 162.

18. Lin, X. Cui, C. H. Yen and C. M. Wai, *Langmuir* (2005) 21 11474.

19. W. Sugimoto, K. Aoyama, T. Kawaguchi, Y. Murakami and Y. Takasu, *J. Electroanal. Chem*. (2005) 576 215.

20. K. Nishimura, M. K-i Machida and M. Enyo, *J. Electroanal. Chem.* (1988) 251 117.

21. V. Ganesh, S. Pitchumani and V. Lakshminarayanan, *J. Power Sources* (2006) 158 1523.

22. J. Bisquert, H. Randriamahazaka and G. Garcia-Belmonte, *Electrochim. Acta* (2005) 51 627.

23. M. Jafarian, M.G. Mahjani, H. Heli, F. Gobal, H. Khajehsharifi and M.H. Hamedi, *Electrochim. Acta* (2003) 48 3423.

24. S. Majdi, A. Jabbari, H. Heli and A.A. Moosavi-Movahedi, *Electrochim. Acta* (2007) 52 4622.

CHAPTER FIVE

Oxygen Reduction Reaction in Alkaline Solution using Ruthenium Tetrakis(diaquaplatinum)-Octacarboxyphthalocyanine Catalysts Supported on Multi-Walled Carbon Nanotube Electrode*

*N.W. Maxakato, S.A. Mamuru, K.I. Ozoemena, Electroanalysis 23 (2011) 325.

This chapter deals with a different catalyst compared to previous studies reported in chapters 3-4. The chapter presents a novel ruthenium tetrakis(diaquaplatinum)octacarboxy-phthalocyanine abbreviated as RuOcPcPt supported on MWCNTs and electrocatalytic performance of oxygen reduction reaction (ORR) in alkaline medium. Figure 5.1 shown below was determined by following the method proposed by Dolotova [1] for cobalt derivative.

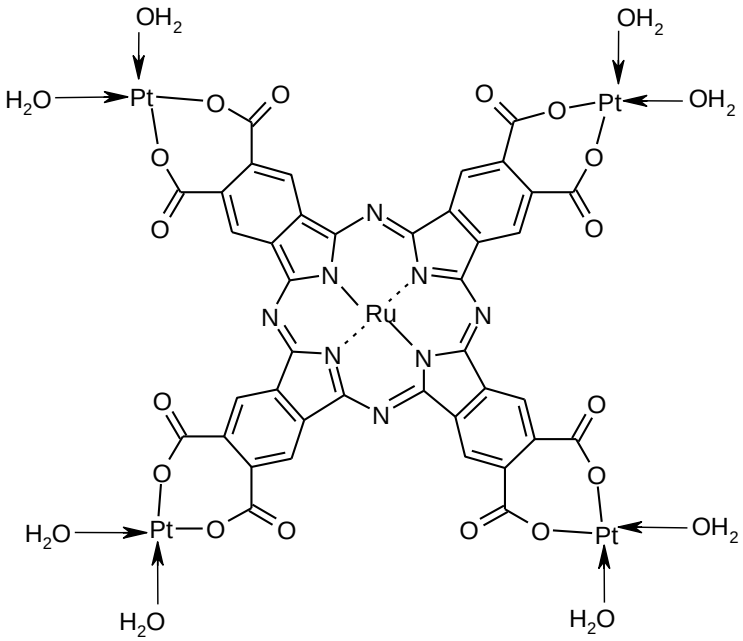

Figure 5.1: Structure of ruthenium tetrakis(diaquaplatinum) octacarboxy phthalocyanine.

The above structure can be represented by the following equation:

$$\textbf{OcPcRuNa} \xrightarrow[\text{H}_2\text{O, MeOH, EtOH}]{\text{K}_2[\text{PtCl}_4]} \textbf{OcPcRuPt}_4\textbf{(H}_2\textbf{O)}_8 \qquad (5.1)$$

Analysis with XRD was used to obtain information on the crystallinity of RuOcPc and RuOcPcPt catalysts. Crystalline structure shows sharp and well-defined peaks while amorphous structure shows narrow peaks. TEM was used to determine the average particle size and particle size distribution of RuOcPc and RuOcPcPt catalysts.

5.1 Spectroscopic and microscopic characterisation

Figure 5.2 presents typical XRD (a) and EDX profiles (b) while Figure 5.3 reports the SEM and TEM images of the RuOcPcPt.

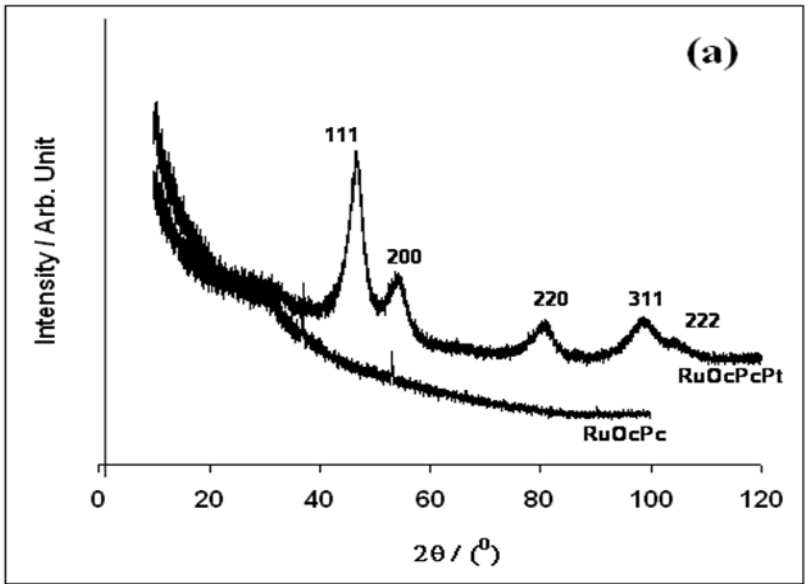

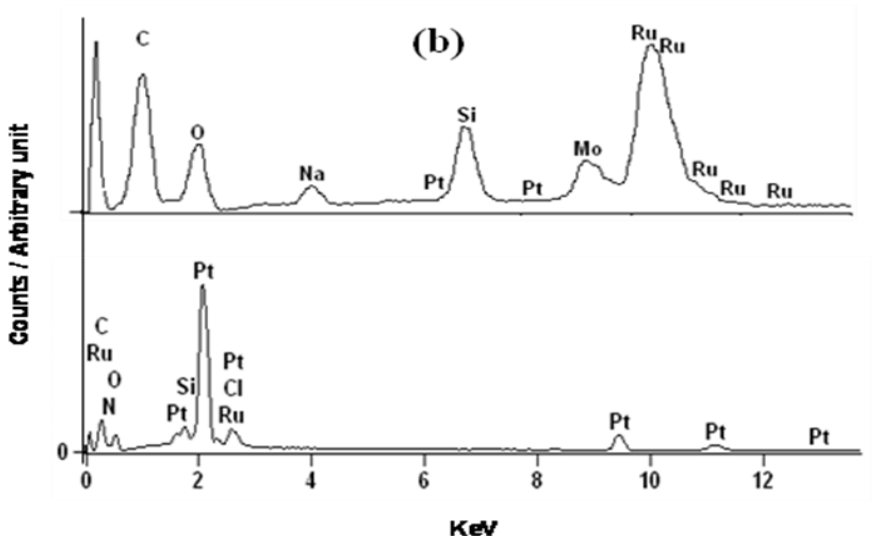

Figure 5.2: XRD pattern of RuOcPc and RuOcPcPt (a) and EDX profiles of RuOcPc and RuOcPcPt (b).

Judging from its precursor RuOcPc, the comparative XRD profiles clearly show the successful introduction of Pt into the RuOcPc. The elemental analysis of the EDX gave atomic ratio of Ru (4.02±0.16): Pt (16.66±0.62), confirming the expected atomic ratio of 1:4 (Ru:Pt). From the SEM and TEM images, the RuOcPcPt show aggregated particles with diameter ≥ 5 nm.

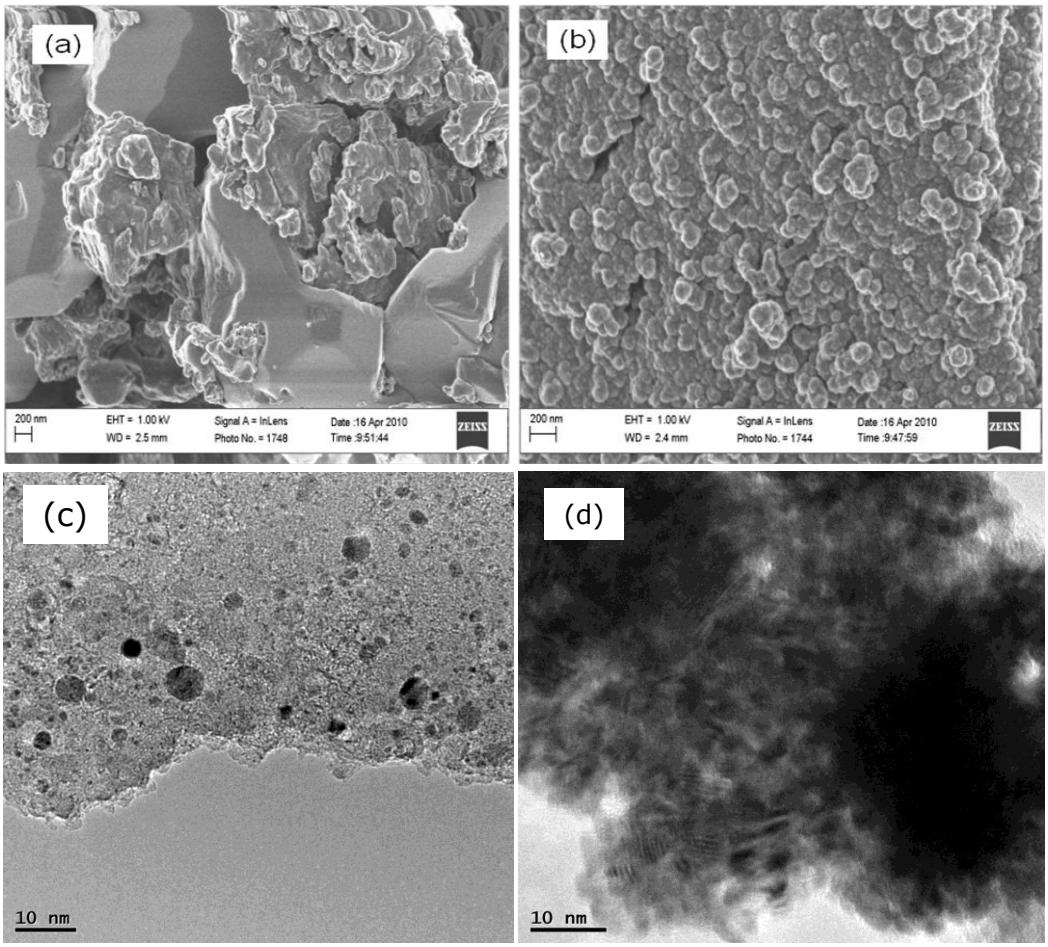

Figure 5.3: SEM images of RuOcPc (a) and RuOcPcPt (b) while (c) and (d) are the TEM images.

5.2 Oxygen reduction reaction (ORR)

From the cyclic voltammetric evolutions in oxygen-saturated 0.1 M NaOH solution (Figure 5.4), it is evident that the BPPGE-fMWCNT-RuOcPcPt showed the least onset potential (–0.12 V) and broad peak potential (~ –0.3 V vs. Ag|AgCl sat'd KCl) compared to other electrodes.

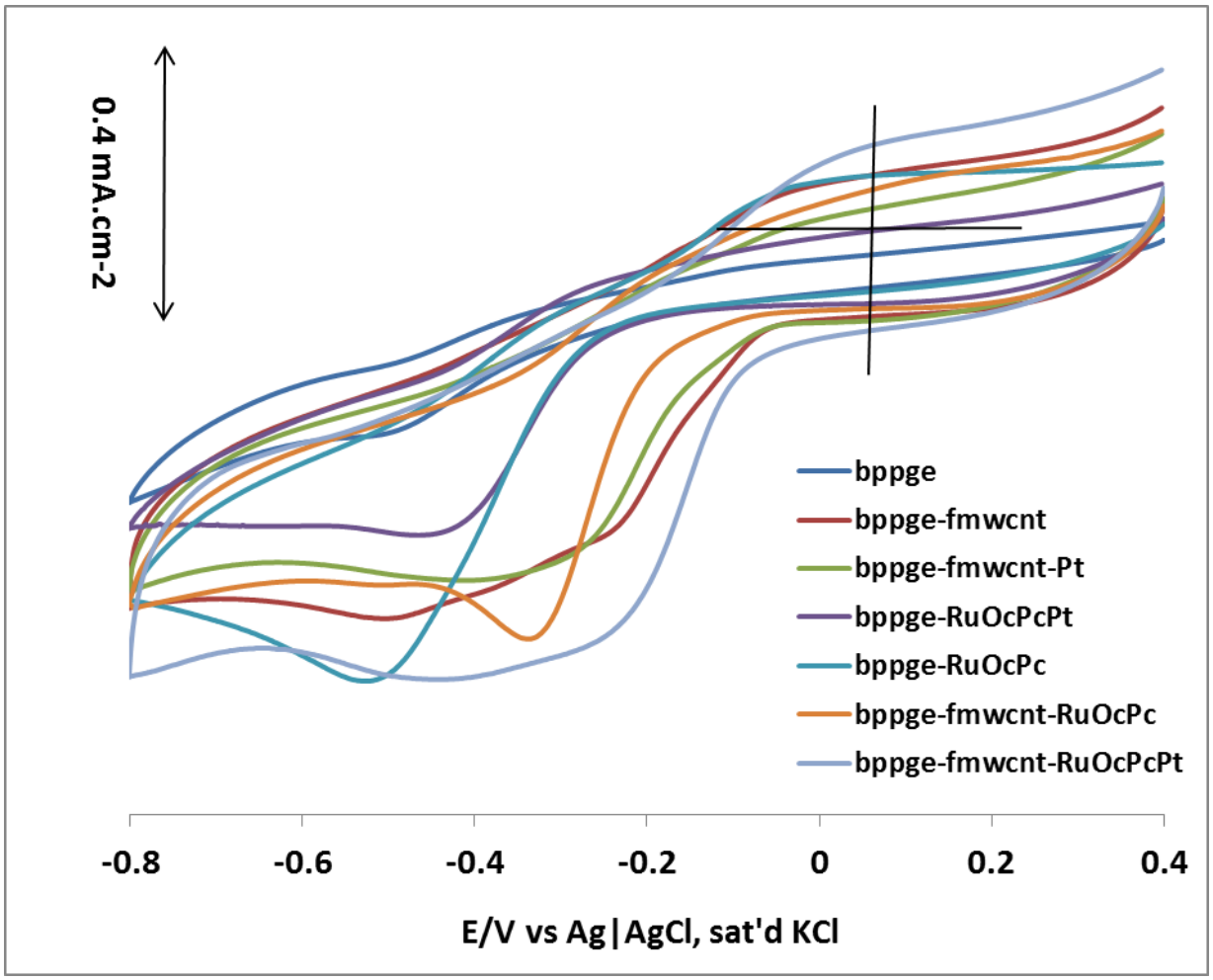

Figure 5.4: Comparative cyclic voltammetric curves in oxygen-saturated 0.1 M NaOH solution scan rate 25 mVs^{-1}.

The broadness of the peak is presumably because the ORR at the Pt and Ru are occurring at almost the same or very close potential. It is interesting to

observe the presence of Pt resulted in huge improvement of the onset potential, from ~ -0.2 V (RuOcPc) to -0.12 V (RuOcPcPt). Also, the presence of conducting MWCNTs increased the ORR response, on BPPGE-fMWCNT-RuOcPcPt compared to BPPGE-RuOcPcPt. The higher performance of the MWCNT-RuOCPcPt electrode (in terms of onset potential, reduction peak potential and current density) clearly indicates faster charge transfer kinetics towards ORR compared to other electrodes. Note that the fMWCNT-RuOcPcPt electrode showed reproducible voltammograms during repetitive scanning in 0.1 M NaOH as well as chronoamperometric response in 0.1 M NaOH saturated with oxygen, confirming electrochemical stability.

The kinetics of the ORR at the MWCNT-RuOCPcPt electrode was explored using the rotating disk electrode (Figure 5.5a). Figure 5.5a clearly shows that the current density increased as the rotation rate is increased, with a limiting current density of 3.06 mA cm^{-2} at 2500 rpm. Figure 5.5b is the plot of j_{lim}^{-1} versus $\omega^{-1/2}$ employing the Koutecky-Levich equation:

$$\frac{1}{J} = \frac{1}{J_{\text{Lev}}} + \frac{1}{J_{\text{kin}}} \tag{5.2}$$

$$J_{Lev} = 0.21nFD^{2/3}\gamma^{-1/6}C_{O_2}\omega^{1/2} \tag{5.3}$$

$$J_{kin} = nFkC_O \tag{5.4}$$

where J is the measured current density, J_{Lev} and J_{kin} are the limiting current density and the kinetic current density respectively, γ is the kinematic viscosity (0.01 cm^2s^{-1} [2], ω is the angular frequency of rotation, D is the

diffusion coefficient of oxygen in an aqueous solution (1.90 x 10^{-5} cm^2s^1 [3]), C_{O2} is the concentration of oxygen in NaOH solution (1.38 x 10^{-6} $molcm^{-3}$ [3-4]), k is the kinetic rate constant for the catalyzed oxygen reduction reaction. The linearity of the plot is indicative that the reaction is first order, and controlled by kinetics at the electrode surface as well as mass transport of oxygen species. From the slope of the Koutecky-Levich plot, the number of electrons (n) transferred per oxygen molecule was calculated as 3.78±0.30, suggesting that ORR at MWCNT-RuOcPcPt electrode proceeds via a single 4-electron transfer mechanism. J_{kin}, obtained from the intercept of the Koutecky-Levich plots, was calculated to be –16.16 mA cm^{-2} at –0.45 V vs. Ag|AgCl (sat'd KCl). The kinetic rate constant (k) was calculated as 3.57 x 10^{-2} cm s^{-1}. This value is in the same magnitude (1.96 x 10^{-2} – 5.87 x 10^{-2} cm s^{-1} range) obtained in alkaline media reported on the gold nanoclusters catalyst [5] and tungsten carbide nanocrystals [6] but slightly better than observed for anthraquinone [7].

Correcting the polarization curve for diffusion effects for first order reaction, one obtains [1]:

$$j_K = \left(\frac{j}{j_L - j} \right) \tag{5.5}$$

The kinetic current density (j_k) is related to the Tafel equation as Eq. 5.7 [1]:

$$E_{app} = E_{eq} - b \log j_k \tag{5.6}$$

$$b = \frac{2.303RT}{\alpha n_{\alpha} F} \tag{5.7}$$

where E_{app} is the applied potential, E_{eq} is the equilibrium potential, j_k is the kinetic current density, j_L is the limiting current density (plateau in RDE voltammogram), j is the measured current density at a given potential, b is the Tafel slope, R, T and F have their usual meaning, αn is the kinetic parameters for the electrode process. The plot of E_{app} versus log j_k yielded a slope of –221 mV dec^{-1}. The high value of the Tafel slope obtained is characteristic of porous electrode with high internal surface area leading to high electrocatalytic activities.

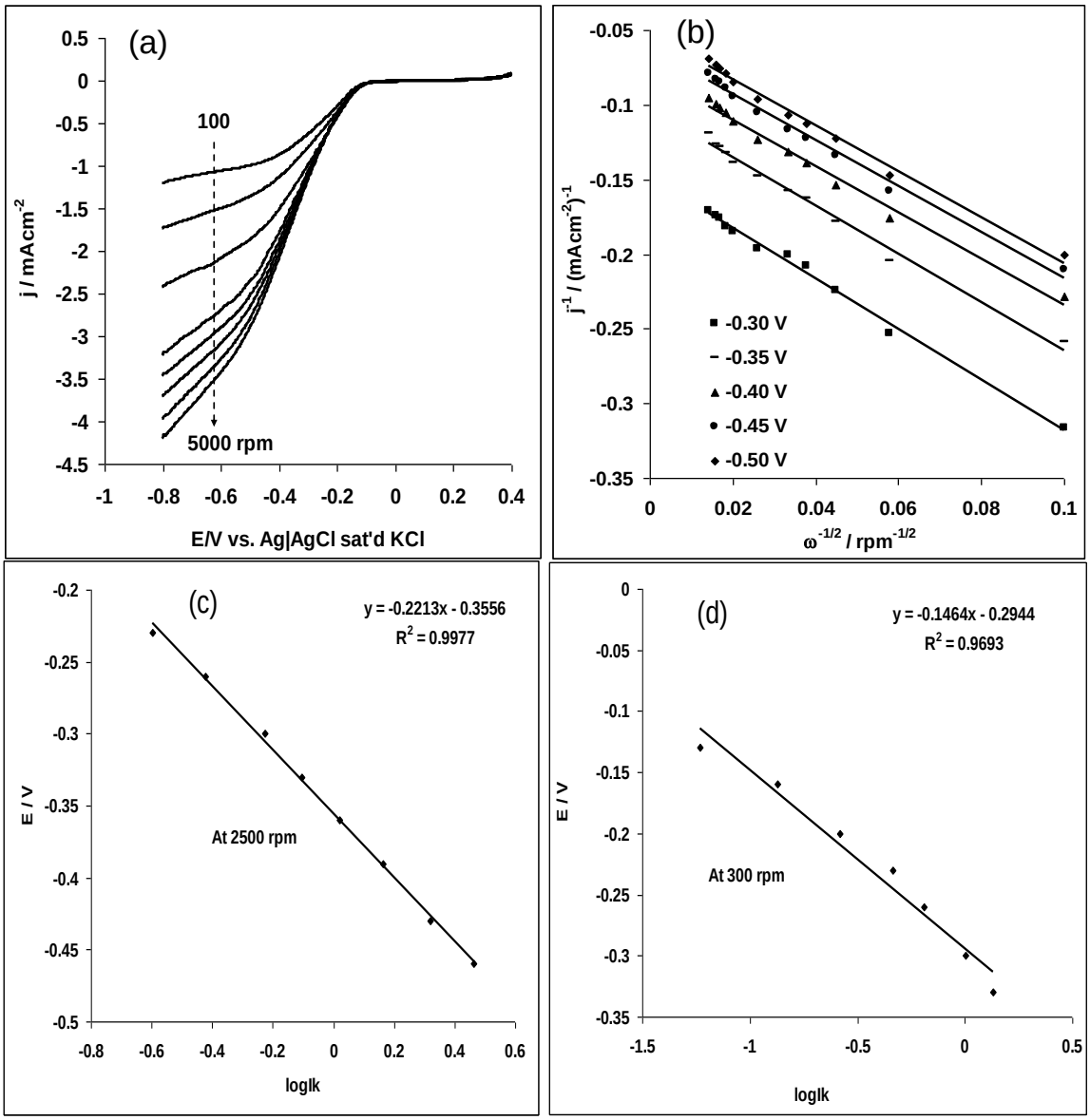

Figure 5.5: (a) RDE polarization curves at different rotation rates for BPPGE-MWCNT-RuOCPcPt in oxygen-saturated 0.1 M NaOH solution at a 10 mVs^{-1}, and (b) Koutecky-Levich plot obtained from RDE data. (c) and (d) are plots for oxygen reduction on BPPGE-fMWCNT-RuOcPcPt electrode in oxygen saturated 0.1 M NaOH at 2500 rpm and 300 rpm.

Figure 5.6 is the comparative cyclic voltammograms for the modified electrodes in 0.1M pH7.0 phosphate buffer solution containing 1 mM $[Fe(CN)_6]^{4-/3-}$ solution. The modified electrodes gave higher current

response compared to the bare BPPGE except for BPPGE-RuOcPc and bppge-Pt which gave about same current response as the bare BPPGE. BPPGE-RuOcPcPt gave much better response due to the RuOcPcPt nanocomposite. The performance was more enhanced in the presence of fMWCNT as shown by BPPGE-fmwcnt-RuOcPcPt modified electrode. The BPPGE-fmwcnt-RuOcPcPt electrode behaves closely to BPPGE-fmwcnt-Pt in terms of electron transport or current response. The results generally emphasised the contribution of fMWCNT in enhancing the current response of Pt and RuOcPc.

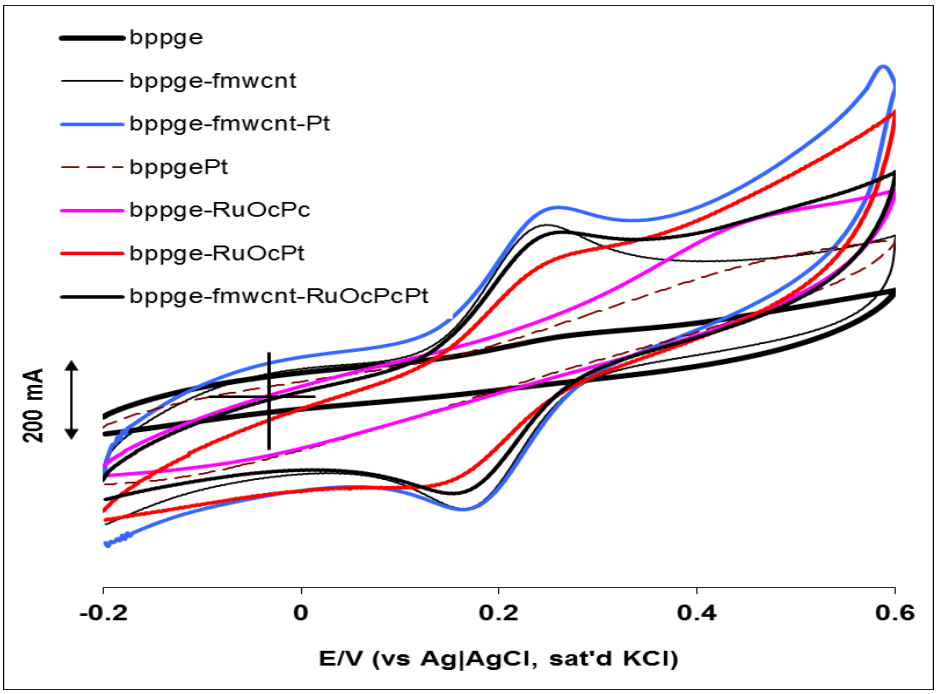

Figure 5.6: Comparative Cyclic Voltammograms of the electrodes studied in 1mM $[Fe(CN)_6]^{4-/3-}$solution containing 0.1 M phosphate buffer solution of pH 7.

Figure 5.7 is the Nyquist plots obtained from the electrochemical impedance study in 0.1M pH7.0 phosphate buffer solution containing 1 mM $[Fe(CN)_6]^{4-/3-}$ solution at $E_{1/2}$ of 0.2 V (vs Ag|AgCl, sat'd KCl). The plots from the experiment were fitted by two circuits model Figure 5.7c (i) and 5.7c (ii). The data obtained from the fitting is presented in Table 5.1. From the Table, BPPGE-fmwcnt, BPPGE-fmwcnt-RuOcPc, BPPGE-fmwcnt-RuOcPcPt, and BPPGE-fmwcnt-Pt have lower charge transfer resistance (Rct) compared to the bare BPPGE.

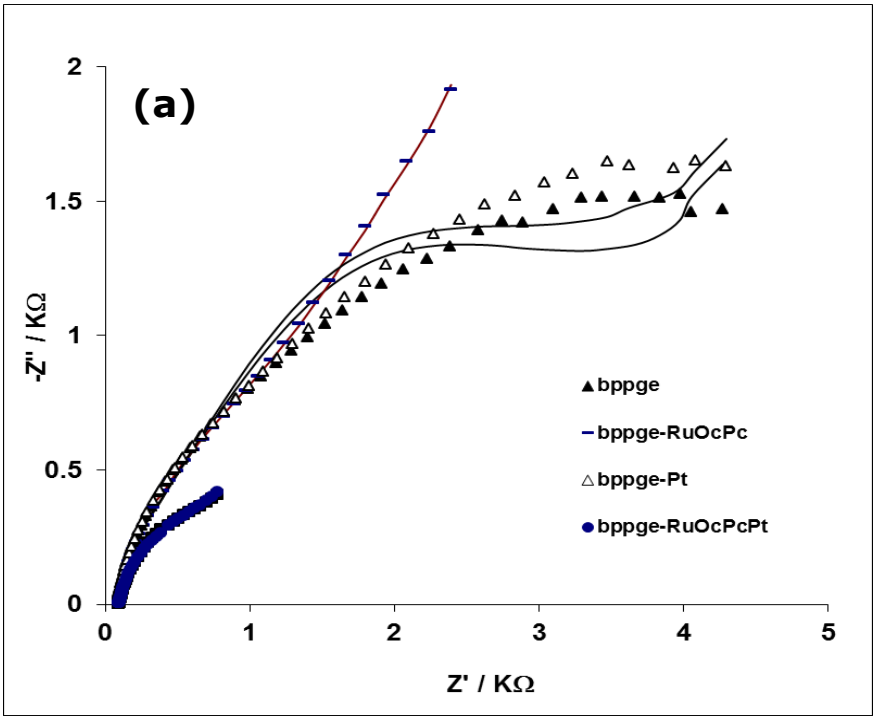

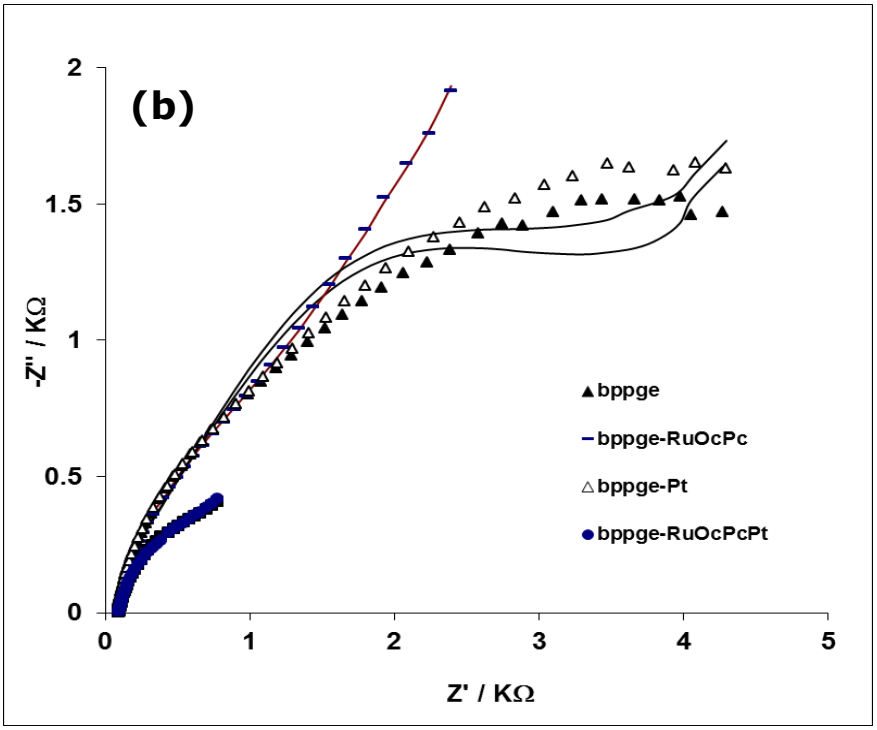

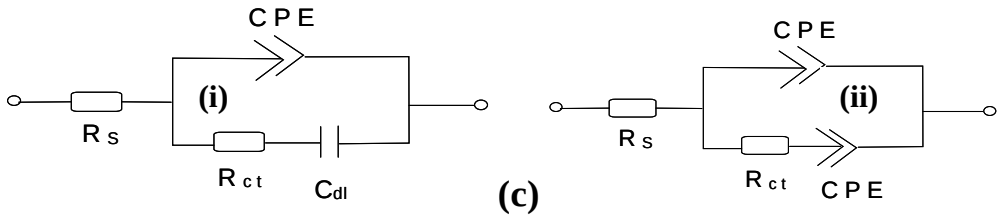

Figure 5.7: Comparative Nyquist plots (a) and (b) obtained for the various electrodes studied in 1mM $[Fe(CN)_6]^{4-/3-}$solution containing 0.1 M phosphate buffer solution of pH 7.0. (c)Electrical Equivalent Circuit Diagrams used for fitting the impedance data obtained in this work are (i) and (ii).

Table 5.1: Impedance data obtained for the modified electrodes in 1mM $[Fe(CN)_6]^{4-/3-}$solution containing 0.1 M phosphate buffer solution of pH 7.0. 1 M $[Fe(CN)_6]^{4-/3-}$ solution at 0.21 V vs Ag|AgCl sat'd KCl.

ELECTRODES	R_s / kΩ	R_{ct} / kΩ	CPE_1 /μF	n_1	CPE_2 / μF	n_2	C_{dl} /μF
BPPGE	0.056 (7.73)	4.75 (4.16)	$0.32E^{-7}$ (17.45)	0.63 (1.70)	-	-	122.4 (22.20)
BPPGE-Pt	0.063 (6.73)	4.82 (5.21)	$0.54E^{-7}$ (18.83)	0.65 (1.90)	-	-	116.6 (26.30)
BPPGE-RuOcPc	0.099 (0.66)	1.091 (8.11)	$0.15E^{-5}$ (5.81)	0.84 (1.00)	$0.32E^{-7}$ (53.54)	0.51 (3.35)	
BPPGE-RuOcPc-Pt	0.095 (0.651)	0.803 (12.9)	$0.49E^{-5}$ (9.92)	0.75 (1.66)	$0.53E^{-5}$ (100)	0.57 (22.7)	
BPPGE-Fmwcnt	0.086 (0.22)	0.009 (10.6)	$0.14E^{-4}$ (12.29)	0.60 (1.18)	-	-	116.2 (5.68)
BPPGE-FMWCNT-Pt	0.086 (1.51)	0.078 (14.6)	$0.33E^{-5}$ (47.42)	0.53 (4.11)	-	-	162.90 (12.00)
BPPGE-FMWCNT-RuOcPc	0.079 (2.60)	0.042 (4.12)	$0.30E^{-8}$ (99.47)	0.36 (4.96)	$0.15E^{-4}$ (9.58)	0.82 (2.91)	-
BPPGE-FMWCNT-RuOcPcPt	0.092 (0.21)	0.32 (9.57)	$0.15E^{-4}$ (5.40)	0.75 (1.14)	$0.29E^{-5}$ (62.73)	0.54 (5.25)	-

Figure 5.8a and 5.8b are the Bodes plots of phase angle against logf (a) and log |Z/Ω| versus logf (b) for the electrodes. The phase angle plots showed that the BPPGE-fmwcnt, BPPGE-fmwcnt-RuOcPc, BPPGE-fmwcnt-RuOcPcPt, and BPPGE-fmwcnt-Pt have lower phase angle compared with the bare. The result support their low charge transfer resistance discussed above because of their fast charge transfer process.

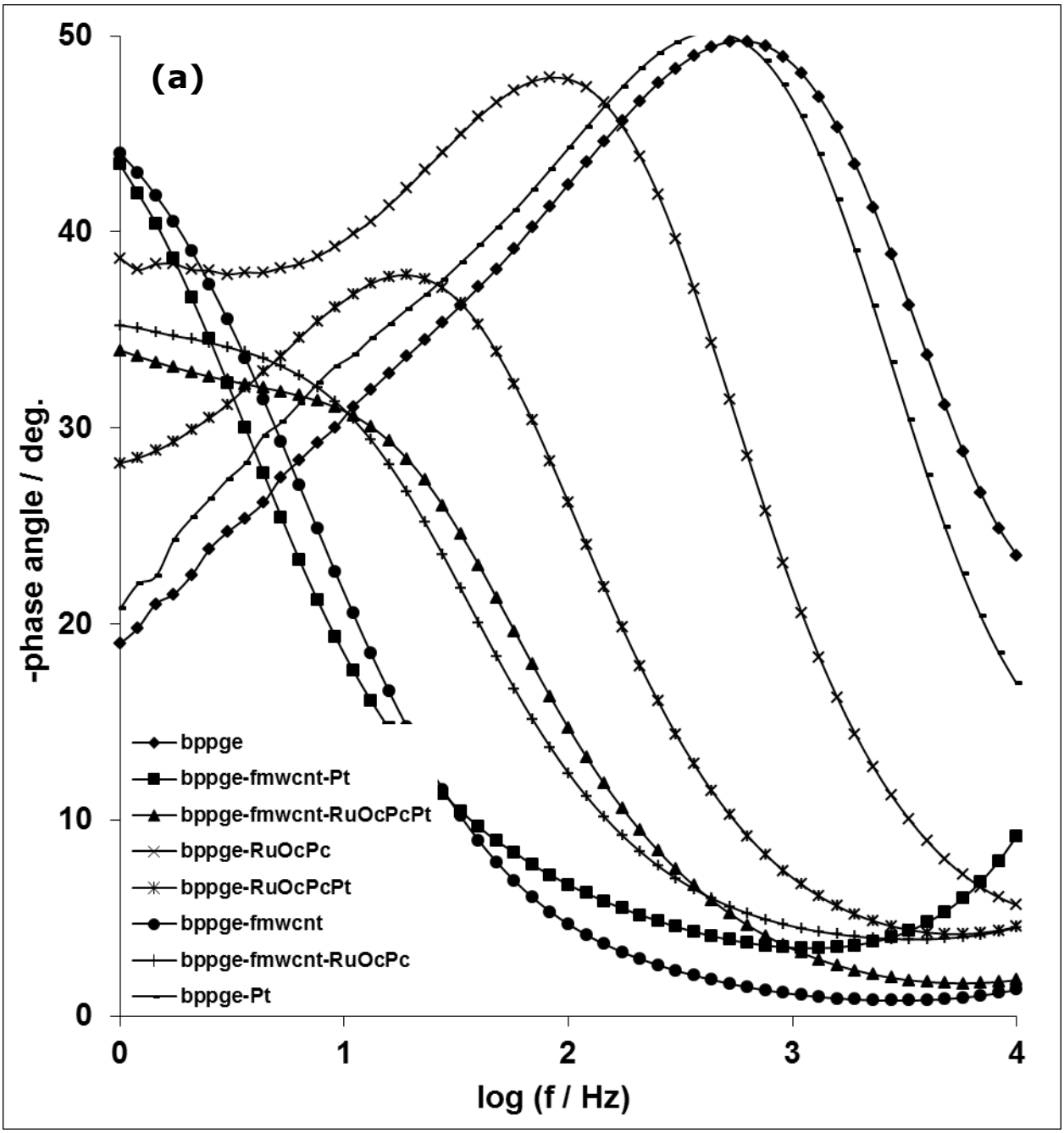

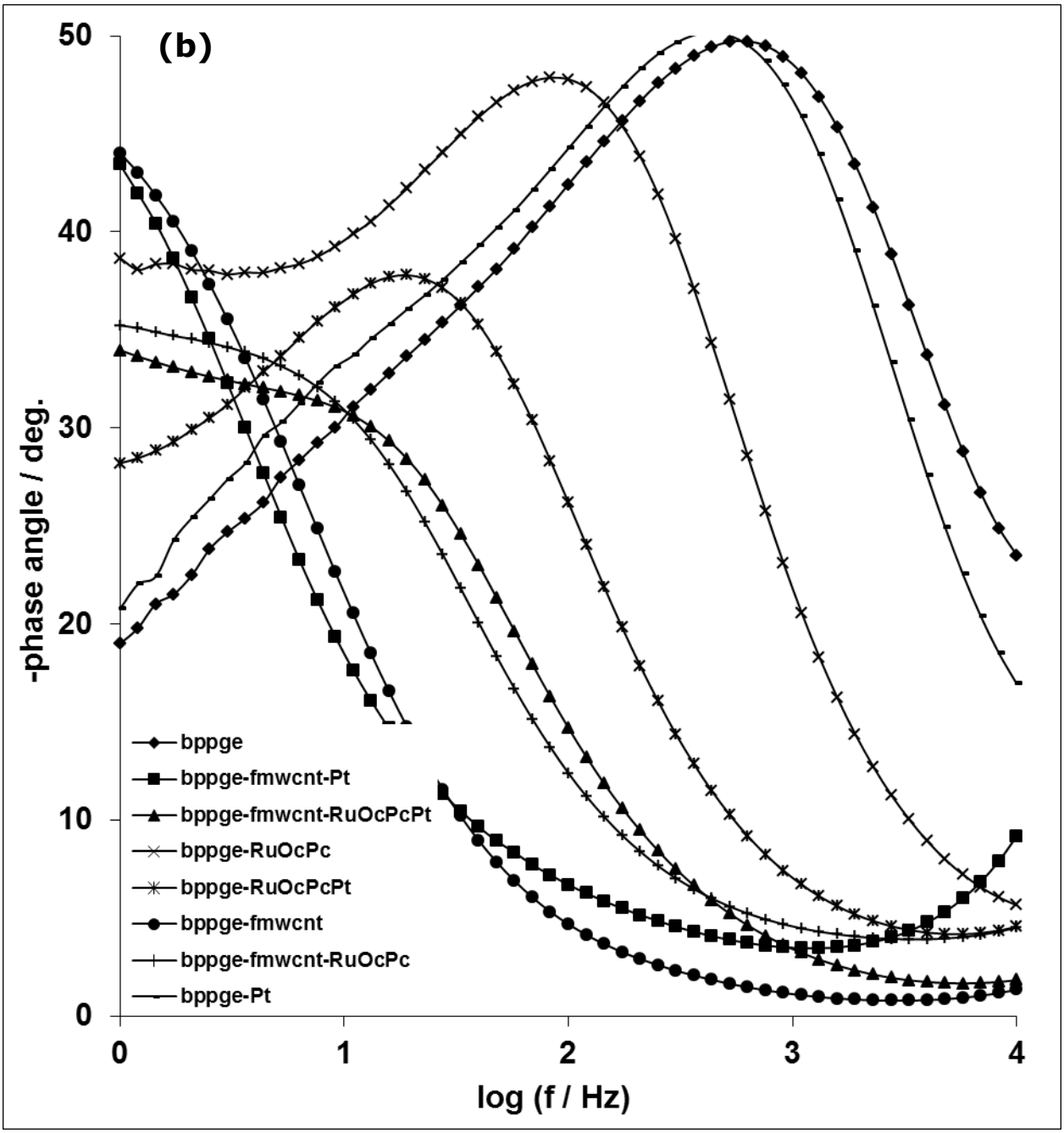

Figure 5.8: Comparative Bode plots (a) and (b) obtained for the various electrodes studied in 1mM $[Fe(CN)_6]^{4-/3-}$ containing 0.1 M phosphate buffer solution of pH 7.0.

References

1. O.V. Dolotova, O.L. Kaliya, Russ. *J. Coord. Chem*. 33 (2007) 111.

2. F. Wang, S. Hu, *J. Electroanal. Chem*. 580 (2005) 68.

3. J. Zagal, P. Bindra, E. Yeager, *J. Electrochem. Soc.* 127 (1980) 1506.

4. W.G. Wilke, Solubilities of Inorganic and Metal Organic Compounds, Vol 2, 4th ed., American Chemical Society, Washington, D.C. (1965) p.1219.

5. K. Vaik, U. Maeorg, F.C. Maschion, G. Maia, D.J. Schiffrin, K. Tammeveski, *Electrochim. Acta* 50 (2005) 5126.

6. H. Meng, P.K. Shen, *Electrochem. Commun*. 8 (2006) 588.

7. I. Koc, M. Camur, M. Bulut, A.R. Ozkaya, *Catalysis Lett*. 131 (2009) 370.

CHAPTER SIX

Electrocatalytic Oxidation of Methanol and Formic Acid at MWCNT Platform Modified with synthesized RutheniumTetrakis(diaquaplatinum)Octacarboxyphthalocyanine*

* **N.W. Maxakato**, N. Kobayashi, K.I. Ozoemena (being prepared for publication).

6.1 Spectroscopic and microscopic characterisation

The microscopic and spectroscopic images of RuOcPc and RuOcPcPt are already described and presented in figures 5.2 and 5.3 under chapter 5.

This chapter reports on how the electrocatalytic oxidation of FC molecules, MeOH and FA behave when using a RuOcPcPt catalyst instead of PtRu catalysts as reported previously. This study was done to improve the electro-catalytic performance of the electrodes modified with Pt/Ru.

6.2 Methanol and Formic acid oxidation

Figure 6.1a presents the voltammograms obtained for the electrodes in 0.5 M H_2SO_4 containing 0.5 M MeOH. The BPPGE-fMWCNT/RuOcPcPt electrode (vii) showed a higher current density in methanol oxidation with well-defined forward and reverse anodic peaks compared to that of the bare BPPGE (i), BPPGE-fMWCNT (ii), BPPGE-fMWCNT-Pt (iii), BPPGE-RuOcPc (iv), BPPGE-fMWCNT-RuOcPc (v) and BPPGE-RuOcPcPt (vi). This is interesting as it agrees with other literature reports where the introduction of macrocycles has led to drastic reduction of poisoning effects due to the electrooxidation of these molecules [1-4]. Unfortunately, oxidation of ethylene glycol was not successful on the modified electrodes. This is strange as our previous report showed successful oxidation of the molecule [5]. The reason for this is not understood at the moment but can be attributed to the different

techniques employed in the electrode modification. Figure 6.1b shows the comparative cyclic voltammograms of the electrodes in 0.5 M H_2SO_4 solutions containing 0.5 M FA. Interestingly, BPPGE-RuOcPcPt electrode has the best performance in terms of current response compared with the other electrodes. The results suggest that formic acid oxidation is enhanced on introduction of the phthalocyanine only without CNT inclusion as compared to MeOH oxidation. Thus, further work was done on methanol using fMWCNT/RuOCPcPt electrode and on formic acid using the BPPGE-RuOcPcPt electrode respectively.

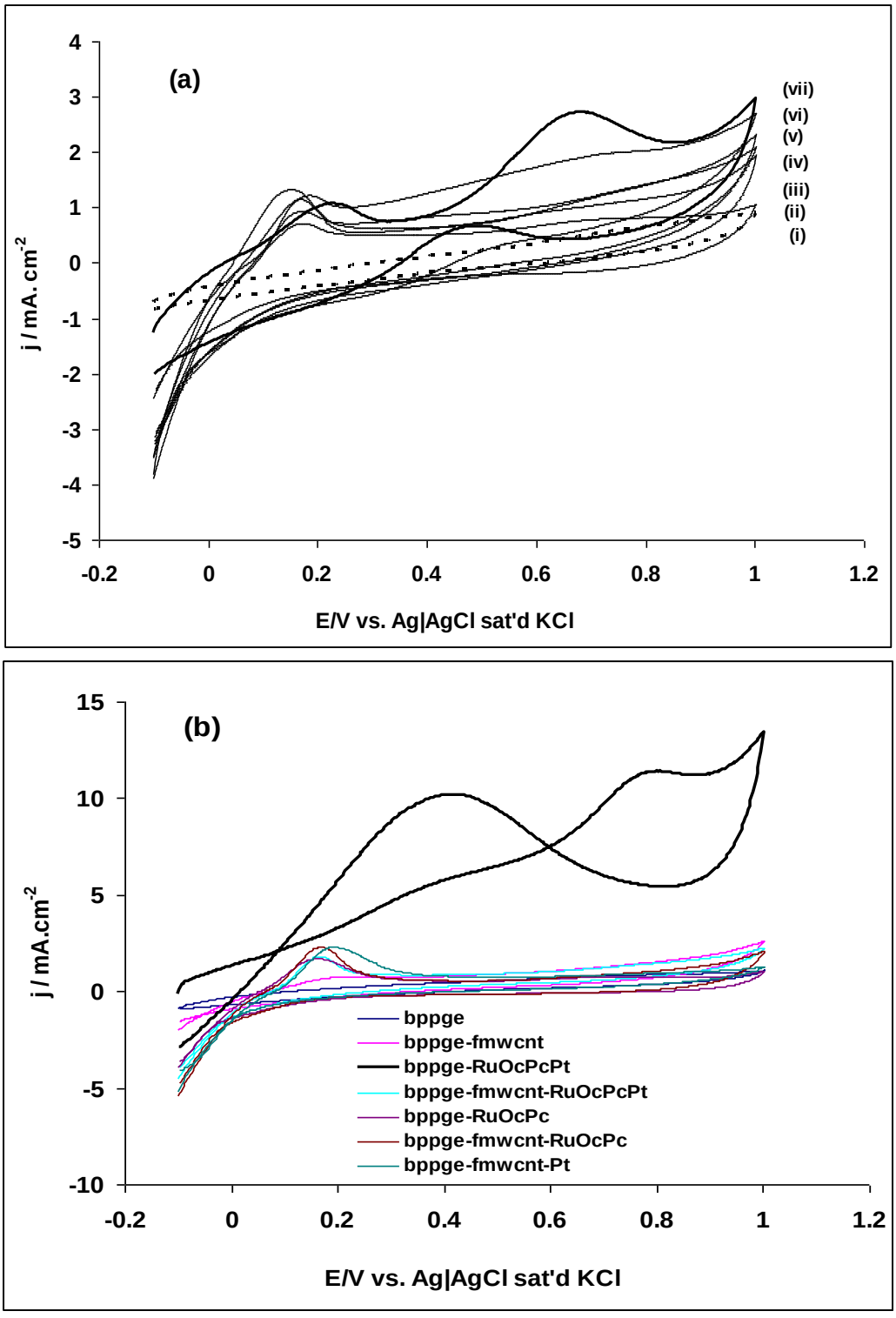

Figure 6.1: Comparative cyclic voltammetric evolutions in 0.5 M H_2SO_4 solutions containing 0.5 M MeOH (a) and 0.5 M FA (b) at different electrodes: (i) BPPGE, (ii) BPPGE-fMWCNT, (iii) BPPGE-fMWCNT-Pt, (iv) BPPGE-RuOcPc, (v) BPPGE-fMWCNT-RuOcPc, (vi) BPPGE-RuOcPcPt and (vii) BPPGE-fMWCNT-RuOcPcPt. Scan Rate = 0.5 Vs^{-1}.

Effect of different concentrations on the electrocatalytic oxidation of the fuel cell molecules using the best electrodes was investigated (Fig. 6.2 (a) and (b)). There is perfect correlation between the current response and concentration. That is, the current increases with increasing concentrations for both methanol and formic acid. The increase of current with increasing concentration obtained in this study is better than that of the previous study where phthalocyanine was not used as part of the electrode modifier [5]. The result further indicates the importance and the catalytic efficiency of phthalocyanine in increasing the oxidation current of the fuel cell molecules as seen in this study.

To evaluate the poisoning effect of CO on the electrodes, the heights of oxidation peaks may be used to estimate the extent to which the nanocomposites tolerate poison. Chen and co-workers [6-7] reported that the ratio of the current density of the forward anodic peak (J_{fa}) to the reverse anodic peak (J_{ra}) [6-7] is a measure of the fraction of the catalyst surface that has not been poisoned, or the higher the value of J_{fa}/J_{ra}, the less poisoned is the electrode. Zhou et al. [8] defined the tolerance to poisoning as the ratio of the first forward peak to that of the second forward peak (J_{fa1}/J_{fa2}). From these three references the J_{fa}/J_{ra} for the MeOH and FA are approximately 4.0 and 1.0, respectively. The result suggests that tolerance to poisoning is better for methanol than formic acid. Compared with our

previous report [5], the contribution of phthalocyanine in reducing the poisoning effect on our electrode is better for methanol.

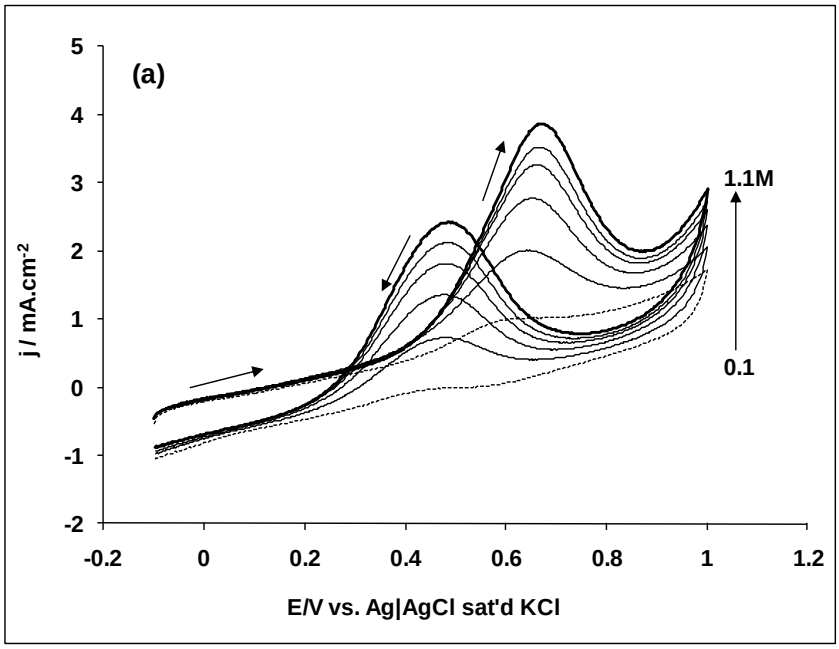

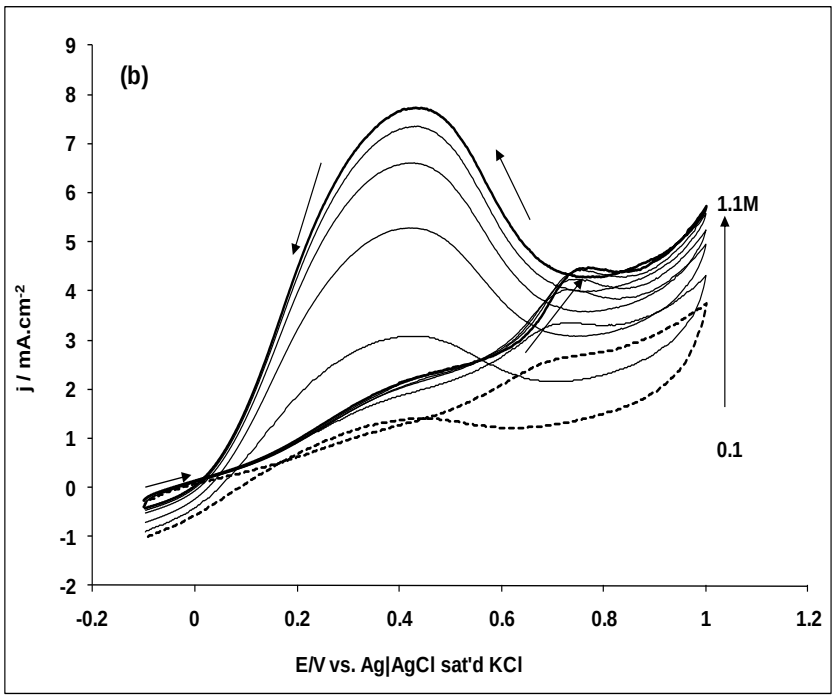

Figure 6.2: Cyclic voltammetric evolutions following changes in concentrations of MeOH and FA (0.1, 0.3, 0.5, 0.7, 0.9 and 1.1 M) at BPPGE-fMWCNT-RuOcPcPt (a) and BPPGE-RuOcPcPt (b). Scan rate = 0.5 Vs^{-1}.

6.3 Impedimetric Experiment

The mechanism of oxidation of FC molecules on the electrodes (BPPG/fMWCNT/RuOcPcPt electrode for methanol and BPPGE-RuOcPcPt electrode for formic acid oxidation) was studied using impedance spectroscopic at different oxidation potentials. The Nyquist plots obtained are represented in Figure 6.3. Figure 6.4 represents the different circuits used in the fitting of the experimental spectra, where R_s is the solution resistance, CPE represent the constant phase element, R_{ads} and C_{ads} represent the adsorption (or partial charge-transfer resistance) and adsorption capacitance arising from the oxidation of adsorbed species on the electrodes surface. Circuits (a) and (b) fitted the experimental spectra obtained in methanol at 0.48 and 0.68 V, while circuits (c) and (d) fitted the experimental spectra obtained in formic acid at 0.41 and 0.80 V respectively. The data obtained from the fittings are presented in Table 6.1. The presence of R_{ads} and C_{ads} in the circuits clearly indicates the adsorption of reaction intermediates arising from the oxidation of methanol and formic acid.

From the Bode plots of log Z/Ω versus log f/Hz (Fig. 6.5a), slope values of -0.44 (i) and -0.65 (ii) were obtained for the forward and the reverse processes in methanol, while a slope value of approximately -0.5 V was obtained at the three oxidation potentials noticed for formic acid oxidation (Fig. 6.5c). The slope values obtained are lower than the -1.0

expected for a pure capacitive behaviour of the electrode in the fuel cell molecules. The results further confirm the inclusion of CPE in the electrical circuit model used in the impedance fitting. Similarly, the plots of –phase angle/deg. versus the log f/Hz for methanol oxidation at 0.48 V (Figure. 6.5b) gave phase angles of 45^0 (at -0.2 Hz) and 51^0 (at 2.4 Hz) respectively, suggesting the involvement of two electrochemical process at this potential, with one of them probably due to the oxidation of the adsorbed intermediates. On the other hand, the highest phase angle of 58.20 was obtained for formic acid oxidation (Figure. 6.5d). The phase angles obtained are lower than the phase angle of -90^0 expected for a true capacitor implying the pseudocapacitive behaviour of the electrodes in the fuel cell molecules.

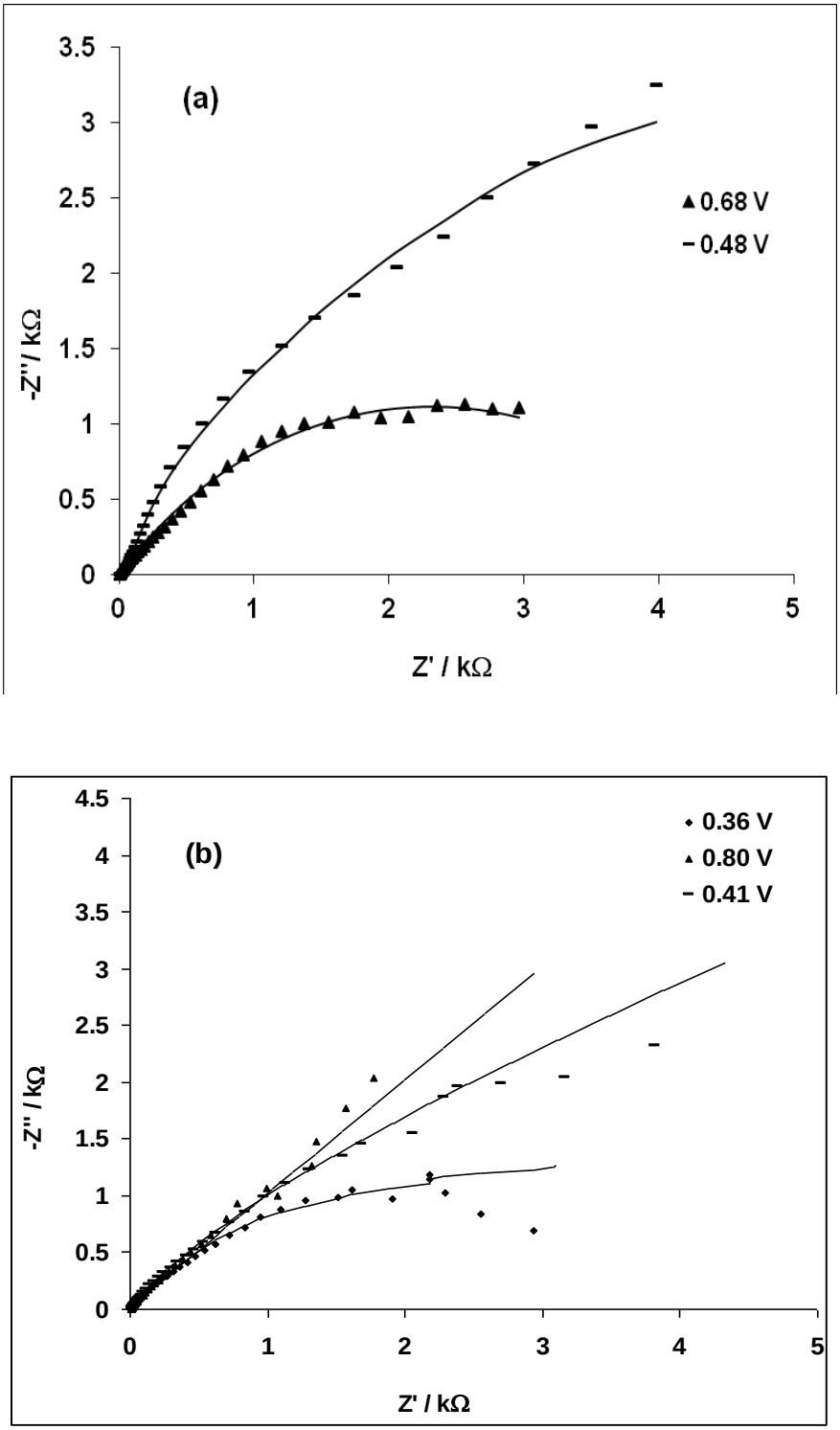

Figure 6.3: Typical Nyquist plots at different potentials of BPPGE-fMWCNT-RuOcPcPt and BPPGE-RuOcPcPt obtained in 0.5M H_2SO_4 solutions containing 0.5M MeOH (a) and 0.5M FA (b) between 10kHz and 0.1 Hz at forward and reverse peak potentials. The data points are experimental while the solid lines represent fitted (theoretical) spectra obtained from the proposed equivalent circuits shown in Figure 6.4 below.

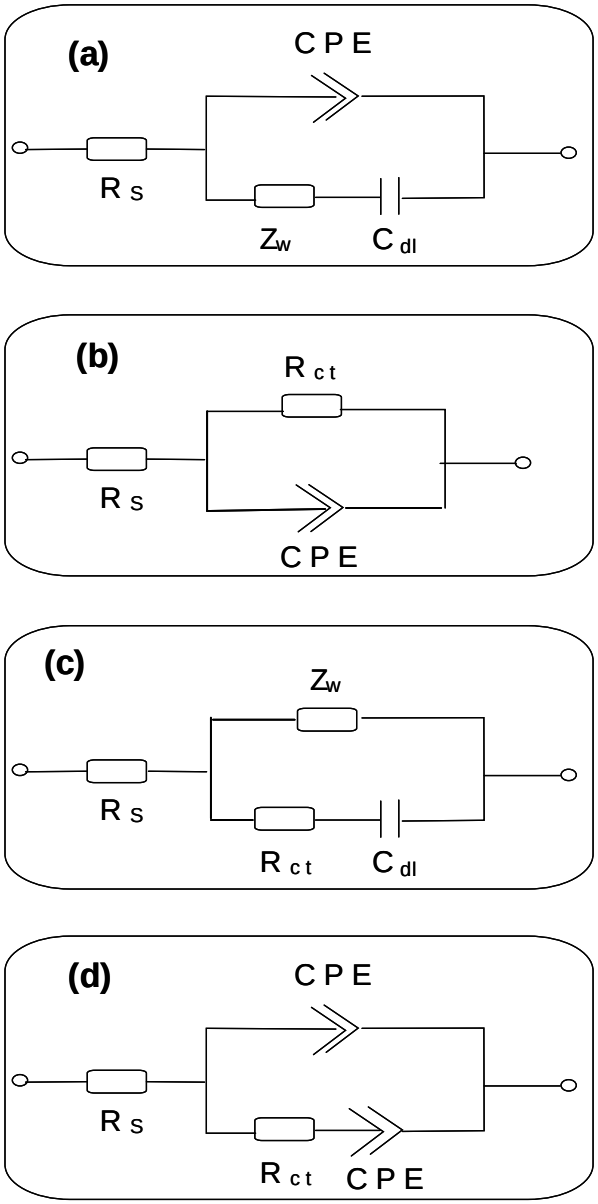

Figure 6.4: Equivalent circuits used to fit the EIS data of BPPGE-fMWCNT-RuOcPcPt and BPPGE-RuOcPcPt in 0.5 M H_2SO_4 solutions containing 0.5 M MeOH and 0.5 M FA.

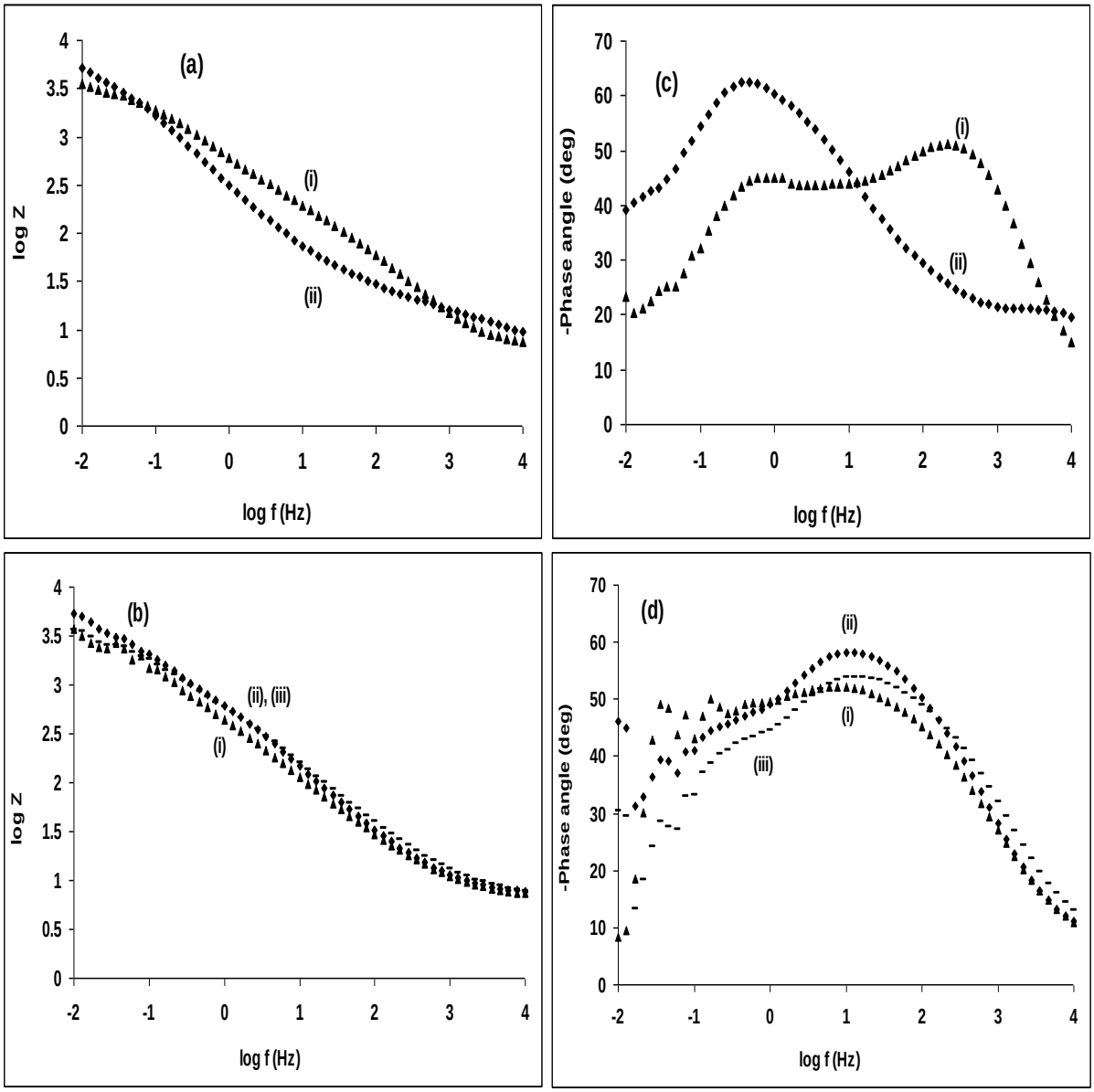

Figure 6.5: Bode plots (log |Z| vs log f) for MeOH (a) and FA (b). Plots (c) and (d) are the corresponding Bode plots (phase angle vs log f); respectively at different voltages as in figure 6.3: 0.68 V and 0.48 V for MeOH; 0.36 V and 0.80 V for FA.

6.4 Effects of scan rate

The impact of scan rates on the current responses of the two FC molecules using BPPG/fMWCNT/RuOcPcPt electrode for methanol and BPPG-RuOcPcPt electrode for formic acid oxidation respectively (Figure 6.6) was studied. The plots of peak current densities (I_p/mAcm^{-2}) against the square root of scan rates ($\nu^{1/2}$), at scan rates ranging from 0.01 – 1.2 Vs^{-1} gave a straight line with intercept around zero (forward process) and intercept deviating from zero (backward process) for methanol oxidation (Figure 6.7a), thus suggesting that the forward process is diffusion-controlled while the backward process is characterized with adsorption of oxidation intermediates. Similar results were obtained for formic acid oxidation (Figure 6.7b). The results obtained here further confirm those already discussed under impedimetric and the cyclic voltammetry experiments for the oxidation of the FC molecules.

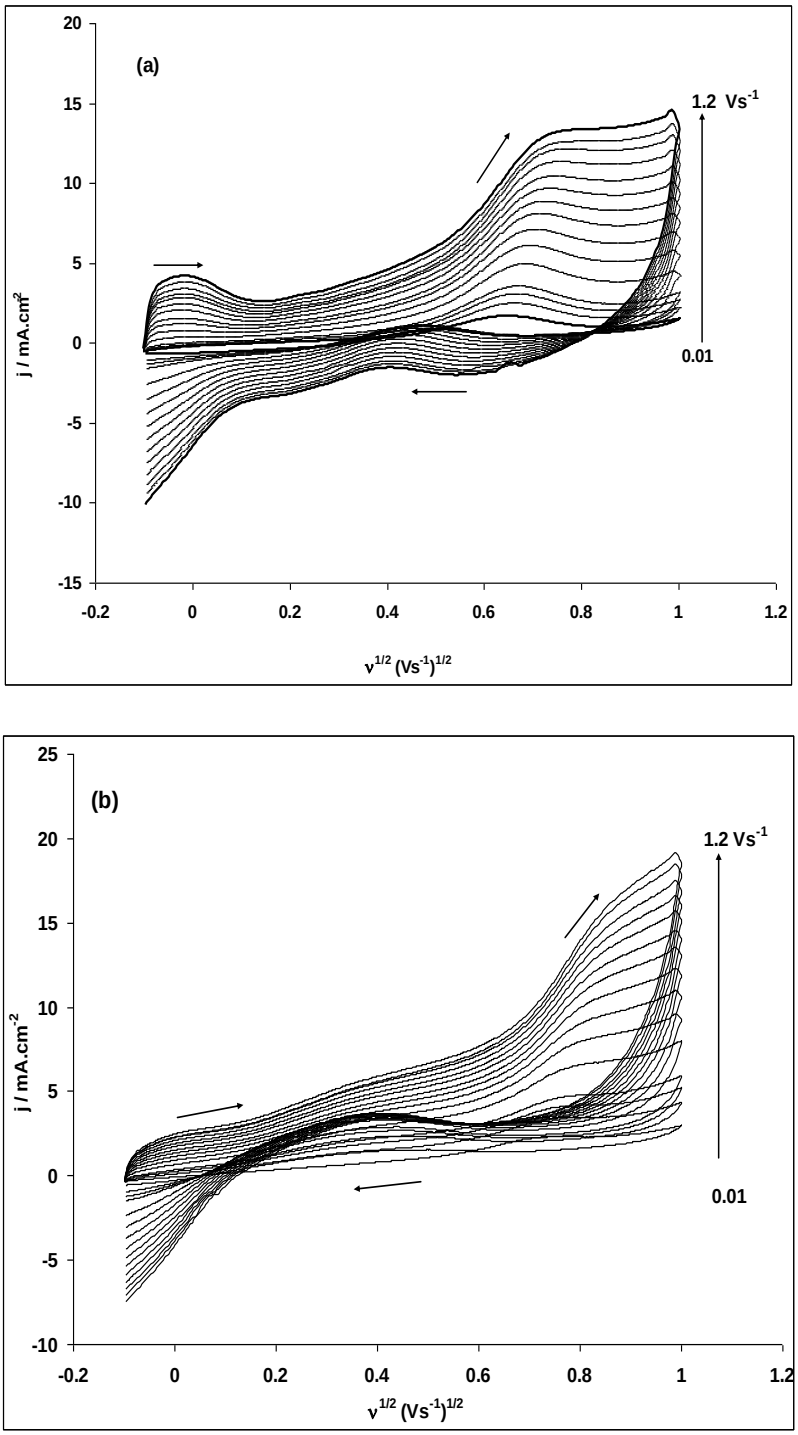

Figure 6.6: Scan rate studies of (a) BPPGE-fMWCNT-RuOcPcPt in 0.5 M H_2SO_4 containing 0.5 M MeOH and (b) BPPGE-RuOcPcPt in 0.5 M H_2SO_4 containing 0.5 M FA at scan rate range of 0.1 to 1.2 Vs^{-1}.

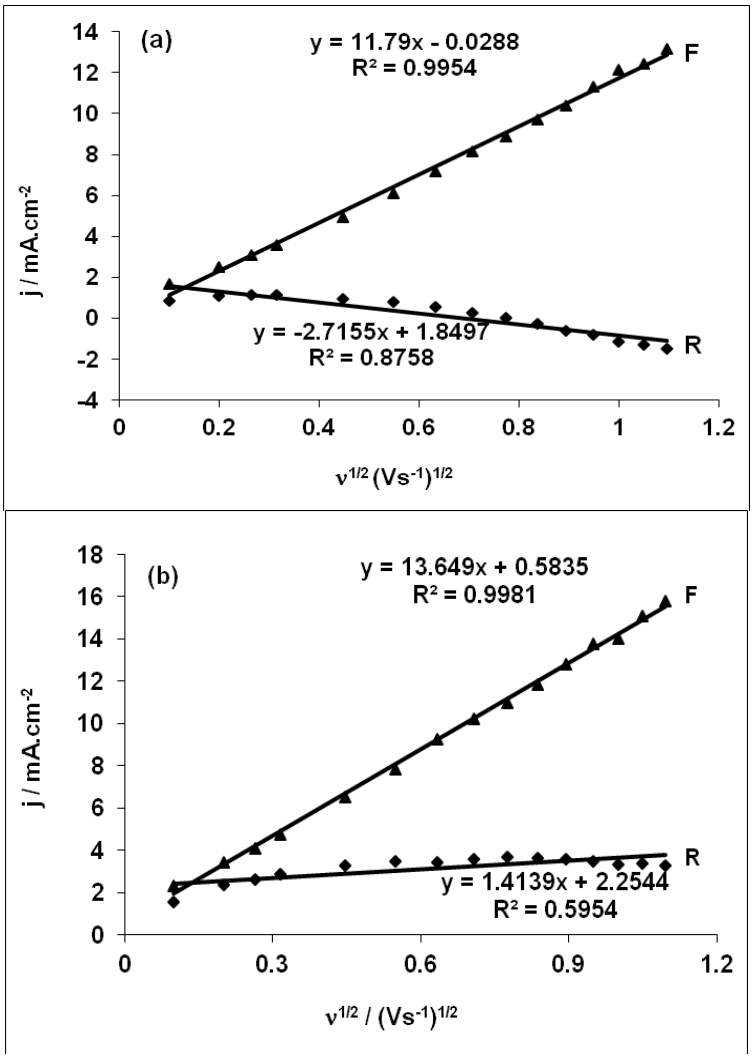

Figure 6.7: Plots of current density versus square root of scan rate for both forward and reverse process in (a) BPPGE-fMWCNT-RuOcPcPt in 0.5 M H_2SO_4 containing 0.5 M MeOH and (b) BPPGE-RuOcPcPt in 0.5 M H_2SO_4 containing 0.5 M FA.

6.5 Effects of scan numbers

Figure 6.8a and 6.8b present the voltammograms obtained for the electrodes in 0.5 M H_2SO_4 containing 0.5 M of the FC molecules (methanol or formic acid). The results agree with the calculations from concentration

studies. The MeOH increases with increasing scan numbers while FA decreases.

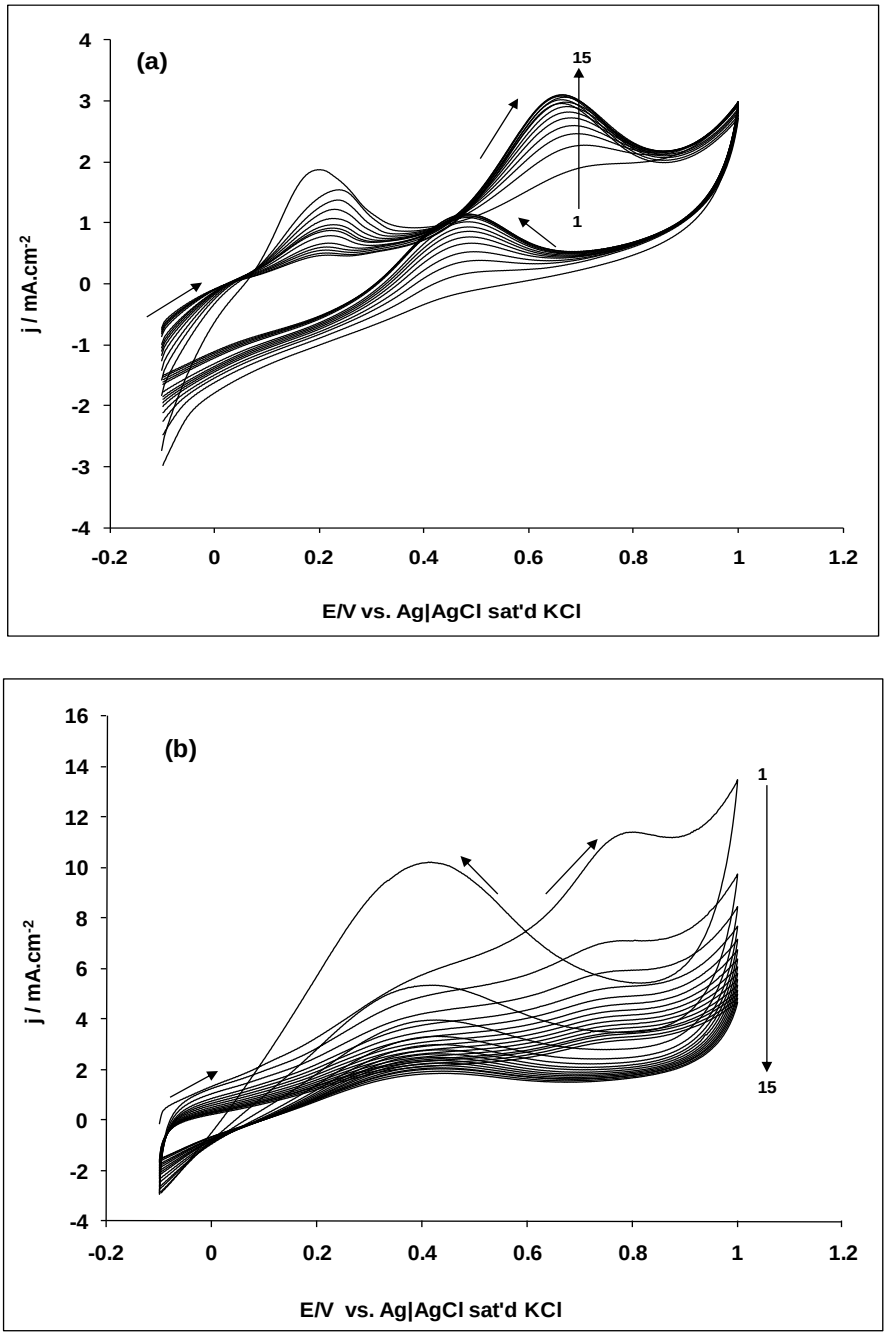

Figure 6.8: Stability of BPPGE-fMWCNT-RuOcPcPt and BPPGE-RuOcPcPt in 0.5 M H_2SO_4 containing 0.5 M of the FC molecules, methanol (a) and formic acid (b). Scan Rate = 0.5 Vs^{-1}

Table 6.1: Impedance data obtained at BPPGE-fMWCNT-RuOcPcPt and BPPGE-RuOcPcPt in 0.5 M H_2SO_4 containing 0.5 M of the fuel cell molecules (methanol or formic acid) at the foward and reverse peak potentials. Value in parenthesis is fitting error in percent.

***Methanol*: Circuit Figures 6.4(a) and 6.4(b) were used to fit the spectrum for the 0.48V and 0.68 V.**

Bias potential /V(vsAg|AgCl sat'd KCl)	R_s / Ω	CPE_1 / mF	n_1	Zw / Ω	C_{ads} / mF	R_{ads} / kΩ	n_2
0.48(Reverse process)	9.22 (4.16)	0.33 (15.32)	0.25 (21.82)	$0.20E^{-2}$ (3.57)	0.87 (13.62)	-	-
0.68(Forward process)	4.09 (9.10)	0.50 (3.39)	0.57 (1.13)	-	-	4.63 (6.26)	-

***Formic acid*: Circuit Figures 6.4(c) and 6.4(d) were used to fit the spectrum for the 0.41V and 0.80V.**

Bias potential/ V(vsAg|AgCl sat'd KCl)	R_s / Ω	CPE_1 / mF And Zw / Ω	n_1	R_{ads}/ GΩ	C_{ads} / μF	CPE_2 / mF	n_2
0.41(Reverse process)	7.32 (2.69)	0.29 (17.83)	0.73 (2.87)	1000 (100)	-	0.37 (7.91)	0.31 (24.40)
0.80(Forward process)	9.68 (7.80)	0.95E-3 (3.98)	-	-2.18 (31.15)	29.62 (15.57)	-	-

References

1. S. Sarangapani, B. Morriseau, Electrochem. Soc. Mtg., Abstract No. 476. Reno, Nevada, 1995.

2. J.S. Bett, H.R. Kunz, A.J. Aldykiewicz Jr., J.M. Fenton,W.F. Baileyb, D.V. McGrath, Electrochim. Acta 43 (1998) 3645.

3. N. Martz, C. Roth, H. Fuess, J. Appl. Electrochem. 35 (2005) 85.

4. J.A.R. van Veen, J.F. van Baar, C.J. Kroese, J.G.F. Coolegem, N. de Wit, H.A. Colijn, B. Bunsenges, Phys. Chem. 85 (1981) 693.

5. N.W. Maxakato, K.I. Ozoemena, C.J. Arendse, Electroanalysis, 22 5 (2010) 519.

6. O.V. Dolotova, O.L. Kaliya, Russ. J. Coord. Chem. 33 (2007) 111.

7. W. Chen, J. Kim, S. Sun, S. Chen, PhysChemChemPhys. 8 (2006) 2779.

8. X. Zhou, C. Liu, J. Liao, T. Lu, W. Xing, J. Power Sources 179 (2008) 481.

CONCLUSIONS AND FUTURE PERSPECTIVE

Various conclusions are drawn, as to determine which electrode amongst the electrodes studied has the potential for fuel cell applications. Also, a comparative investigation on the electrocatalysis of ethylene glycol (EG), methanol (MeOH) and formic acid (FA) fuel cell molecules at MWCNT-Pt/Ru supported on basal plane pyrolytic graphite electrode was undertaken. The main findings emanating from this study are summarized as follows:

From the cyclic voltammetric results, the ratio of the forward anodic to the reverse anodic peak current densities follow this order: MeOH > EG > FA. The impedance spectra for MeOH, EG and FA are dependent on the oxidation potential, and somewhat complicated, but generally follow electrical equivalent circuit models characteristic of adsorption-controlled charge transfer kinetics. EG and MeOH showed conventional positive Faradaic impedance spectra, irrespective of the applied oxidation potential. FA impedance spectra exhibited an inductive loop only at the extreme forward anodic peak potential, characteristic of Faradaic current being governed by the occupation of an intermediate state. The novel results in this work have provided some useful insights into the potential application of these FC molecules in fuel cell technology.

Oxygen reduction reaction (ORR) at ruthenium (II) tetrakis (diaquaplatinum) octacarboxy phthalocyanine (RuOcPcPt) catalyst supported

on multi-walled carbon nanotubes (MWCNTs) has been described. Cyclic voltammetry and rotating disk electrode technique revealed that the MWCNT-RuOcPcPt platform exhibits high activity towards ORR in alkaline medium. The onset potential for the reduction of molecular oxygen is *ca*. +0.003 V vs. Ag|AgCl (sat'd KCl), yielding a 4-electron transfer per oxygen molecule at a kinetic rate constant of 3.57 10^{-2} cm s^{-1}. These results show that the MWCNT-RuOcPcPt is a promising candidate as a catalyst in the cathodic reaction of fuel cell.

The last study of this thesis investigated the oxidation of FC molecules (methanol and formic acid) on basal plane pyrolytic electrode modified with platinum, ruthenium and phthalocyanine supported on multi-walled carbon nanotubes. The results indicated that the modified electrode containing phthalocyanine in the nanocomposite BPPGE-fMWCNT/RuOcPcPt electrode gave the best performance towards methanol oxidation compared to other electrodes studied. Interestingly, formic acid oxidation was favored on the same electrode (BPPGE-RuOcPcPt) but without CNTs support. The oxidation of the FC molecules is characterized by both diffusion (forward) and adsorption controlled (reverse) processes. When comparing with the previous study using electrodeposition (refer to chapter 4) MeOH gave better tolerance to CO poisoning while FA gave about the same J_{fa}/J_{ra}. The presence of phthalocyanine in the modified electrode used for MeOH has improved

their tolerance to CO poisoning and therefore its application in the direct fuel cell oxidation is encouraged.

Future work involves finding a new catalyst that is capable of solving the problem of surface poisoning at low potentials with characteristics of the catalyst that should tackle the weakening of Pt-CO bond to favour poisoning removal, the complete elimination of adsorption and the complete reduction of oxygen on carbon electrode surface decorated with platinum based nanoparticles for fuel cell applications.

APPENDIX A

Publications in peer-reviewed journals form this Thesis

1) **N.W. Maxakato**, K.I. Ozoemena, C.J. Arendse, "Dynamics of electrocatalytic oxidation of ethylene glycol, methanol and formic acid at MWCNT platform electrochemically modified with Pt/Ru nanoparticles", *Electroanalysis* 22 (2010) 519-529.

2) **N.W. Maxakato,** S.A. Mamuru, K.I. Ozoemena. Efficient oxygen reduction reaction using ruthenium tetrakis (diaquaplatinum) octacarboxyphthalocyanine catalyst supported on MWCNT platform, Electroanalysis, 22 December, 23 2 (2011) 325-329.

3) **N.W. Maxakato**, C.J. Arendse, K.I. Ozoemena. Insights into the electro-oxidation of ethylene glycol at Pt/Ru nanocatalysts supported on MWCNTs: Adsorption-controlled electrode kinetics, Electrochemistry Communications, 11 (2009) 534-537.

4) **N.W. Maxakato**, N. Kobayashi, K.I. Ozoemena. Enhanced Electrocatalytic Oxidation of Methanol and Formic Acid at MWCNT Platform Modified with synthesized Ruthenium Tetrakis(diaquaplatinum) Octacarboxyphthalocyanine (being prepared for publication).

APPENDIX B

List of Conference Presentations from this Thesis

1) "Electro-oxidation of Liquid Fuels (ethylene glycol, methanol and formic acid) on MWCNT-Pt/Ru Platform: Establishing the impact of Adsorption on the Reaction Kinetics" **N.W. Maxakato**, C. Arendse and K. Ozoemena, 3rd Nano-africa Conference, Feb. 1-4, 2009, Pretoria, South Africa. (**Poster presentation**).

2) Insights into the Electro-oxidation Properties of Ethylene Glycol at Multi-Walled Carbon Nanotube-Pt/Ru Nanoparticle Platform" **N.W. Maxakato**, C. Arendse and K. Ozoemena, 39th SACI National Convention, Nov. 30 – Dec. 5, 2008, Cape-Town, South Africa. (**Poster presentation**).

3) "Electro-oxidation of Methanol at Multi-walled Carbon Nanotubes Decorated with Metal Nanoparticles" **N.W.Maxakato**, C. Arendse and K. Ozoemena 1st International Symposium on Electrochemistry, Jul. 8-11, 2008, Cape Town, South Africa. (**Poster presentation**).

4) "Electro-oxidatioon of Methanol at Carbon –Nanotube Based Electrodes" **N.W.Maxakato**, C. Arendse and K. Ozoemena International (SA-UK Research Network) workshop on Electrochemistry for Nanotechnology, Apr. 9-11, 2008, Pretoria, South Africa. (**Oral presentation**).

5) "Efficient electrocatalytic oxidation of methanol and formic acid and oxygen reduction reaction in alkaline solution at MWCNT platform modified with synthesised ruthenium tetrakis(diaquaplatinum) octacarboxythalocyanine" **N.W. Maxakato** and K.I. Ozoemena 11th International Conference on Frontiers of Polymers and Advanced

Materials XI (ICFPAM) May 22-27, 2011, Conference Centre University of Pretoria, South Africa. (**Oral presentation)**.